

*SYNTHESIS AND APPLICATION OF
ORGANOBORON COMPOUNDS FOR
CATALYTIC AMIDE FORMATION AND
BIFUNCTIONAL CATALYSIS*

DU, YIHAO

How to cite:

DU, YIHAO (2020) *SYNTHESIS AND APPLICATION OF ORGANOBORON COMPOUNDS FOR CATALYTIC AMIDE FORMATION AND BIFUNCTIONAL CATALYSIS*, Durham theses, Durham University. Available at Durham E-Theses Online: <http://etheses.dur.ac.uk/13731/>

Use policy

The full-text may be used and/or reproduced, and given to third parties in any format or medium, without prior permission or charge, for personal research or study, educational, or not-for-profit purposes provided that:

- a full bibliographic reference is made to the original source
- a [link](#) is made to the metadata record in Durham E-Theses
- the full-text is not changed in any way

The full-text must not be sold in any format or medium without the formal permission of the copyright holders.

Please consult the [full Durham E-Theses policy](#) for further details.



**SYNTHESIS AND APPLICATION OF
ORGANOBORON COMPOUNDS FOR
CATALYTIC AMIDE FORMATION AND
BIFUNCTIONAL CATALYSIS**

A thesis submitted in partial fulfilment of the requirements

for the degree of

DOCTOR OF PHILOSOPHY

Department of Chemistry, University of Durham, UK

Submitted by

Yihao Du

Supervised by

Professor Andrew Whiting

2020

I. Declaration

This work was carried out at the Department of Chemistry, University of Durham (UK), between October 2016 and September 2019, under the supervision of Professor Andy Whiting. The contained content has never been submitted before in any form for a degree at this or any other institution.

The research stated within this thesis was conducted and reported by the author unless indicated otherwise.

YIHAO DU

2020

II. Statement of copyright

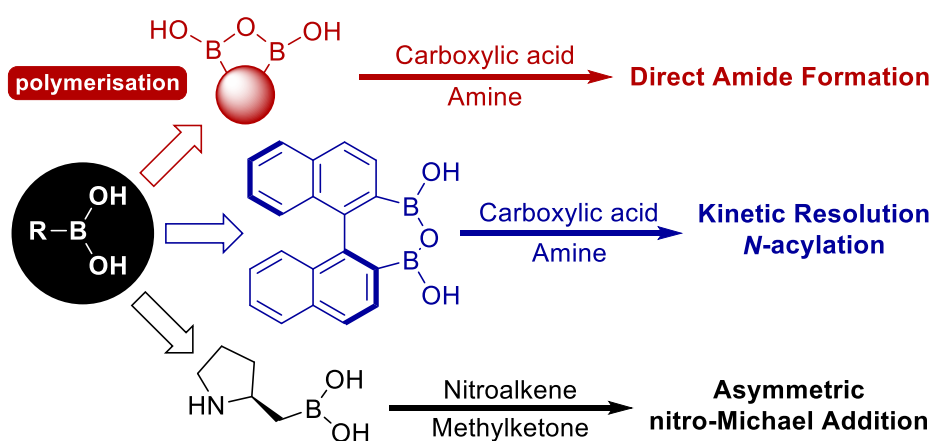
The copyright of this thesis rests with the author. Information derived from it should be acknowledged.

YIHAO DU

2020

III. Abstract

This thesis introduces the synthesis and application of alkyl- and aryl- boronic acids as catalysts for efficient bond formation. Specifically, this thesis mainly focuses on heterogeneous direct amide formation catalysed by solid-phase arylboronic acid, kinetic resolution of asymmetric *N*-acylation by a novel binaphthalene boronic ester species, and pyrrolidine boronic acid-catalysed enantioselective nitro-Michael addition.



The review on reported catalytic direct amide formation, especially organoboron catalysed amidation, gave a general idea of current development on the accessible toolbox towards amide bond construction. Investigation confirmed the existence of a reactive B-X-B bridged species, playing an important role in catalysis. Meanwhile, with increasing interest in solid-phase heterogeneous catalysis, a series of polymer-based catalysts have been prepared neat for amide formation. Some of them possess visible advantages in reactivity, reusability and recyclability over the reported homogeneous catalysts, which raised attention to enhance the overall efficiency of amidation by solid-based arylboronic acid. Careful synthesis gave polymerised catalyst in high conversion (showed in red in the figure above), which was crushed into fine powder for batches. Catalytic performance and

recovery of catalyst were tested in batch. Further employment in flow revealed the potential of the designed polymer catalyst towards an improved performance by optimised reaction conditions.

Apart from the polymer basis, research discovered the likelihood of biaryl scaffold in various types of catalysis. A brief review was given on the kinetic resolution, with focus on kinetic resolution of asymmetric *N*-acylation. As shown in blue in the figure, this thesis suggests an optimised strategy to the kinetic resolution of asymmetric amide formation by a novel system of axially chiral binaphthalene diboronate. It was based on our reported naphthyl diboronate system, including biphenyl-diboronate yet to publish. Under optimised methodology, initial attempt exhibited considerable enantioselectivity in high conversion.

Finally, we continued to look into other asymmetric catalysis. A review on current progress in bifunctional asymmetric was given, including a homoboroproline catalyst reported for catalytic aldol reaction *via* an enamine intermediate. It was believed that boronic acid coordinated the reaction with either its strong Lewis-acidic boron centre or its Brønsted acid site as H-bond donor. Further investigation on the proposed homoboroproline suggested reactivity in catalytic nitro-Michael addition (showed in black in the figure above). The optimised reaction condition enhanced the performance of such catalytic system, with up to 64% e.e. obtained in 99% conversion.

IV. Acknowledgements

The completion of the entire course, inclusive of this thesis, could not have been possible without assistance from many people in my life.

Firstly, I would like to express sincere gratitude to my advisor Prof. Andy Whiting for all the academic support and continuous guidance to my PhD study; for his patience, motivation and immense experience that truly contributed to the completion of degree courses. Meanwhile, from the bottom of my heart, I would like to express my love to my parents, without whom this work will never happen. In the past 27 years, their mental and financial support to the education on me truly affected my life.

Secondly, much appreciated to Prof. Ian R. Baxendale for his assistance during the period of my stay in his lab. Also, thanks to Prof. Patrick Steel, Dr. Elizabeth J. Grayson and Dr. Matthew O. Kitching for their constructive advice and instructions whenever needed. Additionally, special thanks to Dr Andrei S. Batsanov for his help on crystallography, as well as the rest of our analytical team staff for their efforts.

Thirdly, my appreciation and wishes would need to go to Dr. Alba Pujol, Dr. David Chisholm, Melinda Morelli, Jingbiao Chen, Diego Perera, Dr. Sergey Arkhipenko, Dr. Anna Wu and all the other members of our group for their support to my lab work. I do wish you all the best of luck in the life of your future.

Last but not least, I would like to thank all my family and friends for their spiritual support through the toughest moment of my academic career; for any form of encouragement and assistance that will be remembered for long.

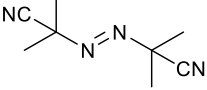
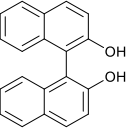
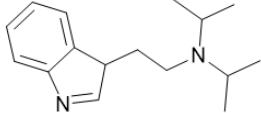
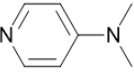
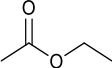
Contents

I.	Declaration	1
II.	Statement of copyright	3
III.	Abstract	5
IV.	Acknowledgements	7
V.	Abbreviations	10
VI.	Introduction	19
1.	Solid-supported catalytic direct amide formation	21
1.1	Catalytic direct amide formation	21
1.2	Organoboron-catalysed direct amide formation	23
1.3	Heterogeneous catalytic direct amide formation	28
1.4	Mechanistic insights.....	31
2.	Bifunctional catalysis of the asymmetric nitro-Michael reaction	36
2.1	Bimetallic asymmetric bifunctional catalysis	37
2.2	Lewis-acid/Lewis-base asymmetric bifunctional catalysis.....	42
2.3	Brønsted-acid induced dual activation in asymmetric catalysis	45
2.4	Boroproline based asymmetric enamine-based addition	51
3.	Kinetic resolution of asymmetric amide formation.....	55
3.1	Kinetic resolution of functional group interconversion	55
3.2	Organo-catalytic asymmetric <i>N</i> -acylation of amines.....	59
3.3	Mechanistic considerations.....	62
4.	Summary	65
VII.	Results & discussion	67
1.	Research target	67
2.	Solid-supported catalytic direct amide formation	68
2.1	Preparation of heterogeneous polymer catalyst	68
2.2	Substrate scope of polymer catalyst.....	72
2.3	Catalytic kinetics and mechanistic studies.....	77

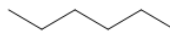
2.4	Polymer catalyst recovery and recyclability	83
2.5	Application in a flow reactor system	84
2.6	Conclusion	94
3.	Bifunctional catalysis of asymmetric nitro-Michael reaction	96
3.1	The synthesis of proline-based catalyst	97
3.2	Preparation of racemic nitro-alkene Michael adduct	100
3.3	Solvent screening of reaction condition.....	102
3.4	Introduction of ligands to catalysed nitro-Michael addition.....	106
3.5	Substrate scope of the catalysed nitro-Michael addition	108
3.6	Conclusion and future outlook.....	111
4.	Kinetic resolution of asymmetric amide formation.....	112
4.1	Preparation of racemic catalyst 108.....	114
4.2	Homogeneous direct amidation catalysed by (\pm)-108	116
4.3	Preparation of (<i>S</i>)-1,1'-diboronate binaphthalene.....	120
4.4	Kinetic resolution of asymmetric <i>N</i> -acylation catalysed by (<i>S</i>)-108	124
4.5	Conclusion and future outlook.....	129
5.	Concluding remarks	130
VIII.	Experimental section	132
1.	General experimental	132
2.	General reaction procedures	136
3.	Procedures and characterisations.....	145
3.1	Organo-boron mediated direct amide formation.....	145
3.2	Bifunctional catalysis of asymmetric nitro-Michael reaction	153
3.3	Kinetic resolution of asymmetric amide formation	165
IX.	References	172
X.	Appendix	187
1.	¹ H NMR spectra	187
2.	HPLC plots	193
3.	Crystallography data.....	200
4.	Major conferences attended.....	211

V. Abbreviations

Solvents and reagents

AIBN	=	azobisisobutyronitrile	
BINOL	=	1, 1'-bi-2-naphthol	
DCM	=	dichloromethane	
DIPT	=	diisopropyltryptamine	
DMAP	=	4-dimethylaminopyridine	
DME	=	dimethyl ether	
DMF	=	dimethylformamide	
DMSO	=	dimethyl sulfoxide	
DVB	=	divinylbenzene	
EtOAc / EA	=	ethyl acetate	

n-Hex. = hexane



c-Hex. = cyclohexane

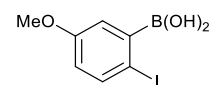


IPA = isopropanol



MCF = mesocellular siliceous foam

MIBA = 5-Methoxy-2-iodophenylboronic acid



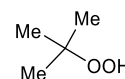
MS = molecular sieves

NHC = *N*-heterocyclic carbene

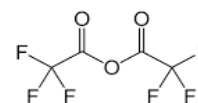
PS = polystyrene

REMB = rare earth-alkali metal-BINOL

TBHP = *tert*-butyl hydroperoxide



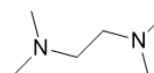
TFAA = trifluoroacetic anhydride



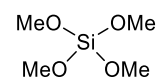
THF = tetrahydrofuran



TMEDA = tetramethylethylenediamine



TMOS = tetramethyl orthosilicate



Structures

Ar	=	aryl-
Bn	=	benzyl-
Boc-	=	<i>tert</i> -butyloxycarbonyl
Bu	=	butyl-
Cp	=	cyclopentadiene
Dipamp	=	bis(<i>o</i> -anisylphenylphosphino)ethane
EBTHI-	=	1,2-ethylene-1,1'-bis(η^5 -tetrahydroindenyl)
Et	=	ethyl-
ⁱ Bu	=	isobutyl-
ⁱ Pr	=	isopropyl-
Me	=	methyl-
Ph	=	phenyl-
Pin	=	pinacol
^t Bu	=	<i>tert</i> -butyl-
Tf	=	trifluorosulfonate
tol.	=	tolyl
Ts.	=	toluenesulfonyl

Others

Å	=	angstrom(s)
br.	=	broad
d.	=	doublet
d.p.	=	degree of polymerisation
E _a	=	activation energy
e.e.	=	enantiomeric excess
E _p	=	polymerisation energy
equiv.	=	equivalent
ES	=	electrospray
FGI	=	functional group interconversion
FWHM	=	full width at half maximum
g	=	gram (1 g = 1000 mg)
GC-MS	=	gas chromatography mass spectrometry
h	=	hour
HPLC	=	high performance liquid chromatography
IR	=	infra-red
<i>J</i>	=	coupling constant

KR	=	kinetic resolution
L	=	litre (1 L = 1000 ml)
LA	=	Lewis-acid
LB	=	Lewis-base
LHE	=	lithium-halogen exchange
M	=	molar (1 M = 1 mol dm ⁻³)
<i>m-</i>	=	<i>meta-</i>
m.	=	multiplet
MAS	=	magic angle spinning
Mol	=	mole(s)
NMR	=	nuclear magnetic resonance
NR	=	no reaction
<i>o-</i>	=	<i>ortho-</i>
p.	=	pentet
<i>p-</i>	=	<i>para-</i>
ppm	=	parts per million
psi	=	pound-force per square inch
q.	=	quartet

<i>rac-</i>	=	racemic
r.t.	=	room temperature
s.	=	singlet
SSNMR	=	solid-state nucleic magnetic resonance
t.	=	triplet
TLC	=	thin layer chromatography
t _R	=	retention time
UV	=	ultra-violent

This thesis is dedicated to my parents, Cheng Du and Wei Zhang, for the toughest but happiest moment we've together been through.

VI. Introduction

For a long time, catalysis has been an inseparable part of Chemistry. People have been fascinated by the state-of-the-art in catalysis and research into its behaviour in most applicable reactions. Generally, small molecules can be modulated by careful design to pursue a specific chemical and kinetic purpose, or a thermodynamically preferred conversion.^{1,2} For some chiral catalyst backbone systems, it is possible to obtain a favoured product through controlling both regio- or stereo-selectivity. Among them, boron-based catalysts have been studied over decades for application in various organic synthetic reactions, including catalytic direct amide formation³⁻⁵ and other asymmetric reactions.⁶⁻⁸

Organoboron compounds come with a trigonal planar structure due to a trivalent sp^2 -hybridized boron centre in their uncomplexed, neutral state. As a result, the property of the resulting boron species depends on the substituents themselves, together with the unoccupied p -orbital which works as a Lewis-acid. In the case of halogen or acyl-substitution on boron, where strong sigma-electron-withdrawing effects work to increase the electrophilicity of boron centre, sensitivity to water or even milder chemical environment becomes crucial as those systems can easily decompose through cleavage of B-X bonds, leading to reduced reactivity and even complete deactivation of the compounds as potential catalysts.⁹

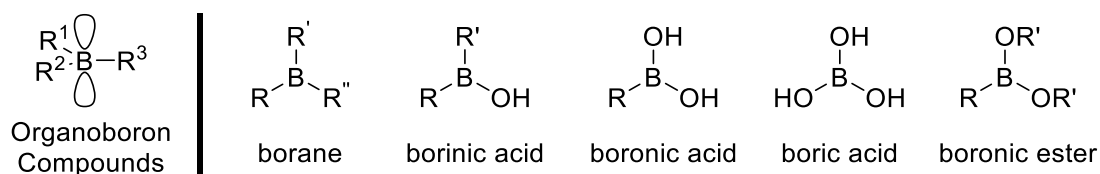


Figure 1. Different oxygenated states of organoboron compounds.

In comparison to the less polar C-B bonding and more polar B-X bonding, B-O bonding is more intermediate, in favour of substitution reactions occurring at the boron centre. Meanwhile, such compounds are generally of moderate reactivity and applicable under milder conditions. Different substitution gives a boron species with different oxygenated substitution patterns (**Figure 1**), providing a readily accessible range of reactive variations. In particular, aryl-substituted boronic acids have been the focus of much research recently because of the advantages mentioned above, as well as their recognised role as Brønsted acids.¹⁰ In this section, some areas where these arylboronic acids behave as catalysts will be discussed, together with how they work, based on the existing evidence.

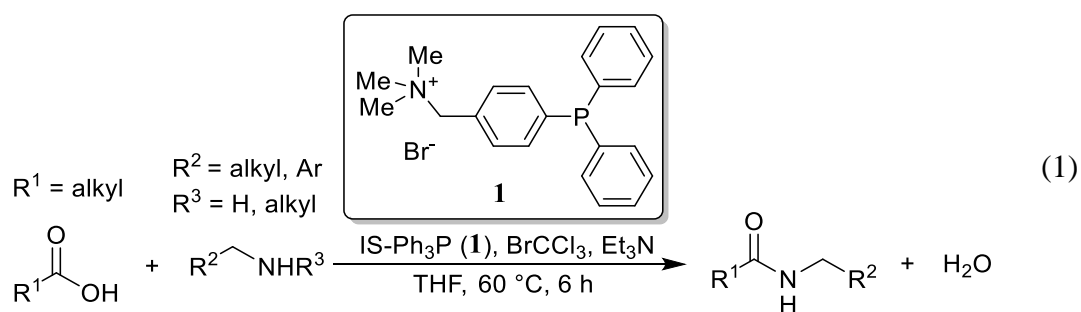
1. Solid-supported catalytic direct amide formation

The amide bond is by far the most widely occurring structural motif incorporated into about 25% of all pharmaceutical compounds,¹¹ with amide formation reactions constituting around 16% of all reactions used by medicinal chemists.¹² There have been a considerable number of synthetic strategies developed towards amide bond formation.³⁻⁵ Most methods developed for amide bond formation between carboxylic acids and amines, particularly those for peptide synthesis, involve the use of carboxylic acid activating agents.^{13, 14} However, such approaches generate stoichiometric amounts of waste,¹⁵ which, therefore, provides a major challenge for new, sustainable amidation to achieve high conversion and catalyst reactivity, coupled with recyclability and low or zero waste or by-products. This has led to the development of direct catalytic amide formation as a more environmentally friendly process and methodology.

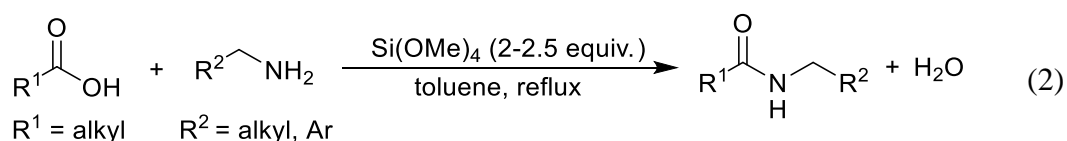
1.1 Catalytic direct amide formation

As realised in recent years, facile direct amide formation from non-activated carboxylic acids and amines has been realised as a desirable target to reach, enabling visible improvements in atom economy since water is the only by-product, as well as providing environmental friendliness. Therefore, to achieve this, new strategies have been developed to prepare amides *via* high yielding and efficient catalytic amidation processes.

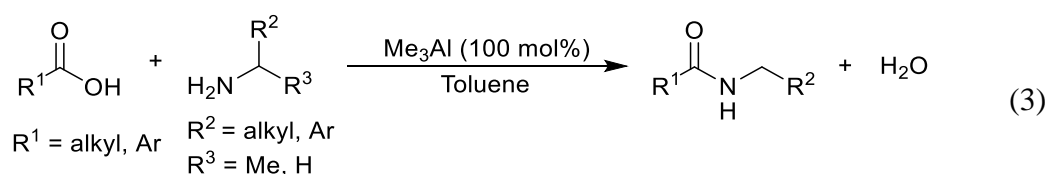
The Kawagoe group suggested an amidation method using an ion-substituted Ph₃P catalyst.¹⁶ They quantified the required catalyst amount of catalyst for the best conditions for both secondary and tertiary amides from various substrates (Equation 1), with the catalyst IS-Ph₃P (**1**) being simply prepared and isolated as required.



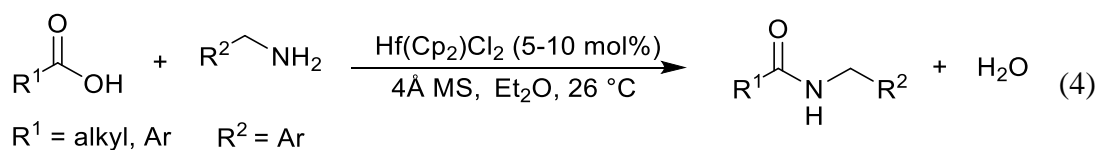
Recent research by Braddock *et al.* introduced TMOS as a mechanistically driven acylating reagent in direct amide formation providing lower process mass intensity conditions (Equation 2).¹⁷ It was treated as an inexpensive and versatile catalyst and considering its high catalytic loading (200-250 mol%), there was still potential for such silyl ester systems being employed after proper modification and optimisation.



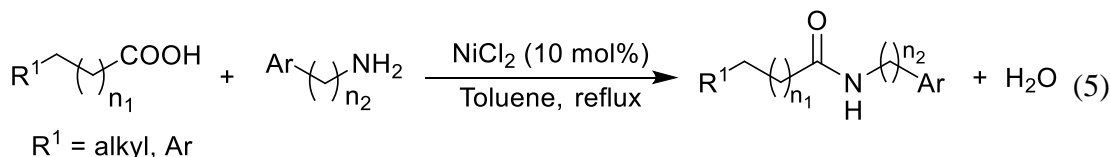
In particular, there has been successful application of metal-catalysed direct amidations. Early explorations such as using trimethylaluminum-based systems, was developed by the Chen group for direct amide formation (Equation 3).¹⁸ Compared to boron, aluminium as a metal, is a stronger Lewis-acid though tuning that Lewis-acidity remains challenging and impacts catalytic loading. This was solved in other applications by the Lundberg group who reported the direct amide formation using a hafnium-based system (Equation 4).¹⁹



In comparison to their reported titanium- and zirconium-based systems,²⁰⁻²² Lundberg group observed good reactivity under mild conditions, presumably by the overall electron dispersity and use of molecular sieves as rate-determining properties. Such methods were applied to wide substrate ranges, retaining the original stereoselectivity when using chiral reagent systems.



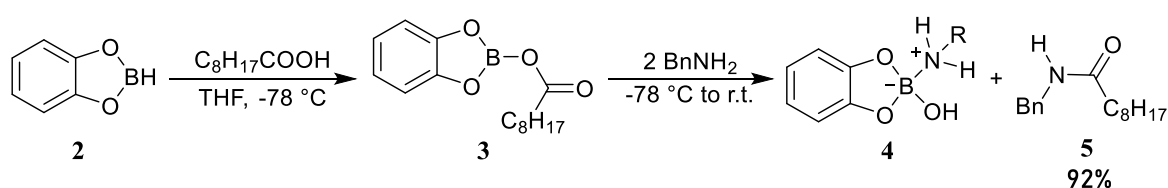
Recently, Cheng *et al.* discovered a route to amides *via* a nickel-based catalyst (Equation 5).²³ Such a process was examined using phenylacetic acid and benzylamine derivatives, giving high efficiency without a need for drying agent.



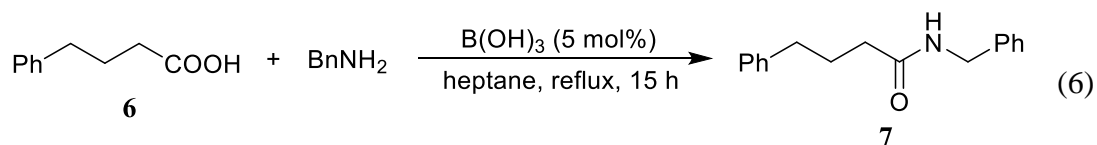
1.2 Organoboron-catalysed direct amide formation

Back in 1970, pioneering efforts were made to develop the first boron-based catalysts for direct amidation.² Over the years, a considerable number of new developments have been reported, showing increasing generality and utility. Initial attempts at developing homogeneous boron-mediated catalysis were introduced by Ganem *et al.*,²⁴ involving

borane systems based on catecholborane **2** for the amidation reaction of aliphatic carboxylic acids and benzylamine in THF between $-78\text{ }^{\circ}\text{C}$ and room temperature (**Scheme 1**). Through the formation of an electron-deficient boronic ester intermediate **3**, the amidation occurred with high rates of conversion. Later, the use of boric acid was introduced by Tang²⁵ for catalytic amidation (Equation 6). Here the reflux process helped increase the reactivity of boric acid catalyst when phenylbutyric acid **6** was reacted with benzylamine.

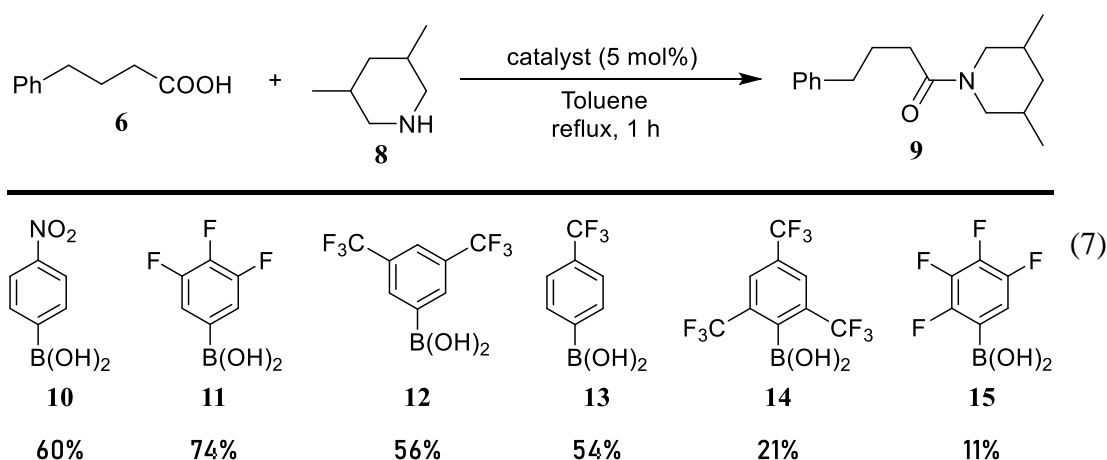


Scheme 1. Catecholborane based catalytic amide formation

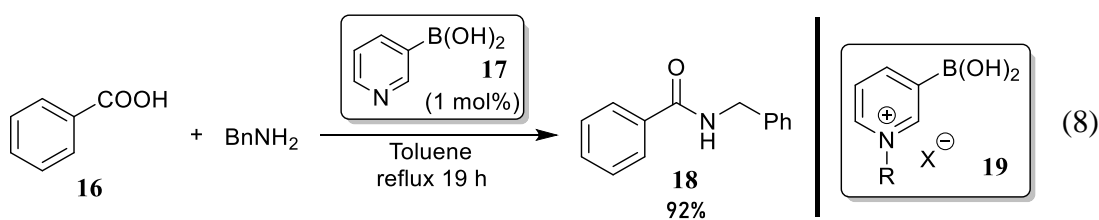


More research has involved developing new generations of boron-based species including arylboronic acids, which are mild Lewis-acid catalysts when applied to direct amide formation, given that the aryl groups are tuneable in terms of their electronic effects. Such systems were first reported by Ishihara and Yamamoto²⁶ in 1996 when they designed a catalytic system involving fluorinated phenylboronic acids **11-15** (Equation 7). They tested the amide formation in the presence of different substitutions on benzeneboronic acid and discovered the types of electronic and steric effects that promoted the process. It was found that substitution of the *ortho*-positions caused negative steric effects and inhibition

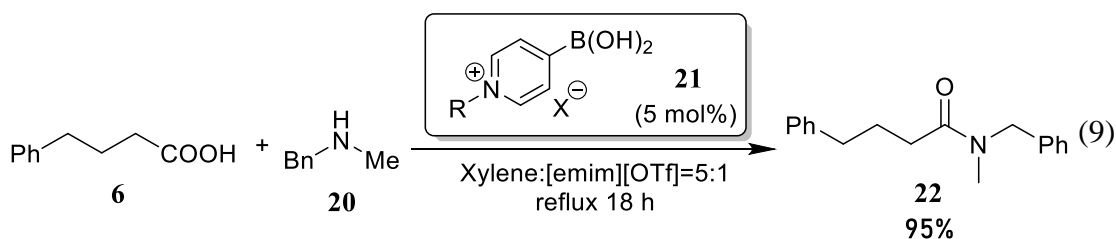
of the catalysis using catalyst **14** and **15**. In contrast, 3,4,5-trifluorophenylboronic acid **11** exhibited the best performance, giving 74% of condensation product in a general azeotropic toluene reflux system. It is believed that the electron-withdrawing effects of the catalyst **11** were better matched for the proposed chemical environment for direct amide condensation. Further examples showed its potential in a wide range of substrates under mild reaction conditions.



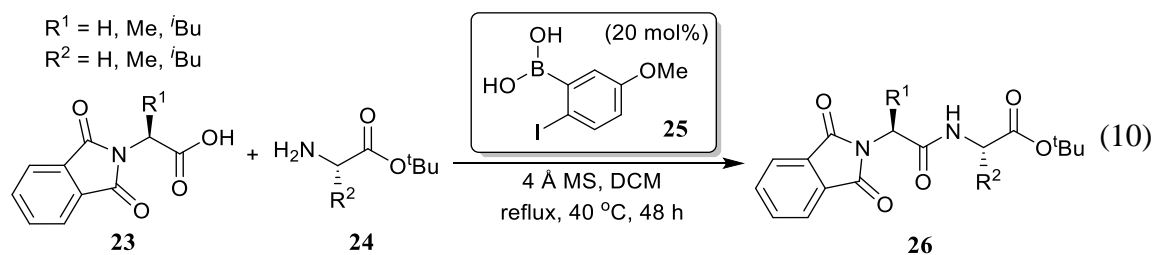
Later, Ishihara and Yamamoto also examined²⁷ further systems using the same ideas,²⁶ with the design of 3,5-bis(trifluoromethyl)phenylboronic acid. Amidation of nonanoic acid with benzylamine gave up to 96% conversion. It was shown that the reactivity of the arylboronic acid catalyst could be enhanced through linkage of fluorinated alkyl sidechains at suitable positions on the aryl ring.



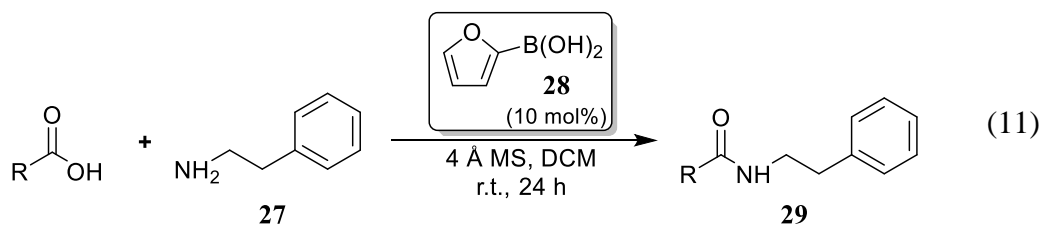
There has been increased focus on the use of boronopyridine systems as electron-deficient arylboronic acid, as introduced by the Wang group for direct amide formation of benzoic acid **16** and benzylamine (Equation 8).²⁸ They designed pyridine-3-boronic acid **17** and *N*-methylpyridine-3-boronic acid **19**, yielding up to 92% of the corresponding amide. Similarly, Maki and co-workers reported the application of *N*-alkylpyridine-4-boronic acid **21** (Equation 9).²⁹ Both of their reports mentioned the utility of pyridinium salts as reusable catalysts, leading to the development of polystyrene-based pyridine-boronic acid species, which will be discussed in the next section.



Efforts to develop amidation catalysts by Sabatini *et al.* focused on the efficient preparation of amides by a newly designed borate catalyst.³⁰ They observed the effects brought about by the use of fluorinated alkoxy groups on the borate system in the acylation process. A new mechanistic role for the borate system was also proposed through a novel catalytic cycle to explain the way such borate catalysts may work. Furthermore, Fatemi *et al.*³¹ recently identified a useful catalyst system based on 5-methoxy-2-iodophenylboronic acid **25** (MIBA), especially useful for peptide synthesis, and illustrating improved atom-economy and environmental acceptability (Equation 10). The resulting peptide products were obtained in high yields and less waste was generated under mild conditions, with reduced amounts of molecular sieves also being used.

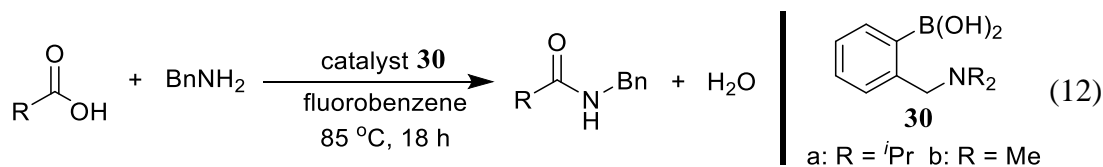


Research by the Chen group reported their efforts in recent studies to access more efficient and environmentally benign amidation methods with lower environmental cost.³² They introduced the application of 2-furanylboronic acid **28** as an inexpensive and effective catalyst for direct amidation at ambient temperature (Equation 11). Yields were claimed to be up to 99% using 10 mol% catalyst loading. Such a catalyst system was shown to apply to a wide range of aliphatic amines though it is important to note that stability to this catalyst was not examined towards protodeboronation.



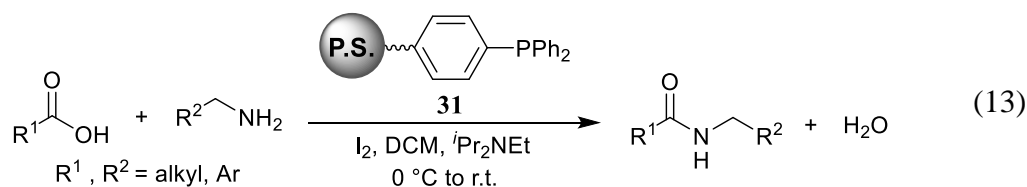
Our group has focused upon the design and application of Lewis acid-Lewis base bifunctional catalytic systems, based on the idea of bringing both amine and acid together while still activating the acid function, and hence, potentially providing enhanced catalytic reactivity. We initially reported the synthesis of 2-*N,N*-diisopropylamino-phenylboronic acid **30a**³³ which unlike other *ortho*-substituted arylboronic acids, the *ortho*-substitution enabled amidation reactivity. Later research discussed the application of these types of bifunctional systems (Equation 12)^{34, 35} including thermodynamic studies for the role of electronic effects of functional groups upon the arylboronic acid on the catalytic direct

amide formation reactions. Meanwhile, mechanistic studies revealed potentially how the bifunctional catalytic behaviour occurred in amidation reactions.

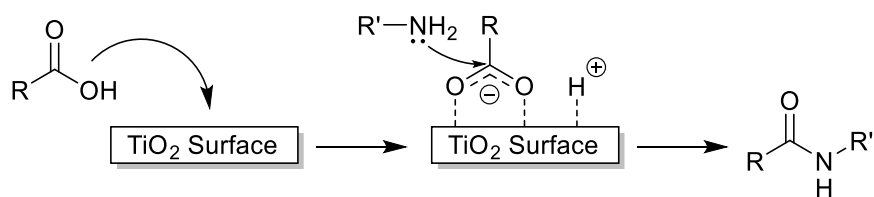


1.3 Heterogeneous catalytic direct amide formation

A key application of ‘greenness’ involving catalytic systems is the recovery and reuse of the catalyst. An early exemplification of this idea was a PPh₃-based polymer catalyst system which has been used as a polymer-based phosphine catalytic agent in a number of applications.^{36, 37} Later, Kumar *et al.* reported a polymer-supported PPh₃/I₂ system **31** for direct amide formation (Equation 13).³⁶ Using *i*Pr₂NEt as deprotonation agent, forming an acyl iodide *via* coupling with a phosphonium species which then enabled catalytic amidation and reached up to 80% conversion.

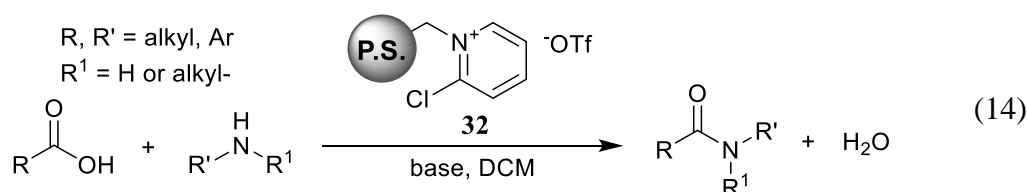


In 2013, Deiana *et al.* provided evidence that supported the role of surface carboxylate species in the process of amide formation (**Scheme 2**) in a solid-phase titanium dioxide catalysed amidation reaction.³⁷



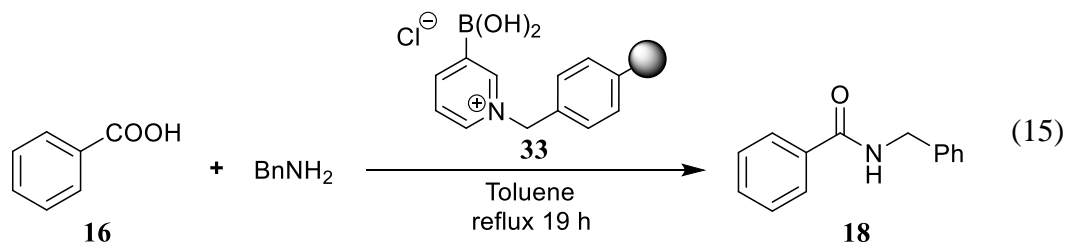
Scheme 2. Surface carboxylate in catalytic direct amide formation

Research by the Comerford group showed that activated Kieselgel 60 (or K60) was a competent heterogeneous catalyst for direct amide formation, showing repeated use with a slight reduction of activity after multiple recycles.³⁸ Similarly, sulfated tungstate was reported as a new solid-phase catalyst.³⁹ The catalyst performance was shown to be linked to the catalytic loading and aggregation/particle size. Later, in 2012, Ghosh *et al.* reported a solvent-free heterogeneous alumina ball system for use in the direct amidation process,⁴⁰ representing a new direction for metal-based heterogeneous catalysis. The chemical properties of alumina balls rely upon higher temperature, according to a study into the surface area and pore volume of different activated states of the catalyst. No major evidence about substrate effects on the catalytic efficiency was observed.

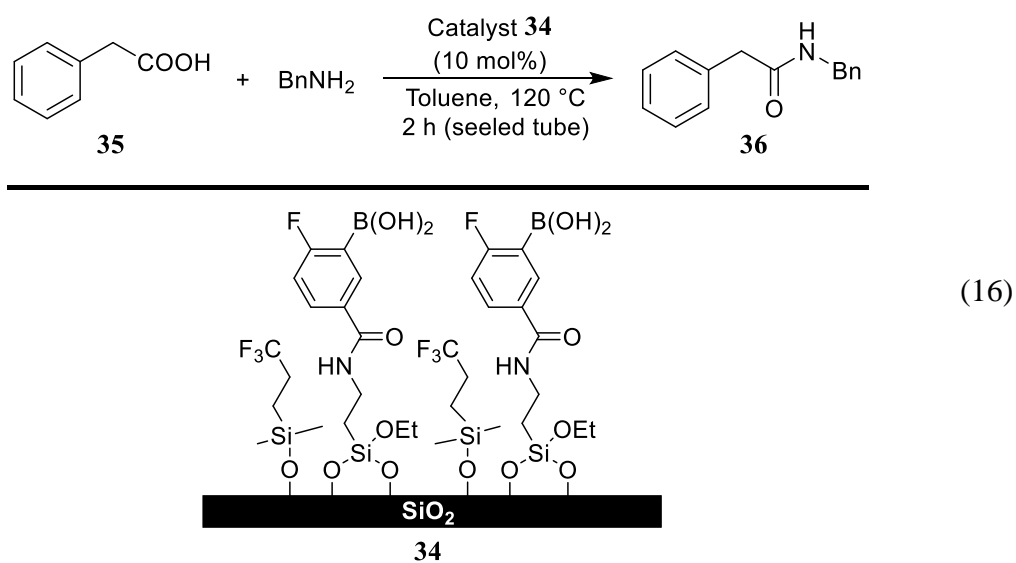


Another heterogeneous polymer-supported amidation catalyst is the Mukaiyama reagent **32** (2-chloropyridinium salt, Equation 14),⁴¹ which has been applied on a range of systems including β -lactam synthesis.⁴² Pandey *et al.* introduced a catalytic direct amide formation reaction using an optimised Mukaiyama reagent⁴³ where inclusion of imidazole

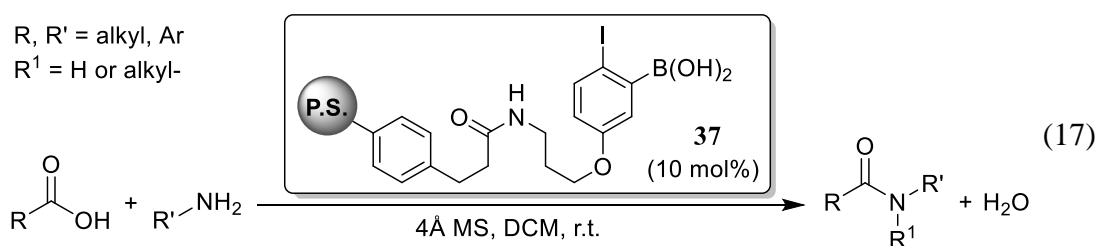
helped to tune the stability, accessibility and reproducibility of the catalyst and delivering improved reactivity.



Over recent years, several researchers have reported the positive effects of linking the reactive boronic acid function to solid support providing for higher catalytic efficiencies and the ability to recycle the catalyst. As discussed above, the Wang group²⁸ introduced the solid-phase supported *N*-alkyl-pyridinium salt **33** as a simple and reusable heterogeneous catalyst, performing high conversion of up to 96% for amide formation low catalyst loading conditions (Equation 15). Similarly, the Yamamoto group suggested a series of *para*-substituted boronopyridinium chloride catalysts,^{29,46} with moderations being made to extend its performance in different reactions including both amidations and esterifications.



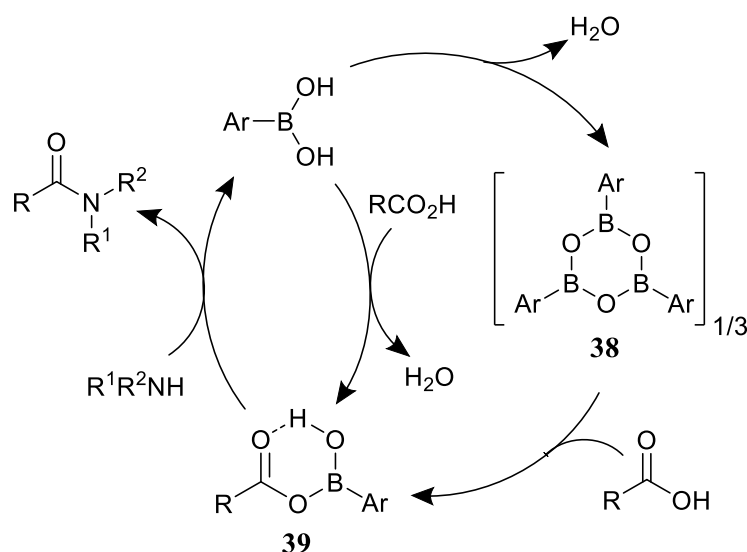
The substrate scope of direct amide formation accomplished using a heterogeneous silica-supported microwave irradiation system was reported by Ojeda-Porras *et al.*,⁴⁴ with the methodology showing good versatility, simplicity and ‘greenness’ in preparative scale processes. Meanwhile, a mesocellular siliceous foam (MCF) has been reported as another form of immobilised-phase silica, as utilised by Gu *et al.* recently for the phenylacetamide **36** formation (Equation 16).⁴⁵ This method, however, suffers from being complicated and expensive while providing only poor atom economy. Gernigon *et al.* also reported the design of a solid-supported boronic acid catalyst **37** (Equation 17).⁴⁶ They discovered an optimised filtration process to recover catalyst **37** when isolating the amide product. Such a method showed impressive substrate tolerance and facile workup procedures.



1.4 Mechanistic insights

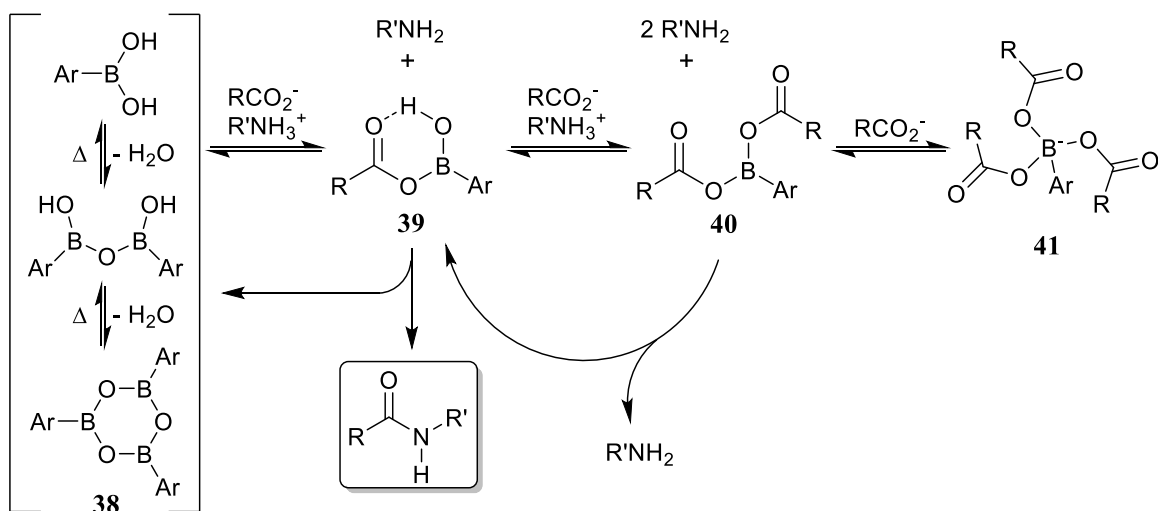
Boronic acids have been shown to be highly applicable in the development of new amidation catalysts due to their reliable stability, synthetic accessibility and wide substrate scope when used in inert solvents and with azeotropic or other water removal conditions. Early attempts at mechanistic research by Ishihara²⁶ involved a possible catalytic cycle as outlined in **Scheme 3**. However, there were flaws in the interpretation of the data reported from their stoichiometric reactions carried out using phenylbutyric acid and benzylamine

catalysed by **12** and as a result, they suggested a rate-determining step involving the generation of **39**, i.e. where an arylboronic acid forms anhydrous boroxine intermediate **38** which then activates the carboxylic acid. That data can now be subjected to a new interpretation involving our group's work showing that the species such as that assigned as **39** were actually bridged diacyl-dicarboxylate systems (*vide infra*).⁴⁷



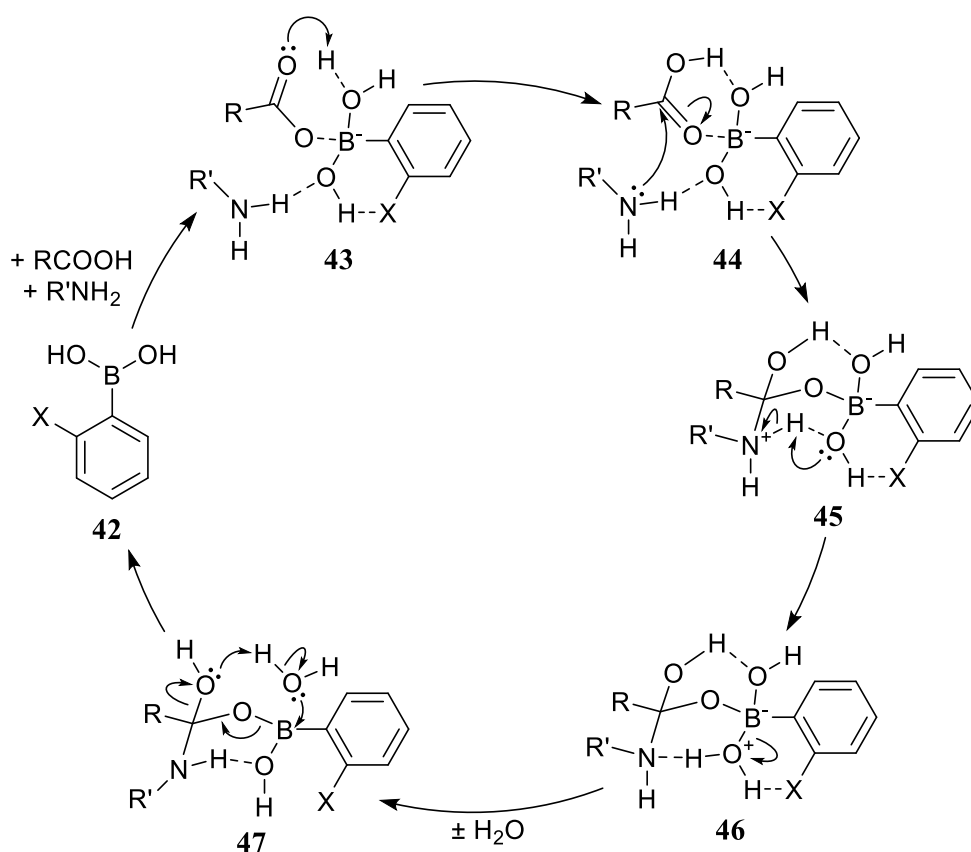
Scheme 3. Proposed arylboronic acid catalytic cycle

Over subsequent years, the Ishihara group continued to maintain this inaccurate view of the types reactive species involved in boronic acid-based amidation reaction and indeed, and it was our group that initially proposed a more general and widely applicable theory about how the boronate-catalysed amidation reaction potentially proceeds (**Scheme 4**),³⁴ suggesting the formation of many species being formed in solution, including acyloxylboronate **39** and diacyloxyboronate **40**, proposing that the latter could function as an acylation reagent and which was detected by MS. It was believed that the formation of intermediate **40** could dominate the catalytic process, considering its thermokinetic efficiency and the behavioural comparison towards other monofunctional catalytic systems, though definitive evidence was not available.



Scheme 4. Our group's proposed mechanistic studies for arylboronic acid-catalysed direct amidation

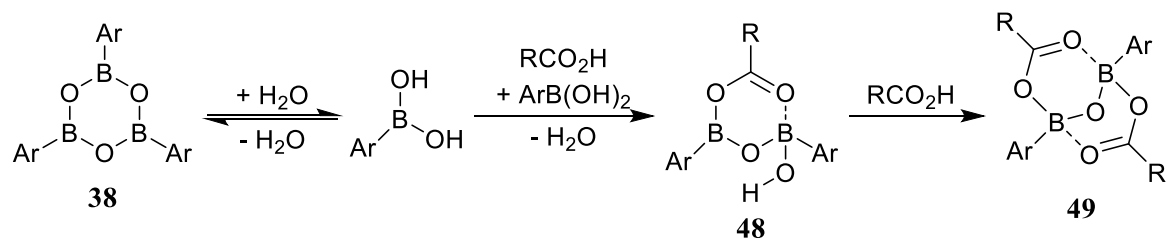
Earlier, Marcelli had used computational methods to examine the proposed catalytic process based on a tetrahedral boronate-'ate' complex system (**Scheme 5**).^{48a} The results suggested that *ortho*-halogenated boronic acid functions had a positive influence on the overall catalytic reactivity due to the generation of a potential O-H--X bond. Later computational work from our group did not corroborate these calculations, highlighting the problems associated with such narrow, theoretical calculations. Marcelli proposed that nucleophilic amide bond formation (transition state **44**) took place after the acylation coordination in **43**, before the rate-determining step of N-H-O proton transfer in **45** taken forward to water elimination transition state **46**. Here the model indicated the isomeric preference by calculating the potential steric effects.



Scheme 5. Proposed catalytic cycle by Marcelli

Furthermore, Wang *et al.* carried these calculations further, examining the importance of water removal throughout the stage of the acylation process.⁴⁹ Computational methods suggested that monoacyloxyl- or diacyloxyl-arylboronic acids system might be involved and even though were thermodynamically unstable. These attempts at theoretical mechanistic proposals for the potentially active boronate catalytic systems in direct amidation, however, contrasts with our much wider-ranging search for the potentially higher catalytic reactivity space. This resulted in revealing a number of more likely mechanistic pathways that would later prove useful for designing novel continuous flow amidation studies (*vide infra*).⁴⁷ From these updated calculations, we proposed the intervention of the B-X-B bridged diboronate **49** system which acts as an acid-activation system (**Scheme 6**), and hence, rather than the intervention of monoacyl-boronate species

39 being involved, diacyl-bridged species of type **38** are **49** are more likely to be key catalytic systems that were also isolated and shown to be reactive in catalytic amidation reactions.⁴⁷



Scheme 6. Observed acid activation process before amide bond formation

2. Bifunctional catalysis of the asymmetric nitro-Michael reaction

There has been increasing interest in the design and application of multifunctional catalysts. As the name suggests, multifunctional catalysts are systems that carry more than one reactive or activating functional group site. In contrast to traditional monofunctional catalysts, they have been designed to activate and guide the reagents towards a desired reaction and even a specific bond construction through assessing reactive or favoured conformations of transition states and intermediates. Among them, bifunctional species have been studied to a high degree, and have resulted in a range of novel and highly effective catalytic systems.⁵⁰ Double-activation processes *via* H-bonding have been particularly effective but wider ranges of approaches are also possible.

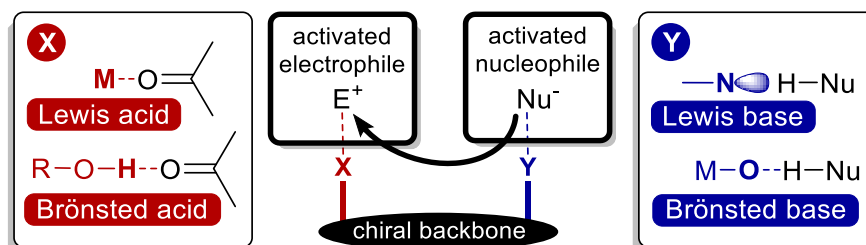


Figure 2. Concept of asymmetric bifunctional catalysis

Bifunctional catalysts consist of two sites and often, by introducing a rigid chiral backbone between the two sites, the resulting catalysts may then be effective for enantioselective control (**Figure 2**). The application of various permutations of such bifunctional systems is becoming increasingly broad, involving a number of key C-C bond constructions to derive enantiomerically enriched compounds and stereoselective intramolecular bond cleavages of symmetric structures. Initial research by Itsuno *et al.*⁵¹⁻⁵⁴

involved the use of different chiral borohydrides for the enantiomeric reduction of aromatic ketones to access chiral secondary alcohols. Matching the right complementarity of functional groups in the bifunctional catalyst to the right substrate, resulting in efficient catalysis though wider substrate scope application remains as a challenge.

Just like the Itsuno system, most catalysts of this type have two components in common. Much effort has been devoted to the design and combination of different reactive functions, among which, metals provide some of the earliest systems. Metals work as either a strong Lewis-acid (LA) or a Brønsted base. Such multi-functionality leads to the development of most heterobimetallic LA-Brønsted base systems or mono-bimetallic LA-LA systems. Later research also proved it was possible to design other types of systems including LA-LB and Brønsted acid-LB systems. In this section, we will briefly examine different types of bifunctional catalytic systems, as well as their uses in organic synthesis.

2.1 Bimetallic asymmetric bifunctional catalysis

Electron-deficient metal systems are commonly used as Lewis acids and can be utilised through coordination to electron-rich functions to activate substrates, and such systems can be combined with Brønsted bases to create combination binding and activation pathways such as *via* hydrogen-bonding. This has led to the development of a range of bifunctional catalysts, including bimetallic systems, some of which have been incorporated into chiral backbones to design chiral bifunctional catalysts (**Figure 3**).

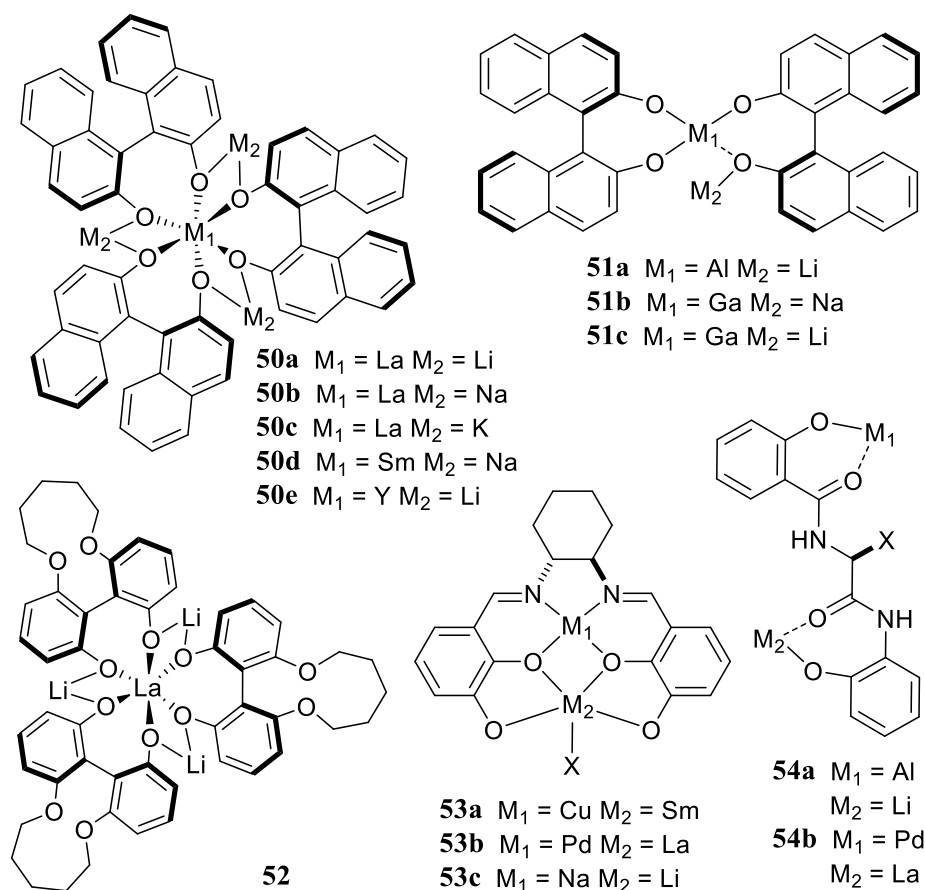
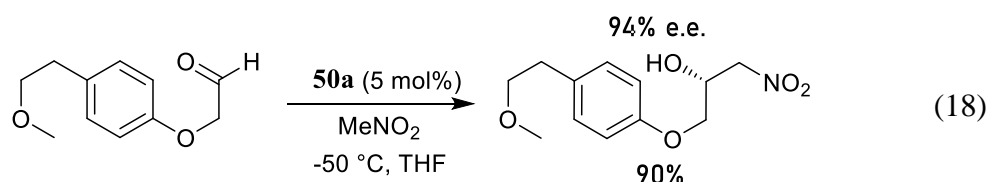


Figure 3. Reported heterobimetallic bifunctional asymmetric catalysts

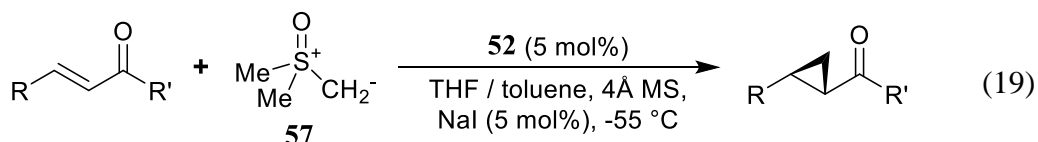
Axially chiral BINOL metal complexes have proved fertile ground for the development of asymmetric catalysts over many years.⁵⁵ However, hydrogen-bonding *via* metal-BINOL complexes was also discovered by the end of last century, with early heterobimetallic-based bifunctional catalysts being reported by the Shibasaki group. As part of developing Lewis acid-Brønsted base bifunctional catalytic systems, a set of rare earth-alkali metal-BINOL (REMB) scaffolds were introduced,^{56, 57} beginning with a lanthanum-lithium-BINOL (LLB) complex **50a**, exemplified in the asymmetric nitroaldol reaction (Equation 18).⁵⁶ Based on the observed results, interactions between the lithium and the asymmetric lanthanoid complex were proposed to dominate the enantioselectivity. The proposed mechanism highlighted the necessity of the lithium being able to fit into the *tris*-dinaphthalene cavity, yet by contrast, sodium was ineffective due to its larger steric

size. However, Shibasaki *et al.* later realised that the less effective lanthanum-sodium-BINOL (LSB) complex **50b** still smoothly promoted asymmetric Michael additions, giving up to 92% e.e. with high conversion.^{59, 60} With an extra linkage between the BINOL ligands to solidify their rigid backbone,⁵⁷ the resulting linked-BINOL-based catalysts enjoyed a broader substrate generality and were active under milder conditions.⁵⁸ Meanwhile, another dimeric BINOL-complexed species were reported, involving Al-Li-BINOL complex (ALB) **51a** and Ga-Na-BINOL (GaSB) **51b** systems, which were reported also to promote the asymmetric Michael addition of different substrates (**Figure 3**).^{59, 60} Mechanistic studies also suggested a likely extension to most types of carbonyl nucleophilic addition.



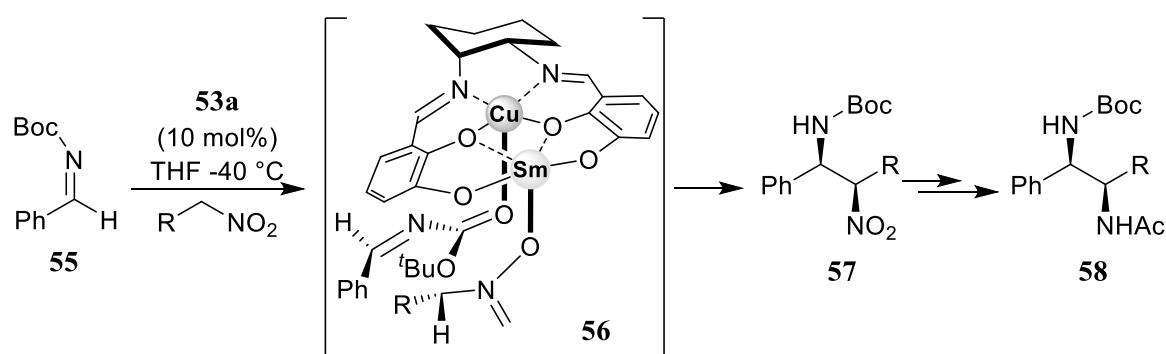
Following these report, other research has involved the design of Sm-Na-BINOL (SmSB) **50d** for 1,4-addition-protonation;⁶¹ La-K-BINOL catalysts (LPB) **50c**,⁶² LLB **50a**^{63, 64} and ALB **51a**⁶⁵ for asymmetric hydrophosphonylation; LLB **50a** for asymmetric direct aldol reaction;⁶⁶ Y-Li-BINOL (YLB) **50d** for chiral cyanoethoxycarbonylation,^{67, 68} and 1,4-addition,⁶⁹ GaSB **51b**, Ga-Li-BINOL (GaLB) **51c** for the asymmetric cleavage of epoxide rings,⁷⁰⁻⁷² Sc-Li-BINOL (ScLB) **51d** for the enantioenriched Strecker reaction (**Figure 3**).⁷³ In addition, it has been reported that the axially chiral binaphthol linker might not be as essential as imagined for catalytic activity and high asymmetric induction. In recent research, substituted biaryl heterobimetallic complexes have been introduced, containing sterically demanding sidechains and bridging strain. The initial design of lanthanum-lithium-*tris*(*S*-biphenyl-diol) complex **52** did not work well when tested on

tertiary nitroaldol resolutions (**Figure 3**),⁷⁴ However, later investigations by Kakei *et al.* looked into the use of complex **52** in the asymmetric cyclopropanation of α,β -unsaturated ketones, and obtained 99% product e.e. and showed broad substrate tolerance (Equation 19).⁷⁵



Time has witnessed the development of a number of bimetallic asymmetric bifunctional catalysts. The functionalisation of Schiff base metal complexes, specifically *N,N'*-bis(salicylidene)ethylenediamine (Salen)-derived metal complexes, have long been recognised and applied in catalysis and organocatalysis.⁷⁶ Usually, the cage-like structures are stabilised by the metal centres which also helps to determine their potential organometallic properties. Mechanistic studies highlighted the customizability of metal-salen complexes as utilised in the stereoselective control of certain reactions.⁷⁷ For systems offering a chiral environment for bimetallic bifunctional catalysis, the rigid salen complex becomes favourable. The overall steric geometry of tetradentate species can be restricted by the shape of alkylamino linkers between symmetric Schiff base moieties. Therefore, most recent research has focused on the two-metal-centred salen complexes for the stereoselective control of several reactions.⁷⁸ Handa *et al.* reported catalytic nitro-Mannich reactions of **55**, catalysed by a Cu-Sm-Schiff base complex **53a** (**Figure 3**) and giving *syn*-adduct **56** in up to 98% optical purity (**Scheme 7**).⁷⁹ In the meantime, another enantiomerically enriched *syn*-diamino product **58** was introduced by the Shibasaki group as an essential building block.⁸⁰ Relevant mechanistic studies suggested the synthetic pathway to **58** *via* formation of plausible transition state **56** involving the Cu-Sm-salen

complex **53a**. This complex relies upon a complex which is stabilised by both transition metals which act as strong Lewis acids and the rare earth metal alkoxides act as Brønsted bases. By designing both substrates to minimise the steric hindrance, stereoselectivity could be established under similar strategies.⁸⁰ Meanwhile, in the presence of a bulky Boc-group on the imine enhanced steric effects provided good diastereoselectivity.



Scheme 7. Asymmetric nitro-Mannich reaction catalysed by Cu-Sm-Schiff Base complex

In further research from the Shibasaki group involving using a Pd-La-Schiff Base system **53b** derived from their initial La-Li-BINOL complex, they demonstrated its application for the diastereoselective nitroaldol reaction of aldehydes.^{86,87} Whereas, the Ni-La-based Schiff base complex **53c** was employed for the asymmetric decarboxylative 1,4-addition reaction,⁸¹ though both catalyst systems demonstrated excellent performance.

Similarly, with the introduction of a structurally rigid chiral arylamide linker, new heterobimetallic complex catalysts can be developed. For example, a Nd-Na-based bimetallic catalyst was created for use in diastereoselective nitroaldol reactions,⁸² for which mechanistic studies provided a better understanding of catalytic *anti*-selective reactions, presumably occurring *via* a planar di-arylamide dinucleating scaffold **54** where both metals worked as Lewis acids and coupled the desired substrates in an opposing *anti*-orientating position (**Figure 3**). This proposal also accounted for the observed results of their later Yb-

K complex derived from **54b** and used for a facile enantioselective nitro-Mannich reaction.⁸³

2.2 Lewis-acid/Lewis-base asymmetric bifunctional catalysis

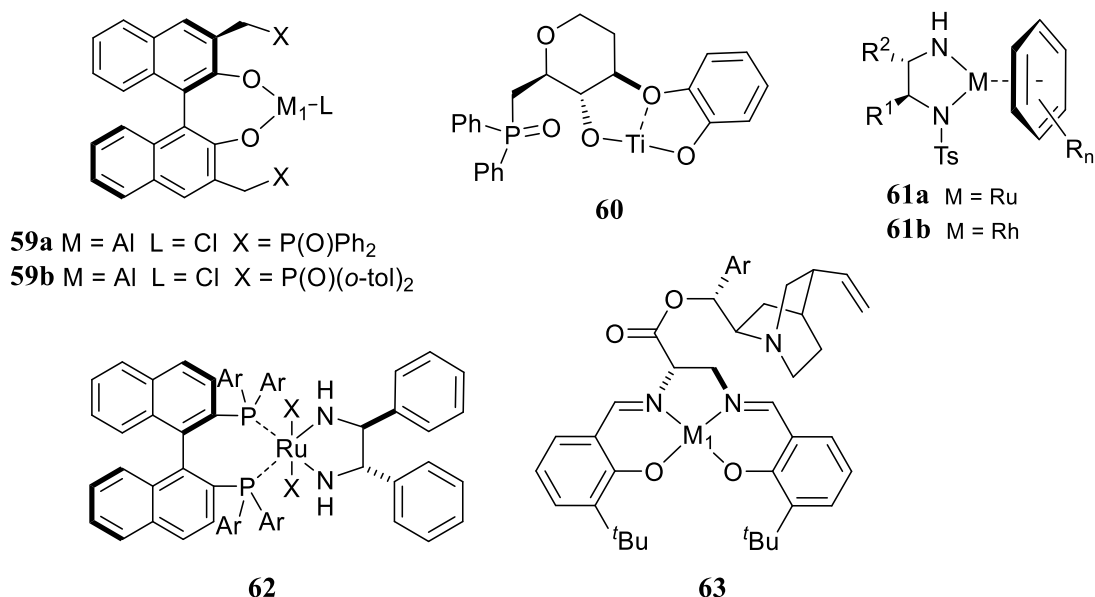
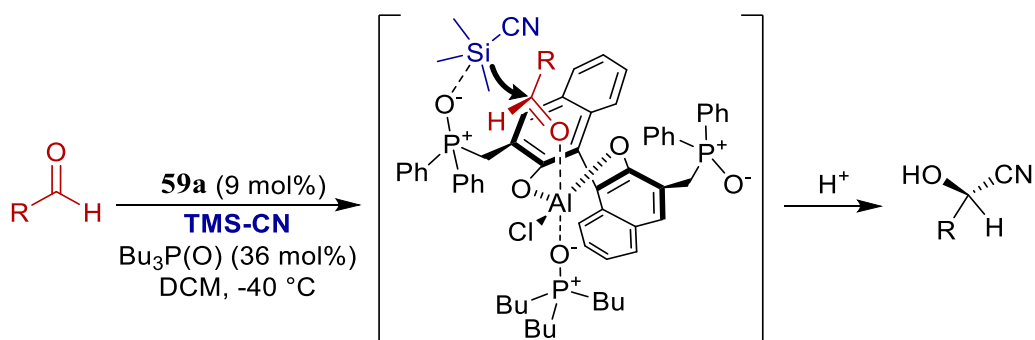


Figure 4. Developed Lewis-acid/base bifunctional catalyst

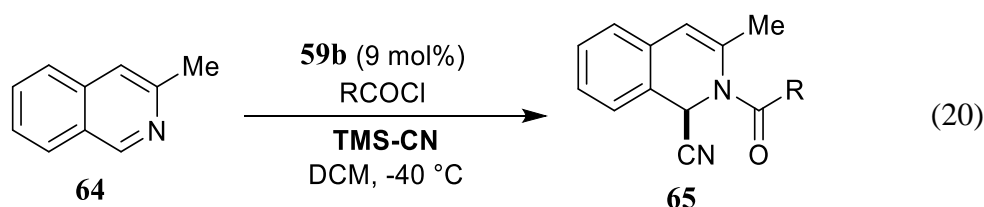
The successful design of heterobimetallic complexes led in many ways to the further development of Lewis-acid/Lewis-base systems, since the replacement of one Lewis-acid with a Lewis-base function enabled access to general and environmentally friendly catalytic systems (**Figure 4**). Using the axially chiral BINOL system for enantiomerically enriched catalysis, Hamashima *et al.* reported the Al-P-BINOL bifunctional catalyst for the stereoselective cyanosilylation of aldehydes (**Scheme 8**).⁸⁴ With the assistance from an appropriate phosphine(V) oxide as additive, reaction with catalyst **59a** reached up to 96%

e.e. for aliphatic aldehydes. Kinetic studies supported the rationale of bonding between the catalyst and carbonyl group, with assisted delivery of the nucleophilic attachment to the silyl cyanide. This system clearly demonstrates the underlying theory of this type of catalytic behaviour and shows the potential for modification to enable broader reaction scope.



Scheme 8. Proposed catalytic asymmetric cyanosilylation of aldehydes

System of **59** was applied further by the Shibasaki group to the asymmetric Reissert-type reaction for the synthesis of quinoline-derived species. Up to 91% e.e. was obtained together with 99% conversion (Equation 20).⁸⁵ They showed that the ditolyl-phosphinoxide species **59b** provided improved Lewis basicity and a more effective catalytic system. Moreover, the BINOL-monometallic system **59** was tested in a solid-phase system for the enantioselective Strecker reaction.⁸⁶



These examples show that facile asymmetric catalysis requires both reactive Lewis-acid and Lewis-base functions and a structurally rigid linker. Chiral binaphthol linkers have proved reliable bridging functions between catalytically reactive centres and many efforts have then involved in tuning steric relationships between the chiral linker and the Lewis-acid and Lewis-base moieties.⁸⁴ BINOL derived systems are not necessarily applicable to all types of reactions, but controlling steric relationships between the Lewis-acid and Lewis-base does seem to provide generally reactive systems, as exemplified by Hamashima *et al.* who developed *D*-glucose derived titanium-diphenyl-phosphine oxide complex **60** for use in the stereoselective cyanosilylation of ketones.^{87, 88}

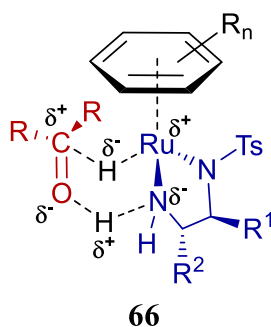
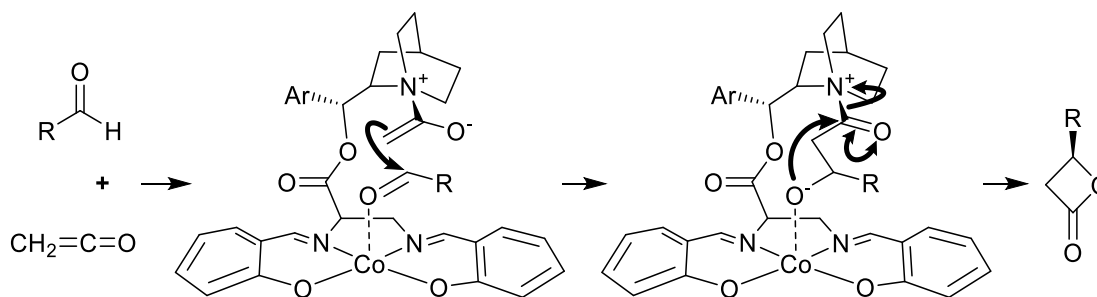


Figure 5. Possible transition state towards asymmetric hydrogenation

Later, the Noyori group reported the catalytic hydrogenation of ketones by a chiral ruthenium(II)-*N*-bifunctional system **61** (**Figure 4**), mechanistically driven by cooperative activation *via* hydrogen-bonding with one preferred face of a five-membered *N*-heterocyclic species (**Figure 5**).⁸⁹ Later, the discovery of a rhodium-based system **61b** for the asymmetric reduction of ketones showed the potential of similar catalysts and their further investigation and wider application.^{90, 91} Muniz *et al.* extended the Ru-N catalyst **61a** for use in the asymmetric aza-Michael reaction, providing up to 97% e.e. with high conversion.⁹² In 2005, Noyori *et al.* updated their Ru-N catalyst with the addition of a

dinaphthalene-based diphosphine complex **62** for use in asymmetric catalytic hydrogenation.⁹³



Scheme 9. Proposed mechanism of asymmetric intramolecular β -lactonisation.

Research by Lin *et al.* introduced the use of a salen-based cobalt complex **63** with the attachment of a Lewis-basic ligand to achieve an enantioselective Wynberg β -lactonisation (**Figure 4**).⁹⁴ Mechanistic studies suggested similar behaviour to salen-based bimetallic systems, except that the Lewis-base moiety was provided by a nucleophilic cinchona alkaloid function acting as an activating function (**Scheme 9**) to provide substrate activation and enabling an intramolecular reaction of both substrates through bringing them together *via* the bifunctional catalyst system.

2.3 Brønsted-acid induced dual activation in asymmetric catalysis

With increasing concern about the environment and the pursuit of atom-economy, metal-mediated catalysis is potentially problematic, because of increased awareness of the need to access metal-free asymmetric bifunctional catalysis. Brønsted acids have been

reported as electrophile activating reagents *via* hydrogen-bonding, particularly including ureas and thioureas, binaphthyl phosphonates, arylboronic acid analogues, and proline derivatives.^{95, 96}

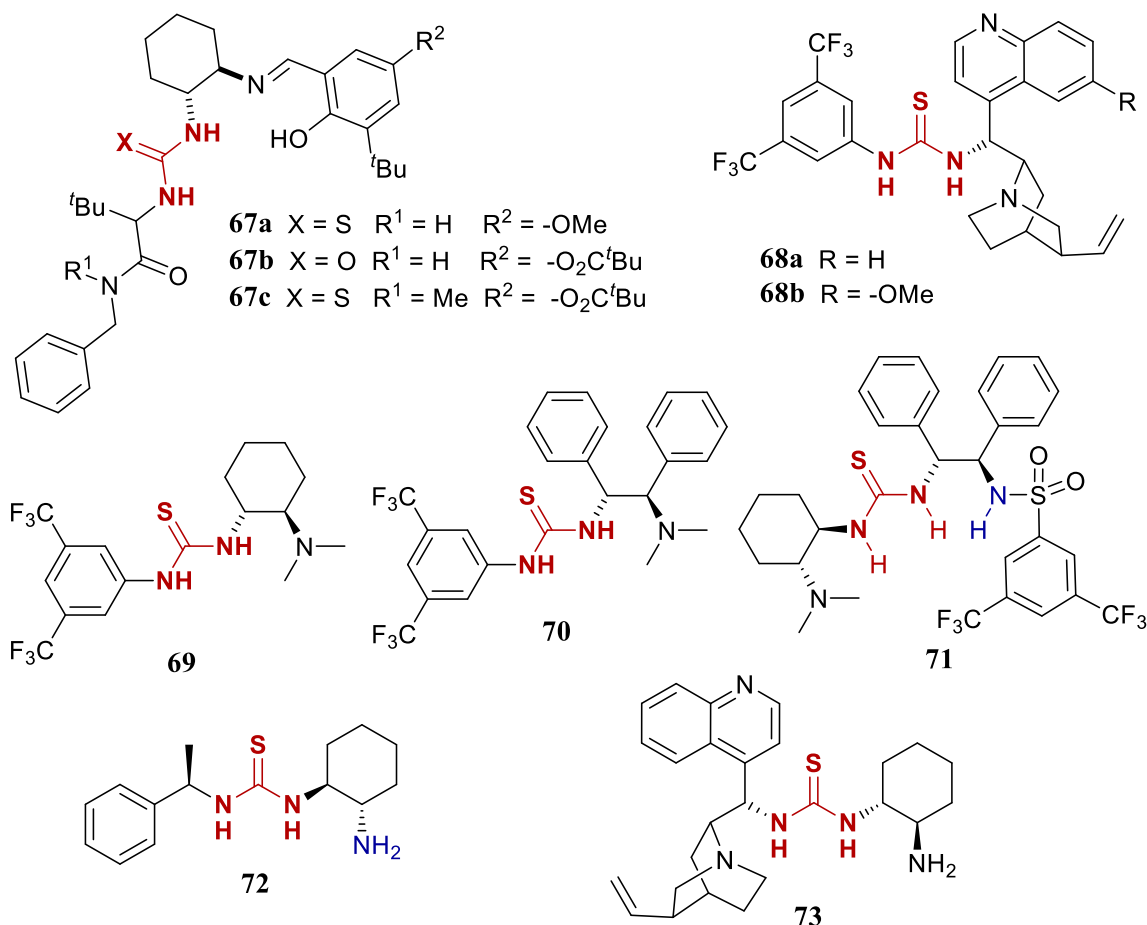
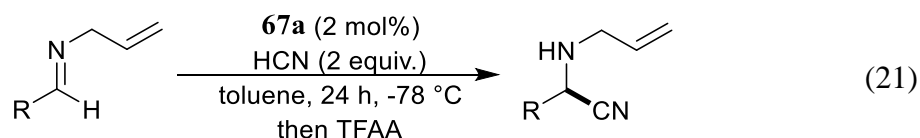


Figure 6. Examples of (thio)urea Bifunctional Catalyst

Catalytic urea and thioureas act as effective hydrogen bond donors and have been recognised for many years for catalytic application.⁹⁷⁻⁹⁹ Early research has shown the ability of (thio)ureas to activate substrates *via* Brønsted acidic proton transfer, and such systems are synthetically accessible as well as catalytically reactive (**Figure 6**).¹⁰⁰



Jacobson *et al.* reported Schiff base (thio)urea chiral catalyst **67a** for the asymmetric Strecker reaction, involving **67b** and its solid-supported form (**Figure 6**) to obtain up to 96% optical purity and 97% yield on large scale (Equation 21).^{101, 102} Theoretical calculations suggested the transition state involved the thiourea activating imines as shown in **Figure 7**, lowering the energy of the subsequent addition reaction.¹⁰³ This transition state enables enantioselective preference to rely on the guiding effect of the *N*-substituent of the Schiff-base (allyl in this case) in relation to the (thio)urea sidechains. This approach provides broad catalytic application and substrate scope, including Mannich,¹⁰⁴ aza-Baylis-Hillman reactions¹⁰⁵ and so on.

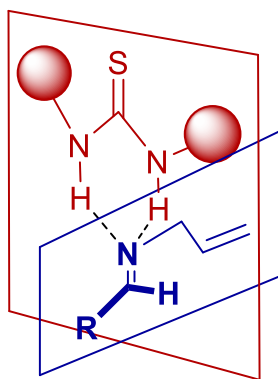
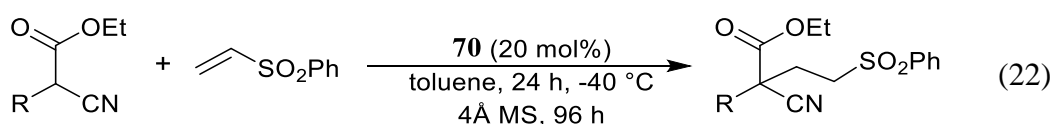


Figure 7. Proposed transition state of urea catalyst-imine.

Following this work, Tsogoeva *et al.* reported an imidazole-linked Schiff base bifunctional thiourea for use on the enantioselective Strecker and nitro-Michael reactions,¹⁰⁶ functioning through imidazole and thiourea sites which led to high e.e.s but low conversions. Such stereoselective control did not work on asymmetric Michael additions, whatever reactive moieties were appended to the catalyst. The reactivity of other

(thio)urea catalytic systems was also revealed in later studies, through looking at different tertiary amine moieties along with the (thio)ureas, as the double hydrogen-bond donor site.^{99,107} Typical examples included the early reports of the cinchona alkaloid-based (thio)urea organocatalyst **68a** (Figure 6) for asymmetric Michael addition,¹⁰⁸ 1,4-conjugate additions of hetero-Michael acceptors and others,¹⁰⁹⁻¹¹¹ including the latest report of enantioselective aza-Henry reaction with a methoxy-quinoline based cinchona alkaloid-based (thio)urea. The Wang group recently reported the use of methoxy-derived alkaloid-based (thio)urea **68b** as Brønsted acid-Brønsted base catalyst for the asymmetric cross aldol reaction¹¹² and found that a bridged tertiary amine was an effective moderate hydrogen bond acceptor. Similarly, another *N,N*-dimethyl substituted amine-thiourea catalytic system **69** was designed by Okino *et al.* and applied it to the enantioselective nitro-Michael reaction.¹¹³ Later, this was updated by the Chen group who reported a more flexible tertiary amine-thiourea catalyst analogue **70** for quaternary C-C bond construction on vinyl sulfones (Equation 22).¹¹⁴



Most of the thiourea based catalysts have monofunctional ureas acting as the Brønsted acid which interact with electron-rich polar substrates such as sulfonyl, carbonyl, imine conjugated alkenes providing electrophilic activation. In addition, activating as a general Lewis base, the tertiary amine moiety works only as a nucleophile in the activation process of the substrate, whereas the multifunctionality of primary and secondary amines has been increasingly recognised as being involved as a multi-H-bonding Brønsted acidic activator. Research by Shi and Liu introduced a bis-thiourea system for asymmetric Morita-

Baylis-Hillman reaction, further proving the importance of multi-hydrogen-bond coordinated stabilization.¹¹⁵ Meanwhile, the Wang group introduced the design and optimization of asymmetric nitro-Michael addition *via* intramolecular coordinated capturing of substrates.^{116,117} It was catalyzed by a versatile chiral secondary amine-thiourea system **71**, obtaining up to 99% e.e. with broad substrate tolerance (**Figure 6**). A similar strategy was applied on enantioselective nitro-Mannich and aza-Henry reactions,^{118,119} as reported by the Wang group, who also suggested a possible transition state by which catalyst **71** operates where the orientation of the Mannich base was guided by the *tert*-butyl and substituted aryl groups, in favour of a less sterically hindered transition state. (**Figure 8**).

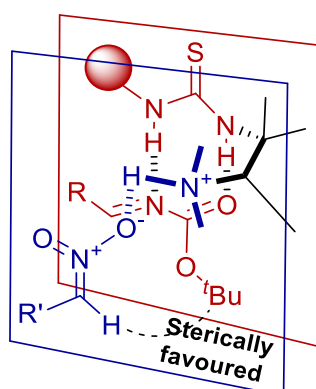


Figure 8. Proposed transition state of Mannich-type reaction

As can be found from above, the catalytic behaviour of bifunctional thiourea-amine catalysts features essential optimizable properties through the presence of substituted amines. Based on the knowledge of primary amines being more flexible and fitting into enzyme binding sites, there has been much investigation into the design of primary amine-urea analogues.¹²⁰ In 2006, the Tsogoeva group revealed the first design of a primary amine-derived thiourea catalyst **72** for asymmetric nitro-Michael additions, obtaining up to 99% e.e. in 88% yield (**Figure 6**).¹²¹ Later, they also reported the use of catalyst **72** in

Mannich-type reactions.¹²² In the same year, Jacobson *et al.* reported a reductive amine from **67c** as catalyst for nitro-Michael reactions, with evidence supporting activation by a Lewis basic primary amine forming a reactive enamine intermediate.¹²³ Additionally, the Jacobson group found that catalysts with primary amine attached to other reported thioureas were more applicable in reactions and substrate scope, such as the cinchona alkaloid-primary amine bifunctional organocatalyst **73** for use in asymmetric Michael addition reactions (**Figure 6**).^{120,124}

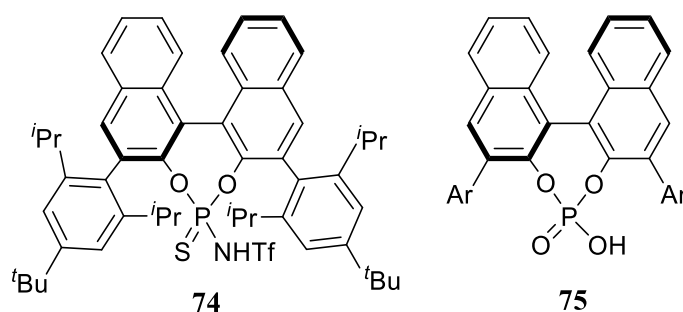


Figure 9. Phosphoric acid as Brønsted Acid and Derived Bifunctional Catalysts

In 2008, the Yamamoto group designed binaphthol phosphine catalyst **74** for the enantioselective silyl enol ether protonation (**Figure 9**)^{125, 126} using a general achiral acid to activate the thiophosphoramidate and generating the chiral phosphoric acid species for catalysis. Recent research suggested a few examples of bifunctional phosphoric acid catalysis, including the introduction of BINOL-phosphoric acid **75** for asymmetric Strecker reaction,^{127,128} Mannich-type reactions,¹²⁹ hetero-Diels-Alder reactions,¹³⁰ Friedel-Crafts reactions,¹³¹ etc. A proposed mechanism for the action of this catalysis involves a dual activation process by the phosphoric acid group where the phosphine oxide works as a hydrogen bond-acceptor, whereas the acidic site acts as the hydrogen bond-donor (**Figure 10**).¹³² Evidence showed the stereoselectivity was determined by the stereoisomer of substrates and the coupling method. Usually, the catalysis would mechanistically avoid the

steric clash caused by either side of *E*-isomer coupling, preventing the formation of the corresponding transition state **76a**, in addition to the generation of **76c**, where a steric collision occurs on the same side with BINOL 3- or 3'- substituent (**Figure 10**).

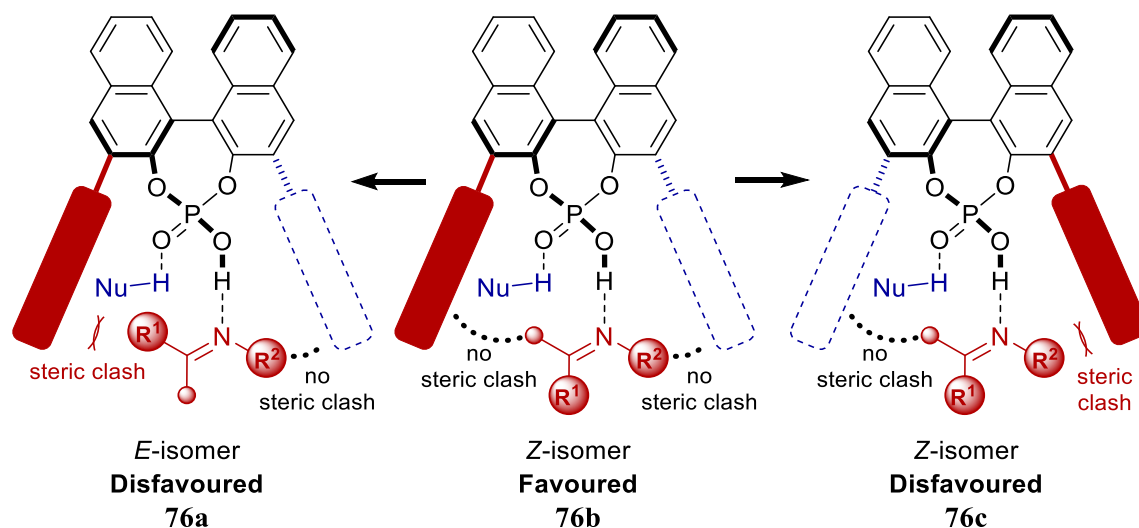


Figure 10. Transition state of bifunctional phosphoric acid-catalysed dual activation.

Based on the above theory, it can be expected that 3,3'-sidechains play an important role in the formation of the desired transition state when accomplishing certain types of stereoselectivity control; the *Z*-isomer was favoured in Mannich-type reactions though *E*-isomers generally occur more frequently being more stabilised.

2.4 Boroproline based asymmetric enamine-based addition

The design of novel bifunctional catalytic systems based organoboron compounds linked to an amino group has become more popular recently, essentially being an early example of organocatalysis.¹³³ Such systems are often seen as both a strongly electrophilic

species (Lewis-acid) and a good hydrogen bond acceptor (base, or Lewis-base, as the Zlatkis group studied and reporting their properties and abilities to behave as a bifunctional catalyst.¹³⁴ Reports from Lestinger *et al.* introduced a set of structurally chiral aryl-borinate compounds,^{135, 136} as well as examining their possible reaction mechanisms and the cooperative behaviour of the amino and borinate groups,¹³⁷⁻¹³⁹ including amino-diboronic acids.¹³⁸ Later, the Lestinger group reported the first B-N based bifunctional arylboronic acid **77** used in organic synthesis (**Figure 11**).¹⁴⁰ Their mechanistic studies suggested that the amine behaved as a cooperative moiety together with the boronic acid in the substrate activation process. The introduction of these amines presented an excellent opportunity for stereoselectivity through bifunctional catalytic reactions.

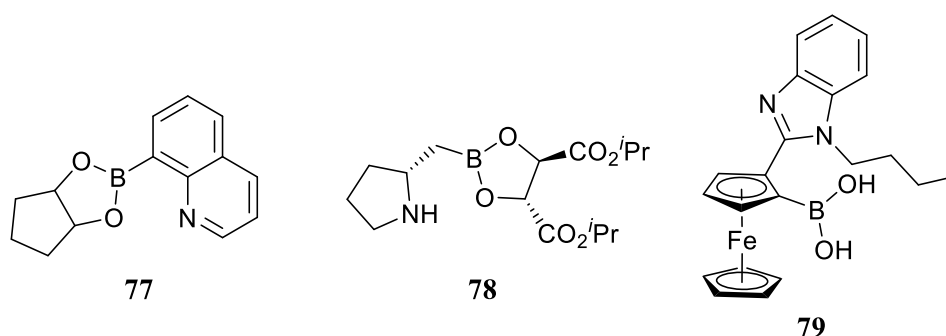
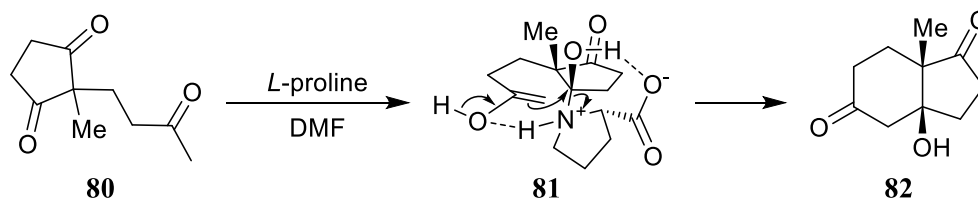


Figure 11. Proposed B-N bifunctional catalysts

On the other hand, the use of easily accessible *L*-proline derived catalysts was first identified in 1971 and exemplified as a bifunctional catalyst for asymmetric intramolecular cyclisation through the aldol condensation (**Scheme 10**).¹⁴¹ Mechanistic investigations by Parrish and Hajos *et al.* proposed an enamine system and a possible transition state **81** in which cooperative hydrogen-bonding helped control the rigidity of the cyclic intermediate providing the stereoselectivity (**Scheme 10**).¹⁴²



Scheme 10. *L*-proline based asymmetric aldol cyclisation

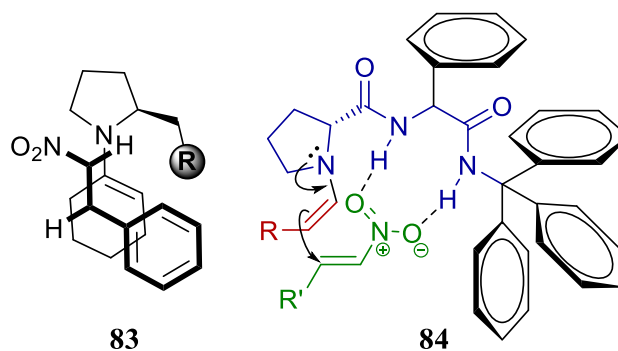
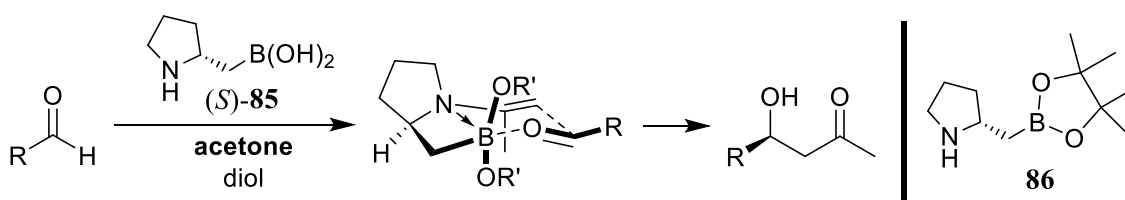


Figure 12. Enamine-based transition states for stereoselective control.

The next development in the pyrrolidine-based asymmetric catalysis systems appeared in 2001 when the Barbas group reported the use of amino-pyrrolidine catalysts for asymmetric Michael additions.¹⁴³ The catalysis reached up to 96% yield and 80% e.e., mediated through a transition state involving an enamine intermediate. Later, Kotsuki *et al.*¹⁴⁴ and Reddy *et al.*¹⁴⁵ introduced a pyrrolidine-pyridine and triazole-based catalyst respectively, obtaining better stereoselectivity in high conversion. In 2006, Luo and colleagues summarised the *in silico* screening of pyrrolidine-type organocatalysts, based on elementary modelling with enamine transition state **83** (Figure 12).¹⁴⁶ They observed the replacement of a structurally hindered R-group to prevent the unfavoured transition state in the process. Similarly, a novel bifunctional *L*-prolinamide catalyst was reported¹⁴⁷ for the asymmetric nitro-Michael reaction, providing high stereoselectivity. A possible transition-state model was proposed where the aldehyde was activated again through the formation of an enamine intermediate **84** (Figure 12) and stabilised through hydrogen-

bonding to the amide. The bulky aromatic amide created steric hindrance which made it possible for preferential nucleophilic attack from one side to take place. This type of transition state control can be realised by either sterically repulsive effects from space-consuming ligands, or by using a hydrogen-bonding donor. The use of a boronic acid function allows the design of catalysts which replaces the hydrogen-bonding group with a Lewis-acidic function, the creating a conceptually novel pyrrolidine-boronic acid, exhibiting potential reactivity for use in organocatalysis.



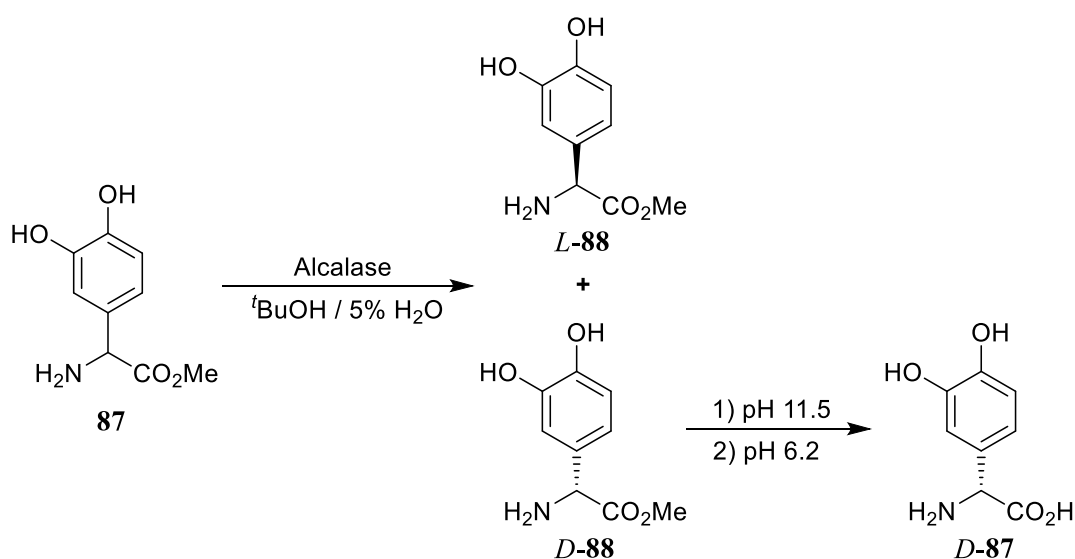
Scheme 11. Proposed enamine transition state with the developed aldol catalyst **85**

Our group's research focused upon the preparation and application of these types of aminoboronic acid catalysts, including an early report in 2009 where Whiting *et al.* suggested pyrrolidinyl-boronic acid **78** for the asymmetric aldol reaction.¹⁴⁸ Besides, a ferrocene-based aryl-boronic acid **79** which was reported for the stereoselective direct amide formation,¹⁴⁹ a proline-based chiral boronic acid system **78** was invented for the catalysis of asymmetric enamine-based reactions (**Figure 4**). Investigation of the proline-based system was successful, where catalyst **78** was the precursor to the formation of the catalyst precursor **83** for the catalytic reaction, resulting in up to 90% e.e. and 94% of yield (**Scheme 11**). Meanwhile, it was necessary to use molecular sieves and enable reaction of the boronic acid to form its corresponding tartrate ester, while preventing the boronic acid from hydrolysing back to its precursor (*S*)-**85** and **86**.

3. Kinetic resolution of asymmetric amide formation

As part of the asymmetric synthetic strategy, kinetic resolution of a racemic substrate has become another recognised pathway towards stereoselectivity.^{150,151} Compared to asymmetric catalysis which creates new chiral centres directly, kinetic resolution (KR) differentiates through chemical or thermodynamic properties, resulting in kinetically controlled separation of racemic products.

3.1 Kinetic resolution of functional group interconversion



Scheme 12. Alcalase-catalysed kinetic resolution

There have been early records of KR using organocatalysts of most FGI reactions, for example, early mechanistic studies suggested an alcalase-catalysed resolution of *D*-amino esters (**Scheme 12**).¹⁵² Herein, the Chen group conducted the separation in a water

(5%) in *t*BuOH solution, keeping the reaction at a fixed *pH* 8.5 at r.t. which gave the hydrolysed *L*-isomer as an insoluble precipitate. Hydrolysis of unreacted *D*-isomer was triggered by an optimised reprecipitation at *pH* 6.2 before the saponification of ester at *pH* 11.5.

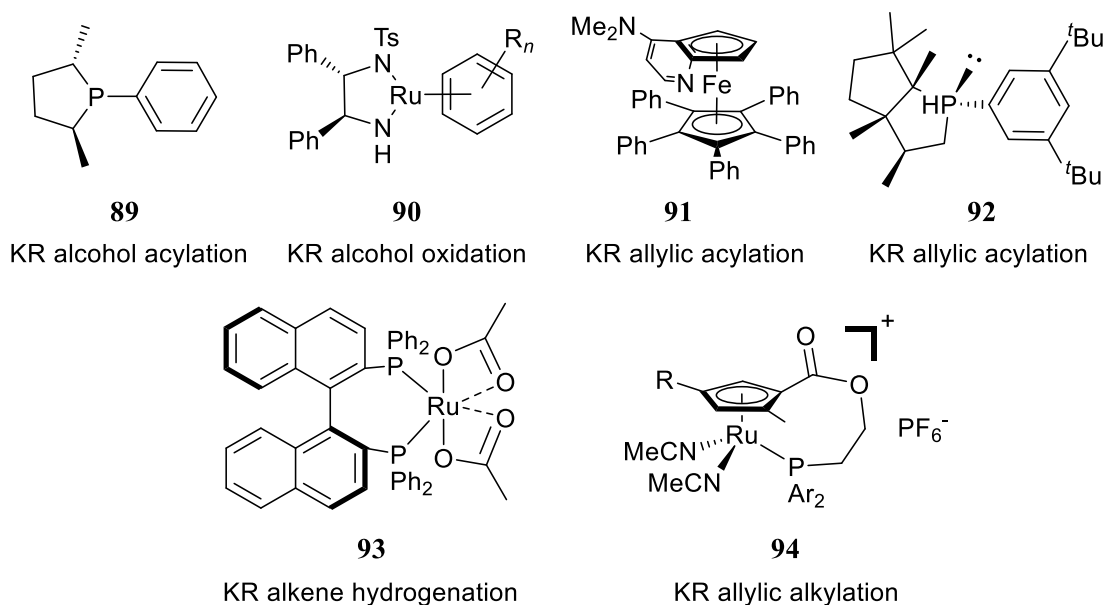
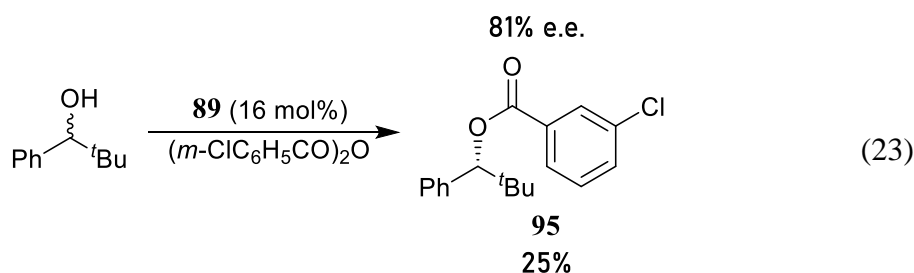
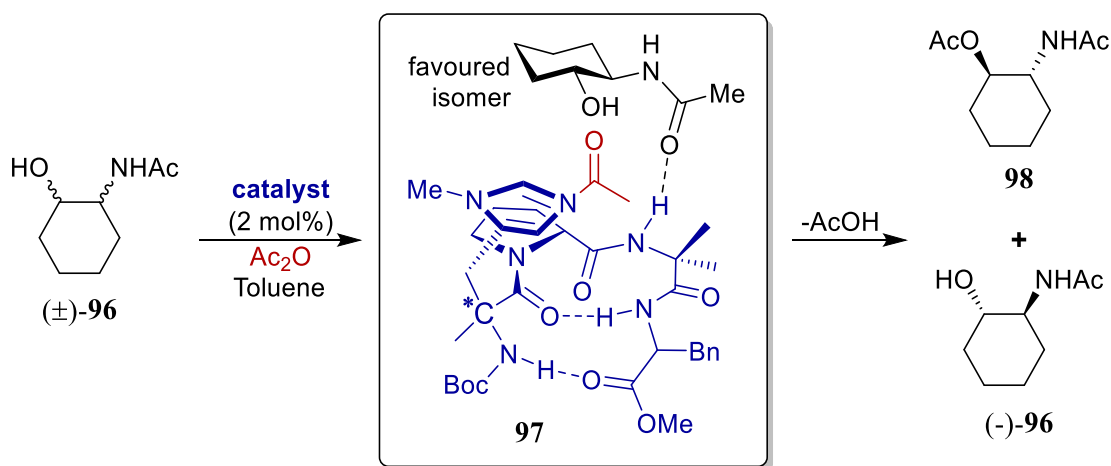


Figure 13. Proposed kinetic resolution of functionalised compounds

Another strategy though is *via* the design of novel, synthetic asymmetric organocatalysts. In 1996, the Vedejs group reported their first attempt at the kinetic resolution of acylation of alcohols, catalysed by a designed chiral phosphine **85** (**Figure 13**).¹⁵³ Their catalyst worked best on hindered secondary alcohols reacting with anhydrides and reaching up to 81% e.e. at 25% yield (Equation 23). These findings inspired a considerable amount of follow up research, creating a real step forward in the design and application of kinetic resolution catalysis.



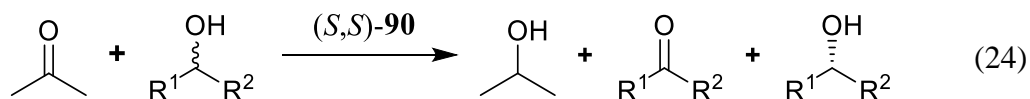
In 2004, Miller group designed a ‘pin’-shaped peptide-based kinetic resolution system from *trans*-1,2-acetamidocyclohexanol **96**, leading to high stereoselectivity (**Scheme 13**).¹⁵⁴ The core of the report was the peptide-based pyrrolidinyl-imidazole catalyst which is constrained by hydrogen-bonding, organised through a chiral centre (highlighted in **97**) which determines the conformation of the favoured transition state **97**. This led to the acylation product **98** in good yields. Following updates then included Mackey’s bridged bicyclic octane catalyst,¹⁵⁵ Levacher’s DMAP analogue,¹⁵⁶ and Nakata’s benzotetramisole,¹⁵⁷ for the enantiomeric acylation of different alcohols.



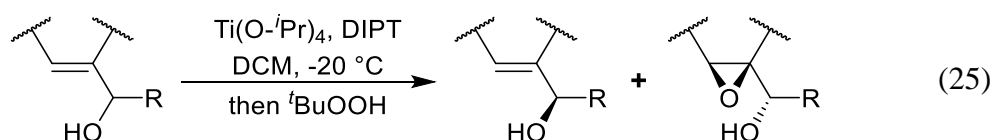
Scheme 13. Proposed peptide-catalysed acylation

In 1995, the Noyori group first reported the kinetic resolution of a ruthenium complex (**90**)-catalysed regioselective hydrogen transfer from racemic alcohols (**Figure 13**)^{158,159} providing up to 99% e.e. (Equation 24) of the unreacted chiral secondary alcohol.

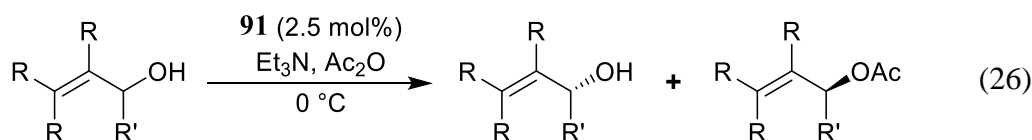
Similar FGIs have been applied enantiomerically *via* design of NHC-Pd complexes,^{160, 161} chiral Schiff base-V complexes,¹⁶² diaminodiphosphine-Ir(I) complexes,¹⁶³ and chiral Mn-salen complexes.¹⁶⁴



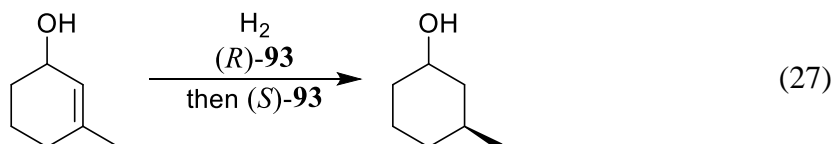
By linking racemic alcohols to C=C bonds Sharpless *et al.* first reported the kinetic resolution *via* allylic alcohol epoxidation of racemic aliphatic allylic alcohols (Equation 25).¹⁶⁵ They tested cyclic and non-cyclic allylic alcohols, both of which produced high e.e.s and high levels of kinetic rate differences explaining the high levels of stereocontrol. In 2005, Yamamoto reported a vanadium complex-catalysed epoxidation of allylic alcohols, demonstrating high enantioselectivity with conversions of up to 91%.¹⁶⁶ Then, the substrate scope of the Sharpless asymmetric epoxidation was expanded to include cyclopropene derivatives by Simaan *et al.*¹⁶⁷



In 2000, the Fu group¹⁶⁸ reported their ferrocene-DMAP derived catalyst **91** (Figure 13) in the KR of allylic alcohol acylation (Equation 26). Later, Vedejs and Mackay¹⁵⁵ broadened the substrate scope to more conjugated systems including aryl allylic alcohols, catalysed by chiral phosphine derivative **92** (Figure 13).



Recent years have seen the development of chiral BINAP-derived compounds for the kinetic resolution of various other FGI reactions. The KR of alkenes through hydrogenation was developed by the Noyori group applying a BINAP-Ru(II) complex catalytic system **93** (Figure 13).¹⁶⁹ The reaction was controlled by the hydrogen pressure and time, generating over 99% e.e. with high conversion (Equation 27). Later, the Faller group reported their use of a BINAP-Ru(II) complex for KR of acyclic allylic acetates and benzoates, giving high stereoselectivity with unsymmetrical substrates.¹⁷⁰ Cp-Ru(II) complexes were also applied in allylic alkylation, with Onitsuka *et al.* reporting their design of catalyst **94** (Figure 13).¹⁷¹ They managed to obtain more than 14 times of rate difference under 2.5 mol% catalytic loading.



3.2 Organo-catalytic asymmetric *N*-acylation of amines

Comparing to most discussions above, asymmetric amide formation is much less developed. Comparing to alcohols, the kinetic resolution of amines is limited by the reactivity of the substrates and due to the wide range of amine nucleophilicities, the KR

effects of a chiral catalyst do not contribute easily to the overall *stereoselectivity* of the reaction. Many of the catalysts for these types of reactions have less nucleophilic amine functions or less reactive electrophilic sites (**Figure 14**).

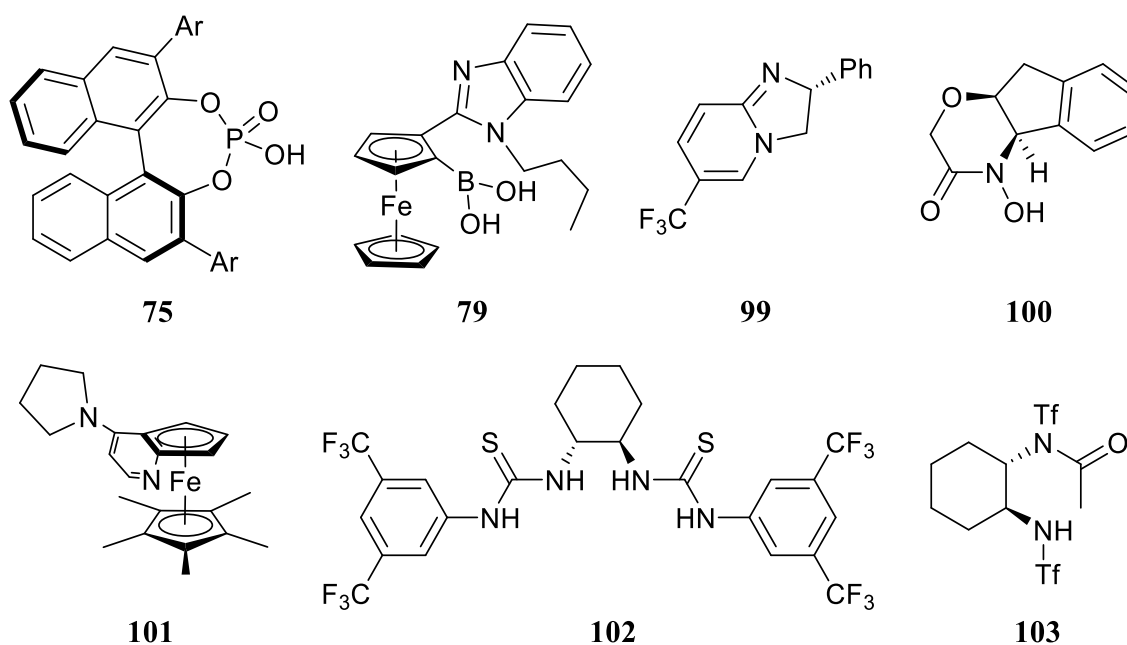
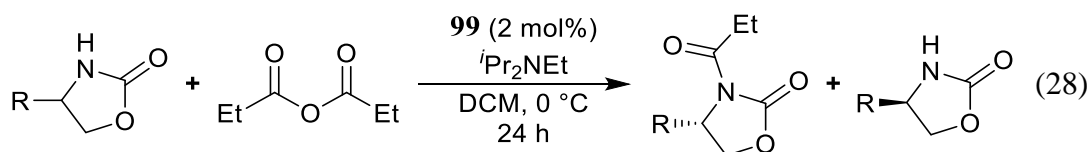
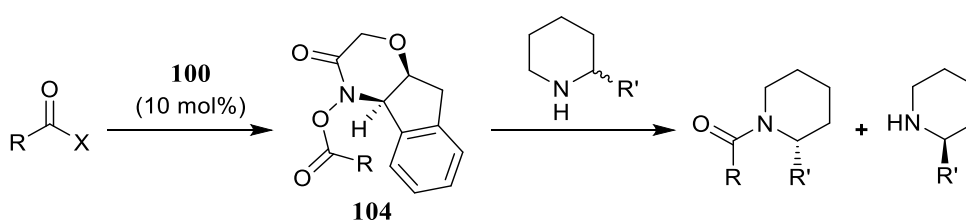


Figure 14. Examples of reported catalysts for *N*-acylation KR of amines.

Research by Sharpless *et al.* stated the kinetic resolution of hydroxy tertiary amines by *tert*-butyl hydroperoxide (TBHP), producing enantiomeric β -hydroxy amine at up to 95% e.e.¹⁷² Another sample was Birman's research in 2006, proposing an efficient *N*-acylation by catalyst **99** (**Figure 14**), giving secondary amide from oxazolidinone and anhydride (Equation 28).¹⁷³

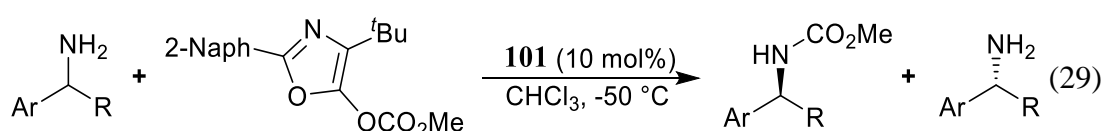


In 2011, Bode group described a cooperative catalytic KR of cyclic secondary amines in the presence of developed aminoindanol-derived hydroxamic acid **100** (Scheme 14).¹⁷⁴ Mechanistic studies suggested a pre-activation process to give intermediate **104**, followed by the *N*-acylation of cyclic amines and the recovery of catalyst **100** by a modified triazolium species.

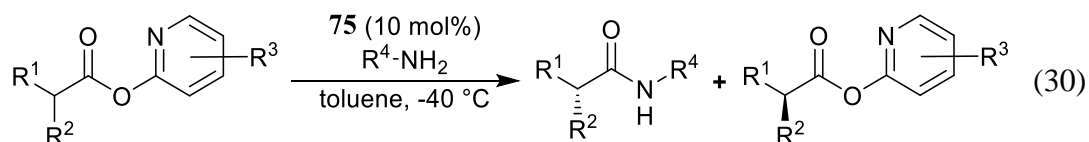


Scheme 14. Reported Cooperative KR of cyclic secondary amines.

Regarding the *N*-acylation of primary amines, a pioneering breakthrough by Fu *et al.* was introduced in 2004, with their ferrocene-fused DMAP derivative **101** for the KR of primary benzylic amines (Equation 29).^{168, 175} This *N*-acylation of primary amines gave acceptable selectivity and broad substrate tolerance (Equation 29) and later Seidel and co-workers discovered the *N*-acylation of amines in the presence of an *in situ* DMAP activation by bis-arylthiourea **102**¹⁷⁶ (Figure 14) and the efficient dual activation process by the anion-binding catalysis (Equation 29).¹⁷⁷⁻¹⁷⁹ The Whiting group also reported a bifunctional arylboronic acid-based ferrocene analogue **79** (Figure 14) which demonstrated a novel asymmetric direct amidation pathway.¹⁴⁹



Recently, Yamamoto *et al.* reported a KR strategy of primary amine acylations catalysed by a Brønsted acidic chiral phosphoric acid **75** (**Figure 14**).¹²⁷ The reaction possessed good substrate tolerance with a range of chiral pyridinyl carboxylic esters being activated for the catalysis (Equation 30).

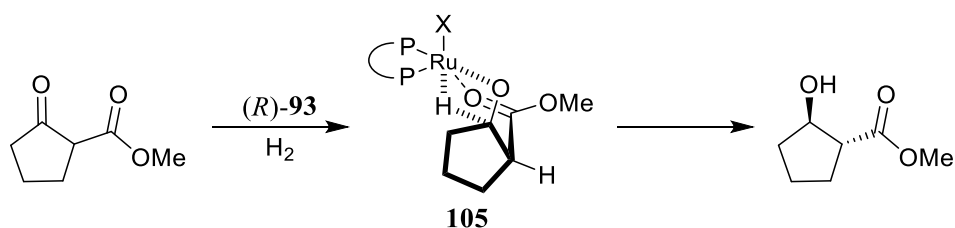


Other research reports include the investigation from the Kim group on the *N*-acylation of primary benzyl amines catalysed by Pd-based nanoparticles,¹⁸⁰ and the Cossy group's development of catalyst **103** for the highly selective *N*-acylation of allylic amines, giving 92% e.e. at 50% conversion.¹⁸¹ Their investigation suggested the introduction of polymer-supported ammonium chloride which helped tuning the solvent polarity while enhancing the overall selectivity. In 2014, Asahara *et al.* applied supramolecular nanocapsule in the enantioselective *N*-acylation of primary amines reacting with an acyl chloride leading to acceptable results and giving up to 90% e.e.¹⁸²

3.3 Mechanistic considerations

Most metal-catalysed kinetic resolutions come with a metal chelation process with a certain isomer fitting the steric restrictions of the catalyst to generate a transition state.¹⁸³ Examples include KR through carbonyl hydrogenation catalysed by a Ru-dipamp complex **93** (**Figure 13**).¹⁸⁴ Evidence showed the formation of enantiomeric products in a highly

pressurised system, giving chelated transition state **105** and producing up to 96 e.e. optical purity.



Similarly, stereoselective control of allylic compounds was generally realised by the formation of transition metal-alkene complexes. For example, Bercaw *et al.*'s catalytic allylic polymerisation involved a zirconium-Cp complex species (**Figure 15**).^{185, 186} Chelation to the C=C prefers a less hindered transition state **106b**, in contrast to **106a** with a potential collision of isopropyl against the polymerised end, or **106c** where a bulky R group was located to be less thermodynamically stable. By placing sidechains as steric hindrance next to Cp rings, transition-metal complexes managed to perform their desired catalytic function with different substrates. Initial research by Collins *et al.* suggested a similar titanium-based complex for the FGI of allylic compounds¹⁸⁷ who introduced a *rac*-EBTHI-mediated titanium complex for the steric restriction and similar strategy has been applied in various other FGI reactions.¹⁸⁸

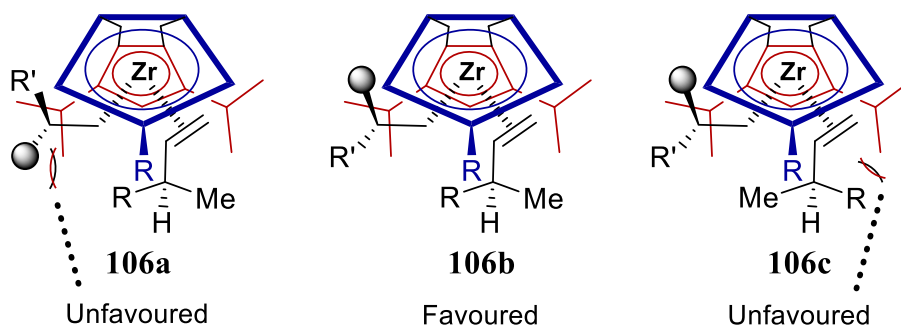


Figure 15. Proposed transition state for KR of allylic polymerisation.

Blackmond *et al.* has studied the resolution process,¹⁸⁹ as outlined in **Figure 16**. It was suggested that energy consumed for this process played an important role in the catalytic process. A decisive factor during the different reaction stages is believed to be the ‘easiness’ of mismatched pairing. As exemplified in this case where an enantiopure (*S*)-catalyst is obtained, the racemic substrates differentiate upon the conformation. With a lower $\Delta G_R + \Delta G_S$, the reaction turns more into a completion, giving higher yield percentages. Meanwhile, a greater energy difference, which is $\Delta G_R - \Delta G_S$, stands for more likelihood to get resolution effects. Besides the kinetically favoured ‘matched’ reaction, strategy to restrict the unfavoured ‘mismatched’ reaction becomes crucial. In most cases, the catalyst is still functioning in the absence of favoured substrates, causing higher energy and lower conversion. (**Figure 16**) Therefore, it is found that design of such a chemically separative catalyst remains challenging.

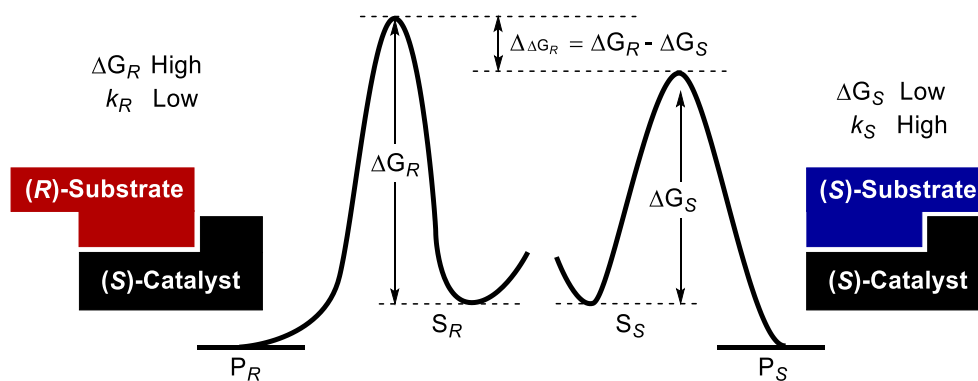


Figure 16. Reaction Mechanism for the proposed kinetic resolution reactions

4. Summary

To summarise, a series of organocatalytic reactions have been reviewed. As one of the most important tools towards efficient C-C bond construction, catalytic direct amide formation has attracted much attention. Usually, a strong electrophile is required to enable the amidation process. There have been various strategies employing different electron-deficient units including phosphine,¹⁶ silane,¹⁷ aluminium,¹⁸ Hafnium,¹⁹ Nickel,²³ etc. As a typical non-metallic electron-withdrawing centre, boron species were introduced more recently for similar purposes, ranging from borane,²⁴ boric acid²⁵ to a series of arylboronic acid.²⁵⁻³⁵ Meanwhile, with the art of heterogeneous catalysis being recognised and more of these types of catalysts being developed to show considerable reactivity with recyclability and reusability (i.e. solid-phase phosphine^{36,37}), plus with the introduction of more environmentally friendly boron species,^{29,46} the future of boron-catalysed heterogeneous direct amide formation is bright.

The role of metals acting as electron-deficient sites is well known. Most chiral bifunctional catalysts have been reported that have one or two metal centres (bimetallic system). Due to the difference in electronic properties, hetero-bimetallic systems normally work as LA-Brønsted base bifunctional system, as research by Shibasaki and co-workers. Under certain circumstances, where non-metallic systems become crucial, bifunctional catalysis is carried out with catalysts composed of active H-bond donor such as urea/thiourea, as well as strong H-bond acceptors with empty *p*-orbital from amines.¹⁰⁰⁻¹⁰³ Since then, new methodologies involving boron-mediated asymmetric synthesis was introduced as an alternative source of reactive activation to H-bond donor sites.^{141,142,148,149} Starting with several basic reactions, the toolbox of organoboron-mediated asymmetric synthesis is expanding. In addition, in order to introduce chirality control, kinetic resolution

has been applied to boronic acid catalytic systems. Although research into efficient kinetic resolution reactions intense,^{150,151,179,190} there is still much to develop, especially given the new reactive systems such aryl-diboronates have only been recently been discovered¹⁹¹ and have not been employed for asymmetric applications to date, although other kinetic resolutions through *N*-acylation has continued in recent years,^{172-175,177-181} including from our own group research,¹⁴⁹ there is much scope for new developments.

VII. Results & discussion

1. Research target

The use of boron-mediated catalysis has been reviewed above, showing an increase in new application over the past few decades.^{6,8} Compared to organometallic catalysis, boron-based systems usually represent a more environmentally friendly catalytic strategy and often effective in air and under mild catalytic reaction conditions.

As part of this project, we investigated the reactions of different boronic acid species using the boronic acids as electrophilic, i.e. Lewis-acid activators¹⁹² through attachment to different functional scaffolds to enable their use in different catalytic applications. **Figure 17** shows some of the structures of interest throughout this thesis, with the design of these molecules being based on their ease of accessibility, and their potential applications in catalysis. The main aims of this project were to design and synthesise a set of organoboron compounds that would act as good catalysts for the following reactions: 1) catalytic direct amide formation using a solid-state, supported boronic acid; 2) an asymmetric direct amidation variant using an asymmetric homogeneous catalyst; 3) an asymmetric nitro-Michael addition using homoboroproline analogues.

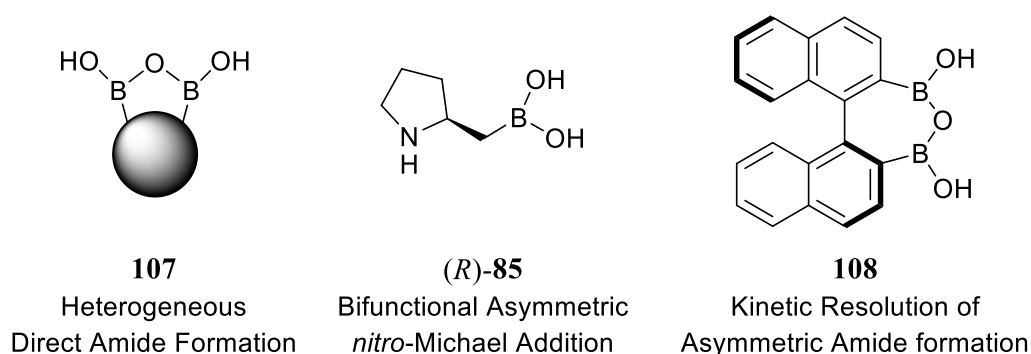


Figure 17. Boronic acid catalysts throughout this thesis

2. Solid-supported catalytic direct amide formation

In this section, a polystyrene-based heterogeneous arylboronic acid catalyst was developed for examining catalytic direct amide formation. Previous research in the group⁴⁷ suggested that a reactive dimeric B–X–B bridged species could be the active catalytic species that accomplished direct amidation, and is formed *in situ*, resulting in a rate-determining step involving acylation of boronic anhydride system. Therefore, the idea of introducing such a system onto a polymer-based backbone would need to be accomplished in a manner where the boronic acid functions could be close enough to form the required boronic anhydride. It was envisaged enhanced catalysis could result from adapting the polymer to have a clustering of the boronic acids resulting in enhanced catalysis and application on a broad range of substrates. Potentially, such a heterogeneous system could combine most advantages of a homogeneous catalyst but in a heterogeneous catalytic system and show robust atom-economic direct amidation capability, with straightforward filtration from the reaction mixture and re-use, with potential for use in flow systems.

2.1 Preparation of heterogeneous polymer catalyst

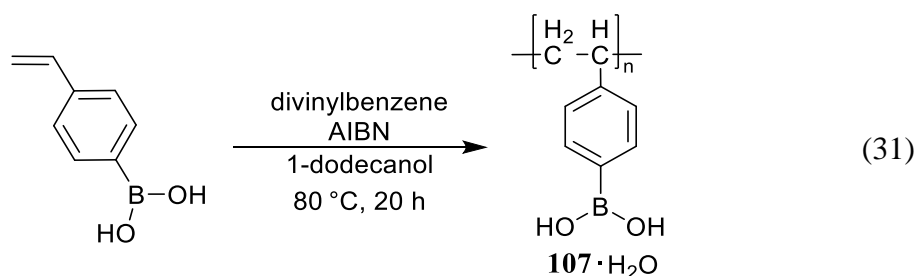
The polymerisation of styrene is a well-studied process¹⁹³ triggered by heating the vinyl monomer with a suitable initiator at a temperature where activation energy (E_a) needs to overcome in order to trigger the later stages of chain propagation and radical transfer.

Table 1. Heating in the vinyl polymerisation

Entry	Monomer Substances	ΔE_p / kcal	T / °C	D.P. / units
1	Styrene (C ₆ H ₅ -CH=CH ₂)	22.1 (±2)	80	5880
2	Styrene (C ₆ H ₅ -CH=CH ₂)	22.1 (±2)	100	4130
3	Styrene (C ₆ H ₅ -CH=CH ₂)	22.1 (±2)	120	2900
4	Styrene (C ₆ H ₅ -CH=CH ₂)	22.1 (±2)	150	1710
5	Styrene (C ₆ H ₅ -CH=CH ₂)	22.1 (±2)	200	827
6	CH ₂ =CH ₂	23.1(±1)	82	- ^a
7	CH ₂ =CH-CH=CH ₂ (1,2-polymerisation)	19.9 (±1)	82	- ^a
8	CH ₂ =CH-CH=CH ₂ (1,4-polymerisation)	20.4 (±1)	82	- ^a

^aThese data have not been recorded in this literature.¹⁹³

For the arylboronic acid-substituted polystyrene synthesis, adequate heating usually gives higher degree of the condensed polymeric product, as results showed a greater degree of polymerisation (d.p.) at 80 °C than those at higher temperatures (Entries 1-5, **Table 1**). Despite previous calculations by Kharasch showing that the styrene polymerisation might cost less energy,¹⁹⁴ reaching a level of about 22 kcal mol⁻¹, in comparison with conjugated dienes at a slightly lower level (Entries 6-8, **Table 1**).



The Coutinho group early discussed the effects of styrene-DVB copolymerisation for better customisation of polymer properties.^{195a} Usually, a 1.2-2.0 equivalent of DVB

was employed with the styrene monomer, leading to a crosslinking free radical polymerisation process. Finally, we chose the well-optimised methodology by the Moad group on, by use of reversible addition-fragmentation chain transfer (RAFT) polymerisation.^{195b} This involves heating of suspended DVB and 4-vinylphenylboronic acid mixture, together with AIBN as free radical initiator and 1-dodecanol as solvent (Equation 31).



Figure 18. Heating unit for polymerisation

Hence, the suspension of vinyl-phenylboronic acid **104**, DVB and styrene in 1-dodecanol was placed in the glass tube by hot air flow, maintaining at a constant 80 °C. After 20 h heating, the reaction mixture turned into a white solid monolith of catalyst **105** (**Figure 19**). The polymer stick was soaked in methanol, followed by DCM washing to get rid of unreacted substances, solvent and some lower molecular weight oligomer. For better drying, the monolith was cut into pieces before placing in a drying oven. For a greater surface area for reactive contact, the fully dried poly-vinyl-phenylboronic acid monolith was ground into a fine white powder and stored for future use.



Figure 19. Synthesised monolith of the polymer catalyst **107**

Characterisation of the polymer catalyst **107** included ^{11}B SSNMR, the results of which are summarised as **Figure 20**. A strong broad peak centred at around 17 ppm was observed indicative of arylboronic acid, including a partial dehydration process, generating what could potentially be identified as a dimeric B–O–B bridged boronate species or boroxine shoulder of the major peak at 23 ppm. For such species to be observed by SSNMR, it strongly suggested that the types of reactive species required for direct amidation catalysis were presented as hoped for in the solid phase catalyst.

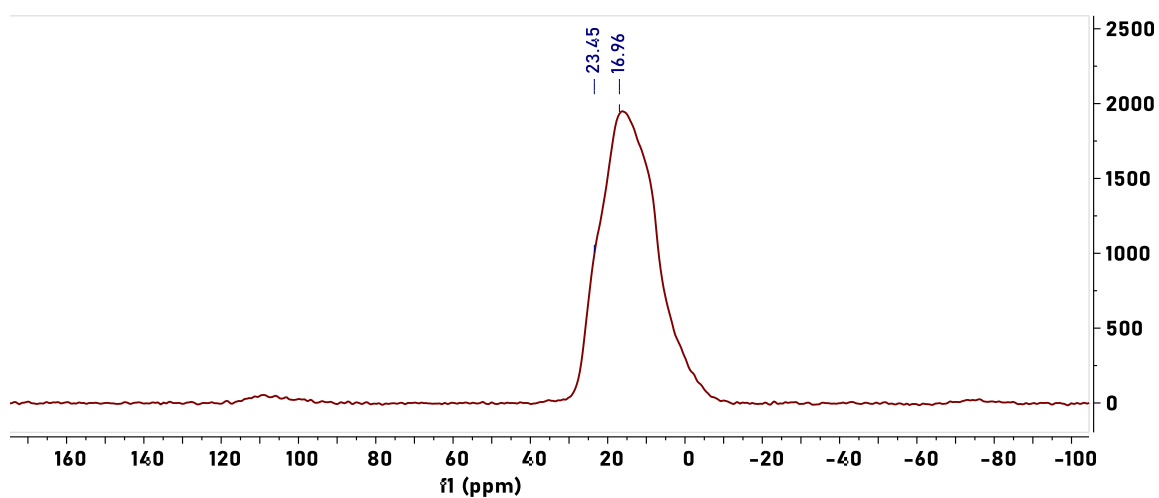
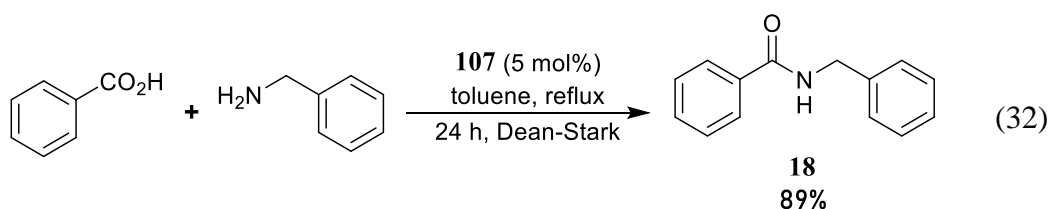


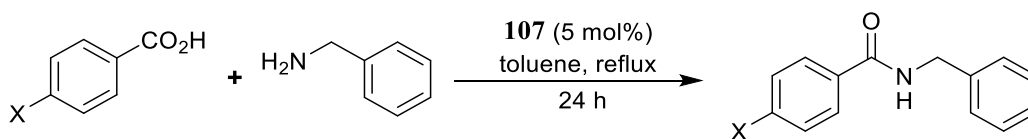
Figure 20. ^{11}B SSNMR of prepared polymer catalyst **107**.

2.2 Substrate scope of polymer catalyst

With a novel solid-phase catalyst in hand, the first thing to evaluate its catalytic reactivity. It is noteworthy that the data consistency and reproducibility of catalytic direct amide formation was carefully examined under controlled reaction conditions, i.e. using a parallel reactor system and GC conversion monitoring. For general conditions check General procedure C. The first chosen amidation was the reaction of benzoic acid and benzylamine, the results of which are shown in Equation 32.



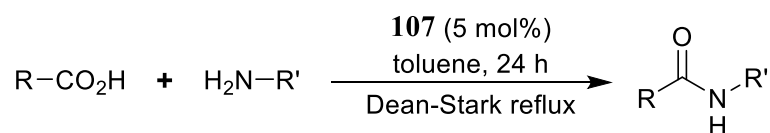
Considering the fact that most homogeneous boron-based amidation catalysts have been reported to be used with a wide range of catalytic loadings from 1 to 20 mol%,^{28,38,40} our initial attempts began with a moderate 5 mol% loading (75.8 mg catalyst to 2.86 mmol substrates as 1 equiv.), but this was also based upon our previous observations for boronic acid catalysts used in previous optimisation studies.³⁵ Selection of solvent began with the reasonably high boiling point solvent toluene under refluxing conditions using a Dean-Stark apparatus for water removal. After final adjustments and repeats of the reaction setup, the optimised conditions were kept constant, generating convincing and reliable data from a series of screening reactions. In this general procedure, 5 mol% of polymer catalyst was added to equal stoichiometric amounts of carboxylic acid and amine dissolved or suspended in toluene before refluxing at 110 °C. An aqueous workup was used to separate unreacted starting materials crude products were analysed before Kügelrohr distillation to give the purified amide product which as a white solid.

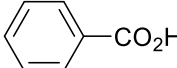
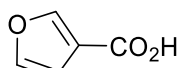
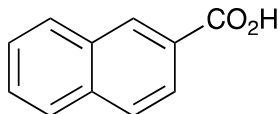
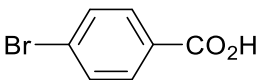
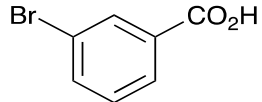
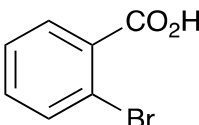
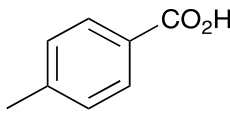
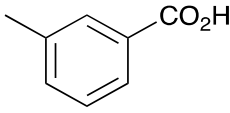
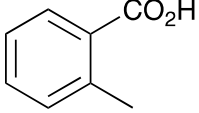
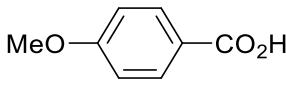
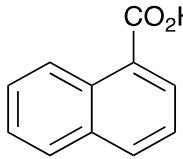
Table 2. Testing of different methods of water removal.

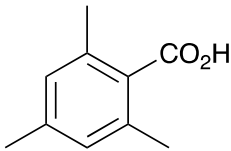
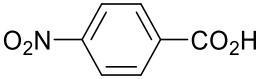
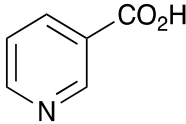
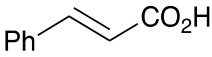
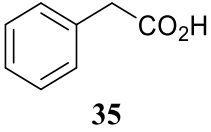
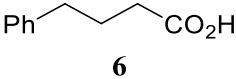
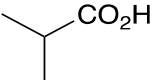
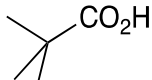
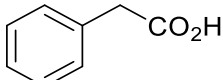
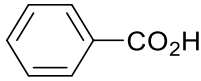
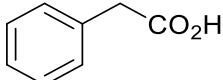
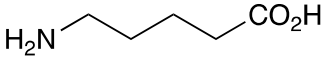
Entry	X	Approach to remove water	Isolated yield ^a
1	-H	with Dean-Stark apparatus	89%
2	-H	with 4Å MS	90%
3	-H	with dried MgSO ₄	76%
4	-H	none	22%
5	-Br	with Dean-Stark apparatus	25%
6	-Br	none	16%

^a Reaction carried out using General Procedure A.

To understand the role of the azeotropic procedure upon the catalysis, different approaches were tested in parallel and the results compared, as listed in **Table 2**. It was obvious that different methods to remove water did not make too much difference to the overall outcomes (Entries 1-3, **Table 2**). Notice that the reaction became more sluggish without any azeotropic water removal (Entries 4 and 6, **Table 2**), presumably, the presence of water slows the formation of key species such as an acyloxy boronate or boronic anhydride,⁴⁸ that are prone to hydrolysis, slowing amide formation. Generally, there was little major impact of substituent effects with benzoic acid analogues, with the exception of *p*-nitrobenzoic acid which was clearly severely deactivated (Entry 2, **Table 3**). In contrast, phenylacetic acid (Entry 11, **Table 3**) was much more reactive, as we would expect with a higher pK_a carboxylic acid.¹⁹⁶

Table 3. Substrate scope of the catalytic direct amide formation with polymer catalyst **107**.

Entry	Carboxylic acid	Amine	Product	Yield ^a / %	
				Crude	Pure
1	 16	BnNH ₂	18	96 35 ^c	90 25 ^c
2		BnNH ₂	109a	86	67
3		BnNH ₂	109b	82	70 42 ^c
4		BnNH ₂	109c	45	25
5		BnNH ₂	109d	35	30
6		BnNH ₂	109e	40	27
7		BnNH ₂	109f	68	32
8		BnNH ₂	109g	45	42
9		BnNH ₂	109h	30	20
10		BnNH ₂	109i	38	29
11		BnNH ₂	109j	84	40

12		BnNH ₂	109k	NR	
13		BnNH ₂	109l	8	5
14		BnNH ₂	109m	Trace conversion	
15		BnNH ₂	110, 112	92	59 ^b +24 ^b
16		BnNH ₂	36	98 92 ^c	92 75 ^c
17		BnNH ₂	7	98 70 ^c 10 ^d	82 64 ^c , 9 ^d
18		BnNH ₂	109n	79	76
19		BnNH ₂	109p	60	42
20		BnNH ₂	109q	Trace conversion	
21		PhNH ₂	109r	-	75
22		PhNH ₂	109s	-	15
23		morpholine	109t	-	79
24			109u	No reaction	

^aUnless otherwise specified, reaction carried out with General Procedure B. ^bBenzylamine (2 equiv.) was used due to both amidation and conjugate addition occurring to give a mixture of both PhCHCHCONHBn and PhCH(NHBn)CH₂CONHBn. ^cHomogeneous catalysis using 5 mol% phenylboronic acid (See General Procedure C). ^d20 mL DCM, 4Å MS, r.t. instead of toluene Dean-Stark reflux.

As shown higher pK_a carboxylic acids were more reactive towards direct amide formation as discussed elsewhere,¹⁶ and importantly, the new heterogeneous catalyst **1** followed the same trend. The aromatic substrates benzoic, furoic, and 2-naphthoic acids showed excellent reactivity (Entries 1-3, **Table 3**). However, a reduction in conversion was observed for those aryl carboxylic acids with a range of substituents including bromine, methoxy and methyl (Entries 4-10, **Table 3**). While some of the effects could be steric in nature 1-naphthoic acid *versus* 2-naphthoic acid for example (Entries 11 and 3, **Table 3**) and mesityl carboxylic acid (Entry 12, **Table 3**), there are clearly other, more subtle effects at work. Furthermore, the more electron-deficient aryl carboxylic acids were much less reactive, as seen with nitrobenzoic acid and 1-nicotinic acid, both of which were unreactive (Entries 13 and 14, **Table 3**). Nonetheless, an efficient direct amide formation from the reaction of *trans*-cinnamic acid (Entry 15, **Table 3**) which showed competitive Michael addition *versus* direct amide formation (**Figure 21**). The crude isolated product NMR showed a mixture of benzylamide **110** and Michael-adduct **112** in an approximate 2.5:1 ratio (Entry 15, **Table 3**). In addition, the general utility of catalyst **1** was further demonstrated through amidation of several other alkyl carboxylic acids (Entries 16-19, **Table 3**).

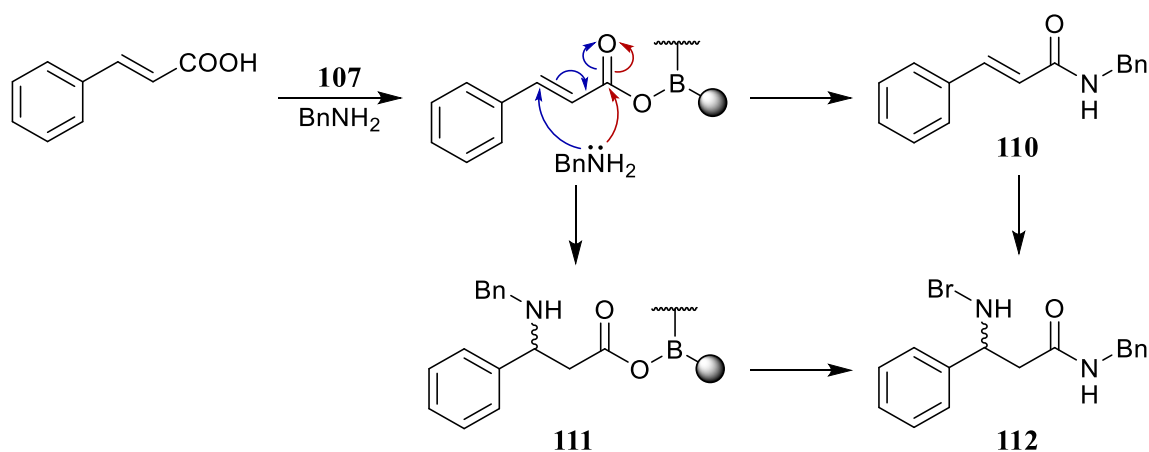


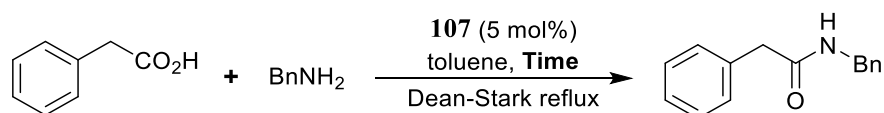
Figure 21. Benzylamide formation (red) was preferred to first time Michael-addition (blue).

The less reactive amines such as aniline and morpholine, also showed good reactivity with phenylacetic acid (Entries 21 and 23, **Table 3**), although the combination of benzoic acid and aniline (Entry 22, **Table 3**) gave low conversion, as might be expected for a lower pK_a carboxylic acid reacting with a less nucleophilic amine. Unfortunately, the potential lactamisation reaction of 5-aminovaleric acid failed (Entry 24, **Table 3**), with the effect of a combination of a volatile secondary amine substrate and a less reactive carboxylic acid, was no reaction at all, as indicated by the result of Entry 25 (**Table 3**).

In terms of heterogeneous *versus* homogeneous phase catalyst, the solid catalyst **1** showed considerably improved reactivity over phenylboronic acid. Hence, although catalyst **1** is electronically similar to phenylboronic acid, its reactivity was shown to be considerably higher (Entries 3, 11, 16 and 17, **Table 3**). In addition, the recovery of catalyst **1** (*vide infra*) added to the general utility of the solid-supported system.

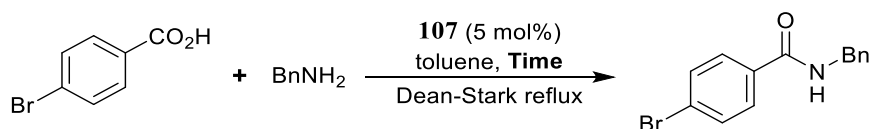
2.3 Catalytic kinetics and mechanistic studies

Following the substrate scope in **Table 3** in which the conversion varied greatly as a function of substrate, we decided to examine the rate of conversion of time, as a function of substitution using two amidation reactions. The two reactions were chosen that had quite different reactivities (Entries 3 and 11, **Table 3**) and by using a parallel reactor system, both reactions could be run at the same time under identical conditions with individual reactions being terminated at different durations. The results are summarised in **Table 4** and **Table 5**.

Table 4. Kinetic studies on heterogeneous catalytic direct amide formation.

Entry	Time / h	Yield / %
1	0.5	17
2	1	28
3	3	66
4	6	69
5	9	70
6	12	71
7	15	75
8	18	76
9	21	79
10	24	80

^aReaction carried out with General Procedure B.

Table 5. Kinetic studies on catalytic 4-bromobenzylamidedirect amide formation.

Entry	Time / h	Yield / %
1	6	9
2	12	10
3	24	46
4	36	48
5	48	62
6	72	73

^aReaction carried out with General Procedure B.

The experiment showed that the more efficient amidation was indeed achieved with phenylacetic acid, which agreed with our previous findings in **Table 3**. The graphical outcome of these series of reactions is shown in **Figure 22**. These plots indicate a sharp

rise of conversion in the first 3 hours for the reaction of phenylacetic acid (**Figure 22**, left), where most products were formed within this timeframe, after which the reaction slowed down until the termination point, and finally producing 80% amide. In contrast, employing bromobenzoic acid resulted in a much slower reaction process which showed a much more moderate rate of conversion of 72 hours, finally reached around 80% conversion. Evidence from these experiments further reinforces the strong relationship between the overall catalytic performance and the pK_a of the substrates and these results show that solid-supported heterogeneous catalyst follows much the same criteria as that which Loupy *et al.* mentioned for homogeneous catalysis.¹⁹⁶

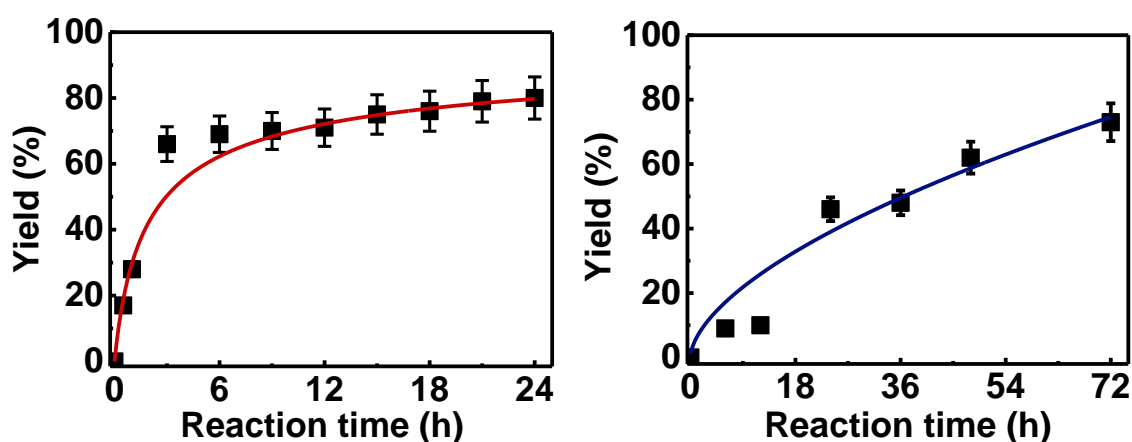


Figure 22 Timescale of catalytic direct amide formation from phenylacetic acid (left) or 4-bromobenzoic acid (right).

Given the previous mechanistic studies proposing the formation of B-X-B bridged intermediates in these types of direct amide formation, it was suggested that the carboxylic acids were ‘activated’ for the direct amide formation *via* a diacyl complex.⁴⁷ Because only one of the bridging carboxylates is reactive towards the amine, the catalytic amide formation reaction should need more than one equivalent of carboxylic acid in order to achieve full conversion. To further clarify the actual catalytic behaviour during this process, SSNMR of polymer catalyst **107** was examined at different stages of the reaction cycle

involving a stepwise addition of phenylacetic acid and benzylamine under stoichiometric, rather than catalytic, conditions, i.e. as shown in **Figure 23**.

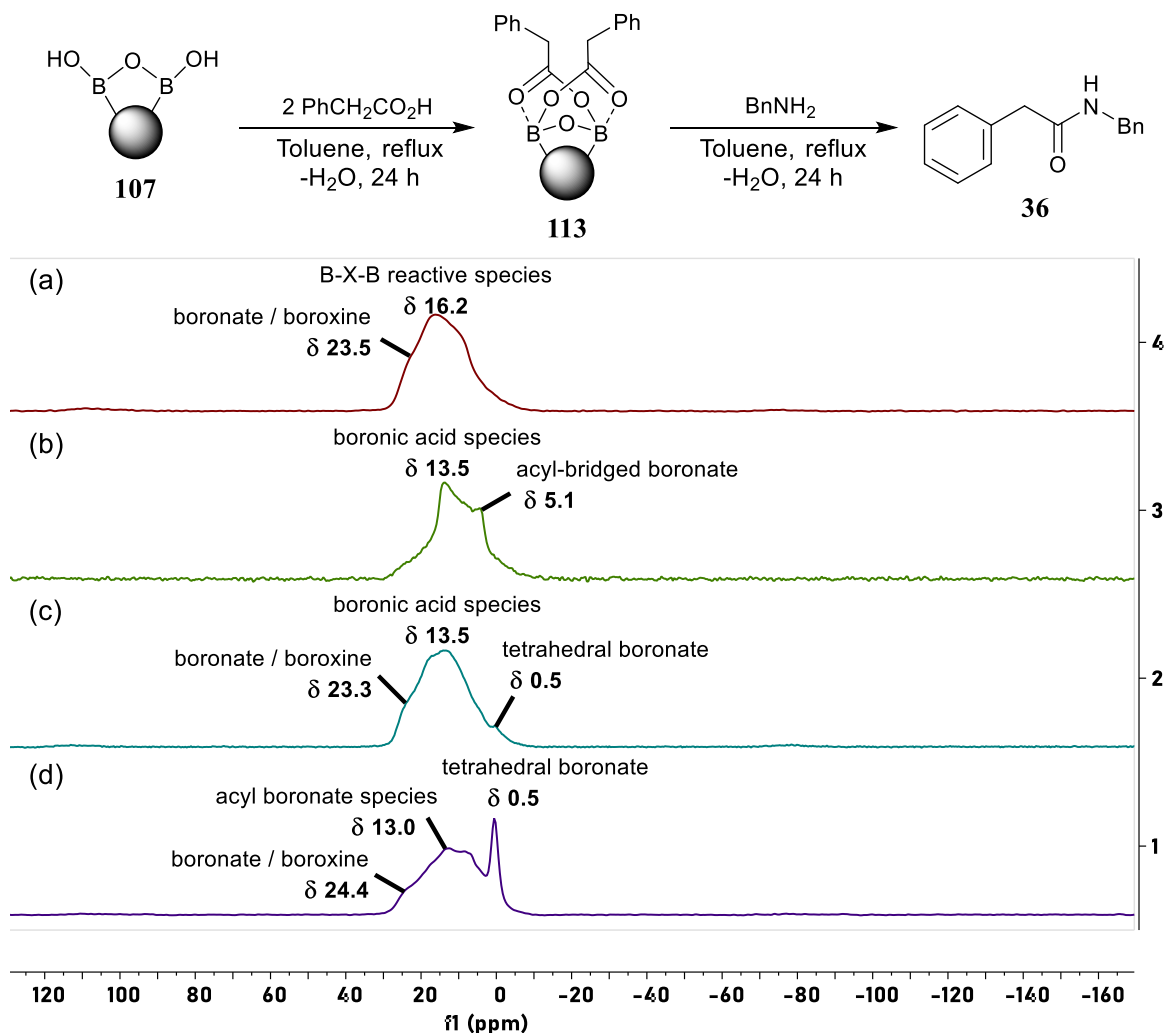


Figure 23. ^{11}B -SSNMR of polymer catalyst **107** under different stages of catalysis.

In the freshly prepared catalyst **107**, a broad peak centred at δ 16.2 and ranging from δ 28 to δ -7 was clearly identified, with the peak at δ 16.2 being typical of the proposed B-O-B bridged starting structure **107**. This peak was merged with a short sharp shoulder peak at δ 23.5, indicative of potential boroxine species (**Figure 23a**). After addition of two equivalents of carboxylic acid, the reactive B-O-B site turned into mostly to the doubly bridged, diacylated coordination species of type **113**, as indicated by the peak at δ 5 ppm

shift (**Figure 23b**). Just after the addition of an equivalent of amine, the diacyl-bridged intermediate went through a rapid conversion to the corresponding phenylacetamide product, leading to a sharp peak at δ 0.5 (**Figure 23c**). That type of peak is typical of a tetrahedral boronate complex, whose intensity increases with time, as revealed by **Figure 23d** and could be indicative of the type of B-N amine complex we have proposed as a key intermediate which forms through coordination of complex **113** with an amide at one of the boron centres prior to amidation occurring.

Furthermore, to better understand the catalytic behaviour shown in **Figure 23**, ReactIR was employed to follow the same reaction after adding each of the reagents (check Experimental Section for the detailed operational procedure for using the ReactIR). This allows the probing the reaction kinetics as a through different functional groups, using the peak intensities in real-time IR. The results of which are illustrated in **Figure 24**.

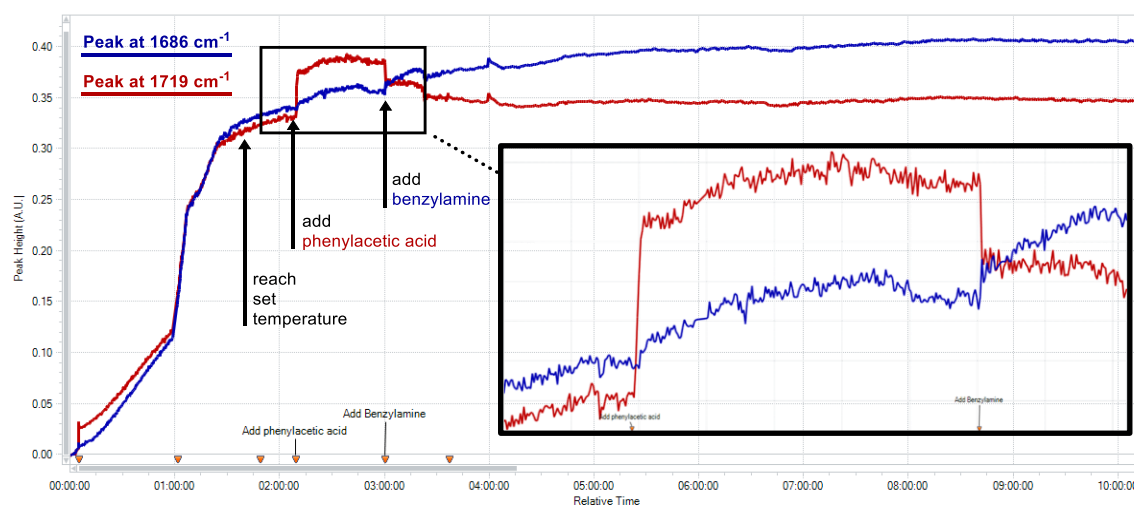


Figure 24. React-IR data of catalytic formation of phenylacetamide.

Hence, the IR probe was placed in toluene together with the solid phase catalyst **107** before heating up to 110 °C. The reaction was refluxed for 20 minutes after which the carboxylic acid was added, which was reflected by an immediate sharp rise in the signal at

1719 cm^{-1} (**Figure 24**) due to the free carboxylic acid. Despite noise on the plot due to the low concentration, the overall trend was clear. When benzylamine was added in after a further 20 minutes, newly formed C=O amide peak at 1686 cm^{-1} quickly appeared (blue), shown by a sudden rise at the beginning followed by a steady increase of concentration (**Figure 24**). Simultaneously, about half of phenylacetic acid was consumed after the addition of amine with the remainder steadily reducing over the next hour, eventually reaching completion after several hours reflux. Notice that the peak height indicating the FG concentration remained a similar level to that at the beginning of the reaction, suggesting the end of conversion. Using a different presentation of this data, i.e. a 3D-stacked IR plot against time, the consumption of substrates and formation of products could be more readily identified, further demonstrating the actual kinetic behaviour from the first moment of reaction through to the end (**Figure 25**).

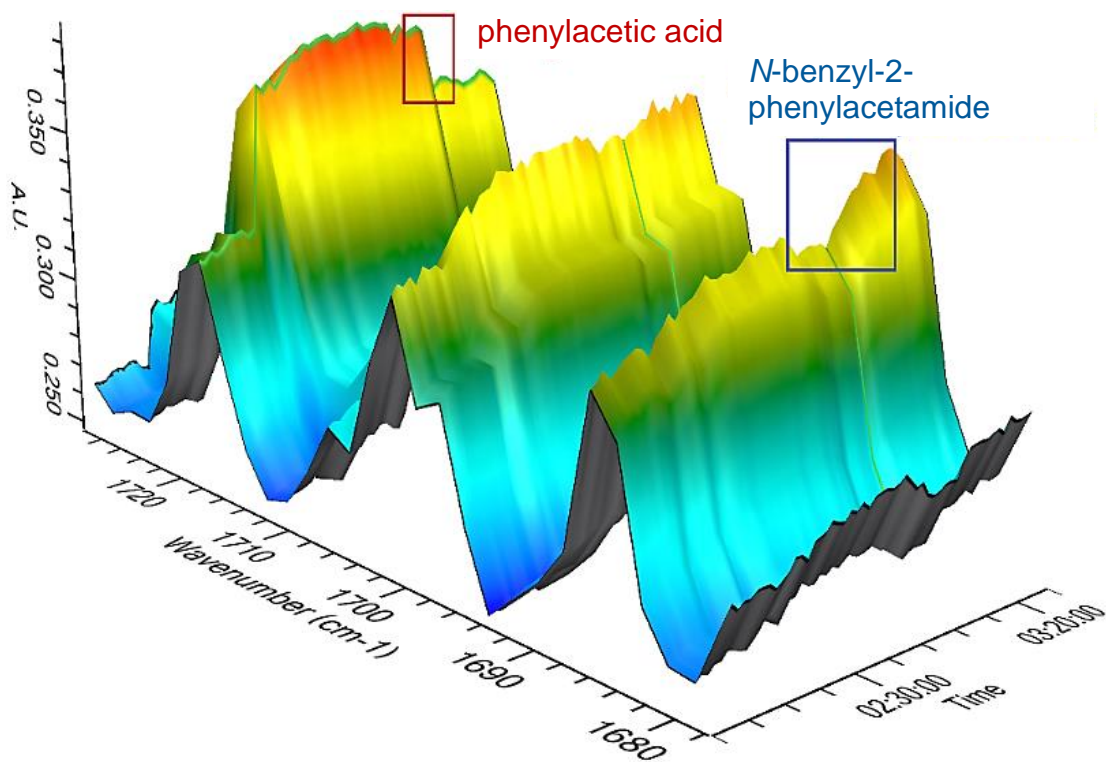
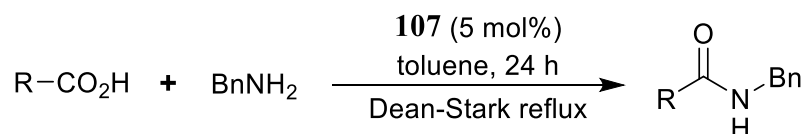


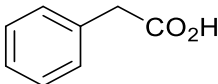
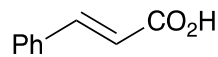
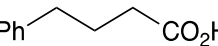
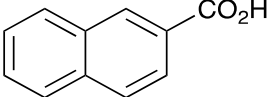
Figure 25. 3D surface stacked IR plots indicates the trend of reaction in a general view.

2.4 Polymer catalyst recovery and recyclability

One reason for employing a solid-based catalyst is its heterogeneity, and therefore, the ability to filter and recover it from the reaction mixture and to then re-use it for the next reaction. The re-use and recyclability of polymer catalyst **107** became a crucial parameter in the evaluation of the catalyst. Hence, a series of reactions were conducted with the catalyst being removed by filtration, followed by being washed and dried for analysis and ready for further use. The results of the re-isolation are shown in **Table 6**.

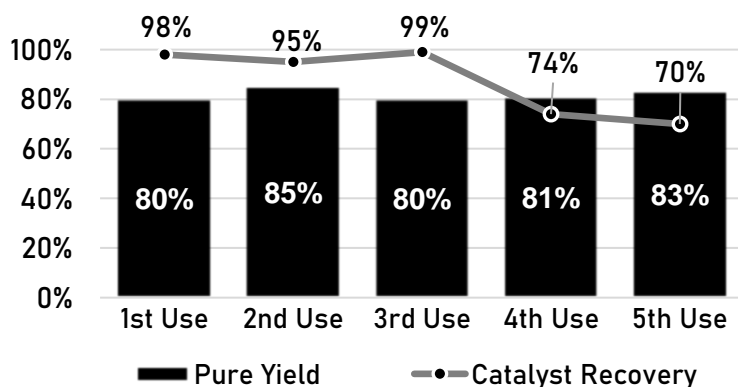
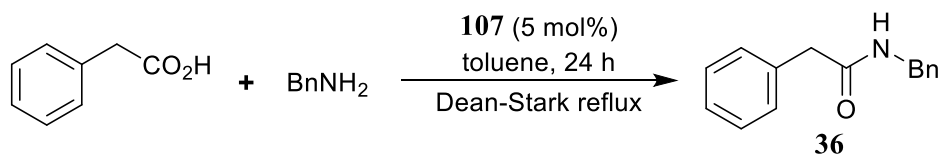
Table 6. Tests on repeated use of recycled polymer catalyst **107**.



Entry	Carboxylic Acid	Yield ^a / %	Catalyst Recovery ^b / %
1		75	98
2		83	88
3		82	92
4		84	87

^aReaction carried under General Procedure E. ^bRecovered under General Procedure E.

After the reaction, the resulting polymer catalyst was collected *via* filtration, washed with different solvents and dried *in vacuo* for more than 10 hours before weighing. The workup procedure demonstrated enough reliability from consistent data and that the catalyst remained intact. Therefore, reaction with phenylacetic acid was then chosen for a series of tests of repeated use of the catalyst. The results of these reactions are shown in **Scheme 15**.



Scheme 15. Recovery test of polymer catalyst **107** in the reaction of phenylacetic acid with benzylamine (Check General Procedure F)

From **Scheme 15**, it is clear that the polymer catalyst remained intact even after 3 reactions, with each involving 24 hours of reflux. After that, a slight drop in mass recovery from the fourth use was observed and is perhaps fully understandable and likely due to experimental considerations. However, the constant performance from the catalyst showed that the consecutive reactions performed highly consistently, and sufficiently so that the catalysts could be considered for use as a stationary phase in a flow reaction system for direct amidation.

2.5 Application in a flow reactor system

The minimal mass loss of polymer catalyst suggested that the catalyst **107** could be the basis of a reliable polymer-based flow reaction system. The Baxendale group has reported the use of modular flow reactors for use in organic synthesis of a number of

compounds.^{197, 198} Such flow systems are effective under many circumstances, and especially where there is a requirement for larger scale synthesis, real-time monitoring, and use of pressurised in-line liquid reactions, as well as improved handling of toxic and hazardous reagents. Due to its modular design, different compartments of the system are readily highly optimizable, and their simplicity makes them ideal for industrial applications (**Figure 26**). Herein, a Vapourtec R₂⁺/R₄ flow reactor was introduced, the workflow for which is shown in **Figure 26**, consisting of a binary pump driving the liquid flow through the reactor, with an automatic heating unit and the attachment of an omnifit glass column loaded with our crushed polymer catalyst. The internal pressure was generated from an in-line 75-psi back-pressure regulator, followed by a digital pressure indicator and finally at the end, a liquid handling robot that enabled collection of the outcoming fluid into fractions.

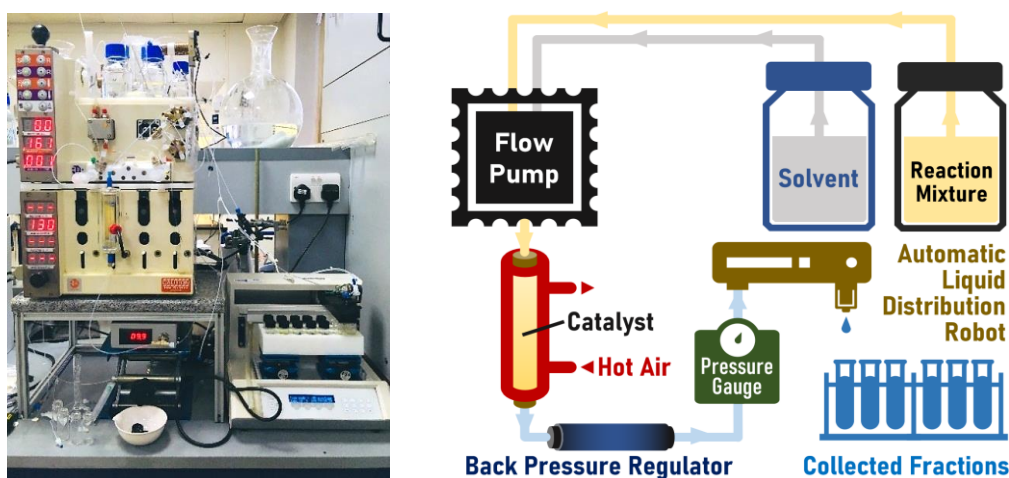
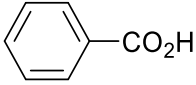
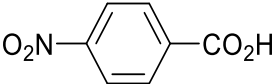
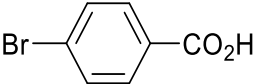
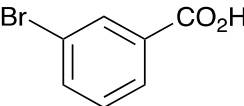
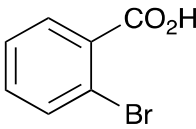
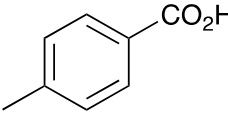
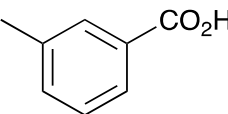
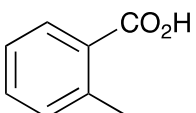
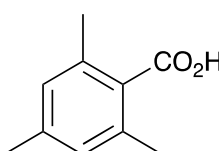
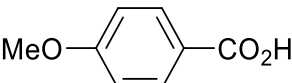
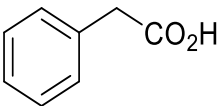
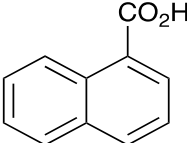
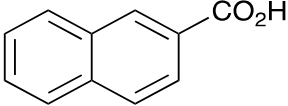
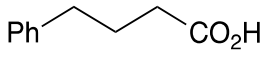
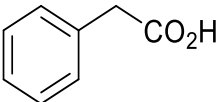
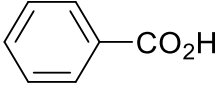
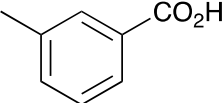


Figure 26. Vapourtec R₂⁺/R₄ modular flow reactor

Initial attempts at use of the system consisted of safety checking posed by potentially hazardous blocking issues of the flow system. One major factor in this is the possible formation of insoluble ammonium carboxylate salts after mixture of both substrates. Hence it was necessary to examine reaction substrate combinations for precipitation at room temperature, as shown in **Table 7**.

Table 7. Precipitation checks of different potential ammonium salt substrates.

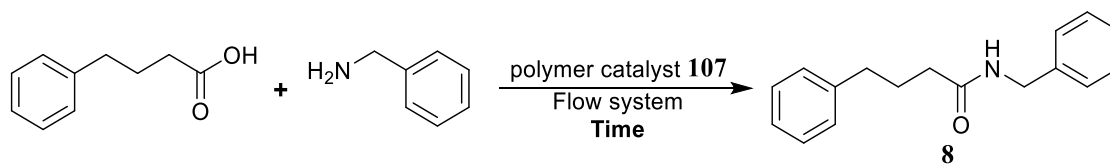
Entry	Carboxylic acid	Amine	Precipitation ^a
1		BnNH ₂	Yes
2		BnNH ₂	Yes
3		BnNH ₂	Yes
4		BnNH ₂	Yes
5		BnNH ₂	Yes
6		BnNH ₂	Yes
7		BnNH ₂	Yes
8		BnNH ₂	Yes
9		BnNH ₂	Yes
10		BnNH ₂	Yes
11		BnNH ₂	Yes
12		BnNH ₂	Yes

13		BnNH ₂	Yes
14		BnNH ₂	No
15		PhNH ₂	Yes
16		PhNH ₂	No
17		diethylamine	No

^a Results observed after 1 h stoichiometric mixture of carboxylic acid amine under r.t. See General Procedure G for details.

Table 7 shows that most amine-carboxylic acid combinations do precipitate at r.t., giving a white solid that does not dissolve in refluxing toluene. However, the cooler parts of a flow reactor system risk being readily blocked by these types of precipitates, yet, and perhaps surprisingly, three combinations were found suitable to test in flow that did not precipitate, i.e. Entries 14, 16, 17, **Table 7**.

Another concern raised about these types of flow applications was from the preparation of polymer catalyst **107**. The catalyst was generated in 1-dodecanol, which has a higher boiling point and can turn solid easily under lower temperature conditions which could in turn cause potential flow system blocking. Therefore, an extra Soxhlet extraction procedure was carried in order to remove any trace amount of 1-dodecanol residue (see Experimental). After 72 h extraction, assuring complete removal of solvents, NMR of the filtrate suggested only a trace 1-dodecanol. Hence, the polymer catalyst was re-isolated and dried before filling into the glass tube reactor for flow system use.

Table 8. Methodology test of flow system under the proposed condition

Concentration of starting materials: 57.2 mmol/L Flowrate: 0.500 mL/min
Column Temperature: 110 °C Back-pressure set: 75 psi

Entry	Fraction No.	Reaction Time	Conversion / %
1	1	0-30 minutes	0
2	2	30-60 minutes	16
3	3	60-90 minutes	18
4	4	90-120 minutes	19

^aConversion rate determined by ¹H NMR after General Procedure H.

Starting with the reliability check of the system to check the methodology, a preliminary amidation reaction was carried out for the reaction of phenylbutyric acid with benzylamine to give corresponding amide **8**. To do this, acid and amine were premixed at the same concentration as the batch reaction, and the mixture was streamed through tubing into the system. After reaching 110 °C in the catalyst column, toluene was introduced through the system. The backpressure was set at 75 psi allowing a higher vaporising pressure for toluene in the reaction mixture, which was then driven through the accumulated hot catalyst. The flow rate was controlled at a level of 0.500 mL/min, assuring enough contact with the catalyst. From the observed rapid conversion to the amide product, the polymer catalyst proved its highly efficient reactivity (Entry 2, **Table 8**). Even after a short period of contact this still gave the corresponding amide in acceptable yields, matching the findings of the kinetic studies, and indeed, the reaction approached a limit of around 20% conversion after 2 hours, but this also reveals the critical role of the contact time between the heterogeneous materials inside the column and the reaction mixture with dissolved reactants. Since the volume of each collected fraction is fixed to the time and flow rate, the

throughput in each time unit is linear to the ratio of amide observed from ^1H NMR compared to the starting material (**Figure 27**). Theoretically, by tuning the flow rate and increasing the temperature, experiments could be enabled with more contact time for the catalysis to take place. The data is summarised in **Table 9**. In this case, the fractions were collected in a gap of every 3 hours in order to keep the same volume collection for each of the reaction tests. Notice that the conversion of each fraction was higher, which proved the previous hypothesis.

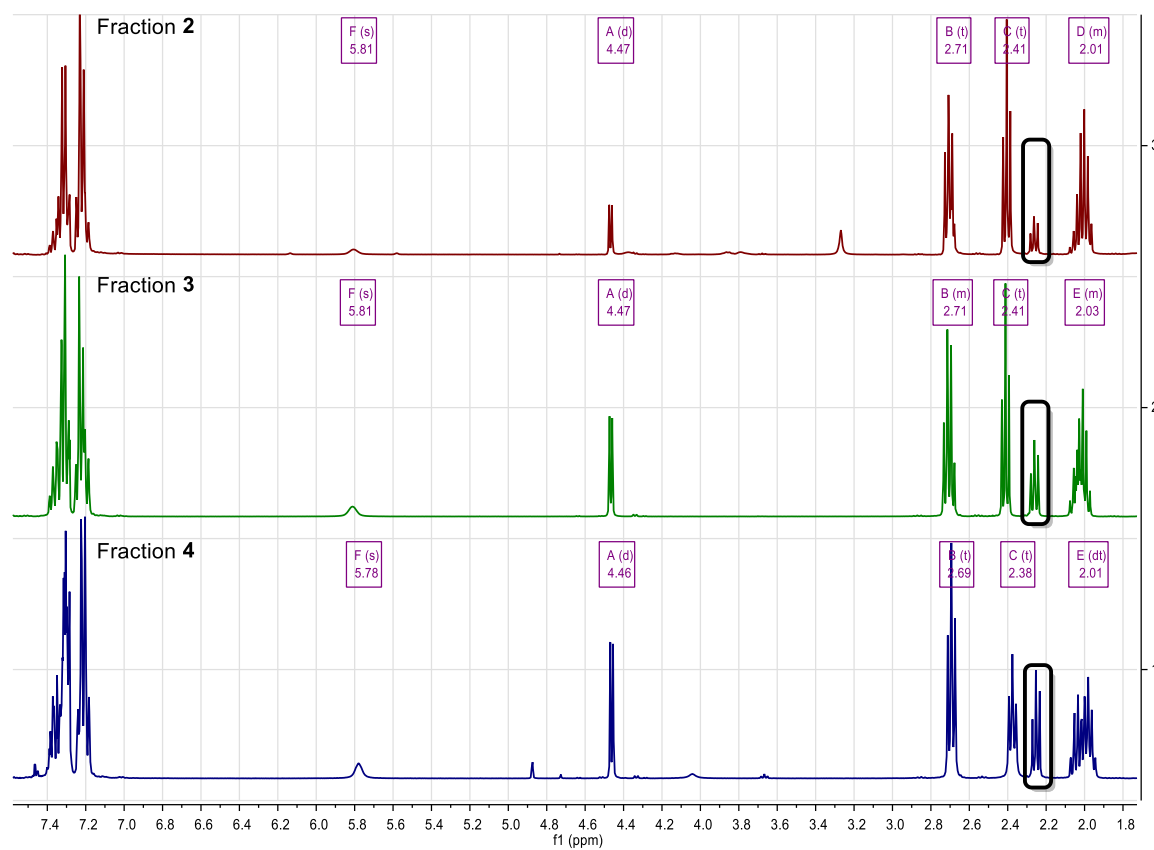
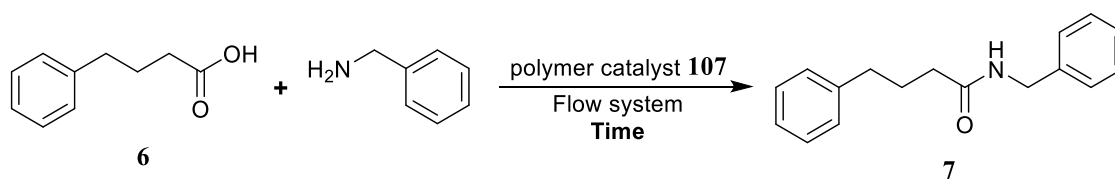


Figure 27. ^1H NMR spectra suggested the conversion in each stage of the catalysis by fractions.

Table 9. Flow system experiments with optimised reaction conditions.



Concentration of starting materials: 57.2 mmol/L Flowrate: 0.100 mL/min
Column Temperature: 130 °C Back-pressure set: 75 psi

Entry	Fraction No.	Reaction Time	Conversion Rate / %
1	1	0-3 h	0
2	2	3-6 h	27
3	3	6-9 h	40
4	4	9-12 h	40

^a Conversion rate determined by ¹H NMR after General Procedure H.

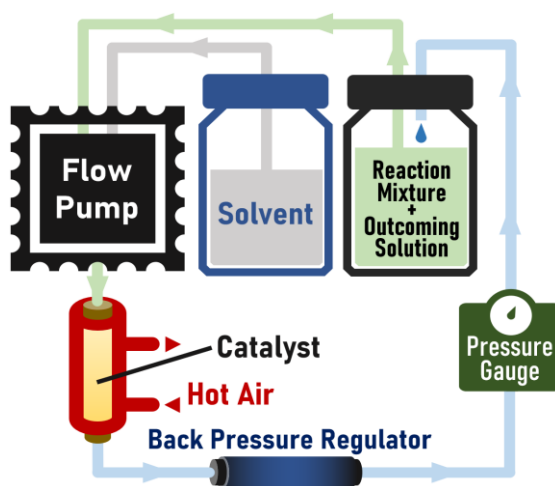


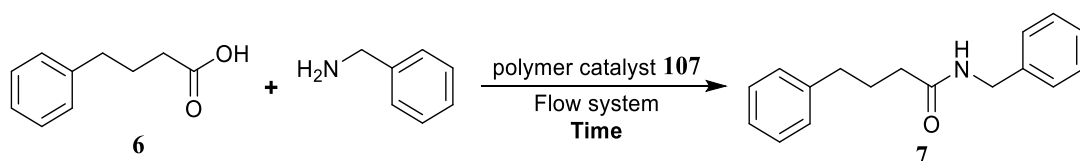
Figure 28. Designed circulative workflow

On the other hand, the flow reactor-solid phase catalyst performance reached a similar limit after a while, which was thought to be connected to the catalytic performance properties of solid phase as utilized in the flow system. To figure out such a connection, a circulating workflow was designed, as described in **Figure 28**. Notice that the outflow liquid was routed back to the starting container, making the remixed solution for a new

cycle. After 3 days of reaction and circulation as shown in **Table 9**, samples were taken at regular time points for NMR analysis, results of which are shown in **Table 10**. It can be seen that the overall amide conversion reached 40% in 2 to 3 days, (Entry 4, **Table 10**).

The overall rate of increase matched the previous test of batch reaction in **Table 9**.

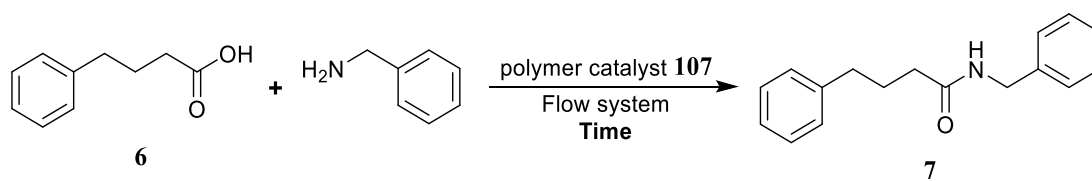
Table 10. Flow system experiment with the optimised condition.



Concentration of starting materials: 57.2 mmol/L Flowrate: 0.100 mL/min
 Column Temperature: 130 °C Back-pressure set: 75 psi

Entry	Reaction Time	Conversion / %
1	6 h	<5
2	24 h (1 day)	18
3	2 days	31
4	3 days	40

^aConversion rate determined by ¹H NMR after General Procedure I.

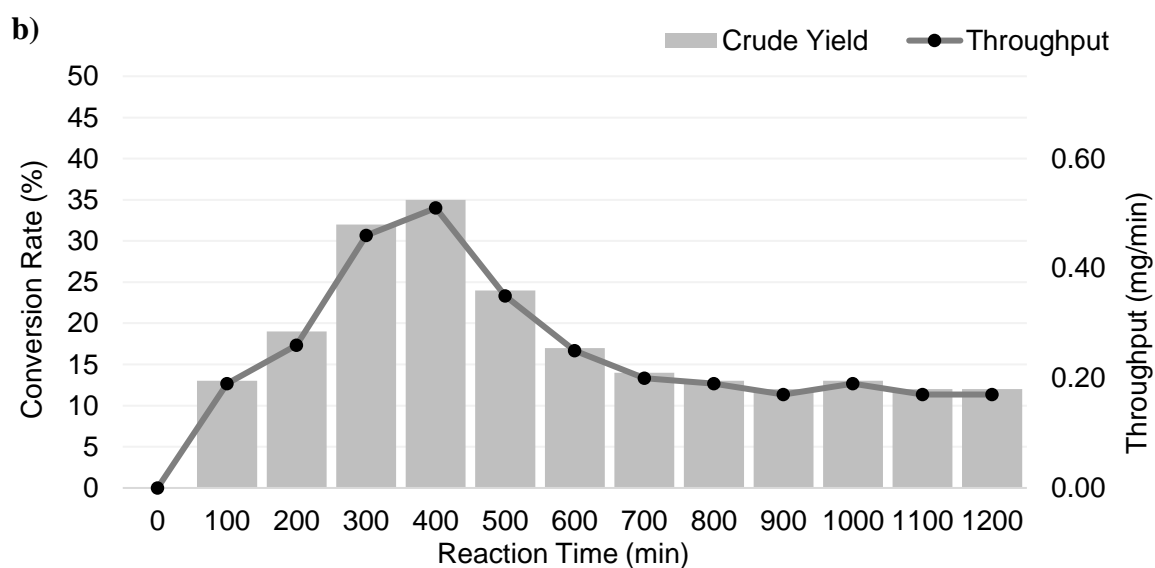
Table 11. Timescale kinetic studies of amide formation in flow.

Concentration of starting materials: 57.2 mmol/L Flowrate: 0.100 mL/min
Column Temperature: 130 °C Back-pressure set: 75 psi

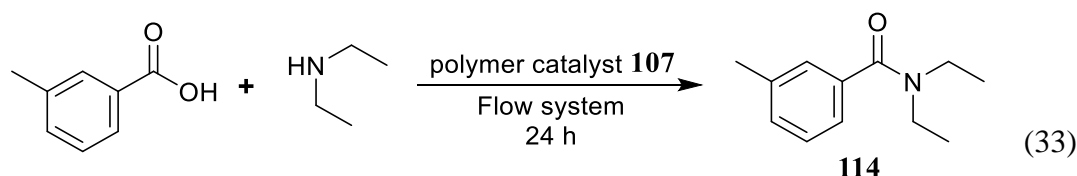
a)

Entry	Reaction Time (min)	Conversion Rate (%)	Flow Throughput (mg/mL)
1	1-100	13	0.19
2	100-200	19	0.26
3	200-300 (5 h)	32	0.46
4	300-400	35	0.51
5	400-500	24	0.35
6	500-600 (10 h)	17	0.25
7	600-700	14	0.20
8	700-800	13	0.19
9	800-900 (15 h)	12	0.17
10	900-1000	13	0.19
11	1000-1100	12	0.17
12	1100-1200 (20 h)	12	0.17

^aConversion rate determined by ¹H NMR after General Procedure H.



Therefore, extra attention was paid to the first 10 hours of the flow reaction where most positive conversion took place (**Table 9**). Each fraction was set in a subdivision of 100 minutes gap. As usual, all samples were evaporated *in vacuo* and then subjected to ^1H NMR analysis. As shown in **Table 11a**, the catalysed conversions were started from a positive rise over the first 400 minutes (Entries 1-4, **Table 11**), reaching up to 35% before dropping down a little and maintaining at a stable throughput (Entries 5-12, **Table 11**). The resulting curve is illustrated in **Table 11b**. To account for such a trend, one possible chromatographic effect was proposed, considering the mechanistic study mentioned in **Scheme 6**, as well as those irrelevant factors such as the latency due to the tubing system. At the beginning of the experiment, the polymer catalyst was saturated in toluene, bearing no activation from the formation of B-O-B bridged diacylated species through reaction with any carboxylic acid. By the time more starting material flowing into the column, the activated polymer catalyst increased in gradients. Inside the column, the generated back pressure supported the catalyst with a more concentrated solution. By the time the amide conversion fell back to a stabilised level, it eventually reached a certain stage where the highest chance of contact between polymeric boronic acids was obtained for pre-activation.



Concentration of starting materials: 57.2 mmol/L Flowrate: 0.500 mL/min
 Column Temperature: 110 °C Back-pressure set: 75 psi

Based on the previously discussed results of the reaction of phenylbutyric acid in the flow systems tests, it was believed that those conditions might be applicable in the other two, non-precipitating amine and carboxylic acid combinations, as previously tested in

Table 7. Hence starting with the catalytic amidation of benzoic acid and aniline (Entry 16, **Table 7**), the same reaction concentration of 57.2 mmol/L for the reaction mixture was prepared for use in flow at 0.100 mL/min. Unfortunately, no conversion was found after 24 h of running through the flow reactor (Entries 16, **Table 7**). Also, the same methodology was then employed for the reaction of *m*-toluic acid and diethylamine under identical conditions (Equation 33) at a flow rate of 0.100 mL at 130 °C, however, again, no product was generated. Hence, although flow systems can indeed be used to carry out amidation reactions using a heterogeneous supported boronic acid catalyst system, this type of application is far from routine and clearly, a considerable amount of further development is required to make such processes of general use.

2.6 Conclusion

To conclude, a new heterogeneous catalytic direct amide formation was developed through co-polymerisation of styrene with styrylboronic acid. Compared to the equivalent homogeneous catalysts, the use of this robust polystyrene-based catalyst **107** as a solid phase system in direct amidation reactions was found to show high catalytic efficiency and generally good substrate tolerance under a minimal 5 mol% loading. The reactivity of the catalyst could be examined by step-wise reaction with a carboxylic acid, followed by amine addition, which could be followed *in situ* using ReactIR and ¹¹B SSNMR which indicated the boron interconversions at different stages and largely as predicted for a system based around a B-X-B key catalytic structure.⁴⁷ Dependable performance was observed as well as excellent recyclability and reusability, also enabling its use in a flow system. Further

investigations could involve further optimisation and use in flow, especially including the potential preparative flow systems studies and broader substrate scope applications. However, for future applications and wider substrate utility, the precipitation of ammonium carboxylate salts issue will need to be solved. The flow-based reaction does proceed to a steady state after long reaction running times, but this has only been demonstrated with a single reaction system to date. Nevertheless, the basic reaction characteristics have been exemplified and the proof of concept demonstrated.

3. Bifunctional catalysis of asymmetric nitro-Michael reaction

In this section, an optimised B-N bifunctional catalytic system, developed from esterified a homoboroproline analogue was designed and applied in asymmetric nitro-Michael addition. Previous work has shown that such compounds can catalyse the formation of a reactive enamine system which can then form transition states of type **115** stabilised through stereoelectronic effects resulting in the desired stereoselective outcome, as mentioned in the previous report for the enantioselective enamine-based aldol reaction (**Figure 29**).¹⁴⁸

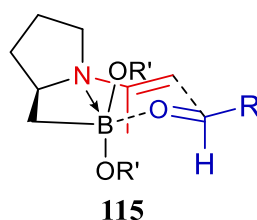


Figure 29. Proposed transition state **115** in B-N bifunctional asymmetric aldol reaction

Barbas *et al.*¹⁹⁹ reported the use of *L*-proline for the asymmetric nitro-Michael addition reaction, with the idea of using the carboxylic acid group to assist the reaction through electrophilic activation *via* hydrogen-bonding (**Figure 30**). However, although catalytically competent, proline failed to affect an efficient asymmetric reaction, and therefore, it was of interest to us to see if a homoboroproline **85** (and its ester analogues)-catalysed asymmetric nitro-Michael addition might be superior. The starting point for this project was to first develop an improved synthetic pathway to the homoboroproline catalyst **85** and then examine its application in the asymmetric nitro-Michael addition reaction. The original reaction process to access homoboroproline²⁰⁰ has several steps which were unreliable and provided varying product yields, especially upon scale-up, and therefore, the overall conversion from starting materials products was optimised and it was then

employed in the asymmetric nitro-Michael addition with a view to develop good enantioselectivity and high catalyst reactivity, especially through tuning reactivity *via* diol esterification.

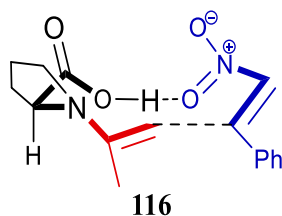
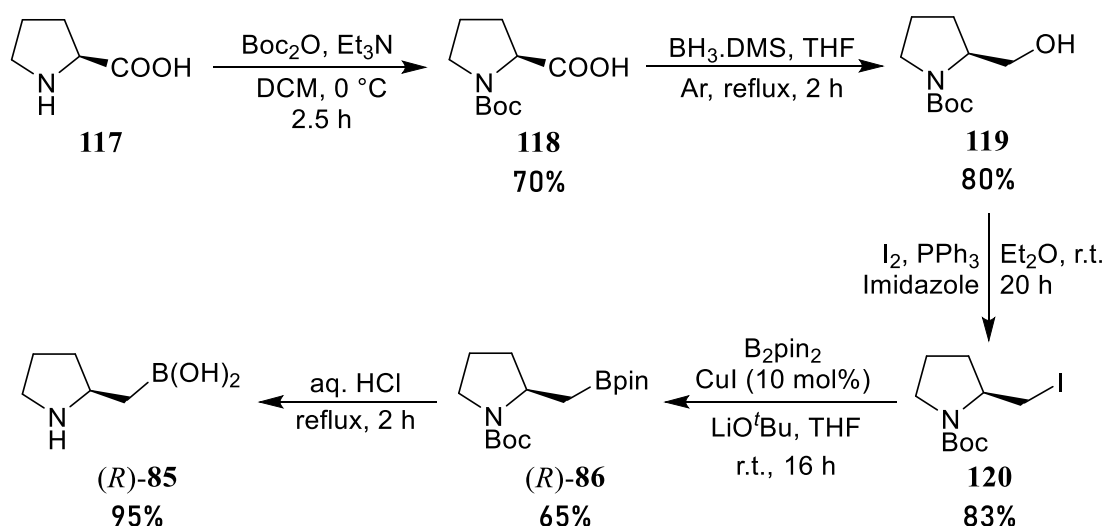


Figure 30. Proposed transition state **116** of proline-based asymmetric nitro-Michael reaction.

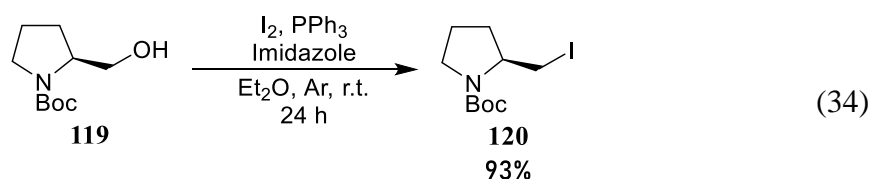
3.1 The synthesis of proline-based catalyst

An updated and robust synthetic pathway to the proline-based catalyst needed to be developed at the outset of this project, and this needed to be based on that previously developed in our group, i.e. as described as outlined in **Scheme 16**.²⁰⁰ Starting with commercially accessible *L*-proline, it was essential to protect the amine prior to a reductive FGI process on the carboxylic acid. *N*-Protection with Boc₂O gave 70% *N*-Boc protected proline **118**, which was followed by borane reduction to the primary alcohol **119** at 80% yield. Treatment with iodine, triphenylphosphine and imidazole in ether, about 83% prolinol **119** was converted to the pyrrolidinyl iodide **120**. Eventually, after great efforts on the testing of a range of possible lithium-halogen exchange reaction conditions, metal-complex catalysed and metal-free catalysis,²⁰⁰ a copper-induced borylation produced a 65% yield of pyrrolidinyl pinacol-boronic ester (*R*)-**86**.



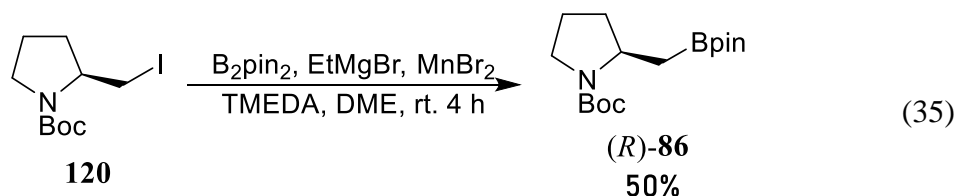
Scheme 16. Reported synthetic pathway to catalyst (*R*)-85

Based on the reported procedures in **Scheme 16**, a few updates were developed for improved and reproducible preparation of catalyst (*R*)-85. Considering the heterogeneous iodination of prolinol **119**, an improved procedure was employed (Equation 34). In this step, the use of a mechanical stirrer was critical to improving the overall reaction performance. By modulating a better stirring effect, introduction of Ar flow, and use of standard column chromatography, the reaction to **120** eventually reached an increased conversion by 93%.



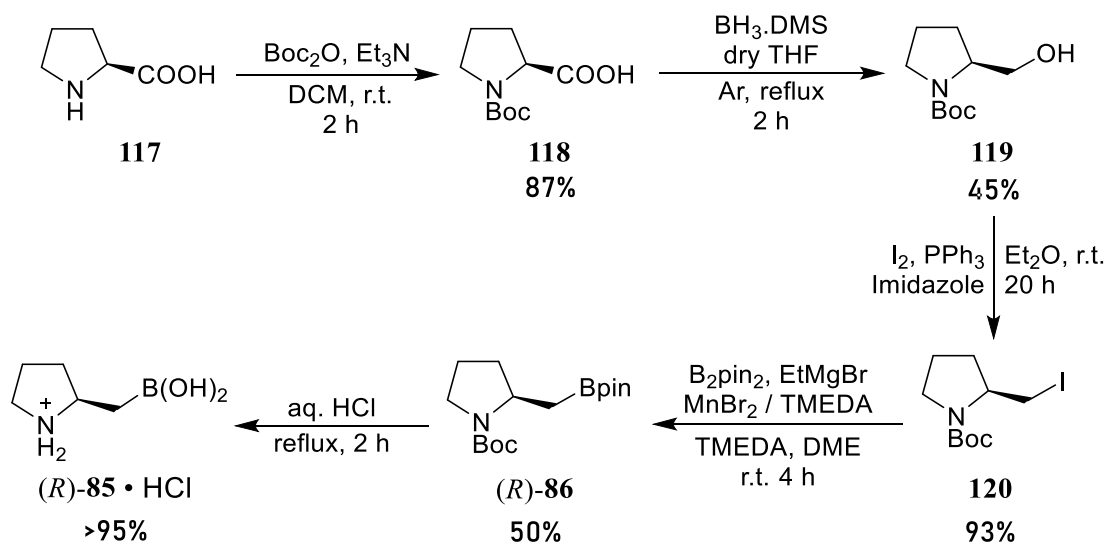
Apart from those methods mentioned in the previous research,²⁰⁰ later literature suggested that a series of novel metal-catalysed borylation of primary alkyl halides might offer improved reliability and conversion for the transformation of iodide **120** to the corresponding boronate (*R*)-86.²⁰¹⁻²⁰⁶ A new manganese (II) catalysed borylation was initially tested for this purpose.²⁰⁷ Manganese bromide was employed in a Mn(II)/TMEDA

catalysed borylation together with B_2pin_2 and $EtMgBr$ to afford an efficient, mild cross-coupling, which after only 4 h converted the primary iodide **120** to the corresponding boronate (*R*)-**86** (Equation 35).



This initial attempt included a 5 mol% $MnBr_2$ and 1 mol% TMEDA catalyst loading dissolved in DME giving a 39% yield after 4 hours. When the manganese complex to TMEDA ratio was adjusted to 1:1 (both 5 mol%), 50% pure prolinyl borylate (*R*)-**86** was produced *via* silica gel chromatography, exhibiting a better catalytic performance. Although, there was not such a dramatic increase of overall conversion, more importantly, the entire process was clean and easily worked up reaction. TLC showed a clean reaction mixture of iodide **120** and product (*R*)-**86** alone. More than 38% of starting material was recovered pure and there was no sign of any by-products being produced.

After isolating boronate ester (*R*)-**86**, treatment with acid achieved efficient hydrolysis and deprotection to provide catalyst (*R*)-**85** as a sticky clear liquid. 1H NMR and HRMS all supported the clean formation of (*R*)-**85**, with the ^{11}B NMR showing a single 30.8 ppm shift indicative of the boronic acid (see Experimental Section). The updated overall synthesis of catalyst (*R*)-**85** is outlined as **Scheme 17**, was suitable for routine and reproducible batch preparations.



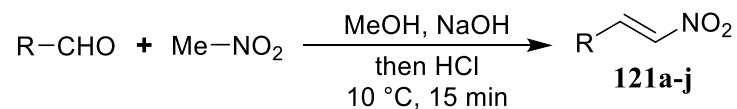
Scheme 17. Updated synthetic pathway to catalyst (R)-85

3.2 Preparation of racemic nitro-alkene Michael adduct

Before employing the catalyst **85** in catalytic asymmetric nitro-alkene Michael addition reactions, we firstly needed to prepare the require nitroalkenes and racemic nitro-alkene Michael addition product standards in order to develop the necessary analytical methods for reaction analysis, especially chiral HPLC. The preparation of racemic nitro-alkene Michael addition products was reported by Barbas *et al.* as part of their attempts to achieve catalytic asymmetric control using *L*-proline.¹⁹⁹ Therefore, we were easily able to adopt this procedure using various nitroalkenes. However, it is also noteworthy that most β -nitrostyrene analogues are not commercially available and therefore needed to be prepared. Fortunately, the synthesis of such series of nitro-alkenes has been reported,^{208, 209} including research by the Zhang group who employed a Henry-type route.²¹⁰ Hence,

following their synthetic strategy, β -nitrostyrene substrates were readily accessed, as shown in **Table 12**.

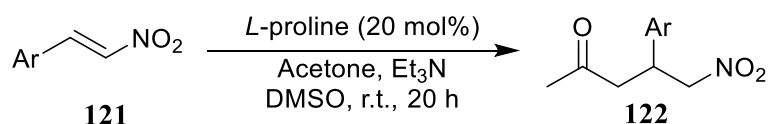
Table 12. Preparation of substituted β -nitrostyrene analogues.



Entry	R	Product	Yield ^a / %
1	<i>p</i> -F-Ph	121a	89
2	<i>o</i> -Cl-Ph	121b	99
3	<i>o</i> -Br-Ph	121c	95
4	<i>p</i> -Br-Ph	121d	99
5	<i>o</i> -CF ₃ -Ph	121e	49
6	<i>p</i> -CF ₃ -Ph	121f	50
7	<i>m</i> -OMe-Ph	121g	56
8	<i>p</i> -OMe-Ph	121h	46
9	Et	121i	44
10	<i>i</i> Pr	121j	92

^aReaction carried out under General Procedure J.

After making a series of β -nitrostyrenes, the formation of the racemic Michael adducts was investigated, with results shown in **Table 13**. The reaction was conducted using 5 mol% *L*-proline using acetone as nucleophile, providing good yields, matching those reported in the literature.¹⁹⁹ Indeed, as expected, none of the acetone Michael addition reactions to the various nitroalkenes exhibited any stereoselectivity, as shown by chiral HPLC analysis.

Table 13. Preparation of racemic nitro-Michael adducts.

Entry	Ar	Product	Yield ^a / %
1	Ph (121k)	122k	79
2	<i>p</i> -F-Ph (121a)	122a	81
3	<i>o</i> -Cl-Ph (121b)	122b	80
4	<i>o</i> -Br-Ph (121c)	122c	88
5	<i>p</i> -Br-Ph (121d)	122d	86
6	<i>o</i> -CF ₃ -Ph (121e)	122e	83
7	<i>p</i> -CF ₃ -Ph (121f)	122f	80
8	<i>m</i> -OMe-Ph (121g)	122g	86

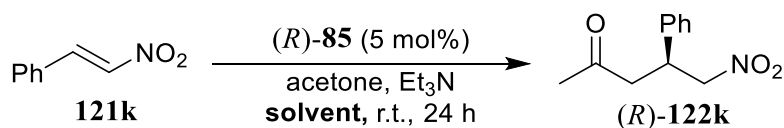
^aReaction carried out under General Procedure K.

3.3 Solvent screening of reaction condition

With the substrates and racemic products in hand, reaction conditions optimisation began with the solvent screening first. β -Nitrostyrene was chosen as the first test substrate for this purpose, by it to the catalyst solution under r.t. in the various solvent, in the presence of acetone. This initial reaction screening was carried out in various solvents without *in situ* water removal or any special drying methods, though we were aware that the hydration levels in these types of amine-ketone condensation reactions deriving enamines. Are particular prone to major effects based upon the amount of water present in the reaction mixture, as noted by the Ley group in related proline-based aldol reactions,²¹¹ and not dissimilar to our own findings.^{200,212-214} However, these undried reactions were reasonably efficient and the resulting nitro-alkene Michael adducts were isolated by column

chromatography and examined by chiral-HPLC to determine the enantioselectivity. The results are shown in **Table 14**.

Table 14. Solvent test of catalytic nitroalkene-Michael addition.



Entry	Solvent	Yield ^a / %	e.e. / %
1	Acetone	63, 33 ^b	15, 30 ^b
2	Toluene	0, 5 ^b	—, 5 ^b
3	2-Me-THF	12, 35 ^b	37, 40 ^b
4	DMF	18, 20 ^b	8, 16 ^b
5	DMSO	14, 20 ^b	0, 0 ^b
6	MTBE	0	—
7	DCM	0, 29 ^b	—, 5 ^b
8	CHCl ₃	0, 15 ^b	—, 5 ^b
9	EtOH	95, 95 ^b	35, 35 ^b
10	MeOH	39, 15 ^b	33, 36 ^b
11	ⁱ Pr-OH	34	33
12	THF	48	14
13	Acetonitrile	44	5
14	ⁱ Pr-CN	15	10
15	1,4-Dioxane	41	20
16	DME	41	24

^aUnless otherwise specified, reaction carried out under General Procedure L ^bReaction carried out with addition of activated 3 Å molecular sieves (see General Procedure M)

The first attempt suggested over 63% of product (*R*)-**122k** was generated in pure acetone environment, which exhibited a more satisfying performance (Entry 1, **Table 14**). Notice that substrates expressed poor solubility in toluene, leading to an understandable trace conversion as predicted (Entry 2, **Table 14**). Surprisingly, despite the low conversion, reaction in 2-Me-THF appeared with a relatively better enantioselective performance,

making 37% e.e. (Entry 3, **Table 14**). Other results varied greatly from low reactive production (for DMF, DMSO, MTBE, DCM, CHCl₃, Entries 4-8 respectively, **Table 14**) to high conversion, such as in ethanol (Entry 9, **Table 14**).

Table 15. Solvent test with *in situ* esterified boronate with (*S,S*)-hydrobenzoin.

$(R)\text{-}121\text{k} \xrightarrow[\text{acetone, Et}_3\text{N, 4 \AA MS}]{(R)\text{-}85 (5 \text{ mol}\%), (S,S)\text{-hydrobenzoin (5 mol\%)}} (R)\text{-}122\text{k}$

Entry	Solvent	Yield ^a / %	e.e. ^b / %
1	Acetone	99	44
2	2-Me-THF	89	54
3	Toluene	99	49
4	DCM	99	36
5	CHCl ₃	80	35
6	DMF	50	20

^aReaction carried out under General Procedure N ^bE.e. determined by chiral-HPLC. AS-H, 1.0 mL/min flow rate, hexane: EA = 60:40

Therefore, we turned to focus on the possible solvent effects that contributed to such findings. The impact of *in situ* solvent drying on the catalysis by the addition of 3 Å molecular sieves was tested. Indeed, results suggested its necessity in this stage, as could be found in some cases that witnessed an increase. Interestingly, use of DMSO, EtOH and MeOH did not bring much of an advantage over the previous attempt (Entries 5, 9 and 10, **Table 14**). In the case of acetone (Entry 1, **Table 14**), sacrifice in conversion by half (63 to 33%) led to doubling the e.e. (15 to 30%), as a result showing the effect by water modulating the catalytic behaviour during the process. Similar doubling effect was observed in DMF reaction, with a better conversion (Entry 4, **Table 14**). Notice that the drying procedure did improve the catalysis in some non-reactive solvents including toluene, DCM and chloroform (Entries 2, 7 and 8, **Table 14**). Of all these examined solvents, the highest e.e. was observed in the reaction with 2-Me-THF, giving 3 times nitroketone adduct over the previous outcomes, together with 40% e.e. of stereoselectivity (Entry 3, **Table 14**).

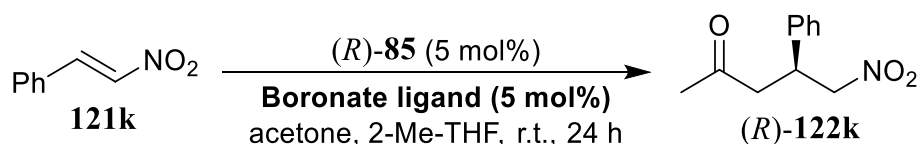
It was encouraging to see such positive solvent effect on both conversion and e.e. indicative of a better performance under use of *in situ* boronate esterification with substituted diol. The functionality of interactive boronic acid-diol complexation has been learnt early for modulation of catalytic environment.²¹⁵ The reservable coupling reaction with boronate ester helped tuning of reagent pK_a while adapting to different substrates. More importantly, chirality of the catalyst could be adjusted and solidified by boronate esterification, as exemplified by Okano's report employing chiral hydrobenzoin coupling.²¹⁶ Further to the reaction optimisation with water properly removed, the results were showed in **Table 15**.

Notice that most enantiomeric excesses did not reach 37% or higher under previous conditions. The performance was impressive after the addition of (*S,S*)-hydrobenzoin. Modulation of catalyst towards a good versatility had a great impact on the reactivity. It was clear that pure acetone gave readily increase in both yield and e.e. (Entry 1, **Table 15**). But in comparison, the most solid breakthrough was found in the 2-Me-THF system, showing the highest e.e. (54%) with stoichiometric substrate addition, as well as a quantitative conversion to the nitroketone adduct (*R*)-**122k** (Entry 2, **Table 15**). Besides, there was an encouraging observation in those non-reactive systems including toluene, DCM and chloroform, showing almost full conversion (Entries 3-5, **Table 15**). Indeed, there was not too much of improvement in the system with DMF, despite the yield doubling presumably by the coordinating effect from (*S,S*)-hydrobenzoin (Entry 6, **Table 15**).

3.4 Introduction of ligands to catalysed nitro-Michael addition

With the best solvent system identified and the effect of diol esterification of homoboroproline (*R*)-**85** using hydrobenzoin demonstrated, we further tested the catalytic nitro-Michael addition in 2-Me-THF of other potentially effective diol systems, in order to probe the Lewis-acidity at boron further. The results are shown in **Table 16**.

Table 16. Diol screening for *in situ* boronate esterification.

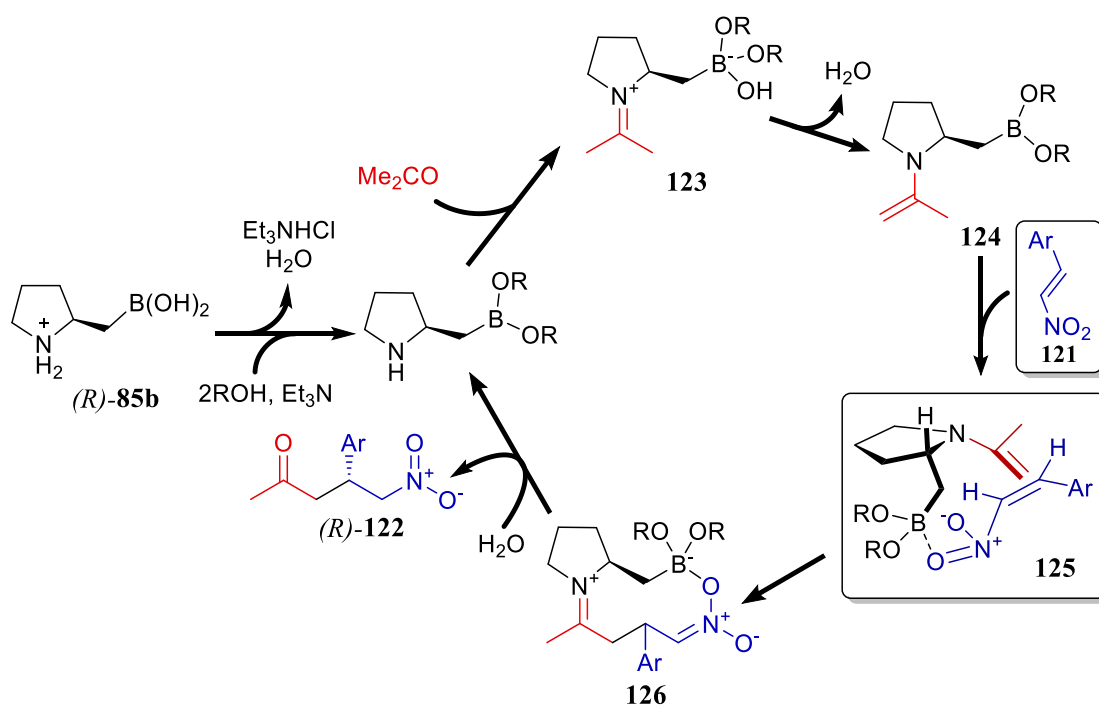


Entry	Ligand	Yield ^a / %	e.e. ^b / %
1	(<i>S,S</i>)-(-)-Hydrobenzoin	89, 99 ^c	54, 52 ^c
2	(<i>R,R</i>)-(+)-Hydrobenzoin	71	57
3	Benzilic acid	43	42
4	2,2-Dihydroxybiphenyl	14	56
5	1,2-Dihydroxybenzene	11	48
6	Tetrabromocatechol	32	6

^aCarried out under General Procedure N, using the stipulated diol in place of hydrobenzoin. ^bE.e. determined by chiral-HPLC. AS-H, 1.0 mL/min flow, hexane: EA = 60:40 ^cReaction conducted at 55 °C.

The data in **Table 16** suggests variable effects during the catalytic process of different esterification systems. It is firstly noteworthy that the chirality of the hydrobenzoin had little impact upon the e.e. and absolute stereocontrol, i.e. there was no sign of any double diastereoselectivity effects. As expected from previous work in aldol catalysis, the diol ligand chirality effect acts predominantly through sigma-bond electronic tuning effects, i.e. tighter Lewis-acidic activation of the aldehyde substrate, now extended to binding a nitro-function.^{208,220-222} This explains the similar catalytic performance

observed from both (*S,S*)- and (*R,R*)-hydrobenzoin diols, resulting in 99 and 71% isolated yields, and 54 and 57% e.e., respectively (Entries 1 and 2, **Table 16**). The potential of a system that might form an acyloxy cyclic boronate ester (Entry 3, **Table 16**) through benzylic acid showed only moderate conversion and e.e. Cyclic phenol-derived boronate ester analogues of **86** (Entries 4 and 5, **Table 16**) gave slower reactions and low to moderate e.e., *i.e.* not as good as hydrobenzoin. It may be the case that boronate esters derived from 2,2-dihydroxybiphenyl and 1,2-dihydroxybenzene are strained and may not be stable under the reaction conditions (Entries 3 and 4, **Table 16**), and certainly, using an even more electron-deficient multi-halogenated catechol also resulted in poor conversion, albeit in improved yield compared to Entries 4 and 5, but at the cost of lowering the e.e. (Entry 6, **Table 16**). There was another attempt to the stereoselective synthesis under higher catalytic loading. It suggested an improved conversion due to the increased amount of reactive intermediate, the overall enantioselectivity remained unchanged (Entry 1, **Table 16**).

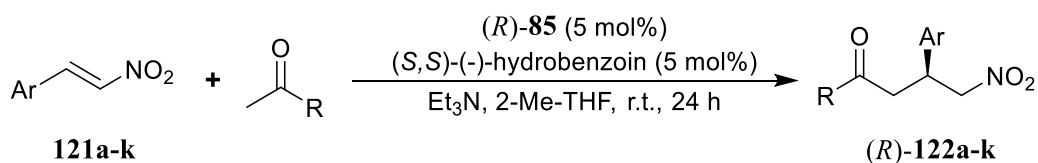


Scheme 18. Proposed mechanistic cycle of catalytic bifunctional asymmetric nitro-Michael addition catalysed by (*R*)-**85**.

Considering the solvent and tuning effects from using *in situ* hydrobenzoin boronate ester formation of catalyst **86**, a mechanism can be proposed involving a catalytic cycle as shown in **Scheme 18**. As discussed, the presence of an enamine analogue **124** of catalyst (*R*)-**85** is required, formed *via* iminium species **123**, which is also the ketone activation step; a step which is the same whether the catalyst is diol esterified or not.^{208, 220-222} As discussed above, a proper dehydration procedure helps maintain the reactivity through the whole process, both of enamine formation and diol esterification. Furthermore, the introduction of nitro-styrene substrates results in strong coordination through Lewis-acid interactions with the boronate centre, forming the transition state **125** where the desired enantiomer is favoured through the mode of addition graphically shown in **Scheme 18**. This orientation triggers the production of nitro-Michael adduct **122**, potentially with high selectivity, and with concomitant re-cycling of the boronate catalyst after iminium ion hydrolysis.

3.5 Substrate scope of the catalysed nitro-Michael addition

After carrying out reaction screening, the optimised conditions were ready for a step further. Using homoboroproline (*R*)-**85** as an enamine catalyst, the substrate scope was conducted using 2-Me-THF as solvent with (*S,S*)-hydrobenzoin to provide *in situ* esterification of the catalyst boronic acid. After a pre-activation process treating with the diol, different aryl-nitroalkenes were used as electrophiles, as well as two additional methyl ketone nucleophiles. The results are summarised as **Table 17**.

Table 17. Substrate scope under optimised reaction condition.

Entry	Ar (nitroalkene)	R-	Yield ^a / %	e.e. / %
1	Ph (121k)	Me-	89	54
2	<i>o</i> -CF ₃ -Ph (121e)	Me-	99, 99 ^b	67, 65 ^b
3	<i>m</i> -OMe-Ph (121g)	Me-	80, 83 ^c	8, 8 ^c
4	<i>o</i> -Cl-Ph (121b)	Me-	99	55
5	<i>o</i> -Br-Ph (121c)	Me-	99, 46 ^b	35, 30 ^b
6	<i>p</i> -Br-Ph (121d)	Me-	99	41
7	<i>p</i> -F-Ph (121a)	Me-	67	20
8	<i>p</i> -CF ₃ -Ph (121f)	Me-	99	51
9	Ph (121k)	Ph-	0, 0 ^c	—
10	Ph (121k)	ⁱ Pr-	0, 0 ^d	—

^aUnless otherwise specified, reaction carried out according to General Procedure N, using the stipulated diol in place of hydrobenzoin. ^bReaction carried out at 55 °C. ^cReaction left for a prolonged 48 hours' time.

Results in **Table 17** suggested a broad substrate tolerance with up to 8 different aryl-nitroalkene substrates were involved in the test, all of which exhibited high conversion after 24 hours. Based on the proposed transition state and the catalytic cycle in **Scheme 18**, it would be expected that a strong electron-withdrawing group, such as CF₃ (i.e. **121e** and **121f**) should enhance nucleophilic attack at the α -aryl alkene carbon, improving the enantiocontrol. The TLC results suggested different chemokinetic performance of the different substrates. Reaction with *ortho*-trifluoromethyl nitroalkene **121e** approached completion after 12 hours, *versus* the other halogenated nitroalkenes. Most reactions reached 99% conversion after 24 hours, among which the *ortho*-trifluoromethyl nitroalkene **121e** stood out by 13% over the general phenyl system (Entries 1 and 2, **Table 17**). Apart from the electronic properties that most substrates have in common, there may be some

expected steric effects, in which case may be beneficial to this type of reaction. As might be predicted with electron donor systems, i.e. a methoxy substituent, the e.e. was moderate, plus the reaction efficiency had dropped even over a prolonged 48 hours reaction time (Entry 3, **Table 17**). The catalytic performance did not strictly follow simple electronic and positioning effects, as demonstrated by the halogen-substituted nitroalkenes (**121a-d**) with the reaction of *ortho*-chloro-nitroalkene **121b** generating 55% e.e. in the nitro-Michael adduct in 99% yield (Entry 4, **Table 17**), whereas the bromo- and fluoro-substituted systems showed variable conversion, and lower e.e.s (Entries 5, 6 and 7, **Table 17**). In addition, with respect to the reaction with bromo-nitroalkene, attempts to push them further by heating up turned to be unsuccessful, showing a similar conversion *versus* room temperature (Entry 5 and 6, **Table 17**). Interestingly, there was no significant change in conversion when this reaction was carried out at 55 °C, with only a slight drop in e.e. (67 to 65%, Entry 7, **Table 17**). Indeed, the absolute stereoselective control of the resulting adducts could still be explained *via* proposed transition state in **Scheme 18**, i.e. a 10-membered Lewis-acid-nitroalkene complex.

In terms of other methyl ketone reactivity, the other methylketone systems examined did not show the high levels of reactivity observed with acetone, as evidenced by Entries 2 and 8, **Table 17**. Hence, acetophenone showed zero reactivity, providing no adduct (Entry 9, **Table 17**). Use of isopropyl-methylketone (Entry 10, **Table 17**) showed some low reactivity, but no enantiocontrol.

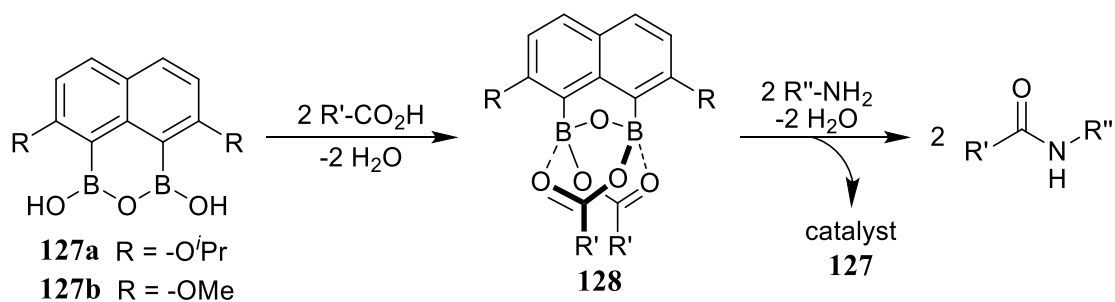
3.6 Conclusion and future outlook

To summarise, a new B-N bifunctional catalyst has been developed for asymmetric nitro-alkene Michael addition. Under optimised reaction conditions, up to 67% enantioselectivity was observed and in high conversion, by employing the homoboroproline catalyst (*R*)-**85**. Enhancement in reactivity, both conversion and e.e. was enabled through suitable diol-esterification, resulting in an efficient methodology for the asymmetric nitro-alkene Michael addition using acetone.

Future applications will be mainly focusing upon improving catalytic reactivity through greater variation and decoration of catalyst (*R*)-**85** to adapt its reactivity to a wider range of substrates. Meanwhile, to avoid the creation of diastereoisomeric products to date, only methyl ketones have been examined, hence, further applications examining regioselectivity effects in more substituted systems is required as well as wider diastereoselective performance possible by increasing the ketone diversity.

4. Kinetic resolution of asymmetric amide formation

Based on the mechanistic studies on the direct amide formation by a reactive B-X-B bridged intermediate species, as outlined in **Scheme 6**,⁴⁷ as well the synthesis of naphthalene-based 2,7-dialkoxy-1,8-disubstituted systems reported by our group,¹⁹¹ there have been few efforts to access diboronic containing compounds to use as potential direct amidation catalyst systems. Research from one of our previous group members involving unpublished results suggested a potential synthetic pathway to the 2,7-diisopropoxy-1,8-diboronic ester compounds **127a**.²¹⁷ From this evidence, a dimerised boronic ester **128** was formed after an acyl activation process using stoichiometric quantities of carboxylic acid substrate (**Scheme 19**). Given this prior work on the formation of the reactive B-O-B bridged intermediates, it was predicted that this system should present catalytic behaviour, however, it was less obvious how such a system could be developed to have chirality introduced due to the rigid conjugated naphthalene backbone. Therefore, it was interesting to look more widely and to see if there were suitable chiral backbones that could carry such diboronic acid functions that could react intramolecularly to form the necessary B-O-B system, which together with a chiral framework would potentially enable kinetic differentiation of the rate of amide conversion from racemic enantiomers of either a chiral amine or carboxylic acid.



Scheme 19. Proposed catalytic cycle with a diacylation process

Compared to catalyst **127**, a more structurally flexible biphenyl catalyst **129** was envisaged as having the ability to form a suitable bridged boronate anhydride system rather than the parent diboronic acid, i.e. as drawn. Our aim, therefore, was to verify if **129**^a was a competent amidation catalyst, and if so, extrapolate to the chiral analogue, i.e. a binaphthyl system of type **108** (**Figure 31**). The fact that such systems have a free rotatable σ -bond allows twisting between the aromatic rings, which should not only enable increased stability in the generation of bridged B-O-B intermediate but also allow flexing of the framework as the amidation reaction proceeds. Of course, the biphenyl catalyst **129** is not chiral, and therefore, in order to introduce asymmetric control *via* a system related to biphenyl, the corresponding binaphthyl diboronic ester catalyst **108** (**Figure 31**). would be expected to be an attractive catalyst target, and potentially able to exercise kinetic resolution effects in amidation reactions of either racemic amine or carboxylic acids

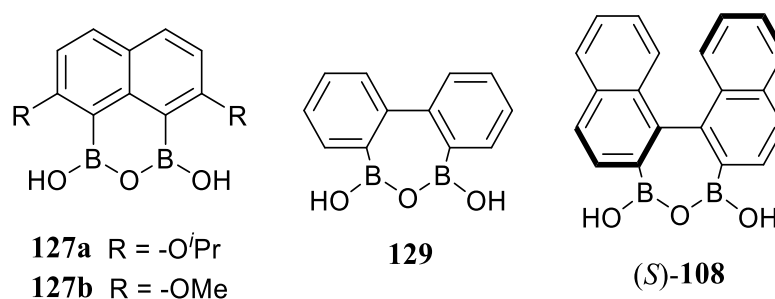


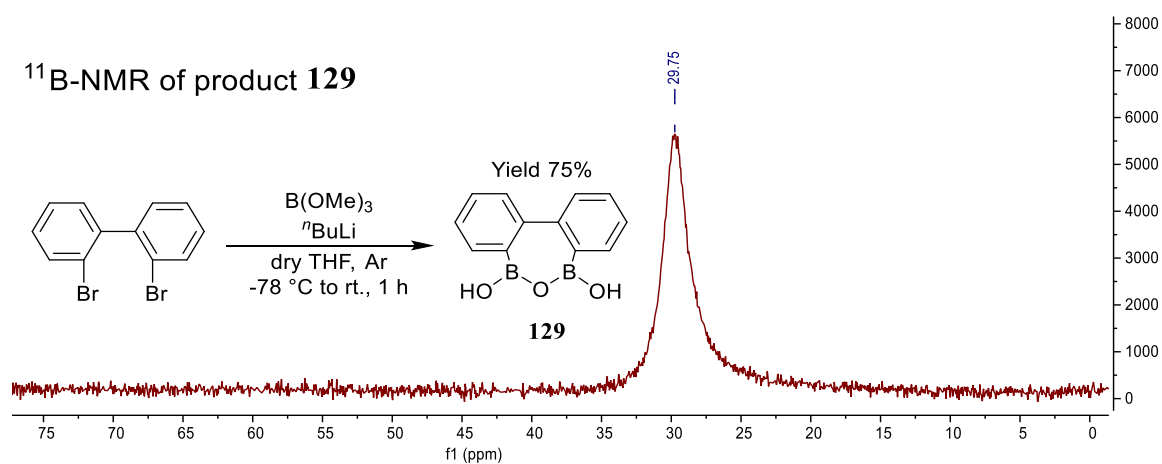
Figure 31. Diboronic Acid Derived Analogues

Thus, this section mainly discusses the synthesis and application of catalyst **129** and **108**, together with their initial applications on the catalytic amidation reaction performance and kinetic resolution of asymmetric *N*-acylation reactions.

^aThe use of biphenyldiboronic acid catalyst **129** was reported for amidation in the process of this work being conducted.²¹⁸

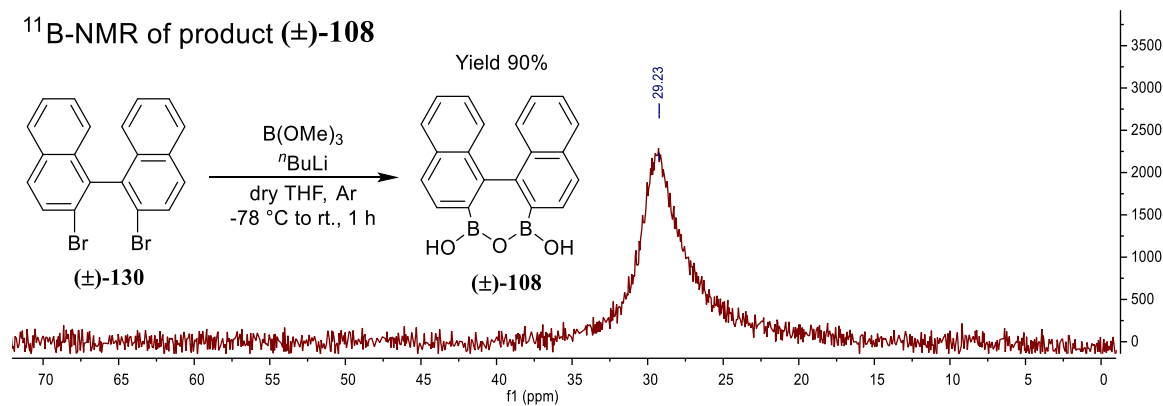
4.1 Preparation of racemic catalyst 108

Based on the synthetic strategy mentioned in earlier reports,²¹⁷ we reproduced the synthesis of catalyst **129** using the same conditions for lithium-halogen exchange (LHE) reaction starting with 2,2'-dibromobinaphthyl and the results of which are outlined in **Scheme 20**. Notice that ⁿBuLi was an excellent lithiation reagent, contributing to a fast overall bromine to boryl substitution to give the desired product **129** in 75% yield. The results were reinforced from ¹¹B NMR which identified a clear signal at δ 30 ppm, indicative of a single boronate species as expected.



Scheme 20. LHE initiated borylation to give racemic product **129**.

Following the same procedure as above, racemic 1,1'-diboronate ester species (\pm)-**124** was generated from commercially available 1,1'-dibromo binaphthalene (\pm)-**108**, the results of which are outlined as **Scheme 21**. Recrystallisation gave 90% of the desired product **108**. ¹¹B NMR showed a single clear peak at δ 29 ppm, likely indicative of the boronate anhydride species which matched that of the biphenyl boronate product **129**.²¹⁷



Scheme 21. LHE initiated borylation to give racemic product (±)-**108**

However, while the highly successful diborylation of dibromide **130** was readily confirmed by single crystal X-ray diffraction analysis (**Figure 32**), the actual structure of **108** observed was an intermolecularly formed boroxine analogue. Whether compound **108** exists as drawn in **Scheme 21**, or as the boroxine system shown in **Figure 32** is not known at this point. The process of recrystallisation and drying for X-ray analysis could lead to the condensed hexameric binaphthalene diboronate system observed, though we have shown in the presence of carboxylic acids and amines,⁴⁷ boroxines are catalytically competent so catalyst **108** would be expected to equilibrate to a reactive form once exposed to amidation conditions. In terms of the crystal structure (**Figure 32**), six binaphthyl units are linked through the boroxines structures, involving the twelve naphthalene boronates acting as linkers, constructing a remarkable hexameric bridged structure. It is also noteworthy that this structure exists as the only diastereoisomer, i.e. made up of only one enantiomer of **108** (*R* in this case), strongly suggesting that the compound crystallises readily in this form and that each crystal is likely to consist of either enantiomeric form, and we happened to pick an "*R*"-derived form in this case. Considering the complexity of the hexamolecular complex shown in **Figure 32**, it is probably not surprising that it crystallises in this homochiral manner.

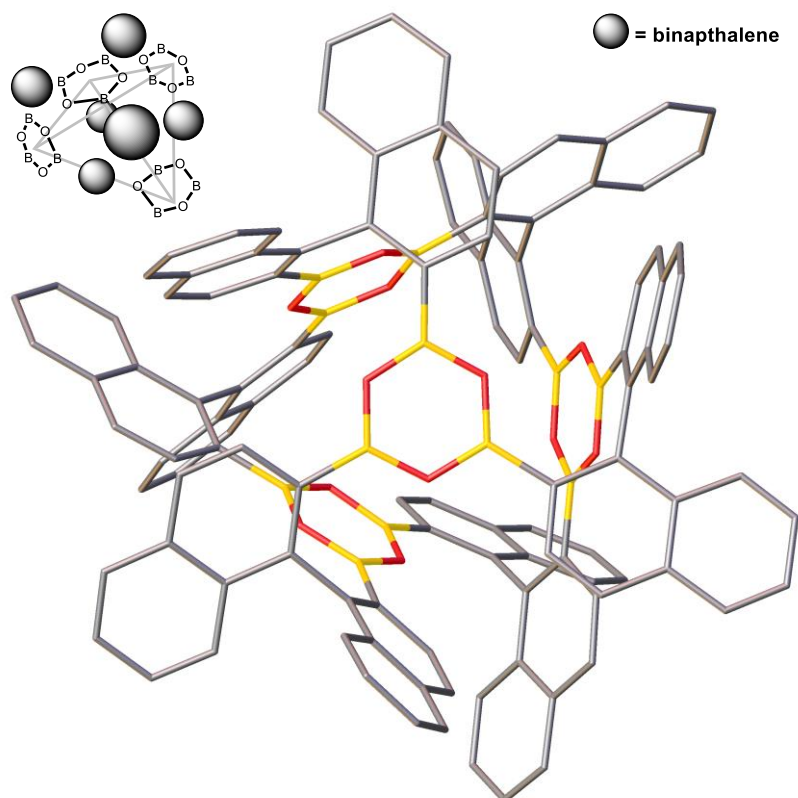
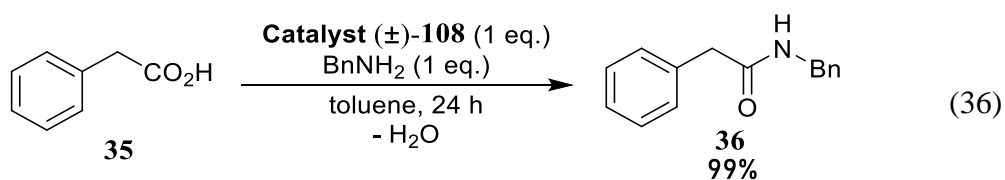


Figure 32. Hexameric structure of (±)-**108** confirmed by XRD analysis

4.2 Homogeneous direct amidation catalysed by (±)-**108**



The catalytic behaviour of racemic catalyst **108** was examined in preliminary experiments, i.e. involving the reaction of phenylacetic acid with benzylamine (Equation 36). A stoichiometric amount of starting materials were employed in the system, and over

99% amide formation was observed after 24 h reflux. Further studies on the process of phenylacetamide formation were suggested by NMR, the results of which were shown in **Figure 33**. The initial catalyst, representative of caged boroxine species was identified at δ 30 ppm chemical shift (**Figure 33a**). immediately after dropping the carboxylic acid, catalyst **108** got activated by an acylation process, indicated as acylated boronated peak at δ 17 ppm (**Figure 33b**). Notice that δ 30 peak did not disappear fully even after a prolonged time with stoichiometric amount of carboxylic acid, presumably by an interconversion equilibrium between the boron species. Next, it was clear to observe the process triggered by the addition of amine, by the time conversion from acyl boronate to the tetrahedral boronate species (indicated at δ 0 ppm) took place (**Figure 33c**). With consumption at δ 17 ppm, the shoulder peak at δ 30 ppm kept dropping to vanish to a point it vanished, indicative of catalyst **108** being activated fully (**Figure 33d**).

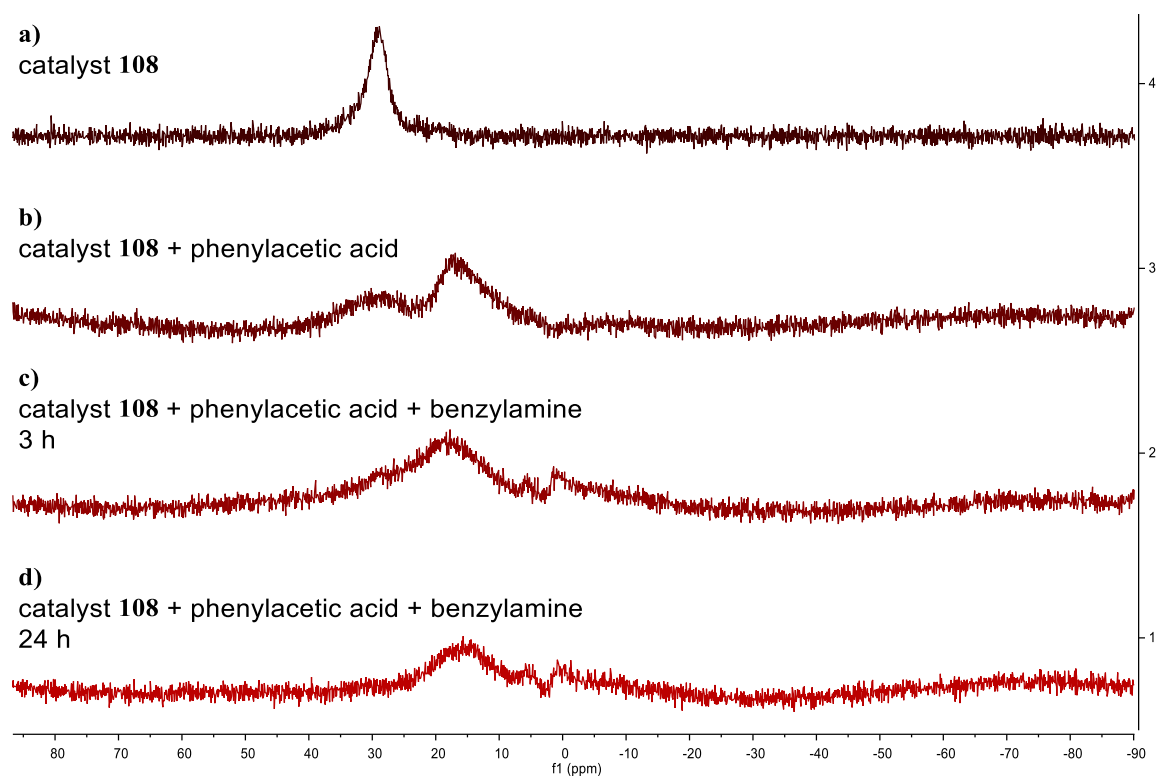
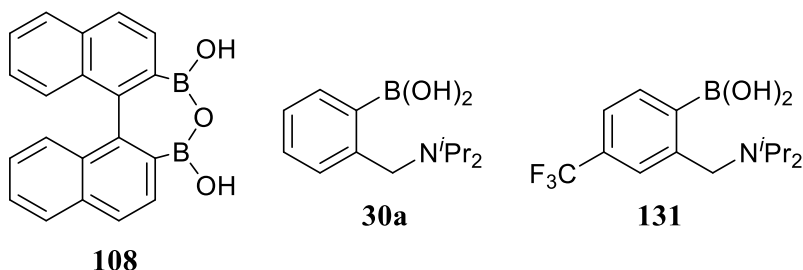
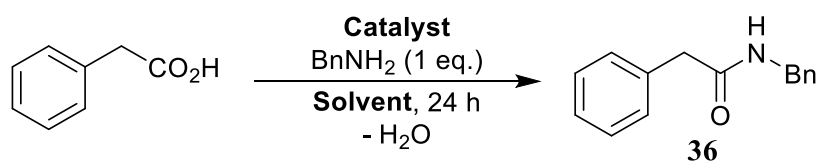


Figure 33. ^{11}B NMR of reaction mixture with catalyst **108** at different stages of stoichiometric amidation.

In others to quantify the catalytic performance of newly made catalyst **108**, a pick of boron-based catalysts from our previous group research³³ was involved for comparison in known reactions (i.e. phenylacetic acid), results of which were summarised in **Table 18**. Starting from the basic condition of Dean-Stark reflux in toluene, direct amidation catalysed by reported catalysts **30a** and **131** was efficient, giving over 90% yield after 24 hours (Entries 1 and 2, **Table 18**). Meanwhile, the first attempt by catalyst **108** was surprisingly successful, giving 99% yield under an equivalent of 5 mol% loading (Entry 3, **Table 18**).

Table 18. Catalytic direct amide formation with phenylacetic acid.



Entry	Catalyst ^a	Solvent	Yield / %
1	30a ^b	Toluene	95 ^c
2	131 ^b	Toluene	65 ^c
3	108	Toluene	99 ^c
4	108 ^b	Ph-F	93
5	30a ^b	Ph-F	74
6	131 ^b	Ph-F	40
7	108	DCM	5 ^d

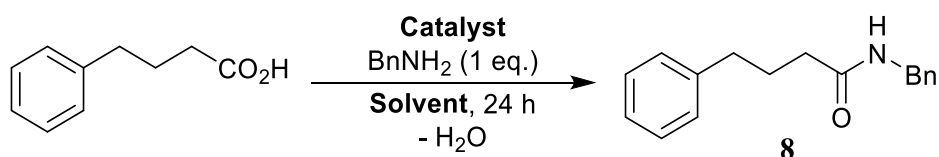
^aUnless otherwise specified, reaction carried out under General Procedure O.

^b10 mol% catalytic loading applied to match equivalent catalytic loading.

^cReflux using a Dean-Stark for water removal. ^dStirring at r.t. using 4 Å MS for water removal.

Next, the catalytic amide formation was conducted in refluxed fluorobenzene. Decrease in catalytic performance with the newly developed catalyst **124** was marginal (6% drop in yield, Entry 4, **Table 18**), comparing to **30a** and **131**, both of which possessed a 20% reduction in conversion (Entries 5 and 6, **Table 18**). Unfortunately, stretching to catalytic amide formation at room temperature was not successful, however, there was still product isolated pure from the system, suggesting a breakthrough towards a potential optimisation of methodology in the future (Entry 7, **Table 18**).

Table 19. Catalytic direct amide formation with phenylacetic acid.



Entry	Catalyst ^a	Solvent	Yield ^b / %
1	108 ^c	Toluene	95
2	30a	Toluene	80
3	131	Toluene	57
4	108 ^c	Ph-F	83
5	30a	Ph-F	41
6	131	Ph-F	36
7	108 ^c	DCM	4 ^d

^aUnless otherwise specified, catalytic loading set as 10 mol%. ^bCarried out using Dean-Stark water removal. ^c5 mol% catalytic loading applied to match equivalent catalytic loading. ^dStirred at r.t., with 4 Å MS for water removal.

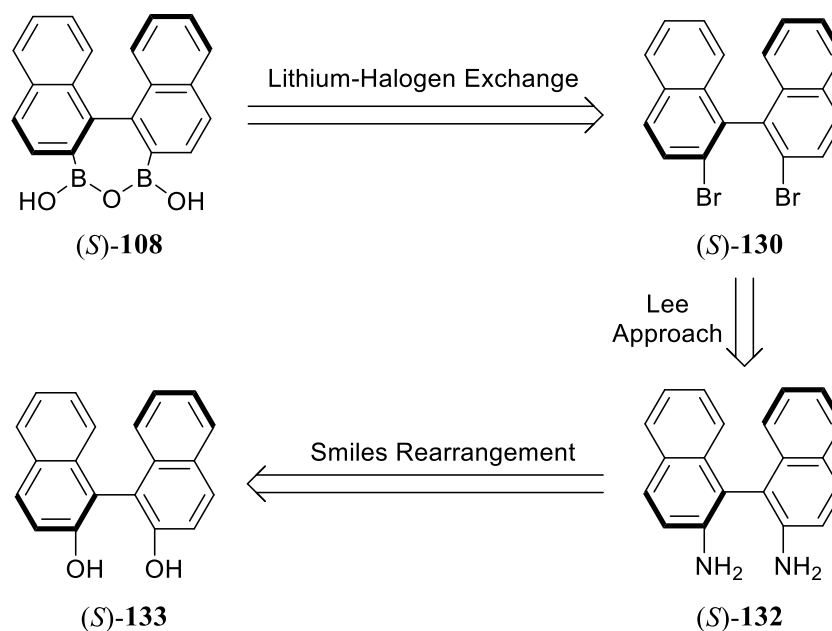
Similar results were observed when a less reactive phenylbutyric acid was employed for catalysis. Better reactivity was found with catalyst **108** *versus* **30a** and **131** (Entries 1-3, **Table 19**), which matched the expectation. Anticipation to that was partially due to the B-O-B bridged species which already existed in catalyst **108**. Unlike the monomeric boronic acid **30a** and **131** that required a dimerisation process to form such a reactive

intermediate before a mandatory diacylation, catalyst **108** came with a ‘B-O-B’ hexamer that rapidly responded to the addition of carboxylic acid.

4.3 Preparation of (*S*)-1,1'-diboronate binaphthalene

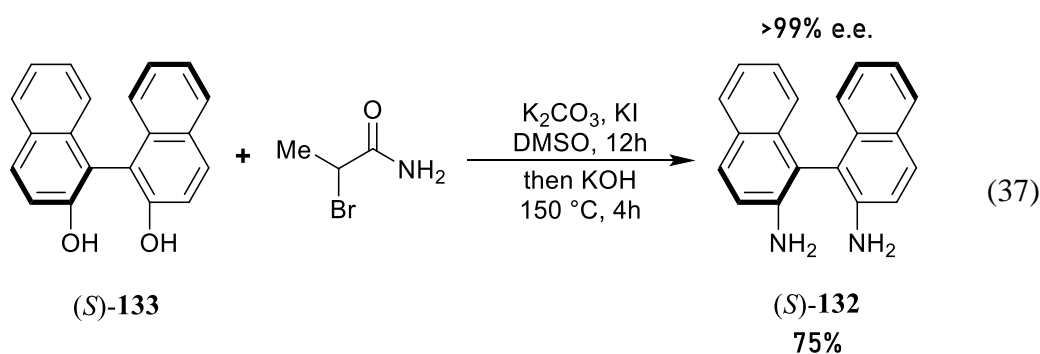
Our initial thoughts for the preparation of enantiopure (*S*)-**108** was to access this compound *via* dibromide **130**, and hence, from bromination of readily available BINOL **133**. However, the direct conversion of (*S*)-**133** directly to (*S*)-**130** requires demanding conditions and reaction efficiency, plus it is a non-trivial process. Despite the use of common brominating reagents including triphenylphosphine dibromide²²¹⁻²²³ and bromine^{224, 225} being used, neither are highly efficient plus requiring heating to more than 300 °C. More importantly, enantiopure starting materials have not been employed in these procedures which could potentially cause an issue with the stereoselectivity control during the process. We therefore considered a milder and more accessible pathway *via* the formation of diamino-binaphthalene (*S*)-**132**, as shown in **Scheme 22**.

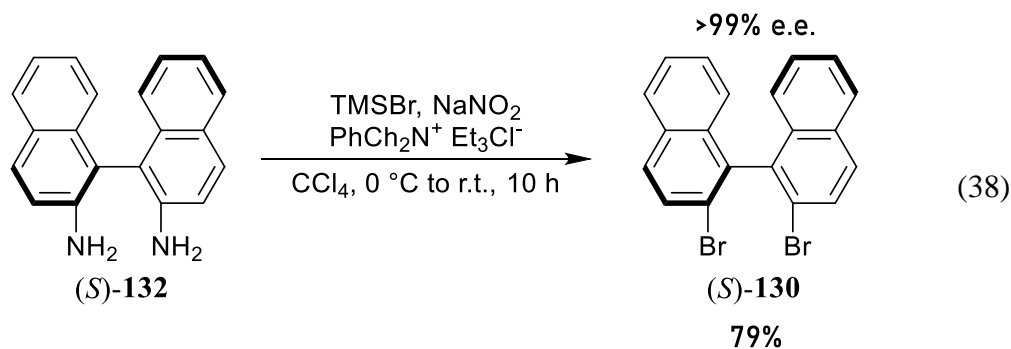
The overall strategy started with a recently reported Smiles rearrangement starting from (*S*)-BINOL (*S*)-**133** to access diamino-binaphthalene (*S*)-**132**,²¹⁹ followed by using the proven approach of Lee *et al.* giving 2,2'-dibromo-binaphthalene (*S*)-**130**.²²⁰ Finally, a similar procedure to those used for **127** and **129** was employed based on lithium-halogen exchange to access the final diboronic ester (*S*)-**108**.^{191, 217} This type of synthetic pathway was believed have less than 1% loss of axial chirality based on the reported stability of these types of binaphthyl systems.²²¹



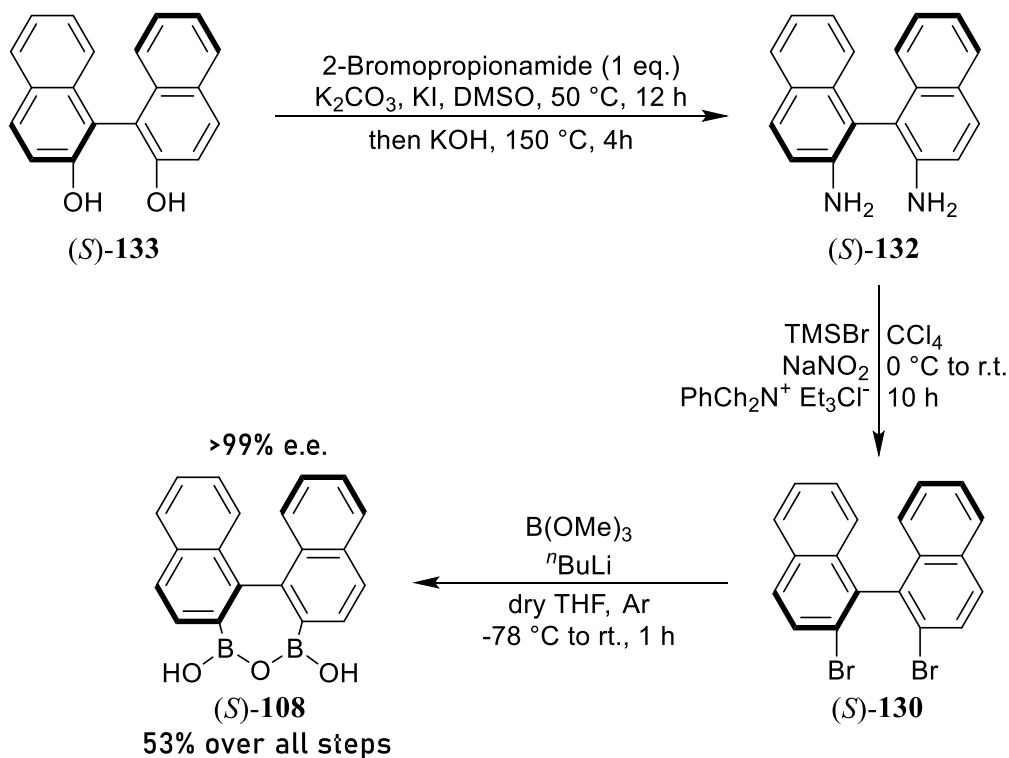
Scheme 22. Retrosynthesis to the formation of enantiomeric catalyst **(S)-108**

Notice the complication from **(S)-133** directly to **(S)-130** is the demanding conditions and reaction efficiency. Despite the two mainstreaming brominating reagents were reported early, including triphenylphosphine dibromide^{222, 223} and bromine^{224, 225}, neither of them was highly efficient, yet still required more than 300 °C heating. More importantly, no enantiopure substance was employed among these researches which potentially caused an issue of the stereoselective control during the process. With discussed factors and cost for the preparation into account, we then considered a milder and more accessible pathway *via* the formation of diamino-binaphthalene **(S)-132**.





Regarding the conversion of diamine **132** to the corresponding aryl dibromide **130**, we examined the approach used by Hagiwara employing zinc(II) bromide as catalyst to give the resulting 2,2'-dibromo-binaphthalene (*S*)-**130** at 99% e.e.^{226, 227} The reaction was neat and easy to handle and was far from satisfactory reaching up to 20% yield. However, a modified Lee's approach, using a halo-trimethylsilane was highly successfully employed which reached 80% yield (Equation 38).²²⁰



Scheme 23. Synthetic strategy to the synthesis of (*S*)-**108**

With the dibromide **130** in hand, the synthesis of chiral catalyst (*S*)-**108** was completed for use in the kinetic resolution- direct amide formation, with the entire process from BINOL summarised in **Scheme 23**. After employing the lithium-halogen exchange-borylation procedure discussed above, this strategy gave a total conversion of 53% to catalyst (*S*)-**108** as a white solid. The preparation was conducted under mild conditions throughout, and hence, the stereoselectivity was maintained at over 99% e.e. ESI-Mass spectrometry confirmed the structure of the catalyst (*S*)-**108**, as showed in **Figure 34** (mass 324.11) and ^{11}B NMR gave the expected, clean signal at δ 29.

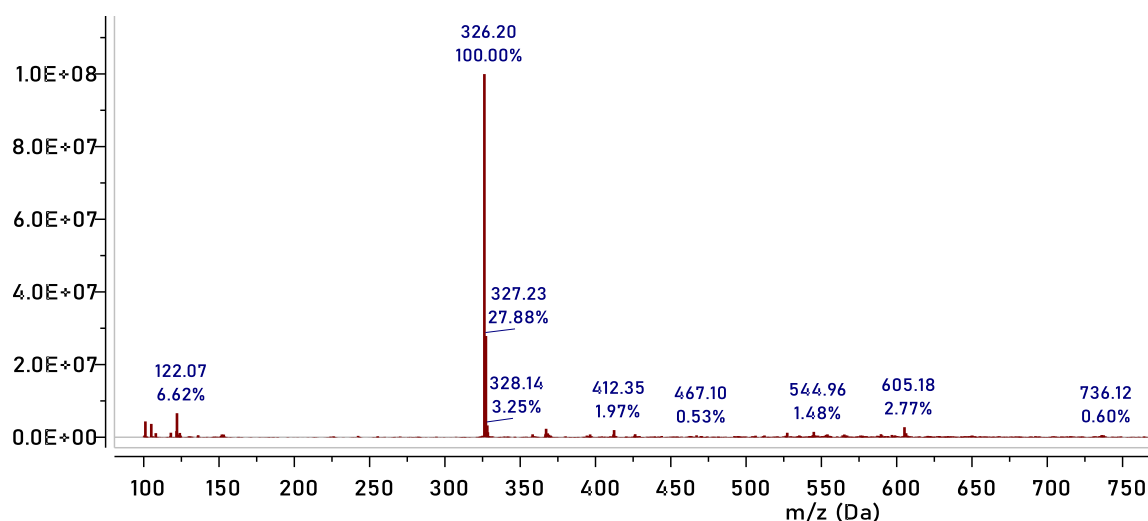
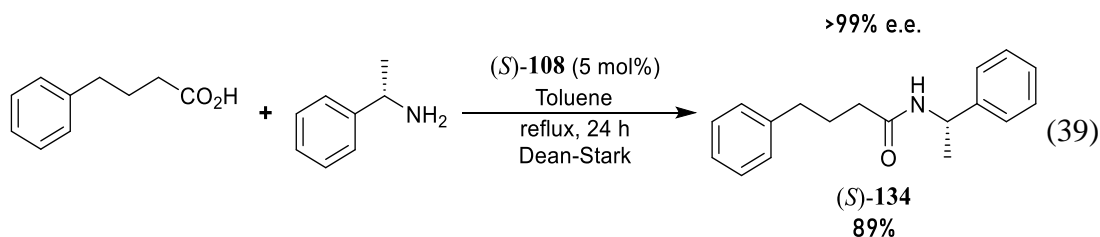


Figure 34. Mass spec result of synthesised compound (*S*)-**108**

4.4 Kinetic resolution of asymmetric *N*-acylation catalysed by (*S*)-**108**

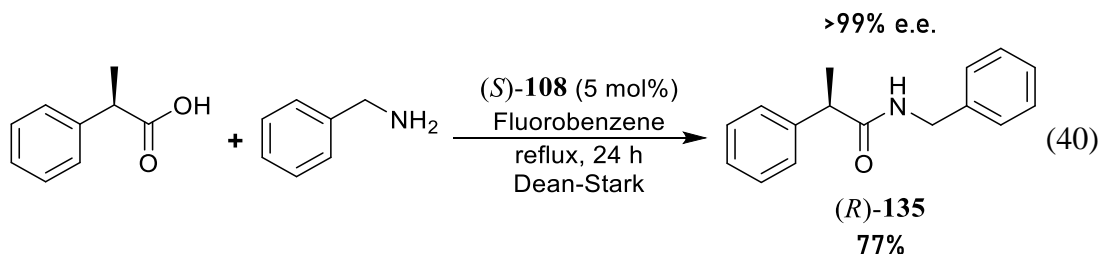
Based on the comparison of the catalyst systems shown in **Table 18**, the reaction tests were initiated in order to determine if the highly reactive catalyst (*S*)-**108** could also affect efficient kinetic resolution. These reactions were initially carried out in either refluxing toluene or fluorobenzene, starting with making enantiopure standards, while examining that racemisation was not occurring. Hence, in the presence of catalyst (*S*)-**108**, enantiopure amides were prepared as reference standards, the results of which are shown as Equations 39 and 40.



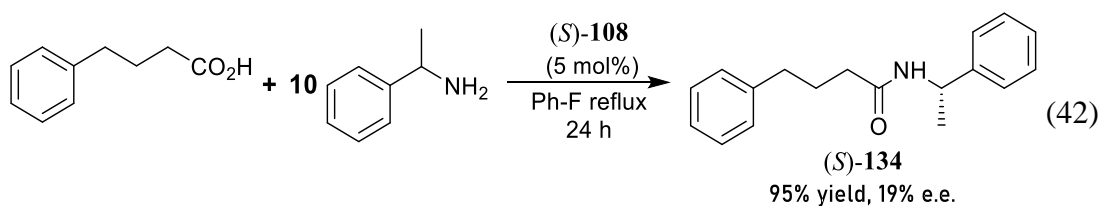
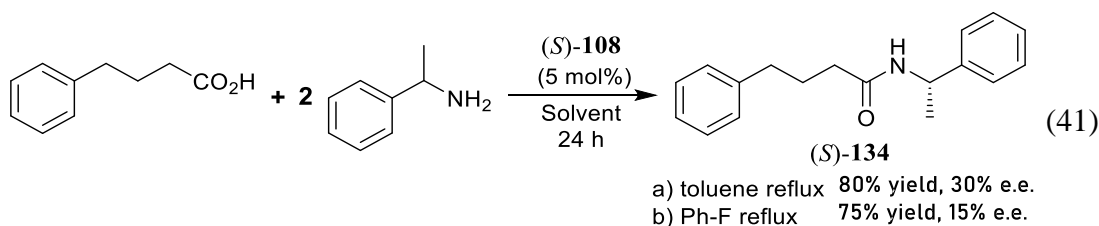
Reaction of phenylbutyric acid with enantiopure alpha-methylbenzylamine in refluxing toluene and 5 mol% catalyst (Equation 39), provided complete conversion to enantiopure amide **134**. The lack of racemisation was important to confirm; however, this standard was used to help with developing chiral HPLC conditions for the KR studies reported below.

Under the milder, lower temperature, reaction conditions using fluorobenzene, standard amide (*R*)-**135** was readily accessed (Equation 40) from the reaction of methyl phenylacetic acid with benzylamine, yielding 77% of the product with no racemisation.

Again, this product was used to assist with developing chiral HPLC conditions to enable e.e. determination in subsequent KR studies.

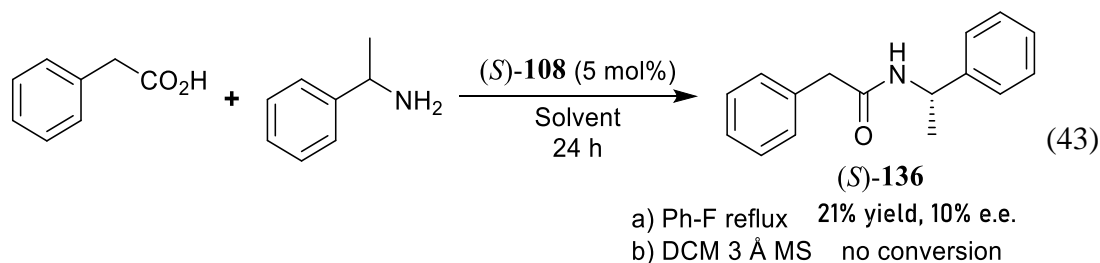


Having assessed the catalytic activity of catalyst **108** and suitable accessed standards, it was then possible to carry out preliminary assessment of the capability of catalyst **108** for kinetic resolution of either racemic amines or carboxylic acids. Hence probing the resolution capability of (*S*)-**108** was carried out using two equivalents of racemic substrates (amine or carboxylic acid) relative to the achiral substrate and the resulting amides were isolated and examined by chiral HPLC to measure its enantiomeric excess and the results of which are shown as follows.



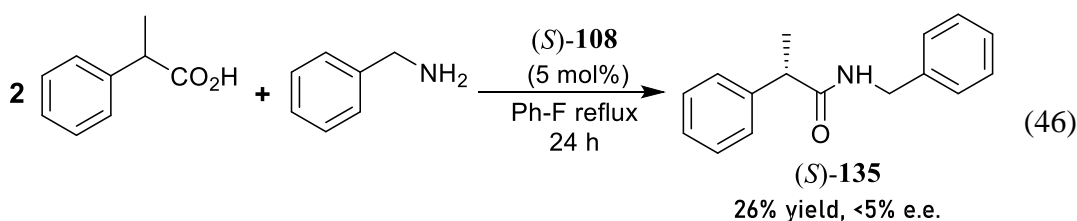
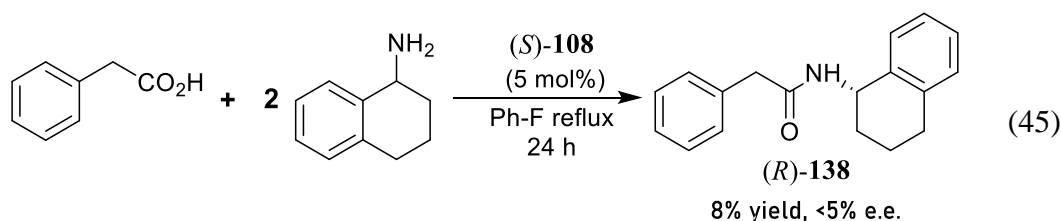
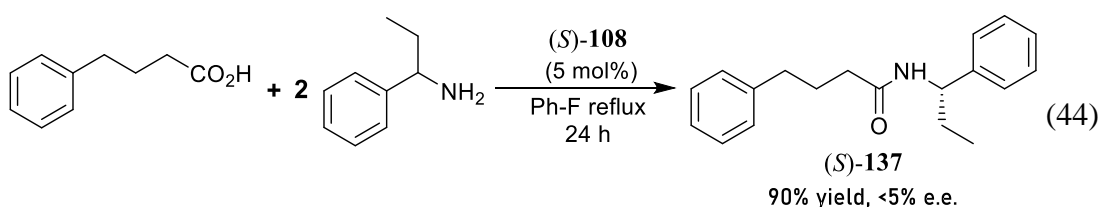
First, racemic amines were tested in the KR-amidation reaction catalysed by **108**, including alpha-methylbenzylamine, starting with reaction with phenylbutyric acid in refluxing toluene (Equation 41, Entry a). After 24 h amide **134** was produced in 80% yield, and chiral HPLC analysis showed a moderate 30% e.e. in favour of the *S*-enantiomer. Interestingly, catalyst (*S*)-**108** showed reduced reactivity under milder, lower temperature conditions, i.e. in refluxing fluorobenzene (Equation 41, Entry b). This reaction generated 75% yield of amide **134**, though with a reduced 15% e.e. according to chiral HPLC analysis. However, increasing the relative amount of racemic amine used in this reaction (Equation 42) did lift the e.e. slightly through the use of 10 equivalents of racemic substrate which generated 95% yield with 19% e.e.

In order to compare reaction with a different carboxylic acid, phenylacetic acid was next examined with alpha-methylbenzylamine in refluxing fluorobenzene (Equation 43, Entry a). Interestingly, this reaction showed considerably reduced conversion to only 21% of amide **136** over 24 h and in addition, there was a reduction in e.e. to only 10%. Given this reduced reactivity compared to phenylbutyric acid, reaction of phenylacetic acid at room temperature in DCM (Equation 43, Entry b) unsurprisingly gave no conversion to amide **136**.



The observation of the higher reactivity of phenylbutyric acid compared to phenylacetic acid was further demonstrated as shown in a series of further reactions (see

Equations 44-46). Hence, reaction of phenylbutyric acid with alpha-ethylbenzylamine in refluxing fluorobenzene provided a high, 90% yield, of amide **137**, though with less 5% e.e. There was a similarly low e.e. producing reaction from the reaction of phenylacetic acid 1-aminotetrahydronaphthalene (Equation 45), which also showed very low conversion. Finally, a racemic carboxylic acid was examined (Equation 46), in the reaction of methylphenylacetic acid with benzylamine, and while the highly reactive benzylamine was employed, only 26% of amide **138** was produced, and again with less than 5% e.e.



To investigate the catalytic KR amidation and catalyst performance during these reactions, Equation 41 was examined over time (see General Procedure O), while running these two reactions in identical reactors and in parallel. The two reactions in both toluene and fluorobenzene were sampled at regular intervals and the conversions and e.e.s

determined. The results of these reactions are shown in **Figure 35**. In refluxing fluorobenzene, the reaction gradually reached 80% conversion after 24 h, though raising to 16% e.e. after only 6 hours, with no further increase in e.e. after that time. In contrast, the performance in refluxing toluene gained 70% of its product within the first 3 hours and 30% e.e. inside the first 3 hours. These differences in kinetic behaviour suggest, unusually, that for these types of reactions, the enantioselectivity is improved at higher temperatures.²²⁸ This suggests that the reactive, enantioselecting species generated is likely different from that produced at lower temperatures. Although these are highly preliminary results, they suggest that further investigations could well shed further light upon the mechanism and speciation involved in these types of catalytic amidation. Due to lack of time, further investigations were not possible, but these results are provocative and at the very least, more substituted analogues of **108** could result in better KR.

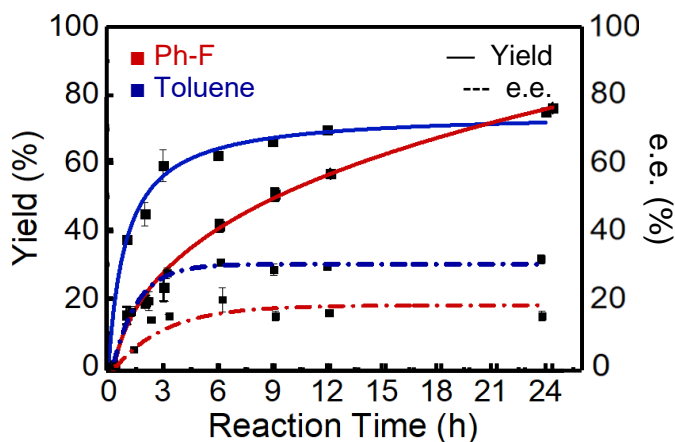
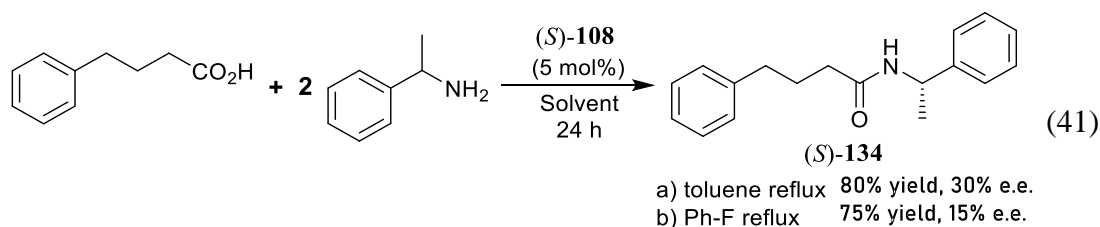


Figure 35. Kinetic studies of asymmetric *N*-acylation to (*S*)-**134** catalysed by (*S*)-**108** in either refluxing toluene or fluorobenzene.

4.5 Conclusion and future outlook

In this section, a novel binaphthalene diboronate catalytic system was designed and synthesised, originally derived from previously discovered naphthyl diboronic ester¹⁹¹ and diphenyl diboronic acid.²¹⁷ Considering the accessibility and procedure convenience, catalyst (*S*)-**108** was synthetically readily obtained *via* a convenient scheme involving a catalytic amination of enantiopure (*S*)-BINOL, followed by a halogenation and lithium-halogen exchange-borylation reaction. Solvent tests and kinetic studies were carried out showing good to poor reactivity upon asymmetric amide formation, with better reactivity at higher temperatures, and the higher KR, which contrasted with milder conditions such as fluorobenzene. These conditions gave lower conversion, but surprisingly, also gave lower e.e. amide.

Further emphasis will be put on the catalytic structure screening, including introduction of 2,7-disubstituted variants of **108**, as suggested previously,¹⁹¹ and other possible decorations to enhance the potential reactivity and KR capability. Subsequent studies of the reaction substrate scope and a possible mechanism will be potentially useful for developing improved catalytic system towards kinetic resolution of asymmetric *N*-acylation, as well as other similar catalysis and mechanistic understanding.

5. Concluding remarks

To conclude, this area of boron-mediated catalysis is fascinating and challenging to work in, not only because such catalysts have a strong Lewis-acidic centre, but also due to their non-metallic and organocatalytic properties. Organoboron catalysis has been broadly applied in various areas in the literature, and in this work, and it still remains exciting with hidden secrets for further application in useful reactions yet to be discovered.

In this work, we examined the catalytic direct amide formation in both heterogeneous and homogeneous reactions. Based on recent calculations revealing a plausible interconversion of B-X-B bridged intermediate during the acid-activation process,⁴⁷ we designed the first polymerized styrylboronic acid catalyst and successfully prepared it through a simple polymerisation reaction to give a polymer monolith which was processed to employ in a number of batch reactions. The conversion of the boron species around the key B-X-B intermediate was examined by *in situ* ReactIR and ¹¹B SSNMR. Substrate scope and recyclability of the catalyst was also tested showing its potential for further application in flow conditions providing a proof-of-concept for use of this type of heterogeneous catalyst system.

Meanwhile, based upon a previous example of using homoboroproline based bifunctional catalysis for asymmetric aldol reactions,^{140, 148} in this work, this type of methodology was employed on the asymmetric nitro-Michael addition. Herein, the B-N bifunctional homoboroproline catalyst (*R*)-**85** was synthesised *via* a scalable pathway from enantiopure proline. Subsequent application in the nitro-Michael showed good stereoselectivity up to 67% e.e. in the presence of an *in situ* boronate esterified system through reaction suitable diols. Broad substrate tolerance was observed under optimised reaction conditions and this convincing performance can enable and inform further

applications in diastereoselective nitro-Michael additions in the future, and even more widely on other C-C bond forming reactions.

Finally, kinetic resolution through the *N*-acylation of amines has been reported by the use of various catalysts.¹⁷¹⁻¹⁸² In this work, we reported the design and synthesis of a novel binaphthalene diboronate catalyst for cooperative kinetic resolution of amide formation. Starting from (*S*)-BINOL, the catalyst was prepared in an enantiopure fashion *via* a series of functional group interconversions to access the diboronic acid (*S*)-**108**. Crystallography data showed the formation of desired diboronate species before application in amidations and subsequent kinetic resolution tests showed some stereoselectivity under toluene reflux conditions, with the performance dropping as the conditions became milder, i.e. lower temperature. The accessibility and functionality of the axially chiral diboronic acid have been confirmed, however, and demonstrated in asymmetric catalysis. It is also a starting point for further research, including optimisation of the structures of the catalysts through functionalisation on 3,3'-positions of the binaphthyl system to amplify stereocontrol effects.

In a summary, all the above cases in this thesis have confirmed the important role of boron compounds in modern catalyst development, not only due to its versatile electronic properties, but also its non-metallic properties that benefit the art of catalyst design. Past reports have demonstrated the rich possibilities of utilisation, yet there is still much more to be discovered. The catalytic behaviour of different boronate species is yet to be understood clearly, after which more structurally diverse catalysts may be designed for different purposes. The work in this thesis tells us that there is a bright future for organoboron catalysis.

VIII. Experimental section

1. General experimental

All the reactions were performed under air unless otherwise specified. The reagents were purchased directly from standard chemical suppliers and used as received from the supplier without further purification unless specified. All solvents were used as received from the supplier, except THF, MeOH and ether which were stored over dehydrating agent and deoxygenated before use. Molecular sieves with 4 Å 1-2 mm beads and 3 Å 3-5 mm pallets were supplied from Alfa Aesar and stored at 220 °C (>48 h), Montmorillonite K10 powder, 250 m²/g, was supplied from Sigma Aldrich and stored at 80 °C (>24 h) and heated under vacuum before use.

The purification of the reaction crudes was performed using medium pressure column chromatography carried out using various sizes of glass columns, sand (40-100 mesh, analytical purity from Sigma-Aldrich) and silica gel (230-400 mesh, 40-63 µm, 60 Å, from Fisher) and monitored by TLC analysis using POLYGRAM[®] SIL G/UV254 (40 x 80 mm) TLC plates from Fisher. In all cases, the TLC plates were visualised under a UV lamp operating at short (254 nm) and long (365 nm) wavelength ranges. The visualisation was aided by dipping the plates into an alkaline potassium permanganate solution or a *p*-anisaldehyde solution. Solvent removal was carried out using Büchi R-114 and R-100 rotary evaporator.

Low pressure for general purposes (i.e. Büchner filtration) was conducted using various mechanical vacuum pumps. Most purified products were placed under a high vacuum environment generated by various high vacuum generators. Low-pressure distillation was carried out using a Büchi B-585 glass oven (Kügelrohr). Pressures were not

controlled, and the values reported are the operating pressure of the vacuum pump used, as indicated by a separate pressure gauge.

Solution state NMR spectra were recorded on a Bruker Avance spectrometer, operating at 400 MHz for ^1H , 100 MHz for ^{13}C and 128 MHz for ^{11}B . Deuterated chloroform (CDCl_3) was used as solvent for routine NMR measurements unless otherwise stated. ^1H NMR spectra were recorded on a Varian-Mercury 400 MHz spectrometer, operating at ambient probe temperature unless specified otherwise. Coupling constants (J) are given in Hz, and the multiplicity of the NMR signals is described as singlet (S), doublet (d), triplet (t), quartet (q) and multiplet (m). ^{13}C NMR spectra were recorded on Varian Brüker Avance 100 MHz. ^1H NMR and ^{13}C NMR chemical shifts are reported in ppm (δ) referencing the chemical shifts of residual solvent resonances. ^{11}B NMR spectra were recorded on a Varian Brüker Avance 400 MHz operating at a frequency of 128 MHz and the chemical shifts are reported in ppm (δ) relative to $\text{BF}_3\cdot\text{OEt}_2$. ^{19}F NMR spectra were recorded on a Varian Brüker Avance 400 MHz operating at a frequency of 376 MHz and the chemical shifts are reported in ppm (δ).

Mass spectra using liquid chromatography-mass spectrometry (LCMS) were obtained using a Waters (UK) TQD mass spectrometer (low-resolution ESI+, electrospray in positive ion mode, ES+) unless stated otherwise. Accurate mass spectrometry was obtained on a Finnigan LTQ-FT.

IR spectra were recorded on a Perkin Elmer Paragon 1000 FT-IR spectrometer with an ATR attachment. ReactIR *in situ* analysis was carried out using a Mettler Toledo ReactIR 15 System.

Single crystal X-ray crystallography data was collected by Bruker Cryostream 700+ diffractometer.

Melting points were measured by *SANYO* Gallenkamp Melting Point Apparatus with *SAMCO* capillary tubes.

The optical rotation of compounds was measured (α) by *Schmidt Haensch GmbH & Co.* Unipol L2000 polarimeter, equipped with a 589.44 nm Na light source. Samples to be measured were kept in constant thermal condition using a Brookfield TC-550MX circulating water bath, and a jacketed 100 mm quartz cell (l). Samples were prepared in HPLC grade solvents. Rotation measurements were repeated in quintuplicate and are reported as an average specific rotation ($[\alpha]_D$), with the concentration (c) and solvent used for each measurement.

$$[\alpha]_D = \frac{\alpha}{c \times l}$$

Flow system experiments were conducted using a commercially available Vapourtec R2+/R4 modular flow reactor. The Vapourtec integrates a twin pumping unit with an independently controlled four-channel air-circulated heating module. A low-pressure input valve is used to route either solvent or bulk stock solutions directly to the self-regulating HPLC pumps. Two additional Rheodyne 6-port–2-position switching valves can be used to introduce reagents or substrates into the main flow line through individual sample loop arrangements of user-defined variable volumes. The positive system pressure was maintained by using an in-line 75 psi back-pressure regulator. The use of an appropriate back-pressure regulator allows superheating of solvents as required. Mixing of the reagent streams is achieved with a simple T-piece and the combined output is then directed through perfluoroalkoxy (PFA) tubing to the convection flow coil (CFC), which can be precisely heated to 150 °C. Upon exiting the CFC, the flow stream is cooled rapidly and is then directed to scavenger cartridges that consist of simple Omnifit glass columns packed with appropriate immobilised materials. The final flow line can then be collected

and evaporated to give the purified product. Rapid screening of reaction parameters was performed, which included reaction temperature, residence time (flow rate), internal pressure, solubility, reagent concentrations and stoichiometry.

2. General reaction procedures

Synthesis of polymer catalyst 107

To a mixture of styrene (12 wt.%), divinylbenzene (mixed isomers, 18 wt.%), 4-vinylphenylboronic acid (12 wt.%) and 1-dodecanol (57 wt.%) was added AIBN (1 wt.%). The mixture was decanted into appropriately sized Omnifit glass tubes and sealed at both ends with PTFE caps. These were placed in a Vapourtec hot air heat exchanger system and heated to 80 °C for 20 hrs. The resulting synthesised polymer monoliths were removed from the tubes and stirred in methanol (6 h) then DCM (6 h) to remove 1-dodecanol, before drying in an oven at approximately 100 °C overnight. The monoliths were crushed into a powder (particle size approx. 1-3 mm). The material was ground more finely (<1 mm) immediately before use. ¹¹B solid state (MAS) NMR (128.3 MHz): δ before use 16.0 (17.1 ppm FWHM); δ after use 12.8 (20.0 ppm FWHM), 0.0 (3.2 ppm FWHM). After washing and drying (removal of 1-dodecanol) the polymer is made up of 27.9% catalytically active monomer by mass, and as such this factor was included when calculating the mass required for use in the reactions below.

The polymer catalyst was further solvent extracted through Soxhlet extraction before filling in the glass column for flow reaction use. To a dry extraction thimble (25 mm \times 100 mm) in a Soxhlet extractor, ground polymer catalyst (10 g) was added, followed by 200 mL of toluene added in the round bottom flask. The Soxhlet extraction was left for 72 hrs before drying in a desiccator under vacuum.

General Procedure A: Batch heterogeneous catalysis

Carboxylic acid (2.86 mmol), polymer catalyst (75.8 mg, 0.143 mmol, 5 mol%), toluene (20 ml) and drying reagent (0.12 g, either dried MgSO₄ or 4Å MS) were added to a 50 mL round-bottom flask. Amine (2.86 mmol, 1 equiv.) was added and the resulting mixture stirred under vigorous reflux using a condenser for 24 hrs. After cooling to rt, the solvent was removed *in vacuo*. The resulting crude solid was redissolved in DCM or chloroform (30 ml), filtered to remove catalyst, washed with 5% HCl (3 × 15 ml), saturated NaHCO₃ (3 × 15 ml), brine (3 × 15 ml) and finally water (15 ml). The resulting solution dried over MgSO₄ before solvent removal *in vacuo* to give the crude amide product. Purifications were then carried out by low-pressure distillation (Kügelrohr).

General Procedure B: Batch heterogeneous catalysis

Carboxylic acid (5.72 mmol), polymer catalyst (151.6 mg, 0.286 mmol, 5 mol%), and toluene (40 ml) were added to a 100 mL Radley's Carousel Reactor azeotropic round-bottom flask with a built-in Dean-Stark trap. Amine (5.72 mmol, 1 equiv.) was added and the resulting mixture stirred for the reported period of time. When finished, the reaction mixture cooled to rt, and the solvent was removed *in vacuo*. The resulting crude solid was redissolved in DCM or chloroform (50 ml), filtered to remove catalyst, washed with 5% HCl (3 × 50 ml), saturated NaHCO₃ (3 × 50 ml), brine (3 × 50 ml) and finally water (50 ml). The resulting solution was dried over MgSO₄ before solvent removal *in vacuo* to give the crude amide product. Purifications were then carried out by low-pressure distillation (Kügelrohr).

General Procedure C: Batch homogeneous catalysis

Carboxylic acid (5.72 mmol), arylboronic acid catalyst (0.286 mmol, 5 mol %), and solvent (40 ml) were added to a 100 mL Radley's Carousel Reactor azeotropic round-bottom flask with a built-in Dean-Stark trap. Amine (5.72 mmol, 1 equiv.) was added and the resulting mixture stirred for the reported period of time. When finished, the reaction mixture was cooled to rt and the solvent was removed *in vacuo*. The resulting crude solid was redissolved in DCM or chloroform (50 ml), washed with 5% HCl (3 × 50 ml), saturated NaHCO₃ (3 × 50 ml), brine (3 × 50 ml) and finally water (50 ml). The resulting solution was dried over MgSO₄ and then the solvent was removed under reduced pressure to give the crude amide product. Purifications were then carried out by low-pressure distillation (Kügelrohr).

General Procedure D: *in situ* ReactIR kinetic analysis

The ReactIR 15 system, including LC2 NCT detector, was set and the probe cleaned with IPA before calibration. Polymer catalyst (151.6 mg, 0.286 mmol, 5 mol%) and toluene (40 mL) was added to a 100 mL 3-neck round bottom flask attached with Dean-Stark apparatus and stirred for 20 minutes. Data collection started with a sampling interval of 15 seconds. Then the reaction mixture was heated to the pre-set temperature. After 20 minutes, phenylacetic acid (11.44 mmol, 2 equiv.) was added, followed by the addition of benzylamine (5.72 mmol, 1 equiv.) after 50 minutes. After another 40 minutes stirring, experimental parameters were changed for a longer-term reaction, with the data sampling interval set to 1 minute. The reaction was refluxed in toluene for another 24 hours after the completion of the data collection. The resulting data was processed by en-suite software, as partially shown in **Figure 24** and **Figure 25**.

General Procedure E: Catalyst recyclability check

To a 100 mL Radley's Carousel Reactor azeotropic round-bottom flask with a built-in Dean-Stark trap, carboxylic acid (1 equiv.), polymer catalyst (5 mol%), and toluene were added, followed by the amine (1 equiv.) before the reaction mixture stirred at a vigorous reflux for 24 hrs. After cooling to rt, the solvent was removed *in vacuo*. The resulting crude solid was redissolved in DCM (50 ml), filtered to remove catalyst, washed with 5% HCl (3 × 30 ml), saturated NaHCO₃ (3 × 30 ml), brine (3 × 30 ml) and finally water (30 ml). After drying over MgSO₄, the solvent was removed under reduced pressure to give the crude amide product. Purifications were carried out by low-pressure distillation (Kügelrohr). The recovered filtered catalyst was refluxed with toluene for 20 hrs before evaporation and drying to get a pale yellow solid. The resulting recovered catalyst was weighed read for reuse.

General Procedure F: Catalyst recyclability check

To a 100 mL Radley's Carousel Reactor azeotropic round-bottom flask with a built-in Dean-Stark trap, carboxylic acid (1 equiv.), polymer catalyst (5 mol%) and toluene were added, followed by the amine (1 equiv.) before the reaction mixture stirred at a vigorous reflux for 24 hrs. After cooling to rt, the solvent was removed *in vacuo*. The resulting crude solid was redissolved in DCM (50 ml), filtered to remove the catalyst, washed with 5% HCl (3 × 30 ml), saturated NaHCO₃ (3 × 30 ml), brine (3 × 30 ml) and finally water (30 ml). After drying over MgSO₄, the solvent was removed under reduced pressure to give the crude amide product. Purifications were then carried out by low-pressure distillation (Kügelrohr). The recovered filtered catalyst was refluxed with toluene for 20 hrs before

evaporation and drying to give a pale yellow solid. The resulting catalyst was reused in the next batch of reactions.

In the first batch of reaction, an equivalent of 7.15 mmol of substrates was added, with polymer catalyst (189.5 mg, 0.358 mmol, 5 mol%). Catalyst recycled to get 185.7 mg (98%) of pale yellow solid.

In the second batch of reaction, an equivalent of 7.01 mmol of substrates was added, with polymer catalyst (185.7 mg, 0.5351 mmol, 5 mol%). Catalyst recycled to get 176.4 mg (95%) of pale yellow solid.

In the third batch of reaction, an equivalent of 6.66 mmol of substrates was added, with polymer catalyst (176.4 mg, 0.340 mmol, 5 mol%). Catalyst recycled to get 174.6 mg (99%) of pale yellow solid.

In the fourth batch of reaction, an equivalent of 6.59 mmol of substrates was added, with polymer catalyst (174.6 mg, 0.337 mmol, 5 mol%). Catalyst recycled to get 129.2 mg (74%) of pale yellow solid.

In the fifth batch of reaction, an equivalent of 4.88 mmol of substrates was added, with polymer catalyst (129.2 mg, 0.249 mmol, 5 mol%). Catalyst recycled to get 90.4 mg (70%) of pale yellow solid.

General Procedure G: Precipitation test

In a clear test tube, carboxylic acid (0.57 mmol, 1 equiv.), amine (0.57 mmol, 1 equiv.) and toluene (4 mL) were added. The reaction mixture was stirred for 1 h at r.t. and then stopped upon visual inspection of precipitation.

General Procedure H: Flow system test

General procedure involving the introduction of a solution of carboxylic acid (14.30 mmol 1 equiv.), amine (14.30 mmol, 1 equiv.) in toluene (250 ml) through a glass column filled with polymer catalyst (6.0 g). The column was flushed with toluene at 0.100 ml/min for 1 h before heating to 130 °C. Then the reaction mixture was pumped through the column and an automatic fraction collector was employed to collect fractions at 100 min per fraction. The system was left overnight, and the fractions were collected constantly. All the fractions were then evaporated *in vacuo* before NMR analysis which indicated the reaction conversion.

General Procedure I: Circulating flow system test

General procedure involving the introduction of a solution of carboxylic acid (14.30 mmol 1 equiv.), amine (14.30 mmol, 1 equiv.) in toluene (250 ml) through a glass column filled with polymer catalyst (6.0 g). The column was flushed with toluene at 0.100 ml/min for 1 h before heating up to 130 °C. Then the reaction mixture was pumped through the column and the outcoming fluid was directed back into the reaction mixture storage flask. At planned time points, a maximum of 5 mL of reaction mixture was taken from the flask, evaporated *in vacuo* before NMR analysis which indicated the conversion of substrates. After the analysis, the sample was redissolved in 5 mL of toluene and added back into the original storage flask.

General Procedure J: Preparation of nitroalkenes²¹⁰

A 3.5 M solution of NaOH (50 mL) was added into a cooled solution of nitromethane (0.50 ml, 10 mmol, 1 equiv.) and aromatic aldehyde (10 mmol, 1 equiv.) in methanol (50 ml) at 10 °C. After the mixture was stirred for 15 min, crushed ice was added until the solid completely dissolved. The resulting clear solution was added into a vigorously stirred solution of 5 M HCl (35 mL) which resulted in some solid product appearing. The mixture was then stored in the refrigerator for another 4 h to precipitate more solid. After Büchner filtration, the isolated solid was washed with water and dried *in vacuo* to obtain pure product as needle-shaped crystals in most cases.

General Procedure K: Racemic nitro-alkene Michael addition using *L*-proline¹⁹⁹

To a mixture of nitro-alkene (1.0 mmol) and acetone (2.0 ml) dissolved in DMSO (8.0 ml), *L*-proline (23 mg) was added. The reaction mixture was stirred at rt for 24 h before being quenched with saturated NH₄Cl (5 ml), extracted with Et₂O, dried (MgSO₄) and evaporated to give the crude product. Purification by silica gel chromatography (EtOAc:hexane gradient, 1:4 - 2:1) gave the product.

General Procedure L: Homoboroproline catalytic nitro-alkene Michael addition

To a mixture of catalyst (*R*)-**85** (5 mol%) and triethylamine (5 mol%) in a solvent (4.0 ml), nitrostyrene (1.0 mmol) in a solvent (1.0 ml) was added after 30 min. Acetone (1.0 mmol) was then added and the reaction mixture stirred at r.t. for 24 h before extraction with Et₂O (3 × 10 ml), drying (MgSO₄) and evaporated *in vacuo* to give the crude product. Silica gel column chromatography gave the purified product. The enantiomeric excess was

determined by chiral HPLC using an AS-H-CHIRALCEL column (250 × 4.60 mm) fitted with guard cartridge (50 × 4.6 mm), 25 °C, flow rate 1.00 ml/min, 210 nm, hexane:IPA (60:40).

General Procedure M: Homoboroproline catalytic nitro-alkene Michael addition with molecular sieves

To a mixture of catalyst (*R*)-**85** (5 mol%) and triethylamine (5 mol%) in a solvent (4.0 ml), 3 Å molecular sieves (1-2 mm, 10 beads, 64 mg) were added, followed by nitro-alkene (1.0 mmol) in the stipulated solvent (1.0 ml) after 30 min stirring. Acetone (1.0 mmol) was then added to the reaction mixture was stirred at r.t. for 24 h before extraction with Et₂O (3 x 10 ml), drying (MgSO₄) and evaporation *in vacuo* to give the crude product. Silica gel column chromatography gave the purified product. The enantiomeric excess was determined by chiral HPLC using an AS-H-CHIRALCEL column (250 x 4.60 mm) fitted with guard cartridge (50 × 4.6 mm), 25 °C, flow rate 1.00 ml/min, 210 nm, hexane: IPA (60:40).

General Procedure N: Homoboroproline catalytic nitro-alkene Michael addition with molecular sieves and hydrobenzoin

To a mixture of catalyst (*R*)-**85** (5 mol%) and triethylamine (5 mol%) in a solvent (4.0 ml), 3 Å molecular sieves (1-2 mm, 10 beads, 64 mg) and (*S,S*)-(-)-hydrobenzoin (5 mol%) were added, nitro-alkene (1.0 mmol) in the stipulated solvent (1.0 ml) was added after 30 min stirring. Acetone (1.0 mmol) was then added to the reaction mixture which was stirred at r.t. for 24 h before extraction with Et₂O (3 x 10 ml), drying (MgSO₄) and

evaporation *in vacuo* to give the crude product. Silica gel column chromatography gave the purified product. The enantiomeric excess was determined by chiral HPLC using an AS-H-CHIRALCEL column (250 x 4.60 mm) fitted with guard cartridge (50 × 4.6 mm), 25 °C, flow rate 1.00 ml/min, 210 nm, hexane: IPA (60:40).

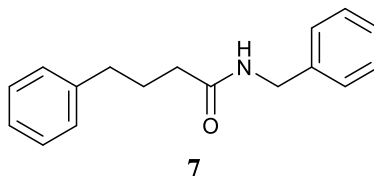
General Procedure O: Kinetic resolution *via* asymmetric *N*-acylation

A racemic carboxylic acid and amine (2.00 mmol, 2 equiv.), catalyst (*S*)-**108** (0.05 mmol, 5 mol%) and fluorobenzene (10 ml) were added to a 25 mL round bottom flask connecting to a Dean-Stark trap [Note: the corresponding non-chiral amine and carboxylic acid (2.86 mmol, 1 equiv.) combination treated similarly] and the resulting mixture stirred for reported number hours and temperature. After completion, the reaction mixture cooled to r.t., the solvent was removed *in vacuo* and the resulting crude was redissolved in DCM or chloroform (10 ml), washed with 5% HCl (3 × 10 ml), saturated NaHCO₃ (3 × 10 ml), brine (3 × 10 ml) and finally water (10 ml). After drying (MgSO₄), the solvent was removed *in vacuo* to give the crude amide product. Purifications were then carried out by low-pressure distillation (Kügelrohr). Any stereoselectivity was confirmed by chiral-HPLC using an AD-CHIRALCEL column (250 x 4.60 mm) fitted with guard cartridge (50 × 4.6 mm), 25 °C, 210 nm, hexane:IPA under specified ratio.

3. Procedures and characterisations

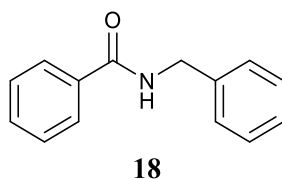
3.1 Organo-boron mediated direct amide formation

N-Benzyl-4-phenylbutanamide (**7**)



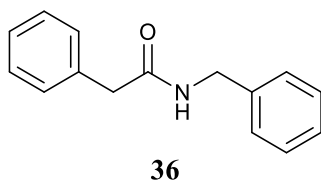
According to General Procedure A, phenylbutyric acid (0.47 g) and benzylamine (0.31 ml) were added for amidation. Kügelrohr distillation (200-210 °C, 0.4 torr) yielded 0.59 g (82%) as a white solid. ¹H NMR (400 MHz, CDCl₃) δ 1.99-2.08 (m, 2H), δ 2.24 (dd, *J* 8.5, 6.8, 2H), δ 2.69 (t, *J* 7.5, 2H), δ 4.46 (d, *J* 5.7, 2H), 5.66 (br. s, 1H), 7.16-7.24 (m, 3H), 7.27-7.33 (m, 5H), 7.33-7.39 (m, 2H). All the other spectroscopic and analytical data are consistent with those reported in the literature.²³⁴

N-Benzylbenzamide (**18**)



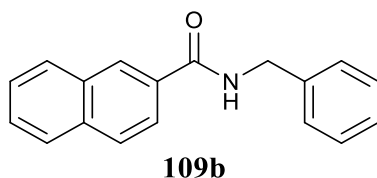
According to General Procedure A, benzoic acid (0.35 g) and benzylamine (0.31 ml) were added for amidation. Kügelrohr distillation carried (175-185 °C, 0.4 torr) and yielded 0.36g (60%) of pure amide product as a white solid. ¹H NMR (400 MHz, CDCl₃) δ 4.64 (d, *J* 5.7, 2H), 6.51 (br. s, 1H), 7.28-7.33 (m, 1H), 7.33-7.37 (m, 4H), 7.40-7.45 (m, 2H), 7.47-7.53 (m, 1 H), 7.77-7.82 (m, 2H). All the other spectroscopic and analytical data are consistent with those reported in the literature.²²⁹

***N*-Benzyl-2-phenylacetamide (36)**



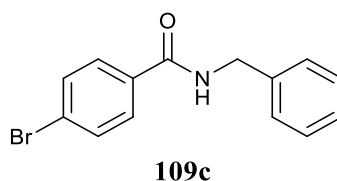
According to General Procedure A, Phenylacetic acid (0.39 g, 2.86 mmol) and benzylamine (0.31 ml, 2.86 mmol) were added for amidation. Kügelrohr distillation carried (175-180 °C, 0.4 torr) and yielded 0.51 g (80%) of pure amide product as a white solid. ¹H NMR (400 MHz, CDCl₃) δ 4.62 (d, *J* 5.7, 2H), 6.47 (br, s, 1H), 7.28-7.39 (m, 5H), 7.55 (dm, *J* 8.6, 2H), 7.65 (dm, *J* 8.6, 2H). All the other spectroscopic and analytical data are consistent with those reported in the literature.²³⁰

***N*-Benzyl-naphthalene-2-carboxamide (109b)**



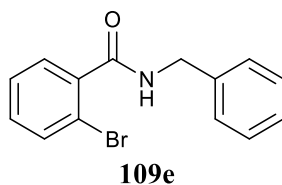
According to General Procedure A, 2-naphthoic acid (0.49 g) and benzylamine (0.31 ml) were added for amidation. Kügelrohr distillation (190-200 °C, 0.3-0.4 torr) yielded 0.50 g (67%) as a white powder. ¹H NMR (400 MHz, CDCl₃) δ 4.72 (d, *J* 5.7, 2H), 6.54 (br. s, 1H), 7.24-7.47 (m, 6H), 7.56 (p, *J* 7.2, 2H), 7.88 (m, 4H), 8.33 (s, 1H). All the other spectroscopic and analytical data are consistent with those reported in the literature.²³³

***N*-Benzyl-4-bromobenzamide (109c)**



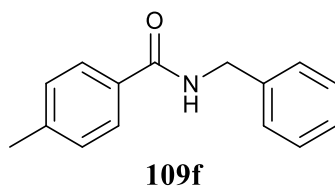
According to General Procedure B, 4-Bromobenzoic acid (1.14 g, 5.72 mmol) and benzylamine (0.62 ml, 5.72 mmol) were added and refluxed for 24 h. Kügelrohr distillation carried (175-180 °C, 0.4 torr) and yielded 0.76g (46%) of pure amide product as a white solid. ¹H NMR (400 MHz, CDCl₃) δ 4.62 (d, *J* 5.7, 2H), 6.47 (br, s, 1H), 7.28-7.39 (m, 5H), 7.55 (dm, *J* 8.6, 2H), 7.65 (dm, *J* 8.6, 2H). All the other spectroscopic and analytical data are consistent with those reported in the literature.²³¹

***N*-Benzyl-2-bromobenzamide (109e)**



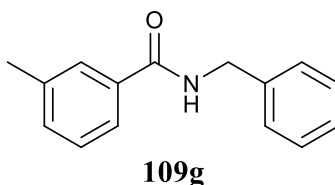
According to General Procedure A, 2-bromobenzoic acid (0.57 g) and benzylamine (0.31 ml) were added for amidation. Kügelrohr distillation (160-170 °C, 0.4 torr) yielded 0.15 g (26.5%) of pure amide product as a white solid. ¹H NMR (400 MHz, CDCl₃) δ 4.69 (d, *J* 5.6, 2H), 6.26 (br, s, 1H), 7.26-7.44 (m, 7H), 7.64-7.57 (m, 2H). All the other spectroscopic and analytical data are consistent with those reported in the literature.²³¹

***N*-Benzyl-4-methylbenzamide (109f)**



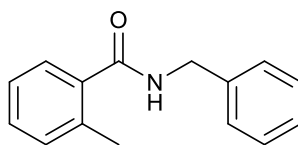
According to General Procedure A, 4-methylbenzoic acid (0.39 g) and benzylamine (0.31 ml) were added for amidation. Crude product was yielded as a pale yellow solid 0.42 g (65%). Kügelrohr distillation (160-170 °C, 0.4 torr) yielded 0.20 g (32%) of pure amide product as a white solid. ¹H NMR (400 MHz, CDCl₃) δ 2.39 (s, 3H), 4.63 (d, *J* 5.5, 2H), 6.50 (br. s, 1H), 7.22 (d, *J* 7.8, 2H) 7.27-7.38 (m, 2H), 7.69 (d, *J* 7.9, 1H). All the other spectroscopic and analytical data are consistent with those reported in the literature.²²⁹

***N*-Benzyl-3-methylbenzamide (109g)**



According to General Procedure A, 3-methylbenzoic acid (0.39 g) and benzylamine (0.31 ml) were added for amidation. Crude product was yielded as a pale yellow solid 0.29 g (45%). Kügelrohr distillation (165-170 °C, 0.3 torr) yielded 0.27 g (42%) of pure amide product as a white solid. ¹H NMR (400 MHz, CDCl₃) δ 2.37 (s, 3H), 4.61 (d, *J* 5., 2H), 6.86 (br. s, 1H), 7.33 (d, *J* 7.8, 2H), 7.60 (d, *J* 6.4, 1H), 7.64 (s, 1H). All the other spectroscopic and analytical data are consistent with those reported in the literature.²²⁹

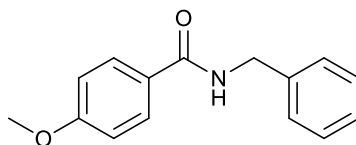
***N*-Benzyl-2-methylbenzamide (109h)**



109h

According to General Procedure A, 2-methylbenzoic acid (0.39 g) and benzylamine (0.31 ml) were added for amidation. The crude product was obtained as a pale yellow solid 0.18 g (30%). ¹H NMR (400 MHz, CDCl₃) δ 2.47 (s, 3H), 4.63 (d, *J* 5.8, 2H), 6.06 (br. s, 1H), 7.16-7.24 (m, 2H) 7.27-7.33 (m, 2H), 7.33-39 (m, 5H). All the other spectroscopic and analytical data are consistent with those reported in the literature.²²⁹

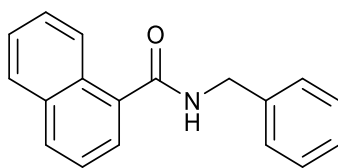
***N*-Benzyl-4-methoxybenzamide (109i)**



109i

According to General Procedure A, 4-methoxybenzoic acid (0.44 g) and benzylamine (0.31 ml) were added for amidation. Kügelrohr distillation (175-190 °C, 0.2-0.3 torr) yielded 0.18 g (26.1%) as a white solid. ¹H NMR (400 MHz, CDCl₃) δ 3.84 (s, 3H), 4.62 (d, *J* 5.7, 2H), 6.42 (br. s, 1H), 6.91 (d, *J* 8.9, 2H), 7.27-7.36 (m, 5H), 7.76 (d, *J* 8.9, 2H). All the other spectroscopic and analytical data are consistent with those reported in the literature.²²⁹

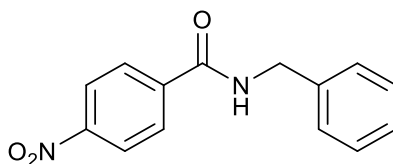
***N*-Benzylnaphthalene-1-carboxamide (109j)**



109j

According to General Procedure A, 1-naphthoic acid (0.49 g) and benzylamine (0.31 ml) were added for amidation. Kügelrohr distillation (190-200 °C, 0.3-0.4 torr) yielded 0.30 g (40%) as a white powder. ¹H NMR (400 MHz, CDCl₃) δ 4.75 (d, *J* 5.7, 2H), 6.28 (br. s, 1H), 7.29-7.48 (m, 6H), 7.50-7.60 (m, 2H), 7.61-7.65 (m, 1H), 7.85-7.94 (m, 2H), 8.34-8.38 (m, 1H). All the other spectroscopic and analytical data are consistent with those reported in the literature.²³³

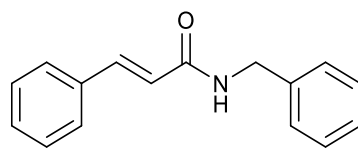
***N*-Benzyl-4-nitrobenzamide (109l)**



109l

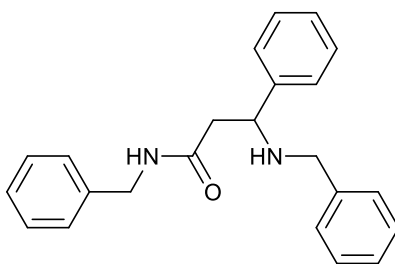
According to General Procedure A, 4-nitrobenzoic acid (0.48 g) and benzylamine (0.31 ml) were added for amidation. The crude product was yielded as a white solid 0.04 g (5%). Kügelrohr distillation (170-185 °C, 0.4 torr) yielded 0.03 g (4%) of pure amide product as a white solid. ¹H NMR (400 MHz, CDCl₃) δ 4.70 (d, *J* 5.6, 2H), 6.45 (br. s, 1H), 7.55 (dd, *J* 7.8, 3.3, 5H), 7.98 (d, *J* 8.9, 2H), 8.32 (d, *J* 8.9, 2H). All the other spectroscopic and analytical data are consistent with those reported in the literature.²³²

(2E)-N-Benzyl-3-phenylprop-2-enamide (110)



Trans-cinnamic acid (0.42 g, 2.86 mmol), polymer catalyst (75.8 mg, 5 mol%) and toluene (20 ml) were added to a 50 mL round-bottom flask. Benzylamine (0.62 ml, 5.76 mmol) was added and the resulting mixture stirred at a vigorous reflux using a Dean-Stark trap for 24 hrs. After cooling to rt, the solvent was removed *in vacuo*. The resulting crude solid was redissolved in DCM or chloroform (50 ml), filtered to remove catalyst, washed with 5% HCl (3 × 20 ml), saturated NaHCO₃ (3 × 20 ml), brine (3 × 20 ml), and finally water (20 ml). The solvent was removed *in vacuo* to give the crude amide product. Kügelrohr distillation (175-185 °C, 0.3-0.4 torr) yielded 0.37 g (54.5%) as a white powder. ¹H NMR (400 MHz, CDCl₃) δ 4.61 (d, *J* 5.7, 2H), 5.93 (br. s. 1H), 6.43 (d, *J* 15.6, 1H), 7.30-7.42 (m, 8H), 7.48-7.56 (m, 2H), 7.71 (d, *J* 15.6, 1H). All the other spectroscopic and analytical data are consistent with those reported in the literature.²³⁵

N-Benzyl-3-(benzylamino)-3-phenylpropanamide (112)

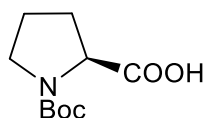


Trans-cinnamic acid (0.42 g, 2.86 mmol), polymer catalyst (75.8 mg, 5 mol%) and toluene (20 ml) were added to a 50 mL round-bottom flask. Benzylamine (0.62 ml, 5.76 mmol) was added and the resulting mixture stirred at a vigorous reflux using a Dean-Stark trap for 24 hrs. After cooling to rt, solvent was removed *in vacuo*. The resulting crude solid

was redissolved in DCM or chloroform (50 ml), filtered to remove catalyst, washed with 5% HCl (3 × 20 ml), saturated NaHCO₃ (3 × 20 ml), brine (3 × 20 ml) and water (20 ml). The solvent was removed *in vacuo* to give the crude amide product. Kügelrohr distillation (190-200 °C, 0.3-0.4 torr) yielded 0.19 g (27.6%) as a pale-yellow oil. ¹H NMR (400 MHz, CDCl₃) δ 1.68 (br. s, 1H), δ 2.55 (dd, *J* 15.6, 3.8, 1H), δ 2.66 (dd, *J* 15.7, 9.7, 1H), δ 3.52 (d, *J* 12.7, 1H), δ 3.65 (d, *J* 12.7, 1H), δ 4.06 (dd, *J* 9.8, 3.8, 1H), δ 4.43 (qd, *J* 14.6, 5.5, 2H), δ 7.10 (dd, *J* 6.6, 2.9, 2H), δ 7.22-7.43 (m, 13H), δ 7.52 (br. s, 1H). All the other spectroscopic and analytical data are consistent with those reported in the literature.²³⁶

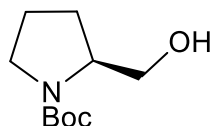
3.2 Bifunctional catalysis of asymmetric nitro-Michael reaction

(2*S*)-1-[(*tert*-Butoxy)carbonyl]pyrrolidine-2-carboxylic acid (**118**)



Add Et₃N (14.2 ml, 102.4 mmol) to an ice-cold suspension of *L*-proline (4.50 g, 39.1 mmol) in DCM (90 ml), followed by Boc₂O (12.0 g, 54.8 mmol) in DCM (10.00 ml). After stirring at rt for 2h, 5% HCl (150 ml) was added. Mixture was extracted into Et₂O, organic layer washed with brine (60.0 ml), water (60 ml) and dried to give crude product. Recrystallisation from hot EtOAc by adding hexane and leaving the mixture in the freezer overnight to give 7.30 g (87%) of solid white product. ¹H NMR (400 MHz) δ 1.35-1.56 (m, 9H, H_{8,9,10}), 1.80-1.99 (m, 2H, H_{3A,4A}), 1.99-2.13 (m, 1H, H_{3B}), 2.20-2.42 (m, 1H, H_{4B}), 3.30-3.60 (m, 2H, H₅), 4.20-4.40 (m, 1H, H₂). All the other spectroscopic and analytical properties were identical to what repeated in the literature.²⁰⁰

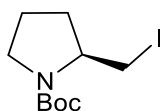
tert-Butyl (2*S*)-2-(hydroxymethyl)pyrrolidine-1-carboxylate (**119**)



To a solution of (2*S*)-1-[(*tert*-butoxy)carbonyl]pyrrolidine-2-carboxylic acid **118** (7.25 g, 33.7 mmol) in dry THF (60 ml) under Ar, BH₃•DMS (3.00 g, 37.1 mmol) was added dropwise and the reaction mixture was refluxed for 2 h. After cooling to rt, ice was

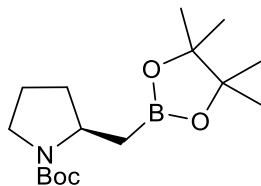
added, the aqueous layer was extracted with Et₂O, washed with 5% aq. NaOH twice, then with water, dried (MgSO₄) and evaporated to yield 2.49 (37%) of *N*-Boc-prolinol as a colourless oil, which crystallised overnight. ¹H NMR (400 MHz) δ 1.44 (s, 9H, H_{8,9,10}), 1.54-1.67 (m, 1H, H_{4A}), 1.69-1.90 (ddt, *J* 12.4, 6.4, 6.4, 2H, H_{4B}, H_{3A}), 1.91-2.04 (m, 1H, H_{3B}), 3.23-3.34 (m, 1H, H_{5A}), 3.36-3.48 (m, 1H, H_{5B}), 3.51-3.63 (m, 2H, hydroxyl methyl H₁), 3.87-4.40 (m, 1H, H₂). All the other spectroscopic and analytical properties were identical to what repeated in the literature.²⁰⁰

***tert*-Butyl (2*S*)-2-(iodomethyl)pyrrolidine-1-carboxylate (120)**



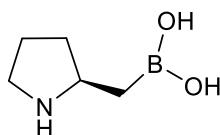
To a suspension of imidazole (1.66 g, 24.4 mmol) and PPh₃ (4.87 g, 18.6 mmol) in Et₂O (150 ml) at 0 °C under Ar, iodine, ground into a fine powder, (4.74 g, 18.60 mmol) was added in portions over 30 min during intense stirring with mechanical stirrer. Solution of *tert*-butyl (2*S*)-2-(hydroxymethyl)pyrrolidine-1-carboxylate **119** (2.49 g, 12.4 mmol) in DCM (20 ml) was added, and the mixture stirred overnight at r.t. The mixture was dissolved in DCM, mixed with silica gel and columned (EtOAc:hexane = 1:1) to yield 3.59 g (93%) of iodomethyl-*N*-Boc-pyrrolidine as white solid. ¹H NMR (with rotamers present, but only some can be distinguished) δ 1.37-1.56 (s, 9H, *tert*-butyl H_{2,3,4}), 1.74-1.98 (m, 3H, H₄, H_{3A}), 1.99-2.12 (m, 1H, H_{3B}), 3.05-3.56 (m, 4H, H₅, H₆), 3.70-3.94 (m, 1H, H₂). All the other spectroscopic and analytical properties were identical to what repeated in the literature.²⁰⁰

***tert*-Butyl (*R*)-2-((4,4,5,5-tetramethyl-1,3,2-dioxaborolan-2-yl)methyl)pyrrolidine-1-carboxylate ((*R*)-86)**



To a mixture of manganese (II) bromide (5.5 mg, 5 mol%), B₂Pin₂ (0.17 g, 0.65 mmol) and TMEDA (3.8 μ L, 5 mol%) dissolved in DME (0.5 ml), ethylmagnesium bromide (220 μ L, 0.65 mmol) was added, followed by the *tert*-butyl (2*S*)-2-(iodomethyl)pyrrolidine-1-carboxylate **120** (0.16 g, 0.50 mmol) under Ar. The reaction mixture turned grey and was stirred at rt for 1.5 h, after which it was quenched with 5 mL 20% HCl, extracted with Et₂O, dried (MgSO₄) and evaporated to give the crude oil, which was then purified by silica gel chromatography (EtOAc:hexane 1:4) to yield 76 mg (49%) of *N*-Boc-homoboroproline pinacol ester as a colourless oil. ¹H NMR (signals for main rotamer) δ 0.96 (d, *J* 5.4, 1H, H_{6a}), 1.21-1.32 (m, 12H, H₁₆), 1.48 (s, 9H, Boc H_{4,5,6}), 1.59 (s, 2H, H_{6b}, H_{3a}), 1.67-1.78 (m, 1H, H_{4a}), 1.78-1.89 (m, 1H, H_{4b}), 1.97-2.09 (m, 1H, H_{3b}), 3.20-3.46 (br, 2H, H₅), 3.84-4.04 (br, 1H, H₂) All the other spectroscopic and analytical properties were identical to what repeated in the literature.²⁰⁰

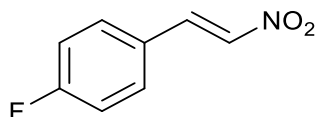
{[(2*R*)-Pyrrolidin-2-yl]methyl}boronic acid ((*R*)-85)



20% HCl (1.7 ml) was added to *tert*-butyl (*R*)-2-((4,4,5,5-tetramethyl-1,3,2-dioxaborolan-2-yl)methyl) pyrrolidine-1-carboxylate (80 mg, 0.26 mmol) and reaction refluxed for 2 h. The mixture was cooled to rt, washed with Et₂O (3 x 20 mL) and

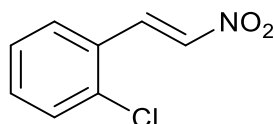
evaporated to isolate homoboroproline hydrochloride **8** a pale brown oil (30 mg, 38%). ^1H NMR (400 MHz in D_2O) δ 1.09 (dd, J 15.8, 9.6, 1H, H_{5a}), 1.22 (dd, J 15.8, 6.5, 1H, H_{5b}), 1.43-1.53 (m, 1H, H_{2a}), 1.80-1.88 (m, 1H, H_{3a}), 1.89-1.97 (m, 1H, H_{3b}), 2.06-2.13 (m, 1H, H_{2b}), 3.10-3.21 (m, 2H, H_4), 3.53-3.62 (m, 1H, H_1). All the other spectroscopic and analytical properties were identical to what repeated in the literature.²⁰⁰

1-Fluoro-4-[(1E)-2-nitroethenyl]benzene (121a)



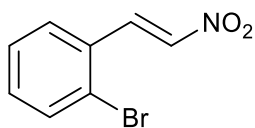
According to General Procedure J, 4-fluorobenzaldehyde (1.24 g, 10 mmol) was applied in the reaction, and a yellow solid was obtained (1.49 g, 89%) ^1H NMR (400 Hz, in CDCl_3) δ 7.18 (t, J 8.5, 2H), 7.63-7.52 (m, 3H), 8.01(d, J 13.7, 1H). ^{19}F NMR δ -105.77 (s). All the other characteristics were identical to those reported in the literature.²¹⁰

1-Chloro-2-[(1E)-2-nitroethenyl]benzene (121b)



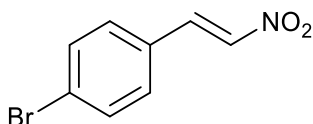
According to General Procedure J, 2-chlorobenzaldehyde (1.41 g, 10 mmol) was applied in the reaction, and a pale yellow solid was obtained (1.81 g, 99%) ^1H NMR (400 Hz, in CDCl_3) δ 7.37 (t, J 7.3, 1H), 7.46 (t, J 7.7, 1H), 7.53 (d, J 8.2, 3H), 7.62 (d, J 13.7, 2H), 8.44(d, J 13.7, 1H). All the other characteristics were identical to those reported in the literature.²¹⁰

1-Bromo-2-[(1E)-2-nitroethenyl]benzene (121c)



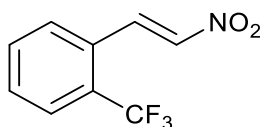
According to General Procedure J, 2-bromobenzaldehyde (1.83 g, 10 mmol) was applied in the reaction, and a pale yellow solid was obtained (2.16 g, 95%) $^1\text{H NMR}$ (400 Hz, in CDCl_3) δ 7.46-7.32 (tm, 2H), 7.63-7.53 (m, 2H), 7.72 (dd, J 7.9, 1H), 8.42 (d, J 13.7, 1H). All the other characteristics were identical to those reported in the literature.²¹⁰

1-Bromo-4-[(1E)-2-nitroethenyl]benzene (121d)



According to General Procedure J, 4-bromobenzaldehyde (1.83 g, 10 mmol) was applied in the reaction, and a pale-yellow solid was obtained (1.84 g, 81%). mp. 140 °C; $^1\text{H NMR}$ (400 Hz, in CDCl_3) δ 7.94 (d, J 13.7, 1H), 7.60 (d, J 8.5, 2H), 7.56 (d, J 13.7, 1H), 7.41 (d, J 8.5, 2H). All the other characteristics were identical to those reported in the literature.²¹⁰

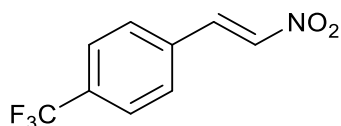
1-Trifluoromethyl-2-[(1E)-2-nitroethenyl]benzene (121e)



According to general procedure J, *o*-trifluoromethyl-benzaldehyde (1.74 g, 10 mmol) was applied in the reaction, and a yellow solid was obtained (1.06 g, 49%): $^1\text{H NMR}$ (400 Hz, CDCl_3) δ 8.38 (dd, J 13.5, 1H), 7.80 (d, J 7.8, 1H), 7.64 (m, 3H), 7.50 (d, J 13.6,

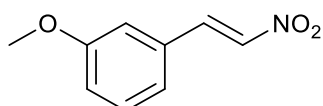
1H). ^{19}F NMR δ 58.78 (s). All the other characteristics were identical to those reported in the literature.²¹⁰

1-Trifluoromethyl-4-[(1E)-2-nitroethenyl]benzene (121f)



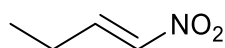
According to general procedure J, *p*-trifluoromethyl-benzaldehyde (1.74 g, 10 mmol) was applied in the reaction, and a yellow solid was obtained (1.09 g, 50%): ^1H NMR (400 Hz, CDCl_3) δ 8.32 (dd, J 13.5, 1H), 7.80 (d, J 7.7, 1H), 7.64 (m, 2H), 7.50 (m, 2H). ^{19}F NMR δ 59.06 (s). All the other characteristics were identical to those reported in the literature.²¹⁰

1-Methoxyl-3-[(1E)-2-nitroethenyl]benzene (121g)



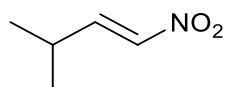
According to general procedure J, 3-methoxybenzaldehyde (1.36 g, 10 mmol) was applied in the reaction, and a pale solid product **122g** was obtained (1.43 g, 80%); ^1H NMR (400 Hz, in CDCl_3) δ 7.97 (d, J 13.7, 1H), 7.57 (d, J 13.6, 1H), 7.37 (dd, J 9.0, 7.6, 1H), 7.14 (m, 1H), 7.03 (m, 2H), 3.85 (s, 3H). All the other characteristics were identical to those reported in the literature.²¹⁰

(1E)-1-Nitrobut-1-ene (121i)



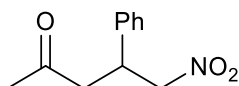
According to General Procedure J, propylaldehyde (0.59 g, 10 mmol) was applied in the reaction, and a pale-yellow oil was obtained (0.44 g, 44%) ¹H NMR (400 Hz, in CDCl₃) δ 1.14 (t, *J* 7.4, 3H), 2.32 (qdd, *J* 7.4, 6.7, 2H), 6.97 (dt, *J* 13.4, 1H), 7.32 (dt, *J* 13.4, 6.7, 1H). All the other characteristics were identical to those reported in the literature.²¹⁰

(1E)-3-Methyl-1-nitrobut-1-ene (121j)



According to General Procedure J, *iso*-butylaldehyde (0.72 g, 10 mmol) was applied in the reaction, and a yellow solid was obtained (1.01 g, 92%) ¹H NMR (400 Hz, in CDCl₃) δ 1.16 (dd, *J* 6.7, 6H), 2.60 (dq, *J* 13.6, 6.8, 1H), 6.95 (dd, *J* 13.4, 1H), 7.26 (ddd, *J* 13.4, 7.1, 1H). All the other characteristics were identical to those reported in the literature.²¹⁰

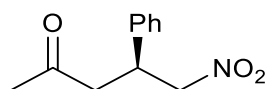
5-Nitro-4-phenylpentan-2-one (122k)



To a mixture of nitrostyrene (0.15 g, 1.0 mmol) and acetone (2.0 ml) dissolved in DMSO (8.0 ml), *L*-proline (23 mg) was added. The reaction mixture was stirred at r.t. for 24 h before being quenched with saturated NH₄Cl (5 ml), extracted with Et₂O, dried (MgSO₄) and evaporated to give the crude product, which was then purified by silica gel column chromatography (EtOAc: hexane gradient, 1:4 - 2:1) to yield 0.15 g (73 %) of white

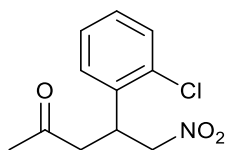
solid. ^1H NMR (400 MHz, CDCl_3) δ 2.15 (s, 3H, H_1), 2.95 (d, J 7.0, 2H, H_3), 4.03 (p, J 7.1, 1H, H_4), 4.63 (dd, J 12.3, 7.6, 1H, H_{5a}), 4.72 (dd, J 12.3, 6.9, 1H, H_{5b}), 7.22-7.26 (m, 2H, phenyl), 7.29-7.39 (m, 3H, phenyl). ^{13}C NMR (101 MHz, CDCl_3) δ 148.8 (RCOR'), 129.1, 127.9, 127.4 (phenyl), 79.5 ($\text{CH}_2\text{-NO}_2$), 46.2 (CH), 39.1 (CH_2), 30.4 (CH_3). All the other spectroscopic and analytical properties were identical to those reported in the literature.²³⁷

(4R)-5-Nitro-4-phenylpentan-2-one ((R)-122k)



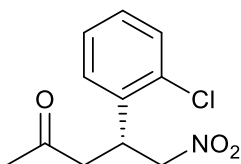
To a mixture of nitrostyrene (0.15 g, 1.0 mmol) and acetone (4.0 ml) dissolved in DMSO (8.0 ml), triethylamine (5 mg) was added, followed by the addition of (*R*)-2-(boronomethyl)pyrrolidine-1-ium hydrochloride. The reaction mixture was stirred at r.t. for 24 h before being extracted with Et_2O , dried (MgSO_4) and evaporated to give the crude product, which was purified by silica gel column chromatography (EtOAc: hexane gradient, 1:5 - 1:1) to yield 0.64 g (61 %) of white solid. ^1H NMR (400 MHz, CDCl_3) δ 2.15 (s, 3H, H_1), 2.95 (d, J 7.0, 2H, H_3), 4.03 (p, J 7.1, 1H, H_4), 4.63 (dd, J 12.3, 7.6, 1H, H_{5a}), 4.72 (dd, J 12.3, 6.9, 1H, H_{5b}), 7.22-7.26 (m, 2H, phenyl), 7.29-7.39 (m, 3H, phenyl). Chiral HPLC: AS-H column, 25 °C, flow rate 1.00 ml/min, 210 nm, hexane:IPA (60:40). $t_R(S)$ = 10.73 min, $t_R(R)$ = 14.37 min. All the other spectroscopic and analytical properties were identical to those reported in the literature.^{199, 237}

4-(2-Chlorophenyl)-5-nitropentan-2-one (122b)



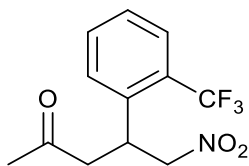
According to General Procedure K, (*E*)-1-chloro-2-(2-nitrovinyl)benzene (0.18 g, 1 mmol) was used for racemic synthesis, and a yellow solid product **123b** was obtained (0.19 g, 80%). ¹H NMR (400 MHz, CDCl₃) δ 3.56 (dd, *J* 6.9, 1H), 4.72 (p, *J* 6.8, 1H), 4.88 (dd, *J* 6.8, 2H), 7.64-7.53 (m, 2H), 7.97 (ddt, *J* 8.1, 6.6, 3H). The enantiomeric excess was determined by chiral HPLC: *t*_R (*S*) = 15.6 min; *t*_R (*R*) = 17.2 min. All the other spectroscopic and analytical properties were identical to those reported in the literature.^{201, 239}

(4*R*)-4-(2-chlorophenyl)-5-nitropentan-2-one ((*R*)-122b)



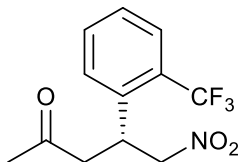
According to General Procedure N, (*E*)-1-chloro-2-(2-nitrovinyl)benzene (0.14 g, 1.0 mmol) was used and a white solid product (***R***-123b) was obtained (0.24 g, 99 %). ¹H NMR (400 MHz, CDCl₃) δ 2.09-2.20 (s, 3H), 2.95 (dd, *J* 17.9, 7.7, 1H, H₃), 3.04 (dd, *J* 17.9, 7.7, 1H, H₃), 4.39-4.50 (p, 1H, H₄), 4.74 (d, *J* 6.4, 2H, H₅), 7.17-7.25 (m, 3H, Ph), 7.35-7.42 (m, 1H, Ph). The enantiomeric excess was determined by chiral HPLC: *t*_R (minor) = 16.7 min; *t*_R (major) = 18.5 min. All the other spectroscopic and analytical properties were identical to those reported in the literature.^{199, 237}

4-(2-Chlorophenyl)-5-nitropentan-2-one (**122e**)



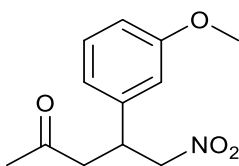
According to General Procedure K, (*E*)-1-trifluoromethyl-2-(2-nitrovinyl)benzene (0.22 g, 1 mmol) was used for the racemic synthesis, and a yellow solid product **123e** was obtained (0.23 g, 83%). ^1H NMR (400 MHz, CDCl_3) δ 3.56 (dd, *J* 6.9, 1H), 4.72 (p, *J* 6.8, 1H), 4.88 (dd, *J* 6.8, 2H), 7.64-7.53 (m, 2H), 7.97 (ddt, *J* 8.1, 6.6, 3H). All the other spectroscopic and analytical properties were identical to those reported in the literature.²³⁷

(*4R*)-5-Nitro-4-(2-trifluoromethylphenyl)pentan-2-one ((*R*)-**122e**)



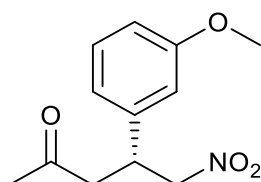
According to General Procedure N, (*E*)-1-trifluoromethyl-2-(2-nitrovinyl)benzene (0.22 g, 1 mmol) was used and a white solid product (*R*)-**123e** was obtained (0.64 g, 61%). ^1H NMR (400 MHz, CDCl_3) δ 2.16 (s, 3H), 2.90 (dd, *J* 17.9, 5.3, 1H), 3.03 (dd, *J* 17.9, 8.4, 1H), 4.35-4.47 (p, 1H), 4.74 (d, *J* 6.7, 2H), δ 7.35 (d, *J* 7.9, 1H), 7.41 (d, *J* 7.8, 1H), 7.54 (d, *J* 7.6, 1H), 7.70 (dd, *J* 7.9, 1H). The enantiomeric excess was determined by chiral HPLC: t_{R} (minor) = 10.7 min; t_{R} (major) = 14.4 min. ^{19}F NMR δ 58.96. All the other spectroscopic and analytical properties were identical to those reported in the literature.¹⁹⁹

4-(3-Methoxyphenyl)-5-nitropentan-2-one (122g)



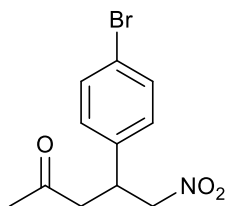
According to general procedure K, (*E*)-1-methoxyl-3-(2-nitrovinyl)benzene (0.18 g, 1.0 mmol) and acetone (2.0 ml) were applied. The resulting product was 0.10 g (42%) and obtained as a white solid. ^1H NMR (400 MHz, CDCl_3) δ 2.13 (s, 3H), 2.92 (d, J 6.8, 2H), 3.80 (s, 3H), 3.99 (p, J 7.1, 1H), 4.60 (dd, J 12.4, 7.7, 1H), 4.69 (dd, J 12.4, 6.8, 1H), 6.86-6.74 (m, 3H), 7.30-7.23 (t, J 7.9, 1H). The enantiomeric excess was determined by chiral HPLC: t_{R} (*S*) = 18.9 min; t_{R} (*R*) = 23.0 min. All the other spectroscopic and analytical properties were identical to those reported in the literature.^{201, 239}

(4*R*)-4-(3-Methoxyphenyl)-5-nitropentan-2-one ((*R*)-122g)



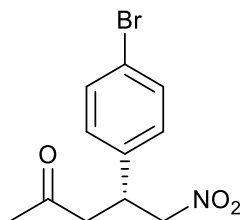
According to General Procedure N, (*E*)-1-methoxyl-3-(2-nitrovinyl)benzene (0.18 g, 1.0 mmol) was used and a white solid product (*R*)-123g was yielded (0.09 g, 38 %). ^1H NMR (400 MHz, CDCl_3) δ 0.81-0.96 (s, 3H, MeO), δ 1.22-1.28 (s, 3H), 2.90 (d, J 7.0, 1H, H_4), 3.76-3.82 (m, 2H, H_3), 4.59 (dd, J 12.4, 7.6, 1H, H_5), 4.67 (dd, J 12.4, 7.0, 1H, H_5), 7.09-7.18 (m, 2H, Ph), 7.20-7.26 (m, 2H, Ph). The enantiomeric excess was determined by chiral HPLC: t_{R} (minor) = 18.9 min; t_{R} (major) = 23.0 min. All the other spectroscopic and analytical properties were identical to those reported in the literature.^{199, 237}

(4-Bromophenyl)-5-nitropentan-2-one (122d)



According to general procedure K, (*E*)-1-bromo-4-(2-nitrovinyl)benzene (0.22 g, 1.0 mmol) and acetone (2.0 ml) were applied. The resulting product was yielded 0.15 g (73 %) as a white solid. ¹H NMR (400 MHz, CDCl₃) δ 2.15 (s, 3H), 2.91 (d, *J* 7.0, 2H), 4.00 (p, *J* 7.1, 1H), 4.60 (dd, *J* 12.5, 7.9, 1H), 4.70 (dd, *J* 12.5, 6.6, 1H), 7.13 (d, *J* 8.6, 2H), 7.48 (d, *J* 8.4, 2H). The enantiomeric excess was determined by chiral HPLC: *t_R* (*S*) = 17.1 min; *t_R* (*R*) = 21.9 min. All the other spectroscopic and analytical properties were identical to those reported in the literature.^{201, 239}

(4*R*)-4-(4-Bromophenyl)-5-nitropentan-2-one ((*R*)-122d)

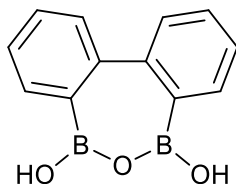


According to General Procedure N, (*E*)-1-bromo-4-(2-nitrovinyl)benzene (0.22 g, 1.0 mmol) was used and the reaction yielded 0.64 g (61%) of product (***R***)-122d as a white solid. ¹H NMR (400 MHz, CDCl₃) δ 1.26 (s, 3H), 2.88 (d, *J* 7.0, 2H), 3.92-4.03 (p, 1H), 4.57 (dd, *J* 12.5, 7.9, 1H), 4.68 (dd, *J* 12.5, 7.9, 1H), 7.06-7.18 (m, 3H), 7.41-7.50 (m, 1H). The enantiomeric excess was determined by chiral HPLC: *t_R* (minor) = 18.2 min; *t_R* (major) = 23.6 min. All the other spectroscopic and analytical properties were identical to those reported in the literature.^{199, 237}

3.3 Kinetic resolution of asymmetric amide formation

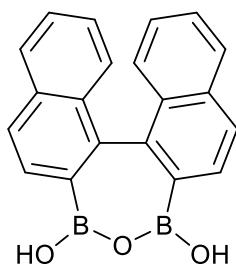
9-Oxa-8,10-diboratricyclo[9.4.0.0^{2,7}]pentadeca-1(11),2,4,6,12,14-hexaene-8,10-diol

(129)^{191, 217}



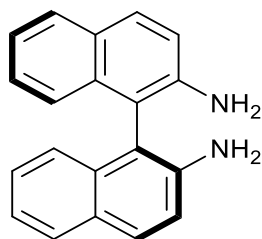
In a 50 mL round bottom flask, ⁿBuLi (0.64 mL, 1.60 mmol) was added to a solution of 2,2'-dibromobiphenyl (0.20 g, 0.64 mmol) in dry THF (10 mL) under argon at -78 °C. After 30 min stirring, trimethyl borate (0.16 mL, 1.41 mmol) was added and reaction mixture warmed up slowly to room temperature. After a further 30 min, the reaction was quenched with 20 % HCl (5.0 mL) for 15 min. The product was extracted with ethyl acetate (3 × 10 mL), washed with brine (3 × 10 mL), dried over MgSO₄ and evaporated *in vacuo* to give a crude solid (0.09 g, 65%). Recrystallisation (toluene-PE) gave pure product **129** as a white solid (75.8 mg, 53 %) ¹H NMR (400 MHz, CDCl₃) δ 4.73 (s, 2H, OH), 7.40 (t, *J* 7.3, 2H), 7.57 (t, *J* 7.4, 2H), 7.65 (d, *J* 7.7, 2H), 7.88 (d, *J* 7.0, 2H). ¹¹B NMR (128 MHz, CDCl₃) δ 29.75. All the other spectroscopic and analytical properties were identical to those reported in the literature.^{191, 217}

13-Oxa-12,14-diborapentacyclo[13.8.0.0^{2,11}.0^{3,8}.0^{18,23}]tricoso-1(15),2,4,6,8,10,16,18(23),19,21-decaene-12,14-diol (108)



In a 50 mL round bottom flask, ⁿBuLi (0.64 mL, 1.60 mmol) was added to a solution of 2,2'-dibromobinaphthyl (0.26 g, 0.64 mmol) in dry THF (10 mL) under argon, at -78 °C. After 30 min stirring, trimethyl borate (0.16 mL, 1.41 mmol) was added and reaction mixture warmed up slowly till room temperature. Stir another 30 min before quenching with 20 % HCl (5.0 mL) for 15 min. The product was extracted with ethyl acetate (3 × 10 mL), washed with brine (3 × 10 mL), dried over MgSO₄ and condensed *in vacuo* to give the crude. Recrystallisation of crude (toluene-PE) gives purified product as a white solid (0.13 g, 64 %), mp: 159-166 °C, ¹H NMR (400 MHz, CDCl₃) δ 8.17-7.73 (m, 12H); ¹³C NMR (100 MHz, CDCl₃) δ 131.6, 130.1, 129.0, 128.0, 127.2, 126.6, 126.0 and 125.7; ¹¹B NMR (128 MHz, CDCl₃) δ 30 (br. s). HRMS (ESI+) calculated [C₂₀H₁₄¹¹B₂O₃+H⁺] 325.1588, found, 325.1215. mp: 159-165 °C.

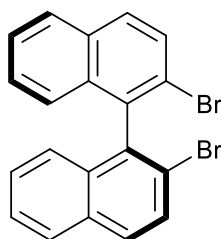
(S)-[1,1'-Binaphthalene]-2,2'-diamine ((S)-132)²¹⁹



(S)-BINOL (0.057 g, 0.2 mmol, 1 equiv.), 2-bromopropionamide (0.09 g, 0.6 mmol, 3 equiv.), K₂CO₃ (0.08 g, 0.6 mmol, 3 equiv.) and KI (3.0 mg, 10 mol%) were dropped in a 10 mL round bottom flask with DMSO (2 mL) at 50 °C. The resulting mixture was stirred for 24 h until complete consumption of starting material. By the time reaction heated to 150 °C, KOH (0.14 g, 2.5 mmol, 12.5 equiv.) was added into the flask. The reaction mixture turned dark brown immediately and was quenched by H₂O (5 mL) after another 4 h stirring. Reaction mixture cooled down to r.t., extracted with EA and evaporated *in vacuo* to give the crude. Silica gel column chromatography (Hex: EA = 75:25) to give the purified product

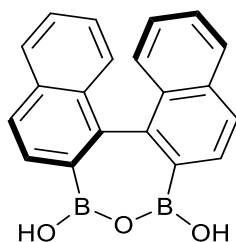
as a yellow solid (0.04 g, 70%). ^1H NMR (400 MHz, CDCl_3) δ 3.52 (br. s, 4H, NH), 7.09 (d, J 8.4, 2H), 7.28-7.18 (m, 6H), 7.83 (t, J 7.7, 4H). The enantiomeric excess was obtained at >99%, which was determined by chiral HPLC using an AS-H-CHIRALCEL column (250 x 4.60 mm) fitted with guard cartridge (50 x 4.6 mm), 25 °C, flow rate 1.00 ml/min, 210 nm, hexane: IPA (80:20). All the other spectroscopic and analytical properties were identical to those reported in the literature.²¹⁹

(*S*)-2,2'-Dibromo-1,1'-binaphthalene ((*S*)-130)²²⁰



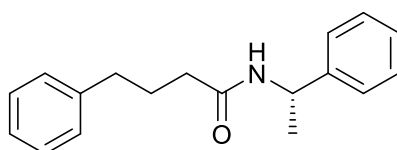
In a 25 mL round bottom flask, TMS-Br (0.92 g, 6.0 mmol, 6 equiv.) was added to the solution of NaNO_2 (0.41 g, 6.0 mmol, 6 equiv.) and triethylbenzylammonium chloride (0.09 g, 40 mol%) in CCl_4 (10 mL) at 0 °C. (*S*)-[1,1'-binaphthalene]-2,2'-diamine ((*S*)-132) (0.28 g, 1 equiv.) was dropped in before stirring for another 1.5 h. Then, reaction warmed to r.t. Solvent removed *in vacuo* after 10 h reaction. Silica gel chromatography (Hex:EA = 75:25) to give the purified product as a yellow solid (0.08 g, 20%). ^1H NMR (400 MHz, CDCl_3) δ 7.10 (d, J 8.5, 2H), 7.32 (m, 2H). The enantiomeric excess was obtained at >99%, which was determined by chiral HPLC using an OD-CHIRALCEL column (250 x 4.60 mm) fitted with guard cartridge (50 x 4.6 mm), 25 °C, flow rate 1.00 ml/min, 210 nm, hexane: DME (75:25). All the other spectroscopic and analytical properties were identical to those previously reported.

**(S)-13-Oxa-12,14-diborapentacyclo[13.8.0.0²,¹¹.0³,⁸.0¹⁸,²³]tricosan-
1(15),2,4,6,8,10,16,18(23),19,21-decaene-12,14-diol ((S)-108)**



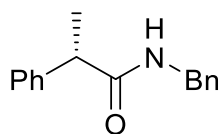
In a 50 mL round bottom flask, *n*BuLi (0.64 mL, 1.60 mmol) was added to a solution of (*S*)-2,2'-dibromobinaphthyl (0.26 g, 0.64 mmol) in dry THF (10 mL) under argon, at -78 °C. After 30 min stirring, trimethyl borate (0.16 mL, 1.41 mmol) was added and reaction mixture warmed up slowly till room temperature. Stir another 30 min before quenching with 20 % HCl (5.0 mL) for 15 min. The product was extracted with ethyl acetate (3 × 10 mL), washed with brine (3 × 10 mL), dried over MgSO₄ and condensed *in vacuo* to give the crude. Recrystallisation of crude (toluene-PE) gives purified product as a white solid (0.13 g, 64 %) IR(neat) ν_{max} : 3208, 3057, 1593, 1502, 1466, 1343, 1328, 1243, 1105, 944 cm⁻¹. ¹H NMR (400 MHz, CDCl₃) δ 7.63-6.98 (m, 4H), 7.53 (q, *J* 7.6, 4H), 8.23-7.80 (m, 4H); ¹³C NMR (100 MHz, CDCl₃) δ 132.5, 131.1, 128.6, 128.0, 127.0, 126.8, 125.7 and 125.3; ¹¹B NMR (128 MHz, CDCl₃) δ 29 (br. s); HRMS (ESI+) calculated [C₂₀H₁₄¹¹B₂O₃+H⁺] 325.1593 found, 325.1215. mp: 158-164 °C. [α]_D = -139.33 (MeOH, *t* = 20 °C, *c* = 1.0).

4-Phenyl-N-[(1S)-1-phenylethyl]butanamide ((S)-134)



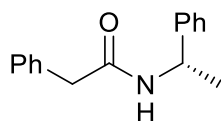
According to General Procedure O, phenylbutyric acid (0.47 g, 2.86 mmol) and (\pm)- α -methyl benzylamine (0.72 ml, 5.72 mmol) were added for amidation. Kügelrohr distillation carried (195-200 °C, 0.4 torr) and yielded 0.65 g (80%) of pure amide product as a pale yellow solid. ^1H NMR (400 MHz, CDCl_3) δ 1.51 (d, J 6.9, 3H), 2.05-1.96 (m, 1H), 2.23-2.17 (m, 1H), 2.67 (t, J 7.5, 2H), 5.17 (p, J 7.1, 1H), 5.64 (d, J 7.9, 1H), 7.24-7.15 (m, 3H), 7.40-7.25 (m, 7H). Chiral HPLC: AD column, 25 °C, flow rate 1.00 ml/min, 210 nm, hexane:IPA (96:4). $t_R(R) = 27.9$ min, $t_R(S) = 37.7$ min. All the other spectroscopic and analytical data are consistent with those reported in the literature.²³⁸

(2S)-N-Benzyl-2-phenylpropanamide ((S)-135)



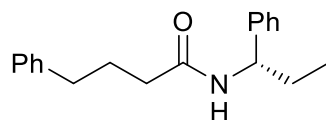
According to General Procedure O, 2-phenylpropionic acid (0.27 mL, 2.00 mmol) and benzylamine (0.11 mL, 1.00 mmol) were added for amidation. Kügelrohr distillation to give 0.07 g (26%) of pure amide product as a pale yellow solid. ^1H NMR (400 MHz, CDCl_3) δ 1.59 (d, J 7.3, 3H), 3.62 (q, J 7.2, 1H), 4.51-4.33 (m, 2H), 5.61 (s, 1H), 7.20-7.13 (m, 2H), 7.41-7.23 (m, 8H). Chiral HPLC: AD column, 25 °C, flow rate 1.00 ml/min, 210 nm, hexane:IPA (95:5). $t_R(S) = 29.1$ min, $t_R(R) = 41.3$ min. All the other spectroscopic and analytical data are consistent with those reported in the literature.²³⁹

2-Phenyl-*N*-[(1*S*)-1-phenylethyl]acetamide ((*S*)-136)



According to General Procedure O, phenylacetic acid (0.14 g, 1.0 mmol) and 2- α -methyl benzylamine (0.25 ml, 2.00 mmol) were added for amidation. Kügelrohr distillation carried (190-195 °C, 0.3 torr) and yielded 0.05 g (21%) of pure amide product as a yellow solid. ^1H NMR (400 MHz, CDCl_3) δ 1.42 (d, J 6.9, 3H), 3.61 (s, 2H), 5.15 (p, J 7.2, 1H), 5.69-5.54 (m, 1H), 7.23-7.18 (m, 2H), 7.42-7.24 (m, 8H). Chiral HPLC: AD column, 25 °C, flow rate 1.50 ml/min, 210 nm, hexane:IPA (97:3). $t_R(R)$ = 23.4 min, $t_R(S)$ = 34.8 min. All the other spectroscopic and analytical data are consistent with those reported in the literature.²⁴⁰

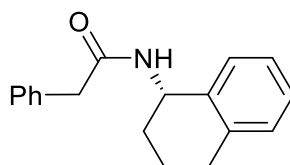
4-Phenyl-*N*-[(1*S*)-1-phenylpropyl]butanamide ((*S*)-137)



According to General Procedure O, phenylbutyric acid (0.16 g, 1 mmol) and 1-phenyl-1-propanamine (0.29 mL, 2.00 mmol) were added for amidation. Kügelrohr distillation carried (220-230 °C, 0.4 torr) and yielded 0.25 g (90%) of pure amide product as a pale yellow solid. ^1H NMR (400 MHz, CDCl_3) δ 0.91 (t, J 7.4, 3H), 1.83 (tt, J 11.1, 5.7, 4.5, 2H), 1.99 (p, J 7.5, 2H), 2.28-2.14 (m, 2H), 2.65 (t, J 7.5, 2H), 4.93 (q, J 7.7, 1H), 5.72 (d, J 8.4, 1H), 7.25-7.13 (m, 4H), 7.40-7.25 (m, 6H). ^{13}C NMR (100 MHz, CDCl_3) Chiral HPLC: AD column, 25 °C, flow rate 1.50 ml/min, 210 nm, hexane:IPA (97:3). $t_R(S)$

= 27.5min, $t_R(R)$ = 40.1 min. All the other spectroscopic and analytical data are consistent with those reported in the literature.²⁴¹

2-Phenyl-*N*-((1*R*)-1,2,3,4-tetrahydronaphthalen-1-yl)acetamide ((*R*)-138)



According to General Procedure O, phenylacetic acid (0.14, 1.00 mmol) and (\pm)-1,2,3,4-tetrahydro-1-naphthylamine (0.28 ml, 2.00 mmol) was added for amidation. Purified to get amide product (0.02 g, 8%) as a pale yellow solid. ^1H NMR (400 MHz, CDCl_3) δ 1.94-1.63 (m, 4H), 2.11-2.00 (m, 2H), 3.03-2.72 (3, 4H), 5.20 (q, J 7.2, 1H), 5.60 (d, J 8.6, 1H), 7.10-7.05 (m, 1H), 7.21-7.11 (m, 4H), 7.32-7.29 (m, 2H), 7.39-7.33 (m, 2H). Chiral HPLC: AD column, 25 °C, flow rate 1.00 ml/min, 210 nm, hexane:IPA (97:3). $t_R(R)$ = 26.5 min, $t_R(S)$ = 60.9 min. All the other spectroscopic and analytical data are consistent with those reported in the literature.²⁴¹

IX. References

1. P. Nelson and A. Pelter, *J. Chem. Soc.*, 1965, **4025**, 5142-5144.
2. A. Pelter, T. Levitt and P. Nelsoni, *Tetrahedron*, 1970, **26**, 1539-1544.
3. V. R. Pattabiraman and J. W. Bode, *Nature*, 2011, **480**, 471-479.
4. X. Wang, *Nature Catal.*, 2019, **2**, 98.
5. R. M. de Figueiredo, J. S. Suppo and J. M. Campagne, *Chem. Rev.*, 2016, **116**, 12029-12122.
6. J. W. ApSimon and Collier, T Lee, *Tetrahedron*, 1986, **42**, 5157-5254.
7. J. Crosby, *Tetrahedron*, 1991, **47**, 4789-4846.
8. L. Deloux and M. Srebnik, *J. Chem. Rev.*, 1993, **93**, 763-784.
9. K. Yoshida, T. Hayashi and D. Hall (2005). *Boronic acids: preparation and applications in organic synthesis and medicine*.
10. M. A. Martinez-Aguirre and A. K. Yatsimirsky, *J. Org. Chem.*, 2015, **80**, 4985-4993.
11. A. K. Ghose, V. N. Viswanadhan and J. J. Wendoloski, *J. Combi. Chem.*, 1999, **1**, 55-68.
12. S. D. Roughley and A. M. Jordan, *J. Med. Chem.*, 2011, **54**, 3451-3479.
13. S.-Y. Han and Y.-A. Kim, *Tetrahedron*, 2004, **60**, 2447-2467.
14. C. A. G. N. Montalbetti and V. Falque, *Tetrahedron*, 2005, **61**, 10827-10852.
15. D. J. C. Constable, P. J. Dunm and T. Y. Zhang, *Green Chem.*, 2007, **9**, 411-420.
16. Y. Kawagoe, K. Moriyama and H. Togo, *Tetrahedron*, 2013, **69**, 3971-3977.
17. D. C. Braddock, P. D. Lickiss and S. Fussell, *Org. Lett.*, 2018, **20**, 950-953.
18. S. Chung, D. P. Uccello and J. Chen, *Synlett.*, 2011, **22**, 2072-2074.
19. H. Lundberg and H. Adolfsson, *ACS Catalysis*, 2015, **5**, 3271-3277.

20. H. Lundberg, F. Tinnis and H. J. Adolfsson, *Chem. Eur. J.*, 2012, **18**, 3822-3826.
21. H. Lundberg, F. Tinnis and H. Adolfsson, *Synlett.*, 2012, **23**, 2201-2204.
22. F. Tinnis, H. Lundberg, H. J. Adolfsson, *Adv. Syn. Catal.*, 2012, **354**, 2531-2536.
23. L. Cheng, X. Ge and L. J. Huang, *R. Soc. open sci.*, 2018, **5**:171870, 1-9.
24. D. B. Collum, S.-C. Chen and B. Ganem, *J. Org. Chem.*, 1978, **43**, 4393-4394.
25. P. Tang, *Org. Syn.*, 2005, **81**, 262-272.
26. K. Ishihara, S. Ohara and H. Yamamoto, *J. Org. Chem.*, 1996, **61**, 4196-4197.
27. K. Ishihara, S. Kondo and H. Yamamoto, *Synlett*, 2001, **9**, 1371-1374.
28. R. Latta, G. Springsteen and B. Wang, *Synthesis*, 2001, **11**, 1611-1613.
29. T. Maki, K. Ishihara and H. Yamamoto, *Org. Lett.*, 2005, **7**, 5043-5046.
30. M. T. Sabatini, L. T. Boulton and T. D. Sheppard, *Sci. Adv.*, 2017, **3**:e1701028, 1-5.
31. S. Fatemi, N. Gernigon and D. G. Hall, *Green Chem.*, 2015, **17**, 4016-4028.
32. E. K.-W. Tam, Rita, L. Y. Liu and A. Chen, *Eur. J. Org. Chem.*, 2015, **5**, 1100-1107.
33. S. W. Coghlan, R. L. Giles, J. A. Howard, L. G. Patrick, M. R. Probert, G. E. Smith and A. Whiting, *J. Organomet. Chem.*, 2005, **690**, 4784-4793.
34. K. Arnold, B. Davies, R. L. Giles, C. Grosjean, G. E. Smith and A. Whiting, *Adv. Syn. Catal.*, 2006, **348**, 813-820.
35. K. Arnold, A. S. Batsanov, B. Davies and A. Whiting, *Green Chem.*, 2008, **10**, 124-134.
36. A. Kumar, H. K. Akula and M. K. Lakshman, *Eur. J. Org. Chem.*, 2010, **14**, 2709-2715
37. C. Deiana, Y. Sakhno, M. Fabbiani, M. Pazzi, M. Vincenti and G. Martra, *ChemCatChem.*, 2013, **5**, 2832-2834.

38. J. W. Comerford, J. H. Clark, D. J. Macquarrie and S. W. Breeden, *Chem. Commun.*, 2009, **18**, 2562-2564.
39. P. S. Chaudhari, S. D. Salim, R. V. Sawant and K. G. Akamanchi, *Green Chem.*, 2010, **12**, 1707-1710.
40. S. Ghosh, A. Bhaumik, J. Mondal, A. Mallik, S. Sengupta and C. Mukhopadhyay, *Green Chem.*, 2012, **14**, 3220-3229.
41. S. Crosignani, J. Gonzalez and D. Swinnen, *Org. Lett.*, 2004, **6**, 4579-4582.
42. D. Donati, C. Morelli, A. Porcheddu and M. Taddei, *J. Org. Chem.*, 2004, **69**, 9316-9318.
43. K. Pandey, M. K. Muthyala, S. Choudhary and A. Kumar, *RSC Adv.*, 2015, **5**, 13797-13804.
44. A. Ojeda-Porras, A. Hernández-Santana and D. Gamba-Sánchez, *Green Chemistry*, 2015, **17**, 3157-3163.
45. L. Gu, J. Lim, J. L. Cheong and S. S. Lee, *Chem. Commun.*, 2014, **50**, 7017-7019.
46. N. Gernigon, H. Zheng and D. G. Hall, *Tetrahedron Lett.*, 2013, **54**, 4475-4478.
47. S. Arkhipenko, M. T. Sabatini, A. S. Batsanov, V. Karaluka, T. D. Sheppard, H. S. Rzepa and A. Whiting, *Chem. Sci.*, 2018, **9**, 1058-1072.
48. a) T. Marcelli, *Angew. Chem. Int. Ed.*, 2010, **49**, 6840-6843. b) H. Charville, D. Jackson, G. Hodgesc and A. Whiting, *Chem. Commun.*, 2010, **46**, 1813-1823
49. C. Wang, H. Z. Yu, Y. Fu and Q. X. Guo, *Org. Bio. Chem.*, 2013, **11**, 2140-2146.
50. M. Shibasaki and M. Kanai, *Chem. Pharm. Bull.*, 2001, **49**, 511-524.
51. S. Itsuno, A. Hirao and S. Nakahama and N. Yamazaki, *J. Chem. Soc. Perkin Trans.*, 1983, **1**, 1673-1676.
52. S. Itsuno, K. Ito, A. Hirao and S. Nakahama, *J. Chem. Soc. Perkin Trans.*, 1984, **1**, 2887-2893.

53. S. Itsuno, M. Nakano, K. Miyazaki, H. Masuda, K. Ito, A. Hirao and S. Nakahama, *J. Chem. Soc. Perkin Trans.*, 1985, **1**, 2039-2044.
54. S. Itsuno, M. Nakano, K. Ito, A. Hirao, M. Owa, N. Kanda and S. Nakahama, *J. Chem. Soc. Perkin Trans.*, 1985, **1**, 2615-2619.
55. Y. Chen, S. Yekta and A. K. Yudin, *Chem. Rev.*, 2003, **103**, 3155-3212.
56. H. Sasai, T. Suzuki, N. Itoh, K. Tanaka, T. Date, K. Okamura and M. Shibasaki, *J. Am. Chem. Soc.*, 1993, **115**, 10372-10373.
57. M. Shibasaki and S. Matsunaga, *J. Organomet. Chem.*, 2006, **691**, 2089-2100.
58. Y. S. Kim, S. Matsunaga, J. Das, A. Sekine, T. Ohshima and M. Shibasaki, *J. Am. Chem. Soc.*, 2000, **122**, 6506-6507.
59. T. Arai, H. Sasai, K. I. Aoe, K. Okamura, T. Date and M. Shibasaki, *Angew. Chem. Int. Ed.*, 1996, **35**, 104-106.
60. T. Arai, Y. M. Yamada, N. Yamamoto, H. Sasai and M. Shibasaki, *Chem. Eur. J.*, 1996, **2**, 1368-1372.
61. E. Emori, T. Arai, H. Sasai and M. Shibasaki, *J. Am. Chem. Soc.*, 1998, **120**, 4043-4044.
62. H. Sasai, S. Arai, Y. Tahara and M. Shibasaki, *J. Org. Chem.*, 1995, **60**, 6656-6657.
63. N. P. Rath and C. D. Spilling, *Tetrahedron Lett.*, 1994, **35**, 227-230.
64. T. Yokomatsu, T. Yamagishi and S. Shibuya, *Tetrahedron Asymmetry*, 1993, **4**, 1783-1784.
65. T. Arai, M. Bougauchi, H. Sasai and M. Shibasaki, *J. Org. Chem.*, 1996, **61**, 2926-2927.
66. N. Yoshikawa, Y. M. Yamada, J. Das, H. Sasai and M. Shibasaki, *J. Am. Chem. Soc.*, 1999, **121**, 4168-4178.

67. Y. Abiko, N. Yamagiwa, M. Sugita, J. Tian, S. Matsunaga and M. Shibasaki, 2004, *Synlett.*, 2004, **13**, 2434-2436.
68. N. Yamagiwa, Y. Abiko, M. Sugita, J. Tian, S. Matsunaga and M. Shibasaki, *Tetrahedron Asymmetry*, 2006, **17**, 566-573.
69. N. Yamagiwa, S. Matsunaga and M. Shibasaki, *J. Am. Chem. Soc.*, 2003, **125**, 16178-16179.
70. T. Iida, N. Yamamoto, H. Sasai and M. Shibasaki, *J. Am. Chem. Soc.*, 1997, **119**, 4783-4784.
71. T. Iida, N. Yamamoto, S. Matsunaga, H. G. Woo and M. Shibasaki, *J. Am. Chem. Soc.*, 1998, **37**, 2223-2226.
72. S. Matsunaga, J. Das, J. Roels, E. M. Vogl, N. Yamamoto, T. Iida, K. Yamaguchi and M. Shibasaki, *J. Am. Chem. Soc.*, 2000, **122**, 2252-2260.
73. M. Chavarot, J. J. Byrne, P. Y. Chavant and Y. Vallée, *Tetrahedron Asymmetry*, 2001, **12**, 1147-1150.
74. S.-Y. Tosaki, K. Hara, V. Gnanadesikan and M. Shibasaki, *J. Am. Chem. Soc.*, 2006, **128**, 11776-11777.
75. H. Kakei, T. Sone, Y. Sohtome, S. Matsunaga and M. Shibasaki, *J. Am. Chem. Soc.*, 2007, **129**, 13410-13411.
76. P. G. Cozzi, *Chem. Soc. Rev.*, 2004, **33**, 410-421.
77. T. Katsuki, *Chem. Soc. Rev.*, 2004, **33**, 437-444.
78. M. Shibasaki and S. Matsunaga, *J. Syn. Org. Chem. Jpn.*, 2010, **68**, 1142-1149.
79. S. Handa, V. Gnanadesikan, S. Matsunaga and M. Shibasaki, *J. Am. Chem. Soc.*, 2007, **129**, 4900-4901.
80. S. Handa, V. Gnanadesikan, S. Matsunaga and M. Shibasaki, *J. Am. Chem. Soc.*, 2010, **132**, 4925-4934.

81. M. Furutachi, S. Mouri, S. Matsunaga and M. Shibasaki, *Chem. Asian J.*, 2010, **5**, 2351-2354.
82. T. Nitabaru, A. Nojiri, M. Kobayashi, N. Kumagai and M. Shibasaki, *Chem. Asian J.*, 2009, **131**, 13860-13869.
83. T. Nitabaru, N. Kumagai and M. Shibasaki, *Molecules*, 2010, **15**, 1280-1290.
84. Y. Hamashima, D. Sawada, M. Kanai and M. Shibasaki, *J. Am. Chem. Soc.*, 1999, **121**, 2641-2642.
85. M. Takamura, K. Funabashi, M. Kanai and M. Shibasaki, *J. Am. Chem. Soc.*, 2000, **122**, 6327-6328.
86. H. Nogami, S. Matsunaga, M. Kanai and M. Shibasaki, *Tetrahedron Lett.*, 2001, **42**, 279-283.
87. K. Yamada, S. J. Harwood, H. Gröger and M. Shibasaki, *Angew. Chem. Int. Ed.*, 1999, **38**, 3504-3506.
88. Y. Hamashima, M. Kanai and M. Shibasaki, *J. Am. Chem. Soc.*, 2000, **122**, 7412-7413.
89. M. Yamakawa, H. Ito and R. Noyori, *J. Am. Chem. Soc.*, 2000, **122**, 1466-1478.
90. K. Muniz, *Angew. Chem. Int. Ed.*, 2005, **44**, 6622-6627.
91. T. Ikariya and A. J. Blacker, *Acc. Chem. Res.*, 2007, **40**, 1300-1308.
92. K. Muniz, A. Lishchynskiy, J. Streuff and M. Belmonte, *Chem. Commun.*, 2011, **47**, 4911-4913.
93. R. Noyori, C. A. Sandoval, K. Muñoz and T. Ohkuma, *Philos. Trans. R. Soc. A*, 2005, **363**, 901-912.
94. Y.-M. Lin, J. Boucau, Z. Li, V. Casarotto, J. Lin, A. N. Nguyen and J. Ehrmantraut, *Org. Lett.*, 2007, **9**, 567-570.
95. P. M. Pihko, *Angew. Chem. Int. Ed.*, 2004, **43**, 2062-2064.

96. M. S. Taylor and E. N. Jacobsen, *Angew. Chem. Int. Ed.*, 2006, **45**, 1520-1543.
97. D. P. Curran and L. H. Kuo, *J. Org. Chem.*, 1994, **59**, 3259-3261.
98. B. Braden, D. Clark, J. Crowcroft and C. Partridge, *Recommendations on queue management and congestion avoidance in the Internet*, Report, 1998, 2070-1721.
99. S. Connon, *Chem. Eur. J.*, 2006, **12**, 5418-5427.
100. P. R. Schreiner and A. Wittkopp, *Org. Lett.*, 2002, **4**, 217-220.
101. M. S. Sigman and E. N. Jacobsen, *J. Am. Chem. Soc.*, 1998, **120**, 4901-4902.
102. J. T. Su, P. Vachal and E. N. Jacobsen, *Adv. Synth. Catal.*, 2001, **343**, 197-200.
103. P. Vachal and E. N. Jacobsen, *J. Am. Chem. Soc.*, 2002, **124**, 10012-10014.
104. A. G. Wenzel and E. N. Jacobsen, *J. Am. Chem. Soc.*, 2002, **124**, 12964-12965.
105. I. T. Raheem and E. N. Jacobsen, *Adv. Synth. Catal.*, 2005, **347**, 1701-1708.
106. S. B. Tsogoeva, D. A. Yalalov, M. J. Hateley and K. Huthmacher, *Eur. J. Org. Chem.*, 2005, **2005**, 4995-5000.
107. S. J. Connon, *Chem. Commun.*, 2008, 2499-2510.
108. B.-J. Li, L. Jiang, M. Liu and Y. Wu, *Synlett.*, 2005, **4**, 603-606.
109. B. Vakulya, S. Varga, A. Csámpai and T. Soós, *Org. Lett.*, 2005, **7**, 1967-1969.
110. A. E. Mattson, A. M. Zuhl, T. E. Reynolds and K. A. Scheidt, *J. Am. Chem. Soc.*, 2006, **128**, 4932-4933.
111. G. Bartoli, M. Bosco, A. Carlone, M. Locatelli, A. Mazzanti, L. Sambri and P. Melchiorre, *Chem. Commun.*, 2007, 722-724.
112. G.-G. Liu, H. Zhao, Y.-B. Lan, B. Wu, X.-F. Huang, J. Chen, J.-C. Tao and X.-W. Wang, *Tetrahedron*, 2012, **68**, 3843-3850.
113. T. Okino, Y. Hoashi and Y. Takemoto, *J. Am. Chem. Soc.*, 2003, **125**, 12672-12673.

114. T.-Y. Liu, J. Long, B.-J. Li, L. Jiang, R. Li, Y. Wu, L.-S. Ding and Y.-C. Chen, *Org. Biomol. Chem.*, 2006, **4**, 2097-2099.
115. M. Shi and X.-G. Liu, *Org. Lett.*, 2008, **10**, 1043-1046.
116. C.-J. Wang, Z.-H. Zhang, X.-Q. Dong and X.-J. Wu, *Chem. Commun.*, 2008, **12**, 1431-1433.
117. X.-Q. Dong, H.-L. Teng and C.-J. Wang, *Org. Lett.*, 2009, **11**, 1265-1268.
118. C.-J. Wang, X.-Q. Dong, Z.-H. Zhang, Z.-Y. Xue and H.-L. Teng, *J. Am. Chem. Soc.*, 2008, **130**, 8606-8607.
119. X. Xu, T. Furukawa, T. Okino, H. Miyabe and Y. Takemoto, *Chem. Eur. J.*, 2006, **12**, 466-476.
120. O. V. Serdyuk, C. M. Heckel and S. B. Tsogoeva, *Org. Biomol. Chem.*, 2013, **11**, 7051-7071.
121. S. B. Tsogoeva and S. Wei, *Chem. Commun.*, 2006, **13**, 1451-1453.
122. D. A. Yalalov, S. B. Tsogoeva, T. E. Shubina, I. M. Martynova and T. Clark, *Angew. Chem. Int. Ed.*, 2008, **47**, 6624-6628.
123. H. Huang and E. N. Jacobsen, *J. Am. Chem. Soc.*, 2006, **128**, 7170-7171.
124. M. Tsakos, C. G. Kokotos and G. Kokotos, *Adv. Syn. Catal.*, 2012, **354**, 740-746.
125. T. Akiyama, J. Itoh, K. Yokota and K. Fuchibe, *Angew. Chem. Int. Ed.*, 2004, **43**, 1566-1568.
126. C. H. Cheon and H. Yamamoto, *J. Am. Chem. Soc.*, 2008, **130**, 9246-9247.
127. M. Rueping, E. Sugiono and C. Azap, *Angew. Chem. Int. Ed.*, 2006, **45**, 2617-2619.
128. M. Rueping, E. Sugiono and S. A. Moreth, *Adv. Synth. Catal.*, 2007, **349**, 759-764.
129. M. Yamanaka, J. Itoh, K. Fuchibe and T. Akiyama, *J. Am. Chem. Soc.*, 2007, **129**, 6756-6764.

130. H. Liu, L.-F. Cun, A.-Q. Mi, Y.-Z. Jiang and L.-Z. Gong, *Org. Lett.*, 2006, **8**, 6023-6026.
131. Q. Kang, Z.-A. Zhao and S.-L. You, *J. Am. Chem. Soc.*, 2007, **129**, 1484-1485.
132. L. Simón and J. M. Goodman, *J. Am. Chem. Soc.*, 2008, **130**, 8741-8747.
133. R. L. Letsinger, I. Skoog and N. Remes, *J. Am. Chem. Soc.*, 1954, **76**, 4047-4048.
134. C. Poole, S. Singhawangcha and A. Zlatkis, *Chromatographia*, 1978, **11**, 347-349.
135. R. L. Letsinger and N. Remes, *J. Am. Chem. Soc.*, 1955, **77**, 2489-2491.
136. R. L. Letsinger and J. R. Nazy, *J. Am. Chem. Soc.*, 1959, **81**, 3013-3017.
137. R. L. Letsinger and I. Skoog, *J. Am. Chem. Soc.*, 1955, **77**, 2491-2494.
138. R. L. Letsinger and D. B. MacLean, *J. Am. Chem. Soc.*, 1963, **85**, 2230-2236.
139. R. L. Letsinger and A. Wysocki, *J. Org. Chem.*, 1963, **28**, 3199-3202.
140. J. D. Morrison and R. Letsinger, *J. Org. Chem.*, 1964, **29**, 3405-3407.
141. U. Eder, G. Sauer and R. Wiechert, *Angew. Chem. Int. Ed.*, 1971, **10**, 496-497.
142. Z. G. Hajos and D. R. Parrish, *J. Org. Chem.*, 1974, **39**, 1615-1621.
143. J. M. Betancort and C. F. Barbas, *Org. Lett.*, 2001, **3**, 3737-3740.
144. T. Ishii, S. Fujioka, Y. Sekiguchi and H. Kotsuki, *J. Am. Chem. Soc.*, 2004, **126**, 9558-9559.
145. S. Chandrasekhar, B. Tiwari, B. B. Parida and C. R. Reddy, *Tetrahedron Asymmetry*, 2008, **19**, 495-499.
146. S. Luo, H. Xu, X. Mi, J. Li, X. Zheng and J.-P. Cheng, *J. Org. Chem.*, 2006, **71**, 9244-9247.
147. D. Xu, J. Wang, L. Yan, M. Yuan, X. Xie and Y. Wang, *Tetrahedron Asymmetry*, 2016, **27**, 1121-1132.
148. I. Georgiou, G. Ilyashenko and A. Whiting, *Acc. Chem. Res.*, 2009, **42**, 756-768.

149. K. Arnold, B. Davies, D. Héroult and A. Whiting, *Angew. Chem. Int. Ed.*, 2008, **120**, 2713-2716.
150. J. M. Keith, J. F. Larrow and E. N. Jacobsen, *Adv. Syn. Catal.*, 2001, **343**, 5-26.
151. H. Pellissier, *Adv. Syn. Catal.*, 2011, **353**, 1613-1666.
152. S. T. Chen and K. T. Wang, *J. Chi. Chem. Sci.*, 1999, **46**, 301-311.
153. E. Vedejs, O. Daugulis and S. T. Diver, *J. Org. Chem.*, 1996, **61**, 430-431.
154. E. A. C. Davie, S. M. Mennen, Y. Xu and S. J. Miller, *Chem. Rev.*, 2007, **107**, 5759-5812.
155. J. A. MacKay and E. Vedejs, *J. Org. Chem.*, 2004, **69**, 6934-6937.
156. T. Poisson, M. Penhoat, C. Papamicael, G. Dupas, V. Dalla, F. Marsais and V. Levacher, *Synlett.*, 2005, **15**, 2285-2288.
157. I. Shiina and K. Nakata, *Tetrahedron Lett.*, 2007, **48**, 8314-8317.
158. S. Hashiguchi, A. Fujii, J. Takehara, T. Ikariya and R. Noyori, *J. Am. Chem. Soc.*, 1995, **117**, 7562-7563.
159. S. Hashiguchi, A. Fujii, K. J. Haack, K. Matsumura, T. Ikariya and R. Noyori, *Angew. Chem. Int. Ed.*, 1997, **36**, 288-290.
160. T. Chen, J.-J. Jiang, Q. Xu and M. Shi, *Org. Lett.* 2007, **9**, 865-868.
161. S. J. Liu, L. j. Liu and M. Shi, *Appl. Organomet. Chem.*, 2009, **23**, 183-190.
162. A. T. Radosevich, C. Musich and F. D. Toste, *J. Am. Chem. Soc.*, 2005, **127**, 1090-1091.
163. Y.-Y. Li, X.-Q. Zhang, Z.-R. Dong, W.-Y. Shen, G. Chen and J.-X. Gao, *Org. Lett.*, 2006, **8**, 5565-5567.
164. Z. Li, Z. H. Tang, X. X. Hu and C. G. Xia, *Chem. Eur. J.*, 2005, **11**, 1210-1216.
165. V. S. Martin, S. S. Woodard, T. Katsuki, Y. Yamada, M. Ikeda and K. B. Sharpless, *J. Am. Chem. Soc.*, 1981, **103**, 6237-6240.

166. W. Zhang, A. Basak, Y. Kosugi, Y. Hoshino and H. Yamamoto, *Angew. Chem. Int. Ed.*, 2005, **44**, 4389-4391.
167. S. Simaan, A. Masarwa, P. Bertus and I. Marek, *Angew. Chem. Int. Ed.*, 2006, **45**, 3963-3965.
168. Gregory C. Fu, *Acc. Chem. Res.*, 2004, **37**, 542-547.
169. M. Kitamura, I. Kasahara, K. Manabe, R. Noyori and H. Takaya, *J. Org. Chem.*, 1988, **53**, 708-710.
170. J. Faller, J. C. Wilt and J. Parr, *Org. Lett.*, 2004, **6**, 1301-1304.
171. K. Onitsuka, Y. Matsushima and S. Takahashi, *Organometallics*, 2005, **24**, 6472-6474.
172. S. Miyano, L. D. Lu, S. M. Viti and K. B. Sharpless, *J. Org. Chem.*, 1985, **50**, 4350-4360.
173. V. B. Birman, H. Jiang, X. Li, L. Guo and E. W. Uffman, *J. Am. Chem. Soc.*, 2006, **128**, 6536-6537.
174. M. Binanzer, S.-Y. Hsieh and J. W. Bode, *J. Am. Chem. Soc.*, 2011, **133**, 19698-19701.
175. S. Arai, S. Bellemin - Laponnaz and Gregory C. Fu, *Angew. Chem. Int. Ed.*, 2001, **40**, 234-236.
176. C. K. De, E. G. Klauber and D. Seidel, *J. Am. Chem. Soc.*, 2009, **131**, 17060-17061.
177. N. Mittal, D. X. Sun and D. Seidel, *Org. Lett.*, 2012, **14**, 3084-3087.
178. N. Mittal, K. M. Lippert, C. K. De, E. G. Klauber, T. J. Emge, P. R. Schreiner and D. Seidel, *J. Am. Chem. Soc.*, 2015, **137**, 5748-5758.
179. N. Busschaert, C. Caltagirone, W. Van Rossom and P. A. Gale, *Chem. Rev.*, 2015, **115**, 8038-8155.
180. Y. Kim, J. Park and M.-J. Kim, *Tetrahedron Lett.*, 2010, **51**, 5581-5584.

181. A. Kolleth, M. Cattoen, S. Arseniyadis and J. Cossy, *Chem. Commun.*, 2013, **49**, 9338-9340.
182. H. Asahara, T. Kida, T. Iwamoto, T. Hinoue and M. Akashi, *Tetrahedron*, 2014, **70**, 197-203.
183. A. H. Hoveyda and M. T. Didiuk, *Curr. Org. Chem.*, 1998, **2**, 489-526.
184. A. H. Hoveyda, D. A. Evans and G. C. Fu, *Chem. Rev.*, 1993, **93**, 1307-1370.
185. C. R. Baar, C. J. Levy, E. Y.-J. Min, L. M. Henling, M. W. Day and J. E. Bercaw, *J. Am. Chem. Soc.*, 2004, **126**, 8216-8231.
186. E. Y.-J. Min, J. A. Byers and J. E. Bercaw, *Organometallics*, 2008, **27**, 2179-2188.
187. S. Collins, B. A. Kuntz and Y. Hong, *J. Org. Chem.*, 1989, **54**, 4154-4158.
188. A. H. Hoveyda and J. P. Morken, *Angew. Chem. Int. Ed. Engl.*, 1996, **35**, 1262-1284.
189. D. G. Blackmond, *J. Am. Chem. Soc.*, 2001, **123**, 545-553.
190. D. E. Robinson and S. D. Bull, *Tetrahedron Asymmetry*, 2003, **14**, 1407-1446.
191. R. Nasser, C. Thirsk, G. E. Hawkes, R. T. Kroemer, K. R. Liedl and T. Loertinh, *J. Chem. Soc., Perkin Trans.*, 2002, **2**, 1510-1519.
192. D. G. Hall, *Boronic acids: preparation, applications in organic synthesis and medicine*, John Wiley & Sons, 2006.
193. P. J. Flory, *J. Am. Chem. Soc.*, 1937, **59**, 241-253.
194. B. S. Kharasch, *Bur. Standards J. Research*, 1929, **2**, 359.
195. a) D. Rabelo and F. Coutinho, *Poly. Bull.*, 1994, **33**, 479-486; b) K. J. Barlow, X. Hao, T. C. Hughes and G. Moad, *Polym. Chem.*, 2014, **5**, 722-732.
196. L. Perreux, A. Loupy and F. Volatron, *Tetrahedron*, 2002, **58**, 2155-2162.
197. I. R. Baxendale, S. V. Ley, A. C. Mansfield and C. D. Smith, *Angew. Chem. Int. Ed.*, 2009, **48**, 4017-4021.

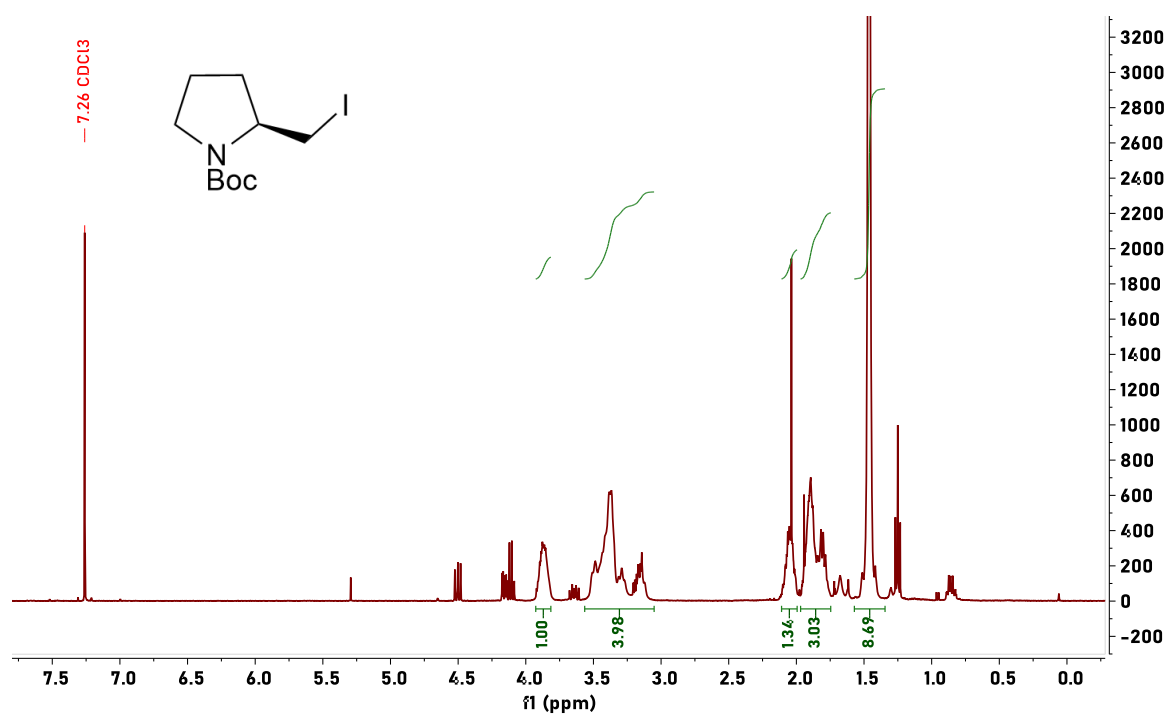
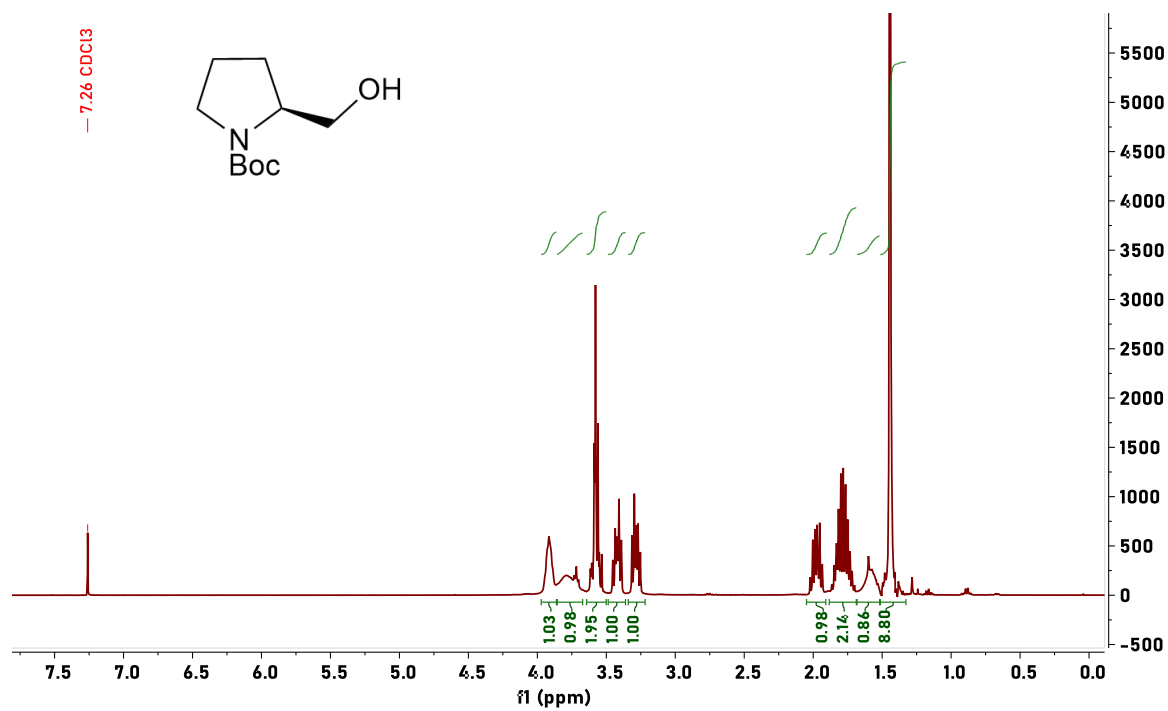
198. I. R. Baxendale, S. C. Schou, J. Sedelmeier and S. V. Ley, *Chemistry*, 2010, **16**, 89-94.
199. K. Sakthivel, W. Notz, T. Bui and C. F. Barbas, *J. Am. Chem. Soc.*, 2001, **123**, 5260-5267.
200. I. Georgiou and A. Whiting, *Eur. J. Org. Chem.*, 2012, **22**, 4110-4113.
201. C. T. Yang, Z. Q. Zhang, Y. C. Liu and L. Liu, *Angew. Chem. Int. Ed.*, 2011, **50**, 3904-3907.
202. H. Ito and K. Kubota, *Org. Lett.*, 2012, **14**, 890-893.
203. A. Joshi-Pangu, X. Ma, M. Diane, S. Iqbal, R. J. Kribs, R. Huang, C. Y. Wang and M. R. Biscoe, *J. Org. Chem.*, 2012, **77**, 6629-6633.
204. H. Xu, C. Zhao, Q. Qian, W. Deng and H. Gong, *Chem. Sci.*, 2013, **4**, 4022-4029.
205. R. B. Bedford, P. B. Brenner, E. Carter, T. Gallagher, D. M. Murphy and D. R. Pye, *Organometallics*, 2014, **33**, 5940-5943.
206. S. K. Bose, K. Fucke, L. Liu, P. G. Steel and T. B. Marder, *Angew. Chem. Int. Ed.*, 2014, **53**, 1799-1803.
207. T. C. Atack and S. P. Cook, *J. Am. Chem. Soc.*, 2016, **138**, 6139-6142.
208. S. Jalal, S. Sarkar, K. Bera, S. Maiti and U. Jana, *Eur. J. Org. Chem.*, 2013, **22**, 4823-4828.
209. H. J. Al-Najjar, A. Barakat, A. M. Al-Majid, Y. N. Mabkhot, M. Weber, H. A. Ghabbour and H. K. Fun, *Molecules*, 2014, **19**, 1150-1162.
210. C. Xu, J. Du, L. Ma, G. Li, M. Tao and W. Zhang, *Tetrahedron*, 2013, **69**, 4749-4757.
211. D. A. Longbottom, V. Franckevicius and S. V. Ley, *Chimia*, 2007, **61**, 247-256.
212. K. Arnold, A. S. Batsanov, B. Davies, C. Grosjean, T. Schütz, A. Whiting and K. Zawatzky, *Chem. Commun.*, 2008, **33**, 3879-3881.

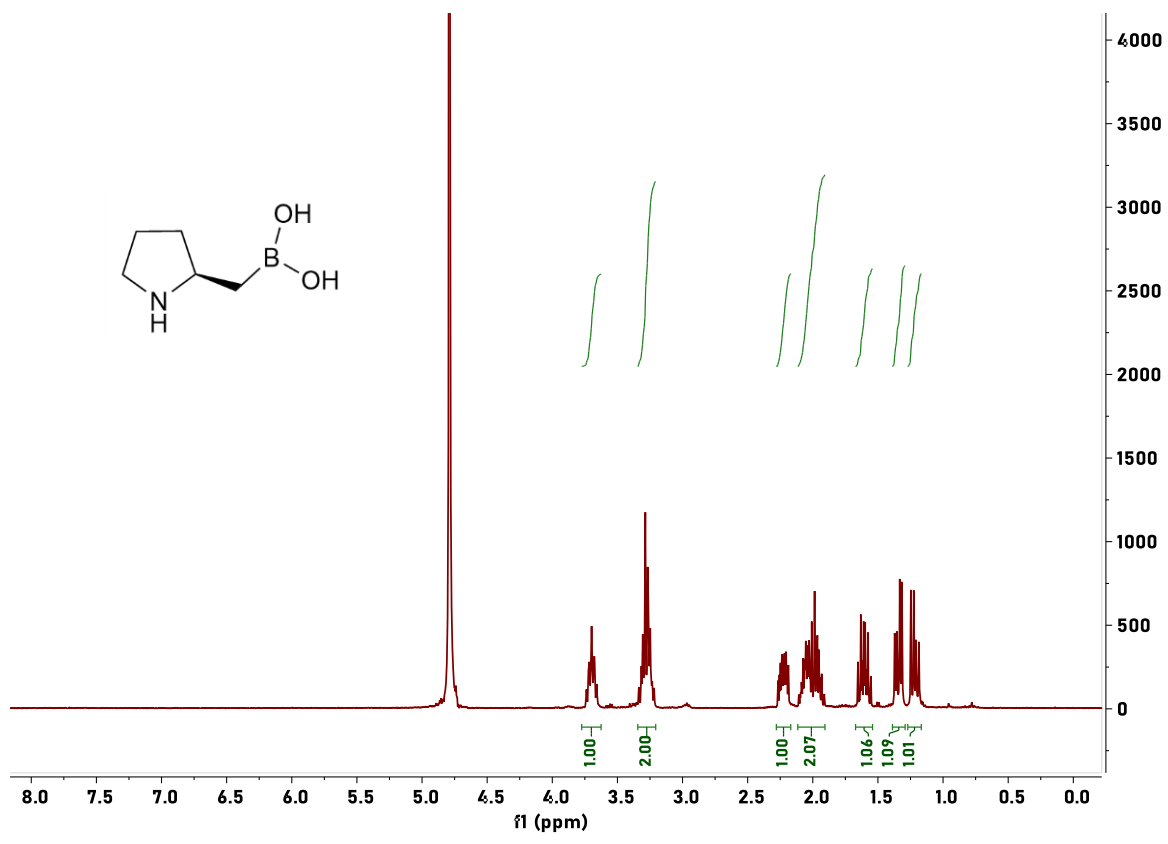
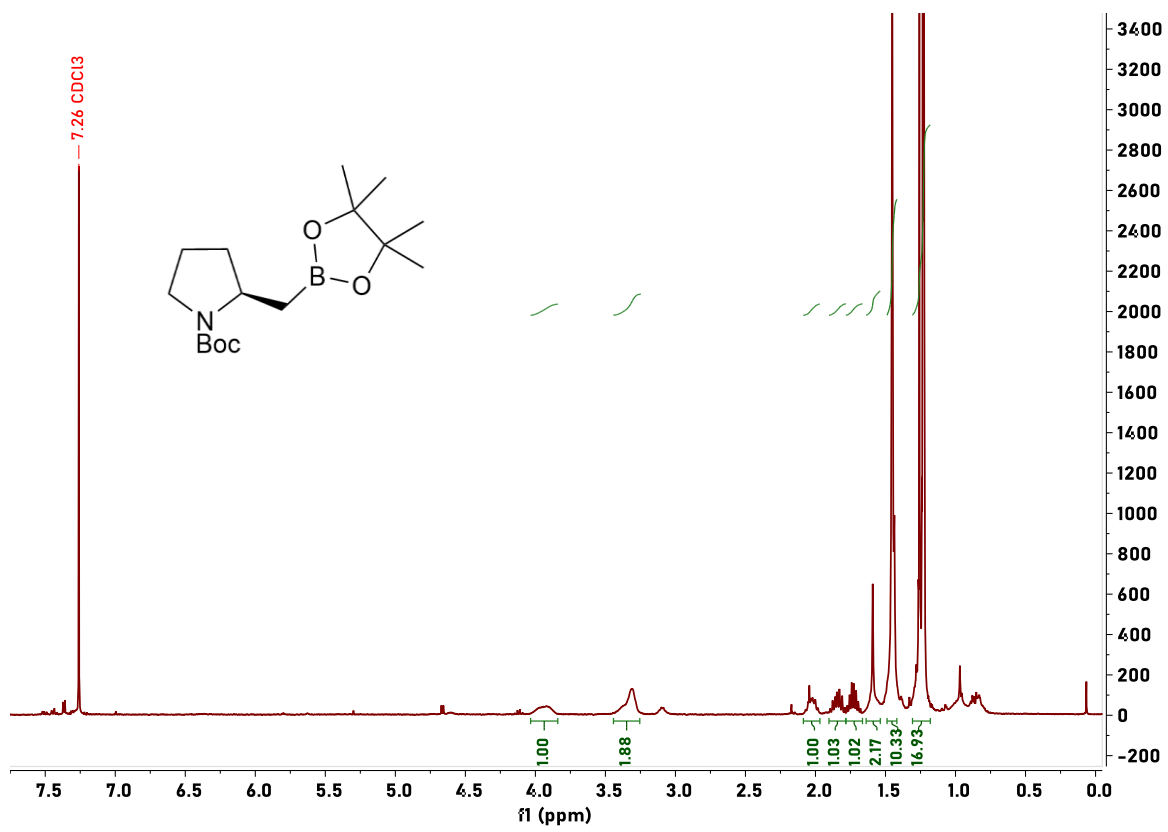
213. I. Georgiou and A. Whiting, *Org. Biomol. Chem.*, 2012, **10**, 2422-2430.
214. A. S. Batsanov, I. Georgiou, P. R. Girling, L. Pommier, H. C. Shen and A. Whiting, *J. Org. Chem.*, 2014, **3**, 470-479.
215. G. Springsteen and B. Wang, *Tetrahedron*, 2002, **58**, 5291-5300.
216. K. Okano, *Tetrahedron*, 2011, **14**, 2483-2512.
217. E. Wan and A. Whiting, *Unpublished report: The synthesis of diboron catalysts*, 2018.
218. a) A. K. Shaneesh, F. N. Hendrika and C. Roberta [NL] +2017, *European Patent* No. WO2017118617; b) A. Das, A. Hübner, M. Weber, M. Bolte, H. W. Lerner and M. Wagner, *Chem. Commun.*, 2011, **47**, 11339–11341.
219. a) X. Chang, Q. Zhang and C. Guo, *Org. Lett.*, 2019; b) C. Guo, X. Chang and Q. Zhang, 2018, *China Patent No.* CN107814729A
220. J. G. Lee and H. T. Cha, *Tetrahedron Lett.*, 1992, **33**, 3167-3168.
221. Cram, D. J. and Cram, J. M., *Acc. Chem. Res.*, 1978, **11**, 8-11.
222. a) A. Miyashita, A. Yasuda, H. Takaya, K. Toriumi, T. Ito, T. Souchi and R. Noyori, *J. Am. Chem. Soc.*, 1980, **102**, 7932-7934; b) H. Takaya, S. Akutagawa and R. Noyori, *Org. Synth.*, 1989, **8**, 20-27.
223. F. Dubois and M. Gingras, *Tetrahedron Lett.*, 1998, **39**, 5039-5040.
224. I. A. Shuklov, N. V. Dubrovina, H. Jiao, A. Spannenberg and A. Börner, *Eur. J. Org. Chem.*, 2010, **2010**, 1669-1680.
225. A. A. Aghshina, G. K. Sterligov, S. A. Rzhnevskiy, M. A. Topchiy, G. A. Chesnokov, P. S. Gribanov, E. K. Melnikova, M. S. Nechaev, A. F. Asachenko and M. V. Bermeshev, *Dalton Trans.*, 2019, **48**, 3447-3452.
226. T. Hoshi, H. Shionoiri, T. Suzuki, M. Ando and H. Hagiwara, *Chem. Lett.*, 1999, **28**, 1245-1246.

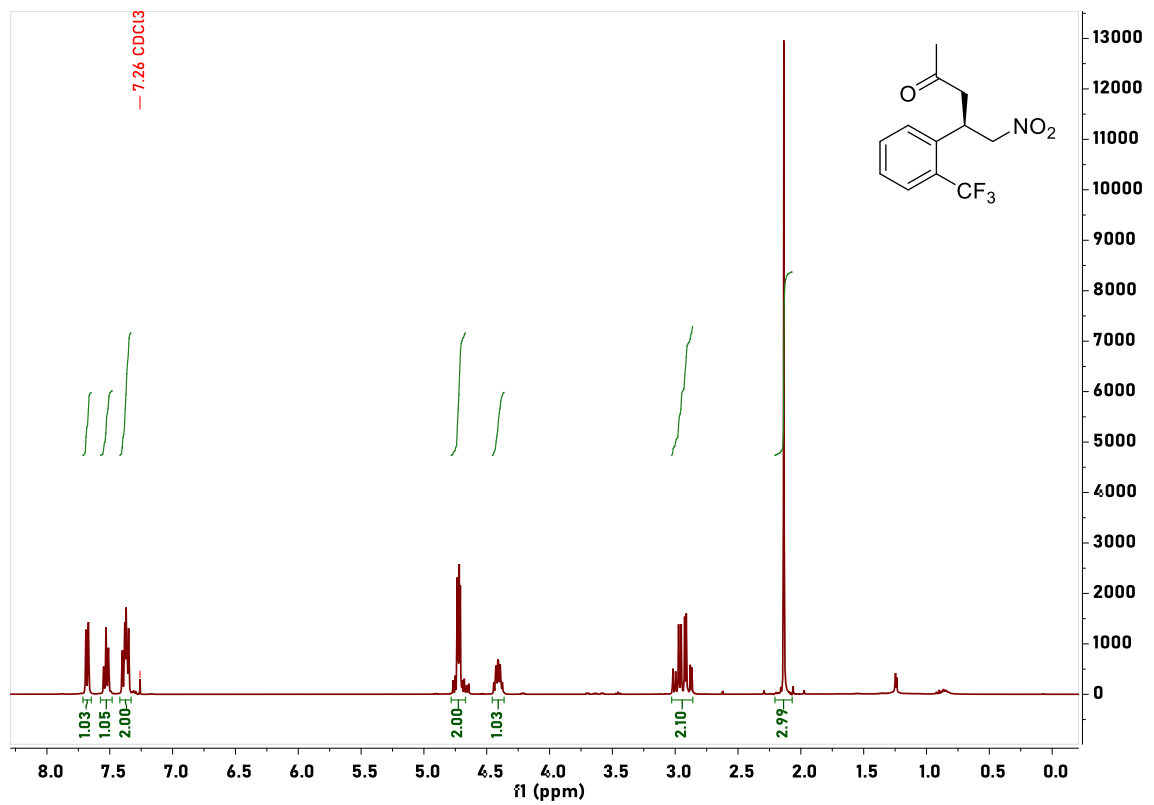
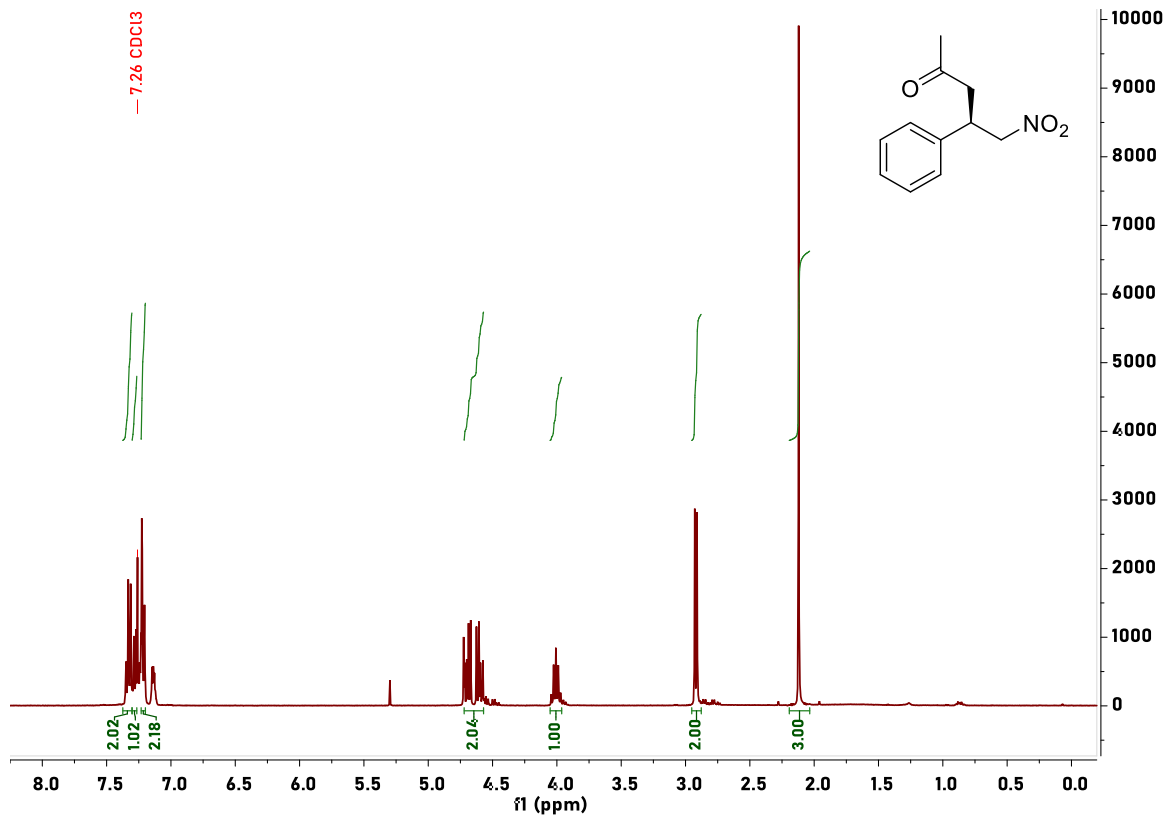
227. M. Mešková and M. Putala, *Tetrahedron Asymmetry*, 2013, **24**, 894-902.
228. S. Guillaume and A. Whiting, *Synlett*, 2004, **04**, 711-713.
229. P. Losch, A. S. Felten and P. Pale, *Adv. Synth. Catal.*, 2015, **357**, 2931-2938.
230. D. T. Nguyen, D. C. Lenstra and J. Mecinović, *RSC Adv.*, 2015, **5**, 77658-77661.
231. S. A. Miller and N. E. Leadbeater, *RSC Adv.*, 2015, **5**, 93248-93251.
232. H. Lundberg, F. Tinnis and H. Adolfsson, *Chem. Eur. J.*, 2012, **18**, 3822-3826.
233. W. Ren and M. Yamane, *J. Org. Chem.*, 2010, **75**, 8410-8415.
234. G. Zhang, B. Gao and H. Huang, *Angew. Chem. Int. Ed.*, 2015, **54**, 7657-7661.
235. Y. G. Zhang, X. L. Liu, Z. Y. He, X. M. Li, H. J. Kang and S. K. Tian, *Chem. Eur. J.*, 2014, **20**, 2765-2769.
236. G. Abbiati and E. Rossi, *Tetrahedron*, 2001, **57**, 7205-7212.
237. L. Peng, X.-Y. Xu, L.-L. Wang, J. Huang, J.-F. Bai, Q.-C. Huang and L.-X. Wang, *Eur. J. Org. Chem.*, 2010, **10**, 1849-1853.
238. T. K. Houlding, K. Tchabanenko, M. T. Rahman and E. V. Rebrov, *Org. Biomol. Chem.*, 2013, **11**, 4171-4177.
239. G. L. Beutner, S. I. Young, M. L. Davies, M. R. Hickey, H. Park, J. M. Stevens and Q. Ye, *Org. Lett.*, 2018, **20**, 4218-4222.
240. Y. Zhou, O. D. Engl, J. S. Bandar, E. D. Chant and S. L. Buchwald *Angew. Chem. Int. Ed.* 2018, **57**, 6672-6675.
241. M. H. Garduño-Castro and M. Hernández-Rodríguez, *Tetrahedron Lett.*, 2014, **55**, 193-196.
242. Dolomanov, O.V., Bourhis, L.J., Gildea, R.J, Howard, J.A.K. and Puschmann, H., *J. Appl. Cryst.*, 2009, **42**, 339-341.
243. Sheldrick, G.M., *Acta. Cryst.*, 2015, **A71**, 3-8.
244. Sheldrick, G.M., *Acta. Cryst.*, 2015, **C71**, 3-8.

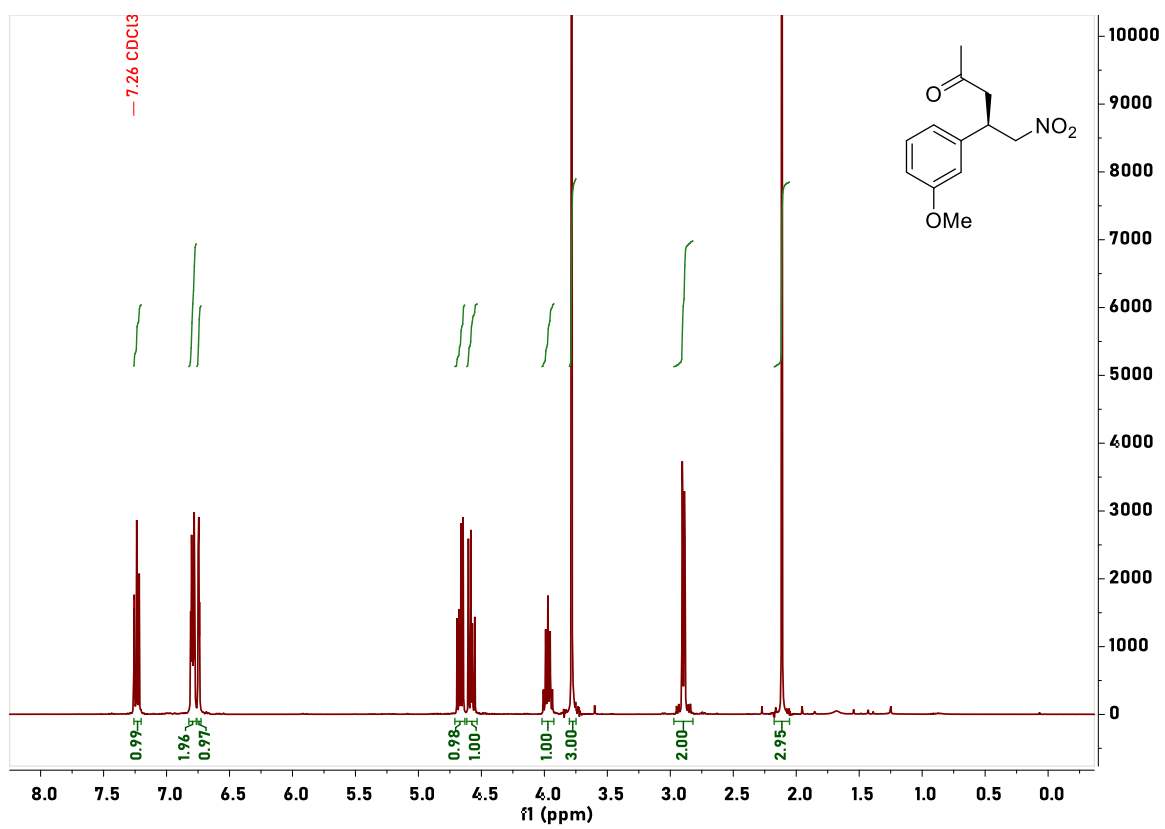
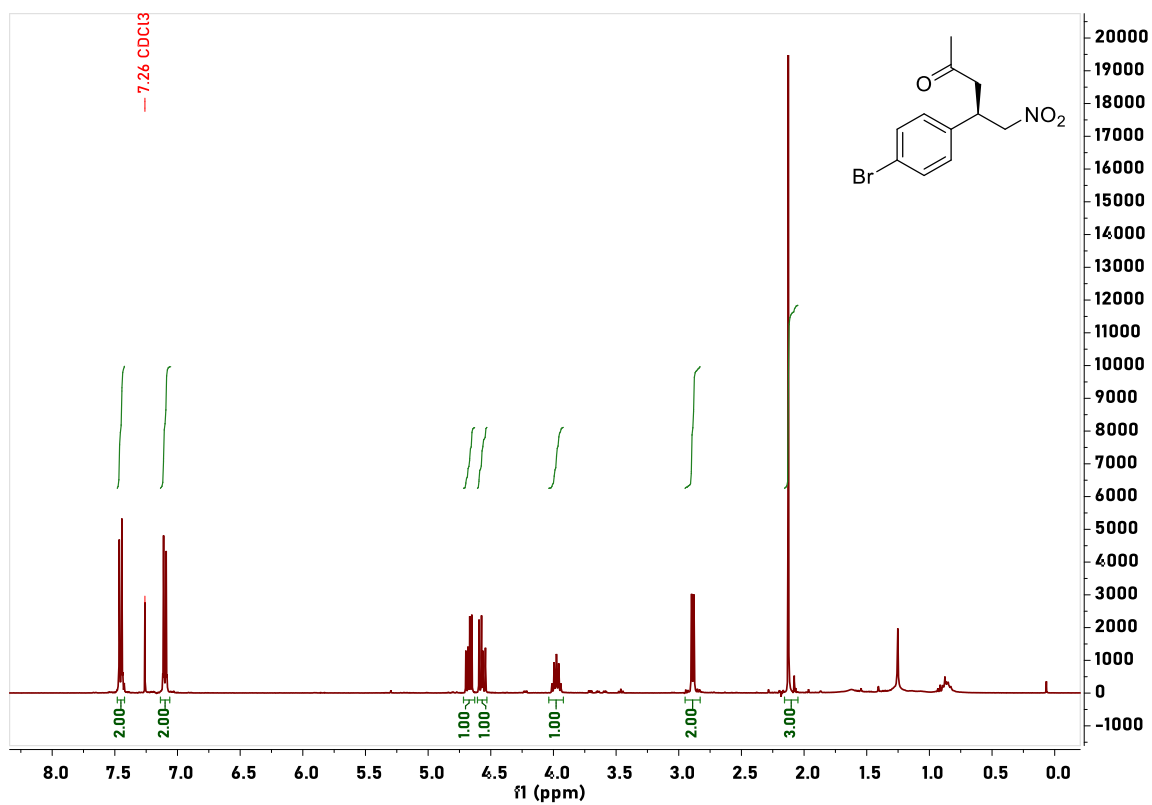
X. Appendix

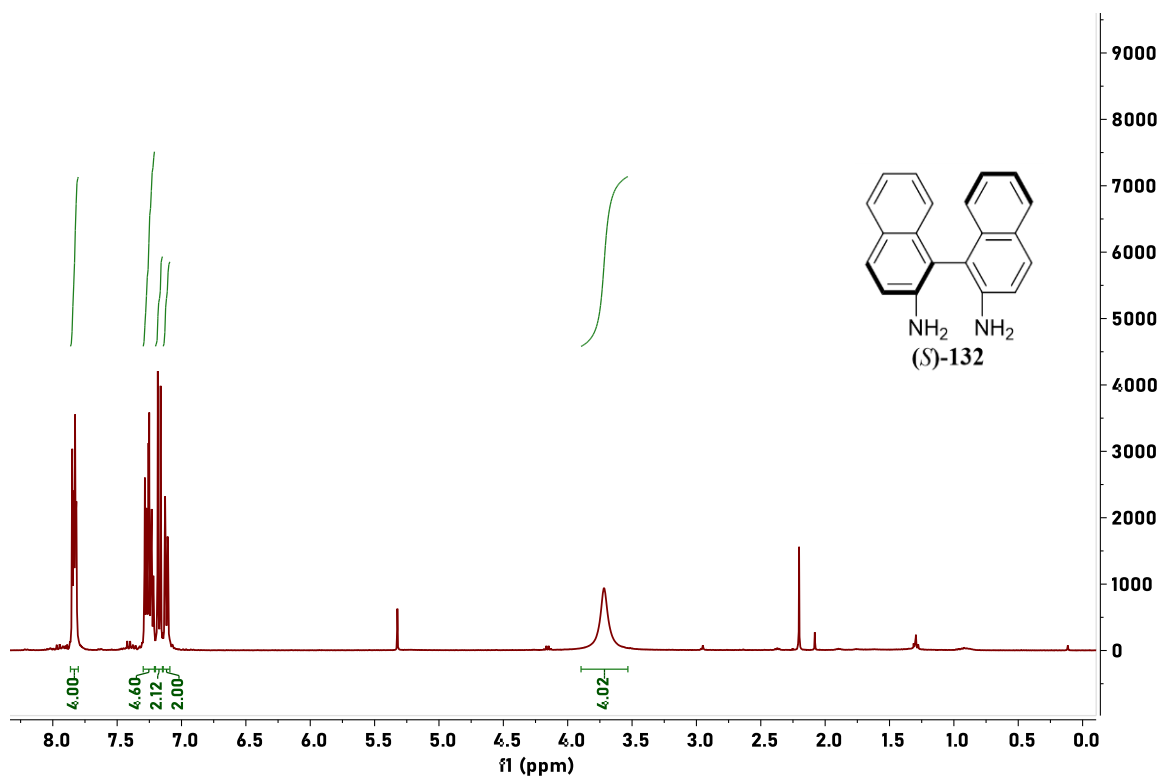
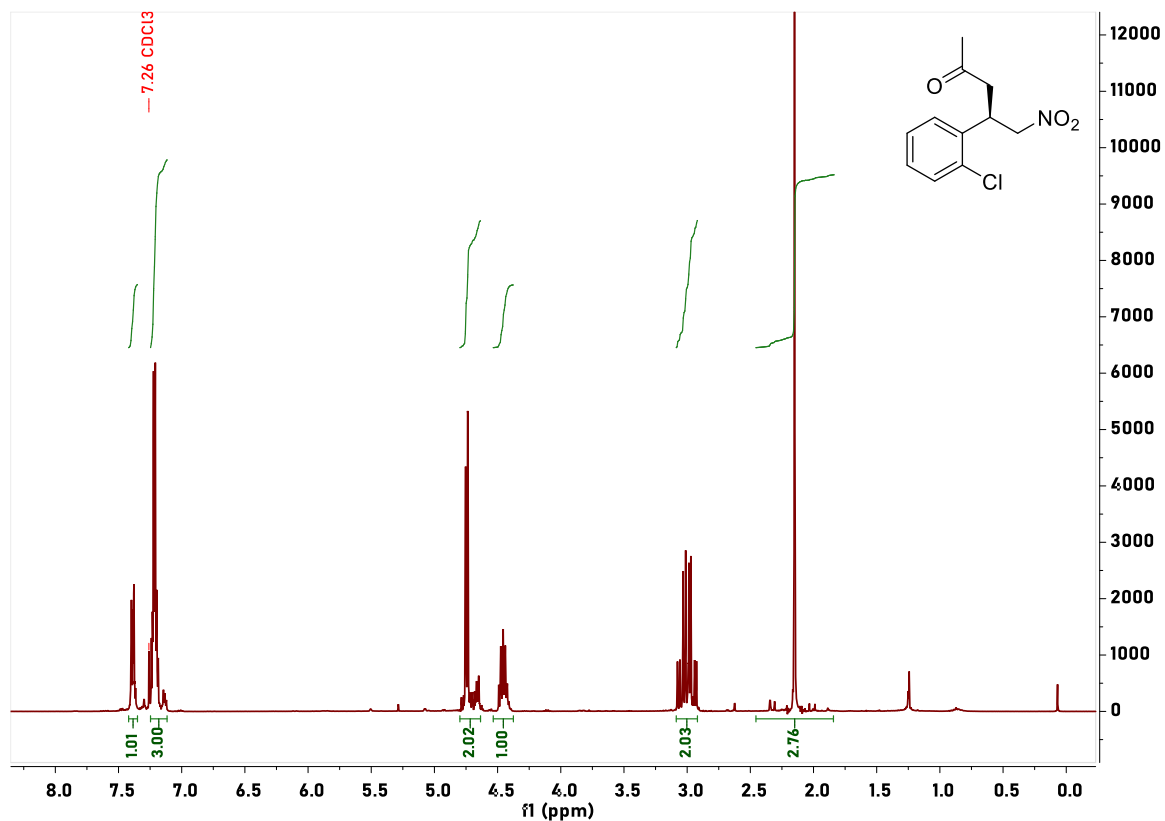
1. ^1H NMR spectra

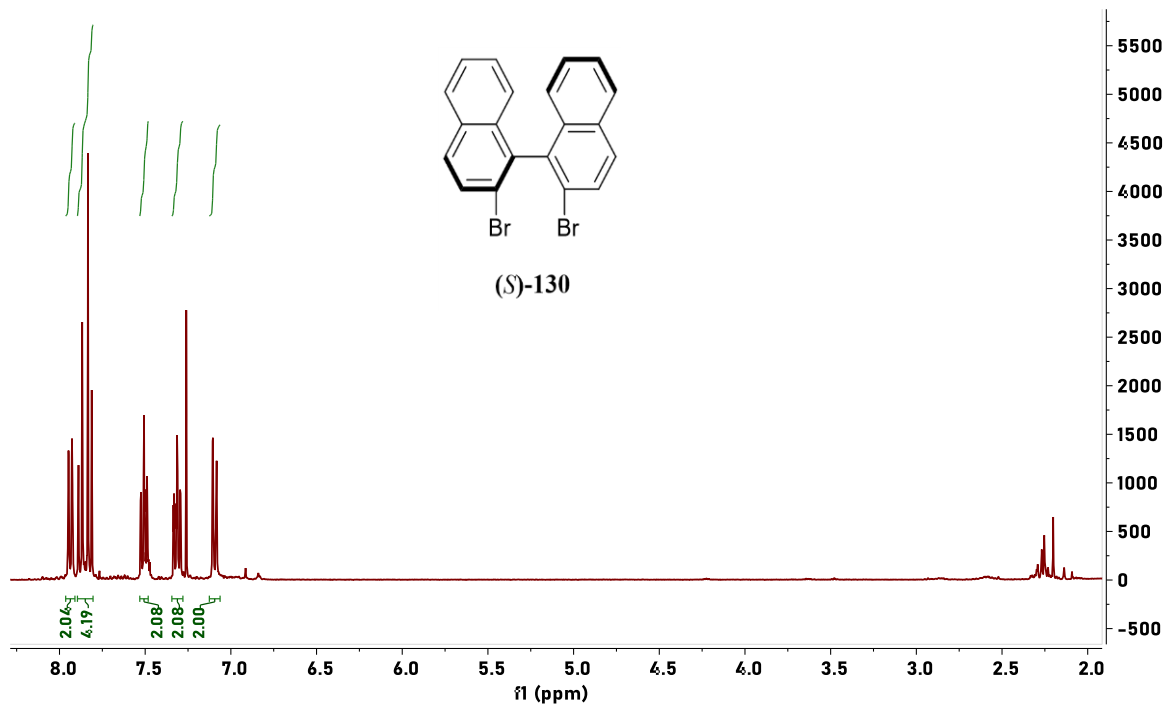




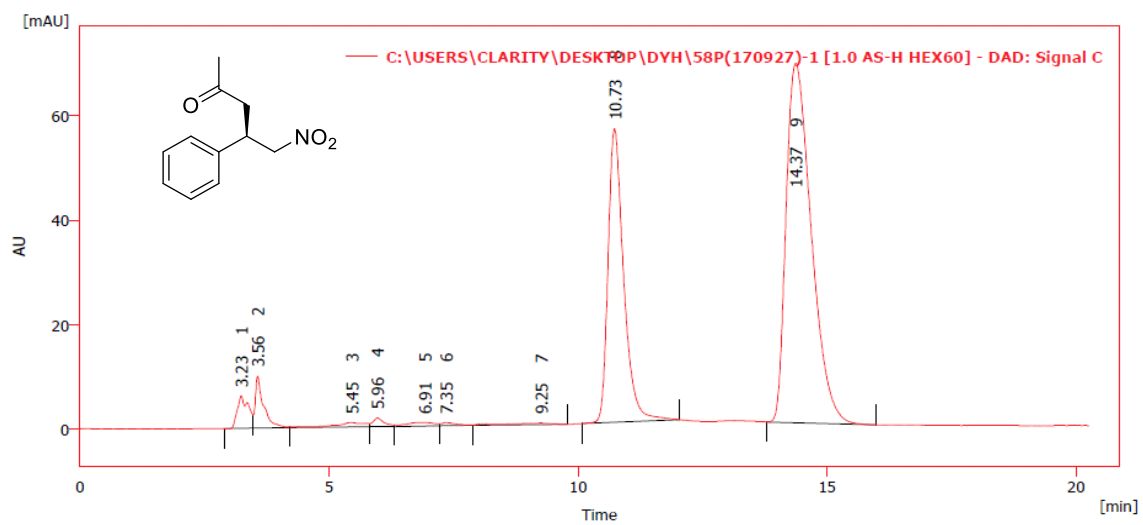
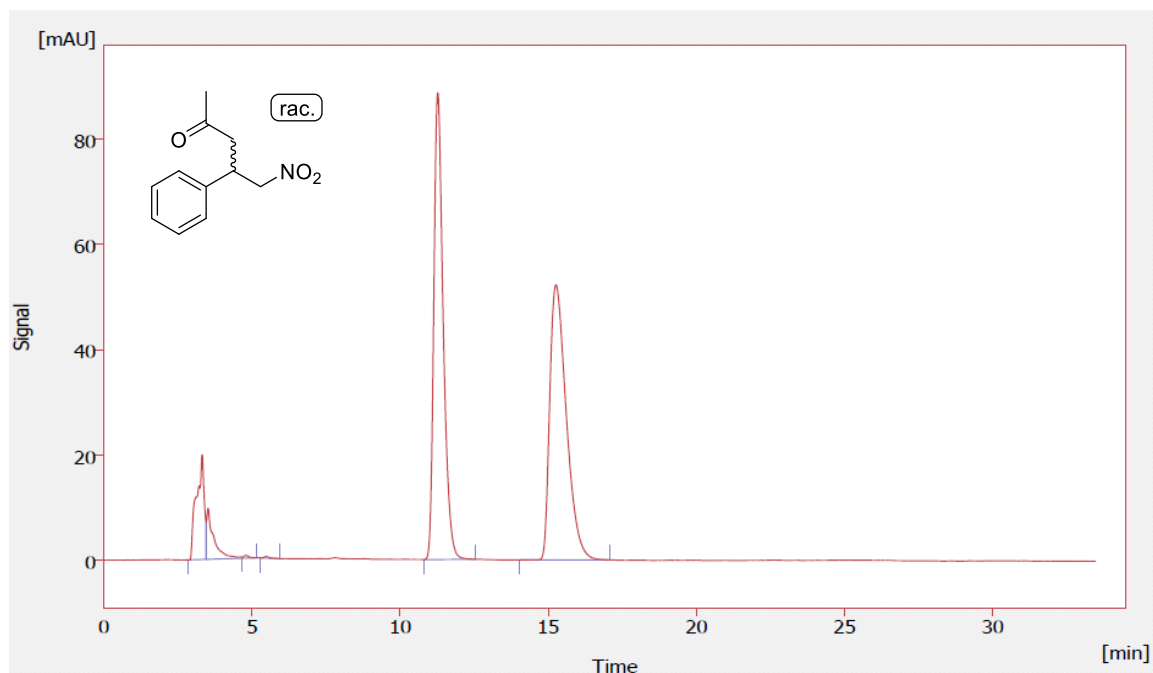


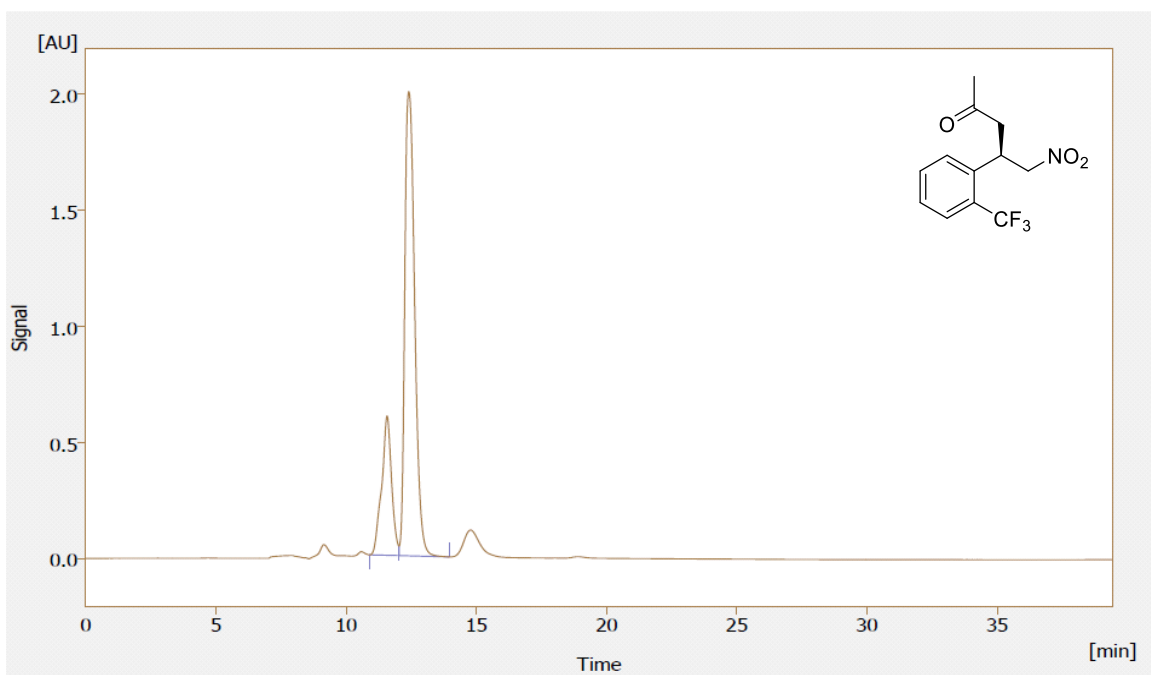
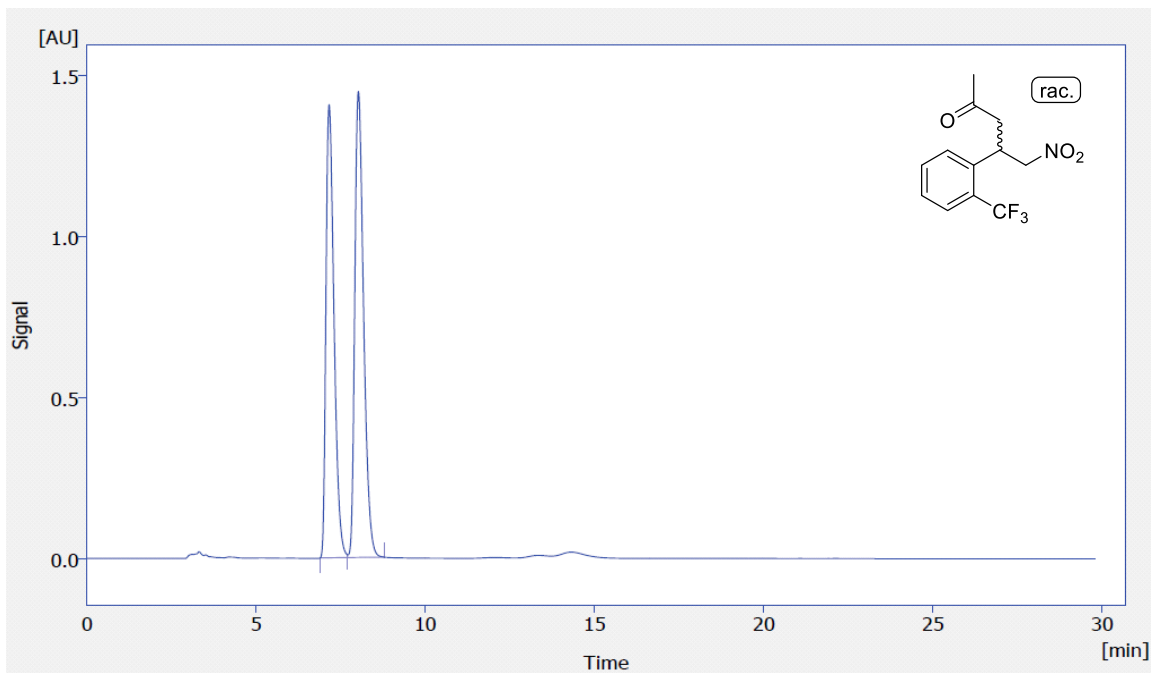


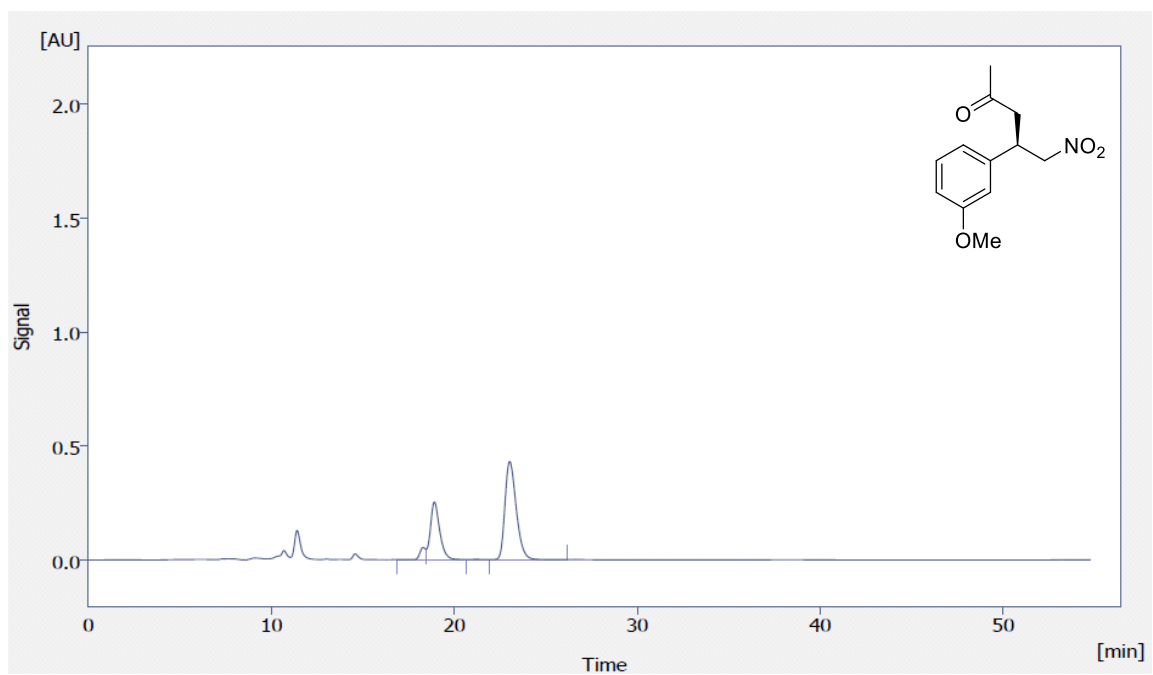
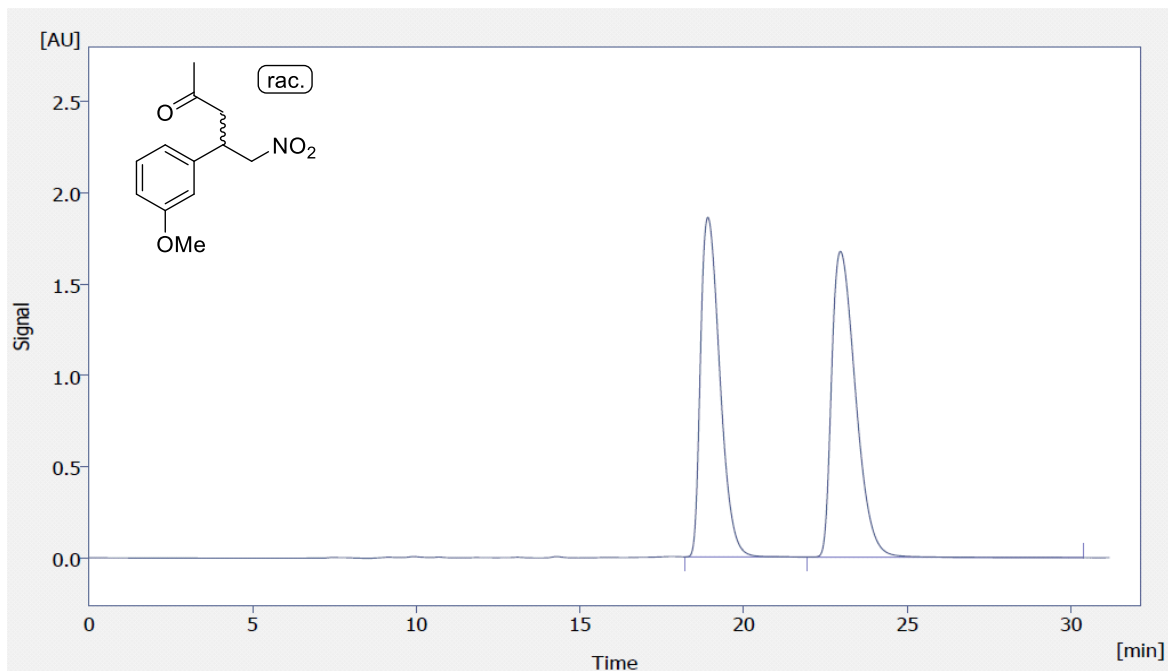


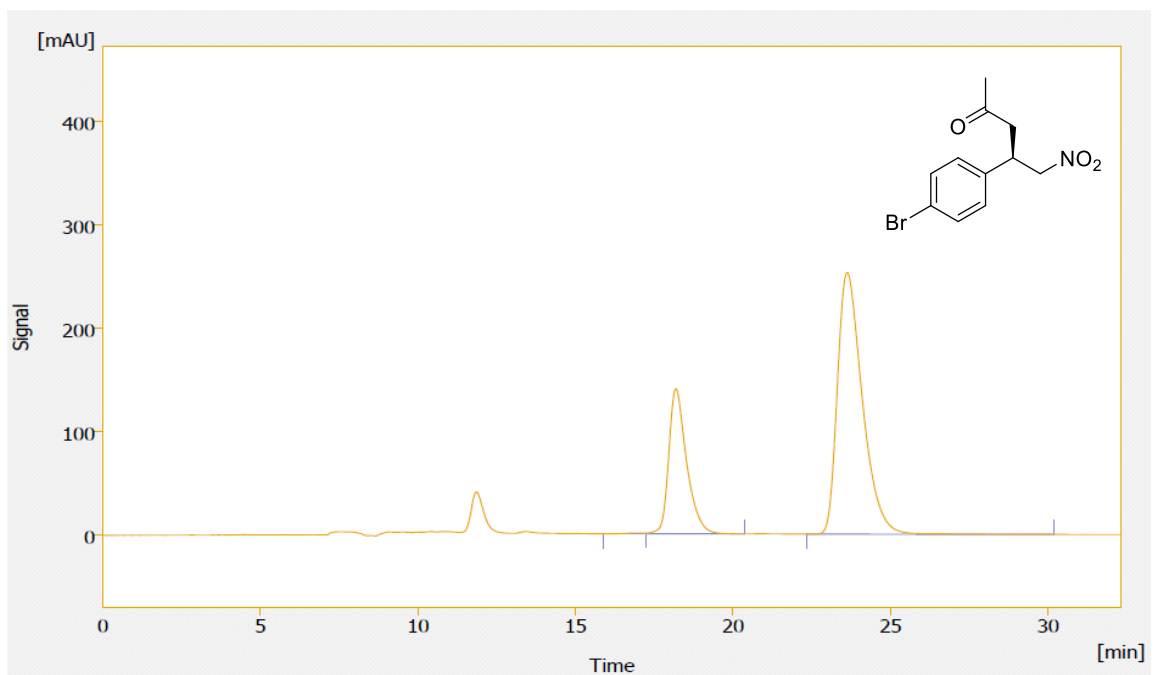
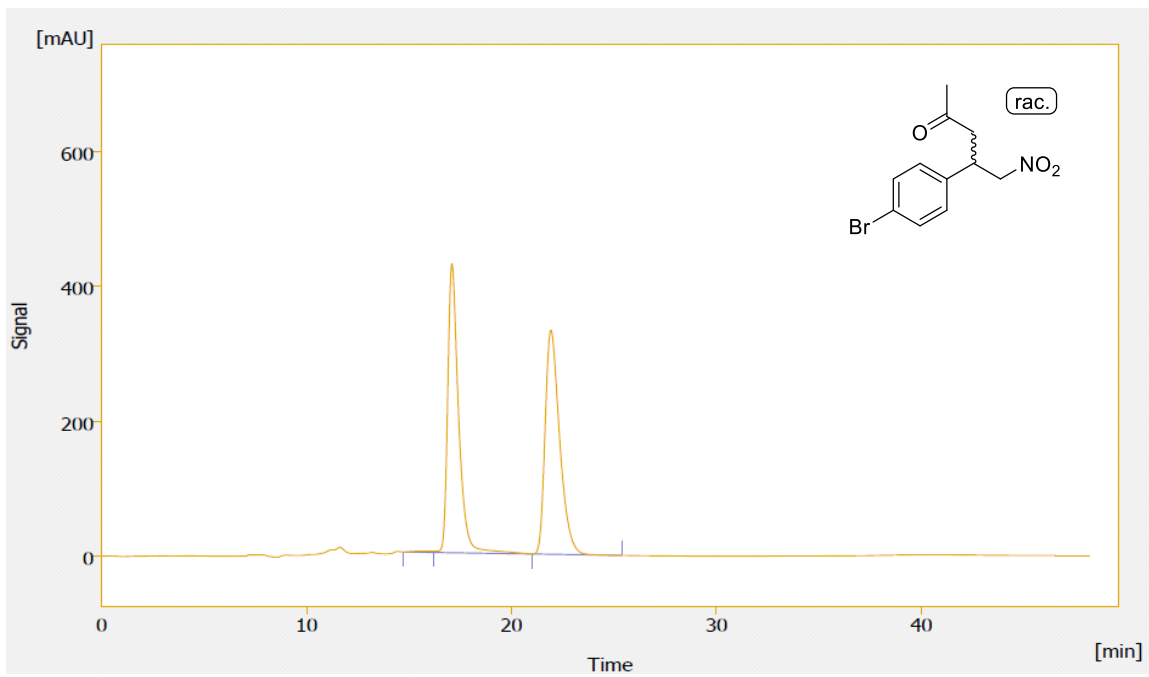


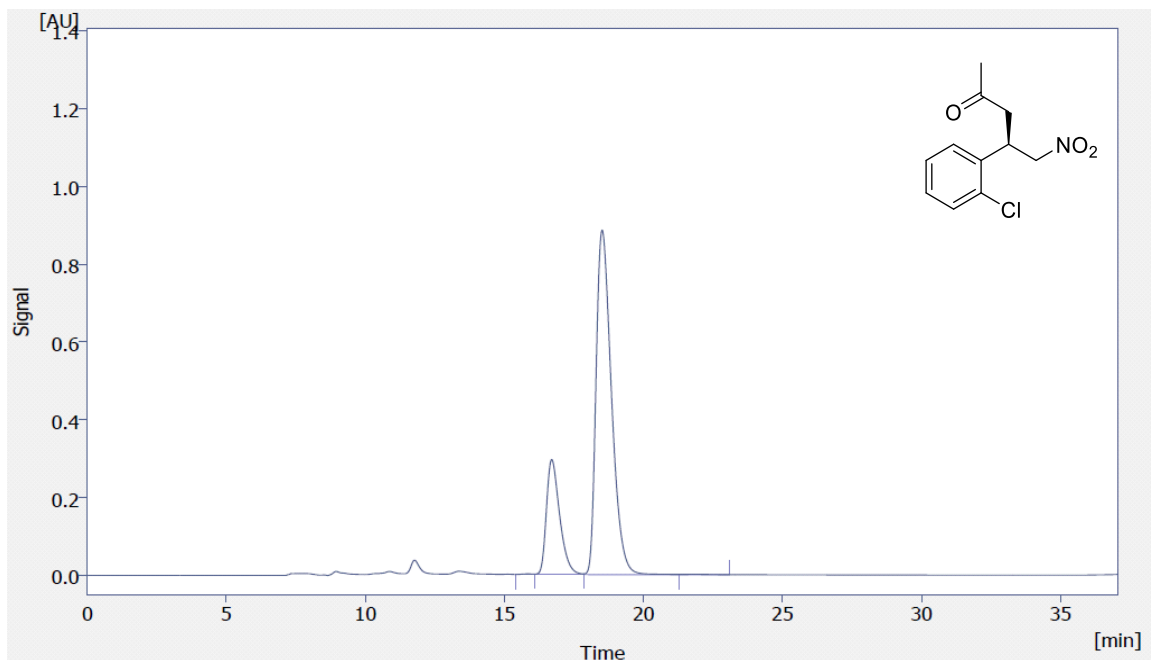
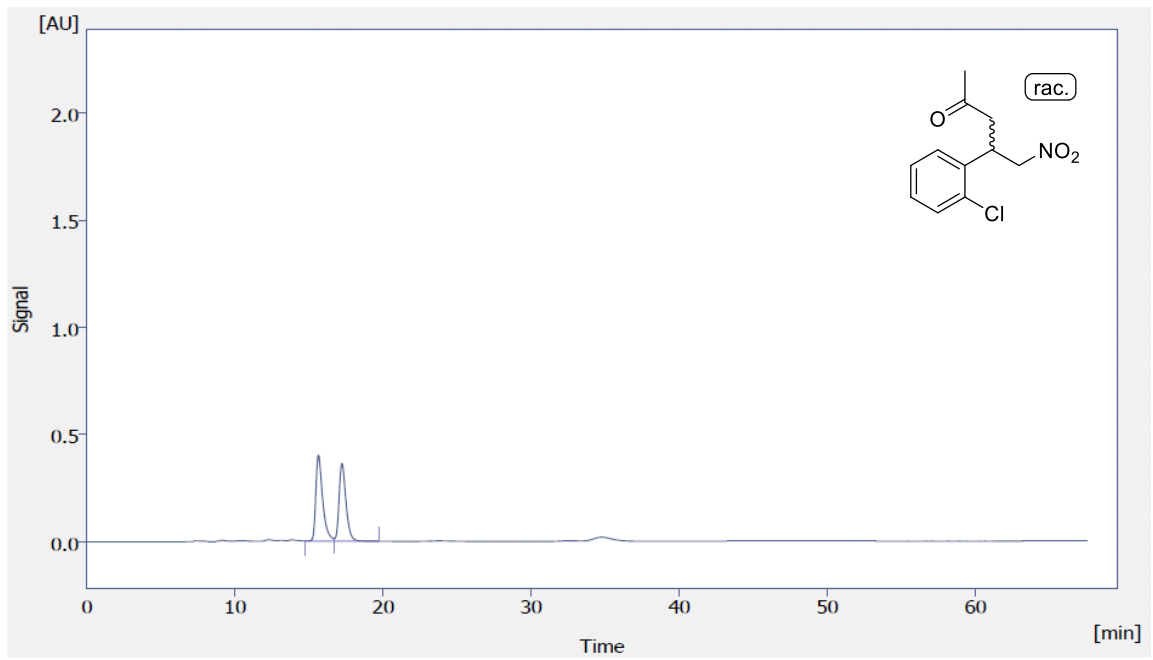
2. HPLC plots

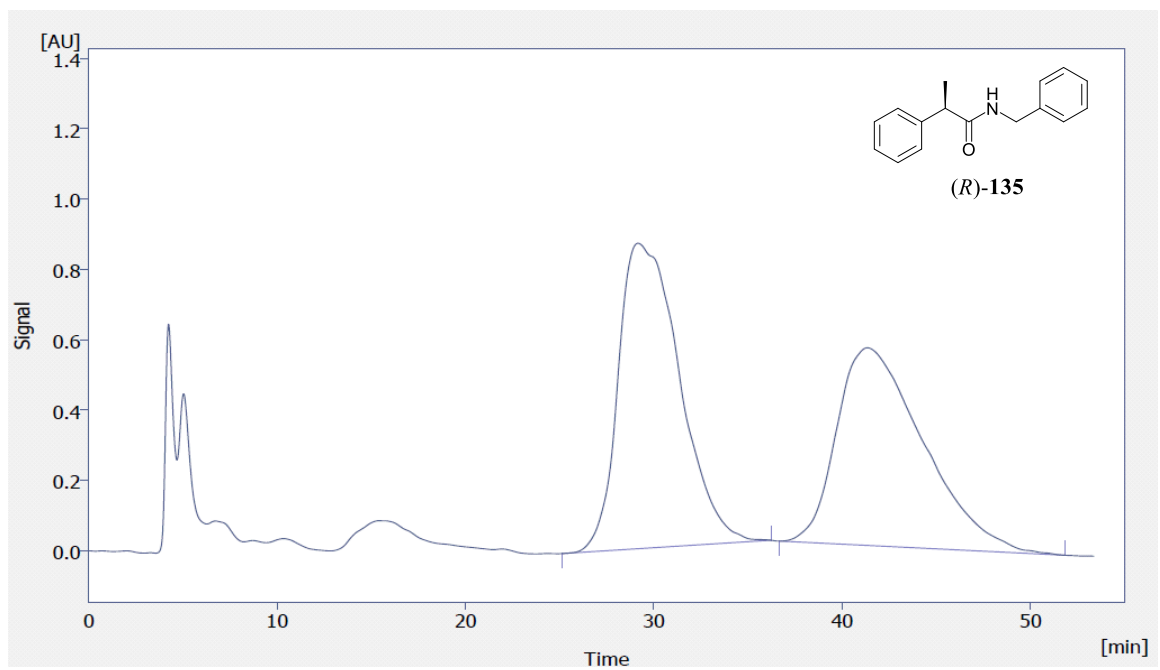
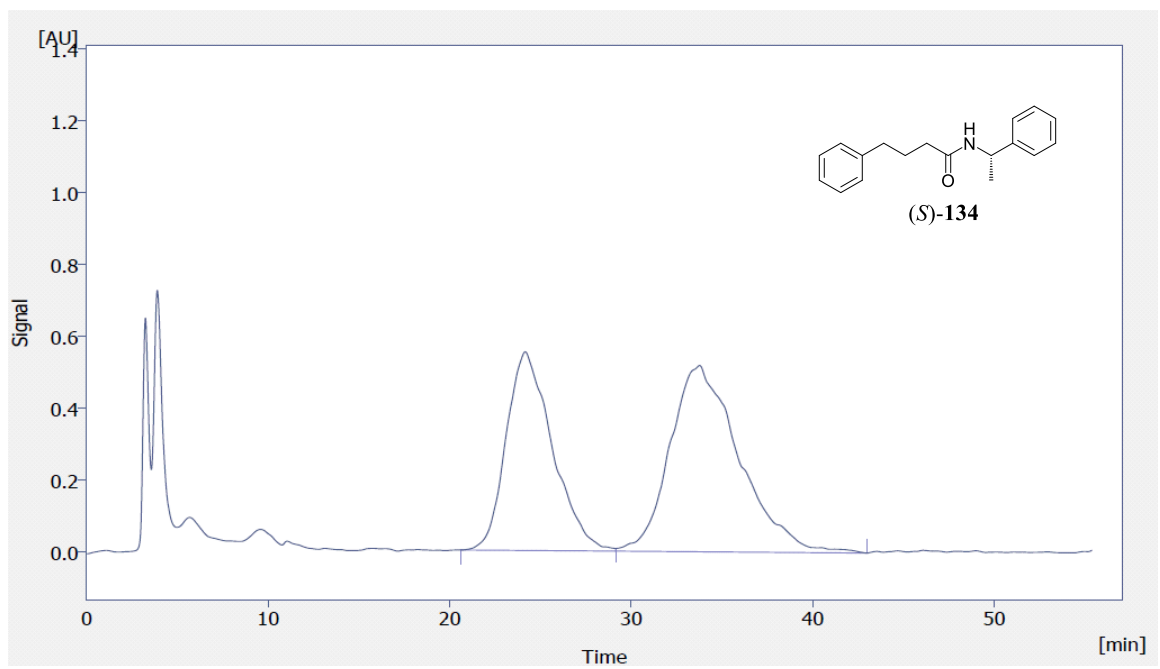


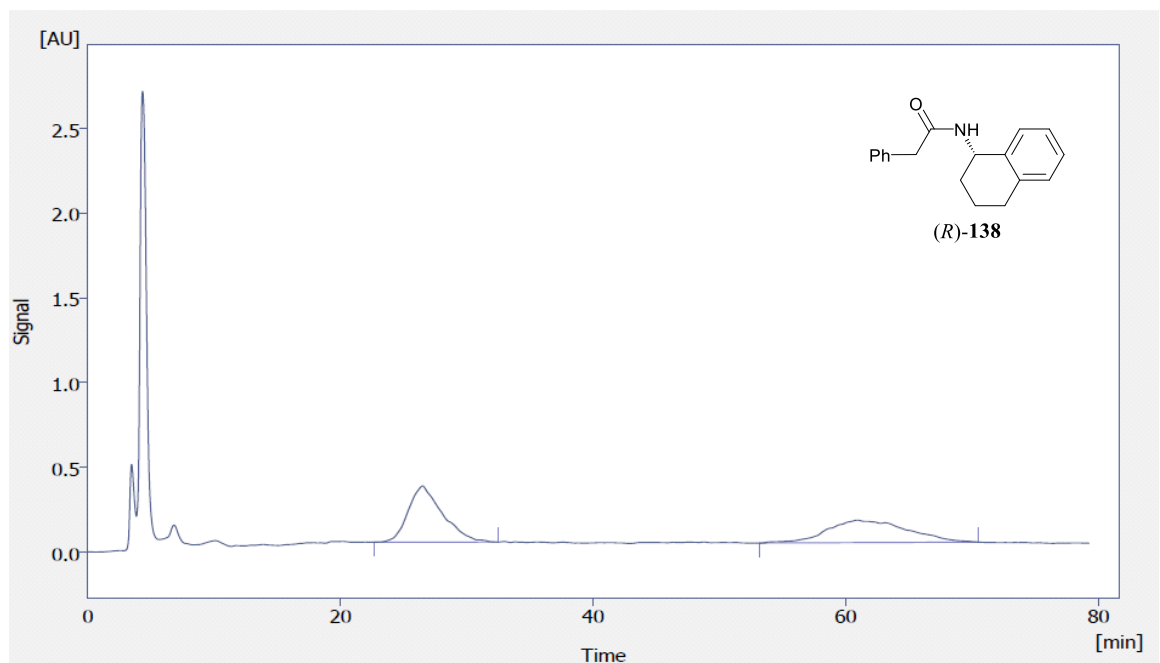
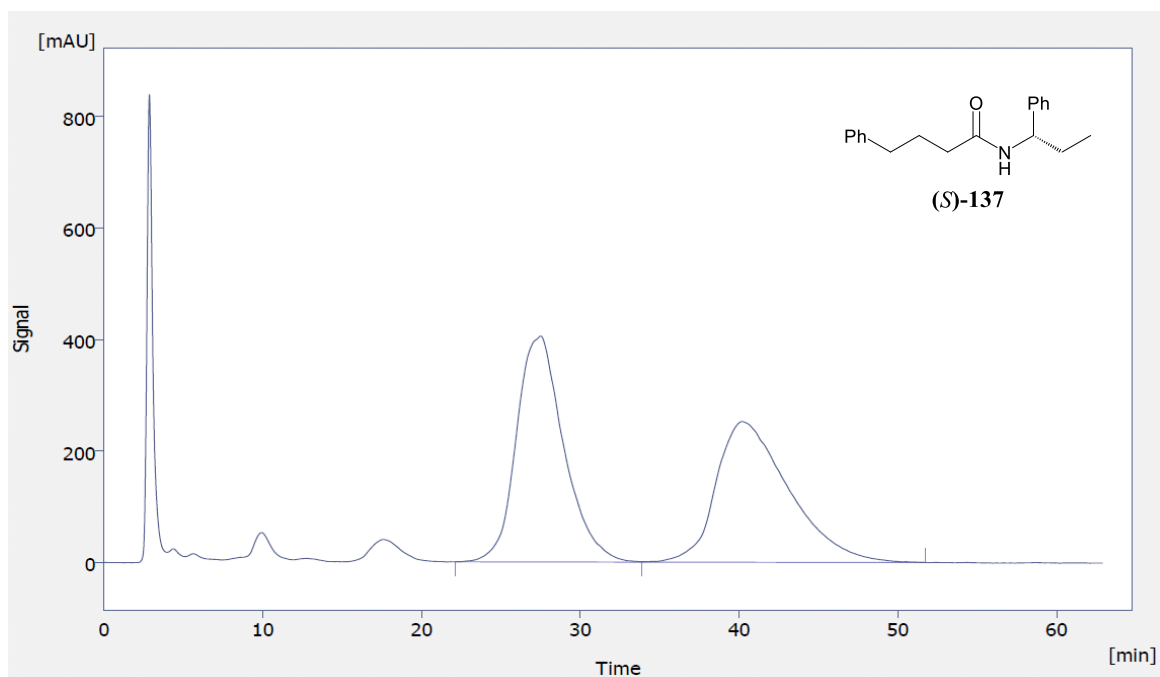












3. Crystallography data

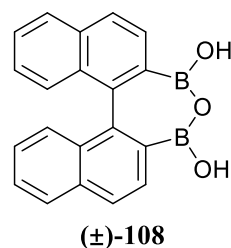
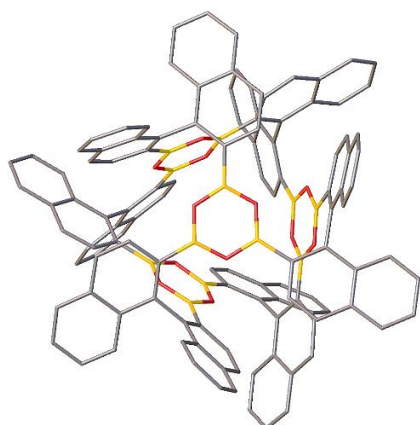


Table 20. Crystal data and structure refinement for **(±)-108**.

Identification code	(±)-108
Empirical formula	$C_{132}H_{84.6}B_{12}Cl_{23.4}O_{12}$
Formula weight	2821.84
Temperature/K	120
Crystal system	trigonal
Space group	P-3
a/Å	20.4108(7)
b/Å	20.4108(7)
c/Å	18.2972(7)
$\alpha/^\circ$	90
$\beta/^\circ$	90
$\gamma/^\circ$	120
Volume/Å ³	6601.4(5)
Z	2
$\rho_{\text{calc}}/\text{g/cm}^3$	1.420
μ/mm^{-1}	0.542
F(000)	2861.0
Crystal size/mm ³	0.288 × 0.207 × 0.162
Radiation	MoK α ($\lambda = 0.71073$)
2 Θ range for data collection/ $^\circ$	3.992 to 50.27
Index ranges	-24 ≤ h ≤ 24, -24 ≤ k ≤ 24, -21 ≤ l ≤ 21
Reflections collected	106131
Independent reflections	7851 [R _{int} = 0.0447, R _{sigma} = 0.0208]
Data/restraints/parameters	7851/24/668
Goodness-of-fit on F ²	1.054
Final R indexes [I ≥ 2 σ (I)]	R ₁ = 0.0585, wR ₂ = 0.1597
Final R indexes [all data]	R ₁ = 0.0747, wR ₂ = 0.1710
Largest diff. peak/hole / e Å ⁻³	0.71/-0.70

Table 21. Fractional Atomic Coordinates ($\times 10^4$) and Equivalent Isotropic Displacement Parameters ($\text{\AA}^2 \times 10^3$) for (\pm)-**108**. U_{eq} is defined as 1/3 of the trace of the orthogonalised U_{H} tensor.

Atom	<i>x</i>	<i>y</i>	<i>z</i>	U_{eq}
O(1)	5700.2(10)	1899.7(11)	5408.7(10)	29.7(4)
O(2)	6603.2(11)	1787.1(12)	6124.4(10)	33.9(5)
O(3)	5438.0(11)	1531.1(11)	6649.5(10)	32.1(5)
O(4)	6752.6(10)	2710.9(10)	8427.2(10)	28.9(4)
C(1)	4198.0(15)	1955.4(14)	5410.0(13)	25.6(6)
C(2)	4427.9(15)	1641.7(15)	5954.9(14)	28.0(6)
C(3)	3916.2(16)	1250.9(17)	6539.0(15)	32.6(6)
C(4)	3215.8(16)	1168.6(17)	6570.0(16)	35.6(7)
C(5)	2971.5(16)	1489.7(17)	6026.5(16)	34.9(7)
C(6)	2241.9(19)	1411(2)	6045(2)	48.7(8)
C(7)	2016(2)	1723(2)	5512(2)	56.1(10)
C(8)	2512(2)	2132(2)	4939(2)	51.0(9)
C(9)	3217.5(18)	2216.0(18)	4902.5(16)	37.5(7)
C(10)	3469.6(16)	1893.7(16)	5441.9(14)	30.1(6)
C(11)	4678.9(15)	2345.7(15)	4753.4(13)	26.1(6)
C(12)	5272.7(15)	3087.4(15)	4770.7(13)	26.8(6)
C(13)	5676.7(16)	3418.4(17)	4109.9(14)	30.0(6)
C(14)	5497.5(17)	3025.6(17)	3471.7(14)	31.2(6)
C(15)	4903.5(16)	2267.7(17)	3438.1(14)	29.8(6)
C(16)	4714.5(18)	1840.3(18)	2781.7(15)	35.5(7)
C(17)	4139.7(19)	1107(2)	2766.5(16)	41.8(8)
C(18)	3727.0(19)	762.9(19)	3403.6(17)	42.8(8)
C(19)	3890.7(17)	1161.0(17)	4044.0(16)	35.6(7)
C(20)	4486.3(15)	1922.1(16)	4084.6(14)	28.1(6)
C(21)	5999.7(15)	1116.0(14)	8079.4(14)	25.5(6)
C(22)	6356.7(16)	1267.3(15)	7404.5(14)	27.5(6)
C(23)	6997.1(16)	1175.9(16)	7321.4(14)	31.2(6)
C(24)	7261.4(17)	927.4(17)	7873.1(15)	33.1(6)
C(25)	6911.2(16)	770.7(15)	8571.0(14)	29.4(6)
C(26)	7184.3(19)	530.3(17)	9166.8(15)	36.7(7)
C(27)	6850(2)	403.2(18)	9835.5(16)	40.3(7)
C(28)	6229.4(18)	510.6(17)	9949.2(15)	35.4(7)
C(29)	5948.9(16)	736.1(15)	9385.7(14)	29.2(6)
C(30)	6279.9(15)	874.5(14)	8677.8(14)	25.1(6)
C(31)	5296.0(15)	1156.5(14)	8206.2(13)	24.4(6)
C(32)	5307.8(15)	1822.6(15)	8386.7(13)	25.1(6)
C(33)	4609.8(15)	1800.1(15)	8521.6(14)	27.4(6)
C(34)	3934.8(16)	1140.9(16)	8491.7(14)	30.9(6)
C(35)	3905.4(16)	458.3(16)	8293.3(14)	30.4(6)

C(36)	3210.3(18)	-230.0(18)	8217.3(16)	41.3(7)
C(37)	3195(2)	-876.6(19)	8005(2)	53.7(9)
C(38)	3872(2)	-872.5(19)	7869(2)	51.7(9)
C(39)	4552.1(19)	-223.7(17)	7934.4(16)	38.5(7)
C(40)	4591.3(16)	466.4(15)	8147.1(13)	28.1(6)
B(1)	5215.7(18)	1696.9(18)	5994.0(16)	27.7(7)
B(2)	6393.6(18)	1944.7(18)	5464.8(16)	28.8(7)
B(3)	6109.8(19)	1538.0(18)	6708.7(16)	29.9(7)
B(4)	6038.9(17)	2613.5(17)	8418.6(15)	25.5(6)
Cl(8)	1826.6(9)	-886.3(9)	7011.6(9)	70.4(4)
Cl(9)	602(5)	-544(4)	7018(7)	144(5)
Cl(10)	847(4)	-1496(3)	8156(3)	86.6(14)
Cl(11)	751(4)	-468(3)	6736(4)	79.8(18)
Cl(12)	431(3)	-1666(2)	7799(3)	86.0(15)
Cl(2A)	1378(5)	163(4)	8075(5)	73(2)
Cl(13)	1357(5)	-703(6)	6836(4)	110(4)
Cl(14)	794(15)	-1458(13)	7824(14)	75(6)
Cl(15)	-150(20)	-1330(20)	7950(20)	68(9)
C(4S)	877(5)	-1229(6)	7235(6)	53.2(19)
C(5S)	884(5)	-1225(6)	6963(6)	53.2(19)
C(6S)	851(19)	-687(18)	7624(18)	74(8)
Cl(16)	1751(2)	480(2)	8480(2)	101.9(10)
Cl(17)	393(3)	-47(3)	9012(3)	59.2(11)
Cl(18)	1673(4)	774(4)	9981(4)	81.6(18)
Cl(19)	1235(3)	-680(3)	9652(4)	91.7(17)
Cl(20)	2286(3)	863(2)	9949(2)	62.2(10)
C(7S)	1301(7)	625(13)	9133(7)	77(6)
C(8S)	1646(13)	336(13)	9487(13)	91(6)
Cl(4)	3901.5(8)	1652.4(8)	10756.0(8)	89.4(4)
Cl(5)	5115.5(6)	1338.9(5)	10923.5(5)	55.9(3)
Cl(6)	5408(2)	2740.2(16)	10298.4(14)	89.3(9)
Cl(7)	5435(6)	2878(6)	10603(5)	85(3)
C(2S)	4744(4)	1777(3)	10377(4)	55.3(15)
C(3S)	4821(10)	1912(10)	10485(17)	55.3(15)
Cl(1)	4078(3)	-249(4)	4947(4)	52.2(11)
Cl(2)	5180.3(19)	169.9(17)	3792.5(16)	55.3(7)
Cl(3)	5600(5)	174(6)	5308(3)	60.2(16)
C(1S)	5027(7)	330(6)	4701(6)	38(2)
C(9S)	4475(5)	-182(5)	5563(5)	45.5(19)
C(10S)	5165(6)	-124(6)	5689(7)	46(2)
C(11S)	5694(18)	62(11)	5137(15)	44(6)
C(12S)	3928(9)	-323(9)	6134(9)	40(4)

Table 22. Anisotropic Displacement Parameters ($\text{\AA}^2 \times 10^3$) for (\pm)-108. The Anisotropic displacement factor exponent takes the form: $2\pi^2[h^2a^{*2}U_{11}+2hka^*b^*U_{12}+\dots]$.

Atom	U ₁₁	U ₂₂	U ₃₃	U ₂₃	U ₁₃	U ₁₂
O(1)	30.7(10)	40.8(11)	18.5(9)	4.3(8)	2.6(7)	18.6(9)
O(2)	35.1(11)	53.3(13)	17.7(9)	8.6(8)	5.5(8)	25.4(10)
O(3)	35.1(11)	46.8(12)	19.1(9)	7.5(8)	5.2(8)	24.0(9)
O(4)	26.5(10)	26.4(10)	34.6(10)	0.8(8)	-0.5(8)	13.9(8)
C(1)	28.1(14)	26.0(13)	18.7(13)	-7.5(10)	-3.3(10)	10.5(11)
C(2)	30.8(14)	30.3(14)	18.7(13)	-2.0(10)	0.3(11)	12.3(12)
C(3)	32.9(15)	38.4(16)	20.8(13)	0.7(11)	0.3(11)	13.5(13)
C(4)	30.2(15)	39.4(16)	28.1(15)	-1.0(12)	4.8(12)	10.5(13)
C(5)	29.8(15)	37.5(16)	31.6(15)	-8.5(12)	-3.5(12)	12.6(13)
C(6)	32.9(17)	59(2)	49(2)	-5.4(16)	1.4(14)	19.3(16)
C(7)	37.0(18)	77(3)	62(2)	-5(2)	-5.4(17)	34.2(19)
C(8)	49(2)	68(2)	48(2)	-6.9(17)	-12.5(16)	38.4(19)
C(9)	39.5(17)	44.5(17)	32.4(15)	-7.2(13)	-6.4(13)	24.0(15)
C(10)	30.5(14)	32.5(15)	24.2(13)	-9.0(11)	-4.8(11)	13.5(12)
C(11)	31.5(14)	35.2(15)	16.3(12)	-2.3(10)	-3.3(10)	20.3(12)
C(12)	31.7(14)	34.1(15)	16.8(12)	-1.1(11)	-1.1(10)	18.0(12)
C(13)	36.3(15)	36.1(15)	19.6(13)	1.6(11)	1.1(11)	19.7(13)
C(14)	40.6(16)	43.7(17)	16.5(13)	3.3(11)	1.5(11)	26.6(14)
C(15)	39.2(16)	43.0(16)	18.5(13)	-4.2(11)	-5.9(11)	29.0(14)
C(16)	45.9(18)	52.8(19)	19.0(13)	-7.0(12)	-6.4(12)	33.1(16)
C(17)	49.4(19)	56(2)	26.2(15)	-19.4(14)	-10.9(13)	31.4(17)
C(18)	43.2(18)	46.6(19)	36.4(17)	-17.8(14)	-9.5(14)	20.9(15)
C(19)	37.8(16)	40.0(17)	29.4(15)	-8.5(13)	-5.8(12)	19.7(14)
C(20)	32.1(14)	37.3(15)	20.8(13)	-5.2(11)	-6.5(11)	21.8(13)
C(21)	32.9(14)	21.3(13)	20.9(13)	-0.7(10)	-0.2(11)	12.5(11)
C(22)	33.9(15)	29.6(14)	19.7(13)	1.2(11)	1.8(11)	16.4(12)
C(23)	38.7(16)	39.2(16)	18.8(13)	-0.1(11)	3.9(11)	21.8(13)
C(24)	42.5(16)	43.3(17)	24.8(14)	-1.4(12)	1.4(12)	30.0(14)
C(25)	41.3(16)	30.9(14)	21.2(13)	-1.3(11)	-1.7(11)	22.1(13)
C(26)	52.5(19)	44.2(17)	27.0(15)	0.4(13)	-1.9(13)	34.4(16)
C(27)	63(2)	46.0(18)	23.8(15)	3.2(13)	-5.9(14)	36.1(17)
C(28)	52.9(19)	38.3(16)	18.3(13)	3.6(12)	1.8(12)	25.1(15)
C(29)	38.2(15)	27.8(14)	22.6(14)	2.1(11)	2.7(11)	17.2(12)
C(30)	35.6(15)	20.4(13)	19.2(13)	1.1(10)	0.7(11)	13.9(11)
C(31)	33.6(14)	26.4(13)	11.3(11)	4.6(10)	1.7(10)	13.6(12)
C(32)	30.2(14)	28.1(14)	15.9(12)	3.7(10)	1.5(10)	13.8(12)
C(33)	28.9(14)	30.9(14)	22.5(13)	0.2(11)	2.5(11)	14.9(12)
C(34)	28.2(14)	40.1(16)	21.4(13)	0.0(11)	3.1(11)	14.8(13)
C(35)	34.2(15)	32.5(15)	16.7(12)	3.4(11)	2.1(11)	10.8(12)
C(36)	35.7(17)	40.0(18)	31.8(16)	0.0(13)	0.9(13)	6.7(14)
C(37)	50(2)	34.1(18)	50(2)	-5.2(15)	-3.5(16)	1.1(16)

C(38)	60(2)	27.9(16)	56(2)	-7.8(15)	-3.6(17)	13.9(16)
C(39)	48.1(18)	32.0(16)	32.8(16)	-2.9(12)	-2.4(13)	18.1(14)
C(40)	36.9(15)	28.4(14)	14.9(12)	2.6(10)	0.6(11)	13.2(12)
B(1)	33.5(17)	30.4(16)	17.8(14)	1.4(12)	0.9(12)	15.0(14)
B(2)	33.3(17)	32.6(17)	20.9(15)	2.0(12)	0.6(12)	16.9(14)
B(3)	35.1(17)	34.5(17)	20.1(15)	2.3(13)	3.0(13)	17.2(14)
B(4)	30.2(16)	29.0(16)	18.7(14)	0.5(12)	1.7(12)	15.9(13)
Cl(8)	55.9(9)	69.6(10)	70.4(10)	-4.8(8)	5.0(8)	19.8(7)
Cl(9)	72(4)	72(3)	310(13)	-26(5)	-72(6)	52(3)
Cl(10)	103(4)	77(3)	62(3)	28(2)	41(2)	32(3)
Cl(11)	60(3)	43(2)	117(3)	-37(2)	-19(2)	12.3(18)
Cl(12)	63(2)	56(2)	104(4)	5(2)	54(3)	3(2)
Cl(2A)	74(5)	50(4)	102(6)	-16(4)	4(4)	37(4)
Cl(13)	58(5)	110(7)	65(5)	28(4)	-44(4)	-31(5)
Cl(16)	115(3)	104(3)	92(2)	-2.0(19)	-2(2)	59(2)
Cl(17)	57(3)	67(3)	60(3)	5(2)	6(2)	36(2)
Cl(18)	80(5)	65(4)	73(4)	1(3)	-21(3)	15(3)
Cl(19)	71(3)	61(3)	145(5)	-11(3)	-36(4)	34(3)
Cl(20)	59(2)	62(2)	67(2)	9.3(19)	3.5(19)	31(2)
Cl(4)	92.0(9)	87.0(9)	113.9(11)	-13.6(7)	-11.3(7)	63.3(8)
Cl(5)	87.5(7)	58.7(5)	39.9(5)	-0.3(4)	5.8(4)	50.3(5)
Cl(6)	133.2(19)	46.9(12)	68.8(15)	11.9(10)	-10.4(15)	30.6(12)
Cl(7)	95(5)	57(4)	103(7)	3(5)	-22(5)	39(3)
C(2S)	85(3)	55(3)	32(3)	-7(2)	-8(2)	39(3)
C(3S)	85(3)	55(3)	32(3)	-7(2)	-8(2)	39(3)
Cl(1)	54(3)	40(2)	62(3)	4.5(18)	7(2)	22(2)
Cl(2)	69.4(19)	49.0(16)	41.9(15)	-6.9(12)	3.7(14)	25.5(15)
Cl(3)	65(5)	61(3)	58(3)	-5(3)	-24(4)	34(3)
C(1S)	50(7)	38(6)	24(5)	1(5)	0(5)	21(6)

Table 23. Bond Lengths for (\pm)-108.

Atom	Atom	Length/Å	Atom	Atom	Length/Å
O(1)	B(1)	1.374(4)	C(31)	C(40)	1.388(4)
O(1)	B(2)	1.375(4)	C(31)	C(40)	1.428(4)
O(2)	B(2)	1.372(4)	C(32)	C(33)	1.424(4)
O(2)	B(3)	1.380(4)	C(32)	B(4)	1.558(4)
O(3)	B(1)	1.383(4)	C(33)	C(34)	1.363(4)
O(3)	B(3)	1.369(4)	C(34)	C(35)	1.412(4)
O(4)	B(4)	1.368(4)	C(35)	C(36)	1.419(4)
O(4)	B(4) ¹	1.383(4)	C(35)	C(40)	1.417(4)
C(1)	C(2)	1.387(4)	C(36)	C(37)	1.361(5)
C(1)	C(10)	1.429(4)	C(37)	C(38)	1.400(6)
C(1)	C(11)	1.503(4)	C(38)	C(39)	1.362(5)
C(2)	C(3)	1.427(4)	C(39)	C(40)	1.425(4)
C(2)	B(1)	1.556(4)	Cl(8)	Cl(14)	2.36(2)
C(3)	C(4)	1.355(4)	Cl(8)	C(4S)	1.748(9)
C(4)	C(5)	1.412(4)	Cl(8)	C(5S)	1.691(9)
C(5)	C(6)	1.416(4)	Cl(9)	C(4S)	1.792(10)
C(5)	C(10)	1.421(4)	Cl(10)	C(4S)	1.762(9)
C(6)	C(7)	1.364(5)	Cl(11)	C(5S)	1.747(10)
C(7)	C(8)	1.405(5)	Cl(12)	C(5S)	1.781(10)
C(8)	C(9)	1.365(5)	Cl(2A)	Cl(15) ³	2.14(4)
C(9)	C(10)	1.418(4)	Cl(2A)	C(6S)	1.73(3)
C(11)	C(12)	1.388(4)	Cl(13)	Cl(14)	2.28(2)
C(11)	C(20)	1.435(4)	Cl(13)	C(6S)	1.78(3)
C(12)	C(13)	1.429(4)	Cl(14)	Cl(15)	2.08(4)
C(12)	B(2) ²	1.567(4)	Cl(14)	C(6S)	1.56(4)
C(13)	C(14)	1.359(4)	Cl(15)	C(6S)	1.89(5)
C(14)	C(15)	1.411(4)	Cl(16)	C(7S)	1.621(13)
C(15)	C(16)	1.420(4)	Cl(17)	Cl(17) ⁴	1.478(8)
C(15)	C(20)	1.422(4)	Cl(17)	Cl(17) ³	1.478(8)
C(16)	C(17)	1.364(5)	Cl(17)	C(7S)	1.679(13)
C(17)	C(18)	1.404(5)	Cl(18)	C(7S)	1.687(13)
C(18)	C(19)	1.369(4)	Cl(19)	C(8S)	1.83(2)
C(19)	C(20)	1.417(4)	Cl(20)	C(8S)	1.47(2)
C(21)	C(22)	1.388(4)	Cl(4)	C(2S)	1.751(7)
C(21)	C(30)	1.432(4)	Cl(4)	C(3S)	1.747(19)
C(21)	C(31)	1.497(4)	Cl(5)	C(2S)	1.748(6)
C(22)	C(23)	1.418(4)	Cl(5)	C(3S)	1.755(18)
C(22)	B(3)	1.568(4)	Cl(6)	C(2S)	1.749(6)
C(23)	C(24)	1.357(4)	Cl(7)	C(3S)	1.742(18)

C(24)	C(25)	1.420(4)	Cl(1)	C(1S)	1.749(12)
C(25)	C(26)	1.419(4)	Cl(2)	C(1S)	1.752(11)
C(25)	C(30)	1.420(4)	Cl(3)	C(1S)	1.755(12)
C(26)	C(27)	1.361(4)	C(9S)	C(10S)	1.372(13)
C(27)	C(28)	1.404(4)	C(9S)	C(11S) ⁵	1.38(3)
C(28)	C(29)	1.366(4)	C(9S)	C(12S)	1.450(18)
C(29)	C(30)	1.422(4)	C(10S)	C(11S)	1.38(3)

¹1-Y,+X-Y,+Z; ²1+Y-X,1-X,+Z; ³-Y,+X-Y,+Z; ⁴+Y-X,-X,+Z; ⁵1-X,-Y,1-Z

Table 24. Bond Angles for (\pm)-108.

Atom	Atom	Atom	Angle/°	Atom	Atom	Atom	Angle/°
B(1)	O(1)	B(2)	121.6(2)	C(33)	C(34)	C(35)	120.5(3)
B(2)	O(2)	B(3)	120.8(2)	C(34)	C(35)	C(36)	122.0(3)
B(3)	O(3)	B(1)	121.0(2)	C(34)	C(35)	C(40)	118.9(2)
B(4)	O(4)	B(4) ¹	121.3(3)	C(40)	C(35)	C(36)	119.1(3)
C(2)	C(1)	C(10)	120.5(2)	C(37)	C(36)	C(35)	121.0(3)
C(2)	C(1)	C(11)	122.5(2)	C(36)	C(37)	C(38)	120.0(3)
C(10)	C(1)	C(11)	117.0(2)	C(39)	C(38)	C(37)	120.9(3)
C(1)	C(2)	C(3)	118.3(3)	C(38)	C(39)	C(40)	120.7(3)
C(1)	C(2)	B(1)	125.1(2)	C(35)	C(40)	C(31)	119.9(2)
C(3)	C(2)	B(1)	116.6(2)	C(35)	C(40)	C(39)	118.2(3)
C(4)	C(3)	C(2)	122.2(3)	C(39)	C(40)	C(31)	121.8(3)
C(3)	C(4)	C(5)	120.6(3)	O(1)	B(1)	O(3)	118.4(3)
C(4)	C(5)	C(6)	121.7(3)	O(1)	B(1)	C(2)	123.2(2)
C(4)	C(5)	C(10)	118.9(3)	O(3)	B(1)	C(2)	118.4(2)
C(6)	C(5)	C(10)	119.4(3)	O(1)	B(2)	C(12) ¹	118.2(2)
C(7)	C(6)	C(5)	120.8(3)	O(2)	B(2)	O(1)	118.8(2)
C(6)	C(7)	C(8)	120.0(3)	O(2)	B(2)	C(12) ¹	123.0(3)
C(9)	C(8)	C(7)	120.8(3)	O(2)	B(3)	C(22)	117.1(3)
C(8)	C(9)	C(10)	120.8(3)	O(3)	B(3)	O(2)	119.0(2)
C(5)	C(10)	C(1)	119.5(3)	O(3)	B(3)	C(22)	123.9(2)
C(9)	C(10)	C(1)	122.3(3)	O(4)	B(4)	O(4) ²	118.7(3)
C(9)	C(10)	C(5)	118.2(3)	O(4) ²	B(4)	C(32)	118.0(2)
C(12)	C(11)	C(1)	122.8(2)	O(4)	B(4)	C(32)	123.3(2)
C(12)	C(11)	C(20)	120.2(2)	C(6S)	Cl(13)	Cl(14)	43.1(12)
C(20)	C(11)	C(1)	116.9(2)	Cl(13)	Cl(14)	Cl(8)	30.8(4)
C(11)	C(12)	C(13)	118.6(2)	Cl(15)	Cl(14)	Cl(8)	131.6(15)
C(11)	C(12)	B(2) ²	125.4(2)	Cl(15)	Cl(14)	Cl(13)	101.0(15)
C(13)	C(12)	B(2) ²	116.0(2)	C(6S)	Cl(14)	Cl(8)	75.8(15)
C(14)	C(13)	C(12)	121.8(3)	C(6S)	Cl(14)	Cl(13)	51.2(14)
C(13)	C(14)	C(15)	121.0(3)	C(6S)	Cl(14)	Cl(15)	60.6(18)
C(14)	C(15)	C(16)	122.1(3)	C(6S)	Cl(15)	Cl(14)	46.1(14)
C(14)	C(15)	C(20)	118.7(2)	Cl(8)	C(4S)	Cl(9)	110.7(6)
C(16)	C(15)	C(20)	119.2(3)	Cl(8)	C(4S)	Cl(10)	102.0(5)
C(17)	C(16)	C(15)	120.8(3)	Cl(10)	C(4S)	Cl(9)	118.5(7)
C(16)	C(17)	C(18)	120.3(3)	Cl(8)	C(5S)	Cl(11)	107.4(6)
C(19)	C(18)	C(17)	120.4(3)	Cl(8)	C(5S)	Cl(12)	111.1(6)
C(18)	C(19)	C(20)	121.1(3)	Cl(11)	C(5S)	Cl(12)	112.4(6)
C(15)	C(20)	C(11)	119.7(3)	Cl(2A)	C(6S)	Cl(13)	109.2(18)
C(19)	C(20)	C(11)	122.1(3)	Cl(2A)	C(6S)	Cl(15)	117(2)
C(19)	C(20)	C(15)	118.2(2)	Cl(13)	C(6S)	Cl(15)	133(2)
C(22)	C(21)	C(30)	120.1(2)	Cl(14)	C(6S)	Cl(2A)	126(2)
C(22)	C(21)	C(31)	122.5(2)	Cl(14)	C(6S)	Cl(13)	85.6(18)

C(30)	C(21)	C(31)	117.4(2)	Cl(14)	C(6S)	Cl(15)	73(2)
C(21)	C(22)	C(23)	118.8(2)	Cl(17) ³	Cl(17)	Cl(17) ⁴	59.995(1)
C(21)	C(22)	B(3)	125.1(2)	Cl(17) ³	Cl(17)	C(7S)	157.7(9)
C(23)	C(22)	B(3)	116.1(2)	Cl(17) ⁴	Cl(17)	C(7S)	98.9(10)
C(24)	C(23)	C(22)	122.3(3)	Cl(16)	C(7S)	Cl(17)	104.5(8)
C(23)	C(24)	C(25)	120.3(3)	Cl(16)	C(7S)	Cl(18)	117.7(10)
C(24)	C(25)	C(30)	118.8(2)	Cl(17)	C(7S)	Cl(18)	118.8(10)
C(26)	C(25)	C(24)	121.9(3)	Cl(20)	C(8S)	Cl(19)	117.9(14)
C(26)	C(25)	C(30)	119.3(2)	Cl(5)	C(2S)	Cl(4)	110.2(4)
C(27)	C(26)	C(25)	120.7(3)	Cl(5)	C(2S)	Cl(6)	109.4(4)
C(26)	C(27)	C(28)	120.6(3)	Cl(6)	C(2S)	Cl(4)	110.4(4)
C(29)	C(28)	C(27)	120.2(3)	Cl(4)	C(3S)	Cl(5)	110.0(12)
C(28)	C(29)	C(30)	121.1(3)	Cl(7)	C(3S)	Cl(4)	111.4(13)
C(25)	C(30)	C(21)	119.6(2)	Cl(7)	C(3S)	Cl(5)	113.8(13)
C(25)	C(30)	C(29)	118.2(2)	Cl(1)	C(1S)	Cl(2)	111.0(7)
C(29)	C(30)	C(21)	122.2(2)	Cl(1)	C(1S)	Cl(3)	109.1(7)
C(32)	C(31)	C(21)	122.9(2)	Cl(2)	C(1S)	Cl(3)	111.7(7)
C(32)	C(31)	C(40)	120.0(2)	C(10S)	C(9S)	C(11S) ⁵	118.5(15)
C(40)	C(31)	C(21)	117.0(2)	C(10S)	C(9S)	C(12S)	123.6(11)
C(31)	C(32)	C(33)	118.9(2)	C(11S) ⁵	C(9S)	C(12S)	117.8(17)
C(31)	C(32)	B(4)	124.2(2)	C(9S)	C(10S)	C(11S)	121.8(14)
C(33)	C(32)	B(4)	116.8(2)	C(9S) ⁵	C(11S)	C(10S)	120(2)
C(34)	C(33)	C(32)	121.8(3)				

¹1-Y,+X-Y,+Z; ²1+Y-X,1-X,+Z; ³+Y-X,-X,+Z; ⁴-Y,+X-Y,+Z; ⁵1-X,-Y,1-Z

Table 25. Hydrogen Atom Coordinates ($\text{\AA}\times 10^4$) and Isotropic Displacement Parameters ($\text{\AA}^2\times 10^3$) for (\pm)-**108**.

Atom	<i>x</i>	<i>y</i>	<i>z</i>	U(eq)
H(3)	4071.89	1041.54	6918.84	39
H(4)	2886.03	892.42	6960.74	43
H(6)	1906.01	1138.68	6433.15	58
H(7)	1523.42	1662.19	5527.53	67
H(8)	2354.03	2354.23	4573.68	61
H(9)	3543.89	2493.56	4510.25	45
H(13)	6081.62	3926.89	4116.79	36
H(14)	5776.16	3264.73	3041.92	37
H(16)	4991.78	2067.5	2347.99	43
H(17)	4017.99	828.92	2322.86	50
H(18)	3331.69	250.14	3390.25	51
H(19)	3600.17	923.07	4468.39	43
H(23)	7249.99	1292.74	6863.43	37
H(24)	7682.54	858.09	7792.04	40
H(26)	7604.86	457.25	9098.39	44
H(27)	7037.65	240.35	10228.69	48
H(28)	6004.15	426.15	10419.58	43
H(29)	5525.61	801.61	9468.08	35
H(33)	4614.78	2256.67	8635.36	33
H(34)	3480.56	1140.86	8605.39	37
H(36)	2748.64	-239.63	8316.09	50
H(37)	2724.29	-1331.06	7949.32	64
H(38)	3857.08	-1328.2	7730.14	62
H(39)	5005.18	-231.67	7836.75	46
H(4S)	559.86	-1695.32	6940.08	64
H(5S)	670.23	-1609.28	6563.28	64
H(7S)	1318.87	1108.46	8999.11	92
H(2S)	4635.3	1542.43	9879.3	66
H(3S)	4802.1	1807	9949.11	66
H(1S)	5155.36	869.43	4747.69	46
H(10S)	5285.29	-205.77	6169.1	55
H(11S)	6169.26	99.91	5233.78	53
H(12A)	4115.51	-400.14	6599.46	61
H(12B)	3856.51	116.86	6172.96	61
H(12C)	3443.31	-773.04	6015.46	61

Table 26. Atomic Occupancy for (\pm)-**108**.

Atom	Occupancy	Atom	Occupancy	Atom	Occupancy
Cl(8)	0.7	Cl(9)	0.35	Cl(10)	0.35
Cl(11)	0.35	Cl(12)	0.35	Cl(2A)	0.15
Cl(13)	0.15	Cl(14)	0.08	Cl(15)	0.03
C(4S)	0.35	H(4S)	0.35	C(5S)	0.35
H(5S)	0.35	C(6S)	0.15	Cl(16)	0.45
Cl(17)	0.2	Cl(18)	0.2	Cl(19)	0.25
Cl(20)	0.25	C(7S)	0.2	H(7S)	0.2
C(8S)	0.25	Cl(6)	0.77	Cl(7)	0.23
C(2S)	0.77	H(2S)	0.77	C(3S)	0.23
H(3S)	0.23	Cl(1)	0.3	Cl(2)	0.3
Cl(3)	0.3	C(1S)	0.3	H(1S)	0.3
C(9S)	0.4	C(10S)	0.4	H(10S)	0.4
C(11S)	0.4	H(11S)	0.4	C(12S)	0.2
H(12A)	0.2	H(12B)	0.2	H(12C)	0.2

Experimental

Single crystals of $C_{132}H_{84.6}B_{12}Cl_{23.4}O_{12}$ (\pm)-**108** were prepared under slow diffusion of deuterated chloroform in test tube. A suitable crystal was selected and analysed on Bruker Cryostream 700+ diffractometer. The crystal was kept at 120 K during data collection. Using Olex2²⁴², the structure was solved with the ShelXT²⁴³ structure solution program using Intrinsic Phasing and refined with the ShelXL²⁴⁴ refinement package using Least Squares minimisation.

Crystal structure determination of (\pm)-**108**

Crystal Data for $C_{132}H_{84.6}B_{12}Cl_{23.4}O_{12}$ ($M = 2821.84$ g/mol): trigonal, space group P-3 (no. 147), $a = 20.4108(7)$ Å, $c = 18.2972(7)$ Å, $V = 6601.4(5)$ Å³, $Z = 2$, $T = 120$ K, $\mu(\text{MoK}\alpha) = 0.542$ mm⁻¹, $D_{\text{calc}} = 1.420$ g/cm³, 106131 reflections measured ($3.992^\circ \leq 2\theta \leq 50.27^\circ$), 7851 unique ($R_{\text{int}} = 0.0447$, $R_{\text{sigma}} = 0.0208$) which were used in all calculations. The final R_1 was 0.0585 ($I > 2\sigma(I)$) and wR_2 was 0.1710 (all data).

4. Major conferences attended

Challenges in Catalysis for Pharmaceuticals and Fine Chemicals V

2nd November, 2016, London

Attendee

RSC Organic Division North East Regional Meeting

29th March, 2017, Durham

Poster Presenter

Dept. Chem. Annual Gala Research Symposium

17th June, 2018, Durham

Poster Presenter

RSC 7th EuCheMS Chemistry Congress

26th August, 2018, Liverpool

Poster Presenter

RSC Challenges in Catalyst VI

14th November, 2018, London

Poster Presenter

Dept. Chem. Annual Gala Research Symposium

21st June, 2019, Durham

Oral Presenter

ACS National Meeting – Chemistry and Water

24th August, 2019, San Diego, USA

Poster Presenter
